Films polymériques pour le développement de stents innovants

Arnaud Pallotta

UNIVERSITÉ DE LORRAINE

Ecole Doctorale BioSE (Biologie-Santé-Environnement)

Thèse

Présentée et soutenue publiquement pour l'obtention du titre de

DOCTEUR DE l'UNIVERSITE DE LORRAINE

Mention : « Sciences de la Vie et de la Santé »

Par Arnaud PALLOTTA

Films polymériques pour le développement de stents innovants

Le 8 décembre 2017

Membres du jury :		
Président :	M. Benoît FRISCH	
Rapporteurs :	M. Benoît FRISCH	DR, UMR 7199, CNRS, Université de Strasbourg, Strasbourg
	Mme Reine NEHME	MCU, UMR 731, Université d'Orléans, Orléans
Examinateurs :	M. Igor CLAROT	PR, EA 3452, Université de Lorraine, Nancy directeur de thèse
	Mme Ariane BOUDIER	MCU, EA 3452, Université de Lorraine, Nancy co-directrice de thèse
Membre invité :	M. Emmanuel LAMOUROUX	MCU, UMR 7565, Université de Lorraine, Nancy

---

EA 3452 CITHEFOR : Cibles Thérapeutiques et Expertise Préclinique du Médicament

5, rue Albert Lebrun, BP 80403, 54001 Nancy Cedex, France

REMERCIEMENTS

Tout au long de cette thèse, plusieurs personnes m'ont permis d'avancer, par leur aide, conseils, ou simplement en étant présentes. Je souhaite donc les remercier profondément.

- *Igor Clarot* et *Ariane Boudier*, respectivement directeur et co-directrice de thèse, merci pour l'aide scientifique, technique et analytique, votre rigueur, les idées « de l'au-delà », les charades … mais surtout pour votre accompagnement sans faille durant ces années.

- *Benoit Frisch* et *Reine Nehmé*, merci d'avoir accepté d'être les rapporteurs de ce travail.

- *Emmanuel Lamouroux*, merci d'avoir suivi l'évolution de ce travail et pour tes conseils avisés.

- *Dominique Decolin*, merci pour ton accueil sur la plateforme de TP, ainsi que pour toutes les discussions, cafés, pâtisseries ou débats que nous avons pu partager depuis mon arrivée.

- *Pierre Leroy*, directeur de l'EA 3452, pour m'avoir accueilli dans le laboratoire tout au long de ces années, et pour votre dynamisme quotidien.

- *Marianne Parent*, pour partager avec moi la valeur inestimable d'une tasse de thé.

❖ Tous les autres membres de l'EA 3452 et tout particulièrement *Caroline Gaucher, Isabelle Fries* et *Anne Sapin-Minet* pour votre bonne humeur quotidienne.

❖ A tous mes collègues doctorants : *Hui, Marie-Lynda, Haiyan, Romain, Yi, Justine*, bon courage à vous pour la suite !

❖ *Valentin*, binôme de choc lors de nos études de pharmacie, merci de t'être replongé avec moi pendant 6 mois dans le bonheur des manipulations.

❖ A tous les étudiants qui ont contribué à ce travail, votre aide est appréciée à sa juste valeur : *Vincent, Aurélien, Célia, Guillaume*.

❖ A nos différents collaborateurs, de Strasbourg (*Philippe Lavalle* et *Annie Tu*) pour leur accueil au sein de l'UMR 1151 de Strasbourg, leurs conseils avisés et l'encadrement sur la microbalance ; de Grenoble (*Lucie Sancey*) pour les études de biodistribution de l'or chez la souris ; et enfin de Nancy (*Murielle Barberi*, *Sophie Pinel* et *Héna Paquot*) pour nous avoir fourni une grande quantité de cellules.

❖ Enfin, à toutes les personnes qui m'ont soutenu durant ce travail, merci de votre (vos) bonne humeur/présence/conseils/compétences culinaires/cave à vin/assurage (rayer la mention inutile).

Pensées doctorales *Ad-Hoc*

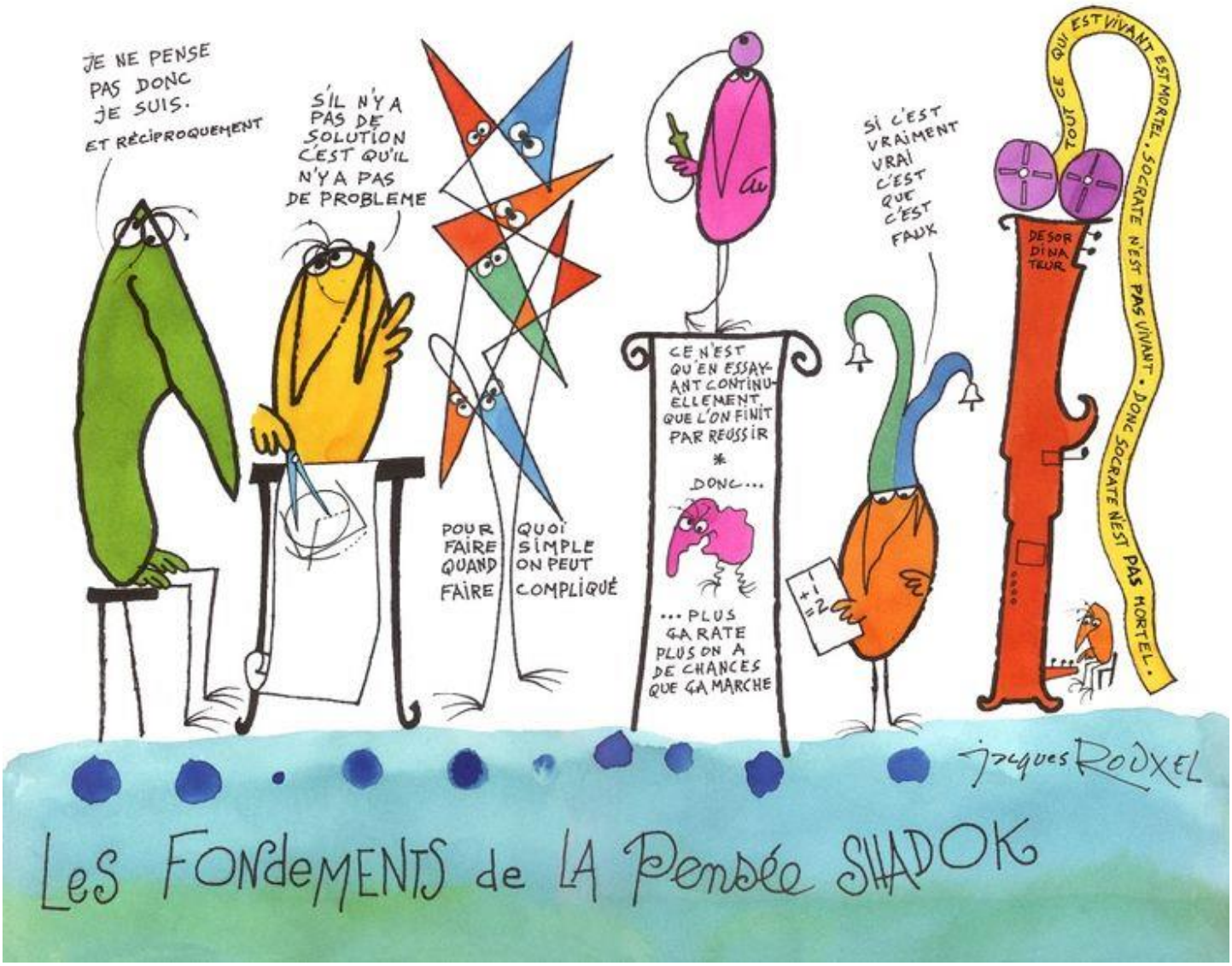

TABLE DES MATIERES

FORMATIONS

2006 : Baccalauréat scientifique option mathématiques : mention assez-bien.

2009 – 2016 : Etudes supérieures pharmaceutiques (faculté de pharmacie de Nancy).

2015 – 2016 : Master 2 : BioSciences et Ingénierie de la Santé, BioIngénierie du Médicament et NanoSanté (BSIS-BIMNS) (faculté de pharmacie de Nancy) : mention bien.

- « Stents recouverts de films multicouches de polyélectrolytes chargés en nanoparticules d'or pour la délivrance prolongée de principes actifs »
- Synthèse, caractérisation physico-chimique et évaluation biologique des films

2016-2017 : Doctorat d'université (laboratoire Cithéfor EA3452, faculté de pharmacie, Nancy).

2017 : Thèse d'exercice de pharmacie : mention très bien.

TRAVAUX SCIENTIFIQUES

PUBLICATIONS

- **A Pallotta**, M Parent, I Clarot, M Luo, V Borr, R Safar, O Joubert, P Leroy, A Boudier, "Blood Compatibility of Multilayered Polyelectrolyte Films Containing Immobilized Gold Nanoparticles", *Particle and Particle Systems Characterization*, **2017**, 34:1600184 (IF : 4,0).

- **A Pallotta**, A Boudier, P Leroy, I Clarot, "Characterization and stability of gold nanoparticles depending on their surface chemistry: contribution of capillary zone electrophoresis to a quality control", *Journal of Chromatography A*, **2016**, 1461:179-184 (IF : 2,3).

- M Luo, A Boudier, **A Pallotta**, P Maincent, J B Vincourt, P Leroy. "Albumin as a carrier for NO delivery: preparation, physicochemical characterization, and interaction with gold nanoparticles" *Drug Development and Industrial Pharmacy*, **2016** 16:1-13 (IF : 4,5).

- **A. Pallotta**, V. Philippe, A. Boudier, P. Leroy, I. Clarot, "High sensitive ion-pairing chromatography with visible detection to easily quantify god nanoparticles in aqueous media", *Talanta*, soumis (IF : 3,8).

COMMUNICATION ORALE

- Groupement de recherche « Or-nano » (Nancy - France) 12-14 juin 2017 : « Multilayered Polyelectrolyte Films Containing Immobilized Gold Nanoparticles »

COMMUNICATIONS AFFICHEES

- Biomaterials 2017 (Ambleteuse – France) 12-15 juin 2017 : « Contribution of capillary electrophoresis for the optimization of LbL film design » **A. Pallotta,** A. Boudier,P. Leroy, I. Clarot

- Groupement de recherche « Or-nano » (Nancy - France) 12-14 juin 2017 : « Quantification of gold in nanoparticles with ion pairing extraction and liquid chromatography: applications to nanoparticle quality control and biological matrices » V. Philippe, **A. Pallotta**, P. Leroy, A. Boudier, I. Clarot

- 2nd European Conference on Pharmaceutics (Cracovie – Pologne), 3-5 avril 2017 : « Blood compatibility and NO delivery of functionalized films »; **A. Pallotta**, I. Clarot, P. Leroy, A. Boudier.

- Société Française de Nanomédecine (SFnano – Paris – France), 5-7 décembre 2016 : « Characterization and stability of gold nanoparticles depending on their surface chemistry »; **A. Pallotta**, A. Boudier, P. Leroy, I. Clarot.

- Hyphenated Techniques in Chromatography and Separative Technology-14 (HTC-14 - Ghent - Belgique), 27-29 janvier 2016: « Characterization and stability of gold nanoparticles depending on their surface chemistry »; **A. Pallotta**, A. Boudier, P. Leroy, I. Clarot.

ENCADREMENTS

Formation et caractérisation de films multicouches de polyélectrolytes :

- Vincent Borr (Stage d'Initiation à la Recherche) : du 1er mars au 28 avril 2016
- Aurélien Renaudin (Stage d'Initiation à la Recherche) : du 1er juin au 28 juillet 2016

Quantification des espèces dérivée du NO par électrophorèse capillaire :

- Célia Boukoufi (Stage d'Initiation à la Recherche) : du 1er juin au 28 juillet 2016
- Guillaume Loeuille (Stage Recherche) : du 3 avril au 30 mai 2017

Quantification de l'or par chromatographie liquide haute performance :

- Valentin Philippe (M2) : du 4 janvier au 4 juillet 2017

ENSEIGNEMENTS

2017-2018 (69 h)

Etudes de pharmacie :

- Deuxième année :
  - ✓ Sciences et techniques analytiques pharmaceutiques : travaux pratiques (15 h)
  - ✓ Qualité et produits de santé : travaux pratiques (15 h)
  - ✓ Formulation – fabrication et aspects biopharmaceutiques des médicaments : travaux pratiques (15 h)

Licence professionnelle :

- Contrôle qualité : travaux pratique (9 h)

Master 1 BioIngénierie du Médicament (BIM) :

- UE 7.308, contrôle du médicament et qualité : travaux pratiques (15 h)

2016-2017 (93 h)

Etudes de pharmacie :

- Deuxième année :
  - ✓ Sciences et techniques analytiques pharmaceutiques : travaux pratiques (60 h)
  - ✓ Qualité et produits de santé : travaux pratiques (15 h)
  - ✓ Formulation – fabrication et aspects biopharmaceutiques des médicaments : travaux pratiques (15 h)
- Quatrième année :
  - ✓ Développement analytique et galénique : travaux pratiques (9 h)
  - ✓ Management de projet R&D par la pratique : le principe actif, de la synthèse à l'évaluation (9 h)

LISTE DES FIGURES

LISTE DES TABLEAUX

LISTES DES ABREVIATIONS

AFM : *Atomic force microscopy*
AuNP : Nanoparticules d'or
AVC : Accident vasculaire cérébral
CML : Cellules musculaires lisses
CQ : Contrôle qualité
DHLA : Acide dihydrolipoïque
DLS : *Dynamic light scattering*
DM : Dispositif médical
DMI : Dispositif médical implantable
DMIA : Dispositif médical implantable actif
ECZ : Electrophorèse capillaire de zone
FDA : *Food and Drug Administration*
FEO : Flux électroosmotique
GSH : Glutathion
GSNO : *S*-nitrosoglutathion
ICH : *International Conference on Harmonization*
IEC : Inhibiteurs de l'enzyme de conversion
IRM : Imagerie par résonnance magnétique
LbL : *Layer-by-Layer*
LIBS : *Laser induced breakdown spectroscopy*
MEB : Microscope électronique à balayage
MET : Microscope électronique à transmission
NDMA : *N*-méthyl-*D*-aspartate
NOS : NO synthase
NP : Nanoparticule
OMS : Organisation mondiale de la santé
PA : Principe actif
PAA : Acide polyacrylique
PAH : Chlorhydrate de polyallylamine
PBS : *Phosphate buffered saline*

PEG : Poly(ethylène glycol)

QCM : *Quartz cristal microbalance*

RSNO : *S*-nitrosothiols

S/B : Rapport signal sur bruit

INTRODUCTION GENERALE

Dans le domaine pharmaceutique, en complément des médicaments se trouvent les dispositifs médicaux (DM). Le nombre de DM commercialisés dans le monde est estimé à environ 20 millions de références réparties dans plus de 22 000 groupes différents [1]. Les DM implantables (DMI) représentent une part non négligeable des DM délivrés. En 2016 en France, on dénombre plus de 17 000 DM stériles à visée implantable sur le marché [2].

Le problème de biocompatibilité de ces dispositifs représente un challenge important à relever. Des solutions ont été envisagées et commercialisées, notamment avec la création de DMI pouvant délivrer des principes actifs ou ayant une activité au sens large (délivrance d'impulsions électriques, stimulateurs …) formant ainsi la classe des DMI actifs (DMIA). Le nombre de DMIA commercialisés en France est estimé à plus de 1000 toutes applications confondues [2]. Il existe une réelle innovation dans ce domaine avec une augmentation de la commercialisation de ces DMIA, 65 % d'entre eux ayant été mis sur le marché après 2010. Dans leur design, les chercheurs se tournent de plus en plus vers des technologies faisant appel à la science des polymères ou celles des nanoparticules. En effet, une modification de surface par l'un ou/et l'autre apporte des propriétés nouvelles à un objet, propriétés pouvant être exploitées pour améliorer, modifier ou moduler le comportement d'un DM vis-à-vis de son environnement biologique.

Dans ce travail, nous nous focalisons sur le domaine cardiovasculaire dans lequel les DMI sont associés sur le long terme à un risque élevé d'effets indésirables graves avec une mise en jeu du pronostic vital du patient. Le monoxyde d'azote (NO), un gazotransmetteur physiologique, joue un rôle clé dans l'homéostasie vasculaire. Le développement de DMI le libérant selon un profil physiologique sur une longue période améliore leur tolérance. Malgré une preuve de concept validée par la littérature [3], le profil de libération de NO reste un point critique à améliorer. Pour atteindre un temps de libération adapté, un réservoir de principe actif d'une capacité suffisante est nécessaire. La solution peut être apportée par

l'utilisation de nanoparticules incorporées dans une matrice. En effet, celles-ci peuvent être fonctionnalisées avec des rendements importants [4], permettant une charge utile importante.

Le but de cette thèse consiste à développer un matériau capable de libérer du NO. Pour cela, des films composés de différentes couches de polyélectrolytes alternativement cationiques et anioniques dans lesquels sont immobilisées des nanoparticules d'or (AuNP) seront construits et caractérisés. Les films ainsi créés devront répondre à terme à un cahier des charges strict : être le plus biocompatibles possible, être capables de libérer du NO avec un profil adapté et posséder une stabilité importante (pas de dissémination des AuNP *in vivo*).

Ce manuscrit est organisé en trois chapitres. Le premier chapitre présente une revue de la littérature se focalisant sur l'association entre les nanotechnologies et les DM pour en améliorer leurs qualités intrinsèques, diminuer leurs effets secondaires et leur conférer de nouvelles propriétés. Cet aspect fait l'objet d'une revue générale qui sera soumise prochainement (**article 1**).

Le second chapitre est consacré au contrôle analytique essentiel au développement de DMI nanostructurés par des AuNP. Dans un premier temps, nous avons optimisé une méthode pour quantifier l'or (à état ionique et nanoparticulaire) dans des milieux aqueux, la méthode est adaptée de celle décrite par Tournebize et al. [5]. Son optimisation ainsi que sa validation ont fait l'objet d'un article soumis dans *Talanta* (**article 2**). Dans un second temps, afin de considérer les AuNP comme une matière première pharmaceutique, nous avons développé une méthodologie capable de les caractériser en fonction de leur diamètre hydrodynamique, charge et composition. Cette méthode est basée sur l'électrophorèse capillaire de zone (ECZ) et est complémentaire aux méthodes de caractérisation classique des nanoparticules (spectrophotométrie UV-Vis., diffusion dynamique de la lumière couplée ou non à de l'électrophorèse…). Cette méthode a été publiée en 2016 dans *Journal of Chromatography A* (**article 3**, Pallotta A. et *al.*, *J. Chrom. A*, 2016 (1461), 179-184). Enfin,

la fonctionnalisation d'une macromolécule par des *S*-nitrosothiols (RSNO) et notamment par le *S*-nitrosoglutathion a été étudiée comme modèle des AuNP. Dans cette partie, le transfert de NO par transnitrosation est montré comme une étape nécessaire à l'obtention de nanoparticules capables de libérer du NO. Ces travaux ont été publiés en 2016 dans *Drug Delivery and Industrial Pharmacy* (**article 4**, Luo et *al.*, *Drug Dev. Ind. Pharm.*, 2016 (16), 1-13).

Le troisième chapitre est consacré à la formation et à l'étude des films de polyélectrolytes nanostructurés par les AuNP. Leur stabilité et des preuves préliminaires de biocompatibilité ont été mises en évidence. Ces travaux ont été publiés en 2017 dans *Particle and Particle Systems Characterization* (**article 5** : Pallotta et *al*., *Part. Part. Syst. Charact.*, 2017 (34), 1600184). Dans un deuxième temps, nous nous sommes employés à enrichir les films en AuNP. Ces films ont été étudiés et caractérisés grâce à différentes techniques : ECZ, microbalance à cristal de quartz (quartz crystal microbalance, QCM) … Les résultats font partie d'une publication en préparation et qui sera prochainement soumise (**article 6**).

Ce mémoire se termine par une discussion et une conclusion générale résumant les faits marquant des travaux réalisés. Les points clés de ce travail peuvent être résumés en deux points : développement d'un contrôle des AuNP et la création d'une couverture innovante, facile à manipuler et extrêmement stable intégrant des AuNP. Enfin nous développerons les principales perspectives à court et long termes ainsi que les verrous qui devront être levés pour poursuivre le développement de la fonctionnalisation de surface.

CHAPITRE I ETAT DE L'ART

1. Monoxyde d'azote et physiologie cardiovasculaire

1.1. Pathologies cardio-vasculaires

Selon l'Organisation Mondiale de la Santé (OMS), les maladies cardio-vasculaires représentent la première cause de mortalité dans le monde (Figure 1) [6]. En France, malgré quatre décennies de baisse de morbi-mortalité grâce à la prévention et aux progrès thérapeutiques, les maladies cardio-vasculaires restent à l'origine d'environ 140 000 morts par an. Elles sont aussi l'une des principales causes de morbidité avec 3.5 millions de personnes traitées en 2012.

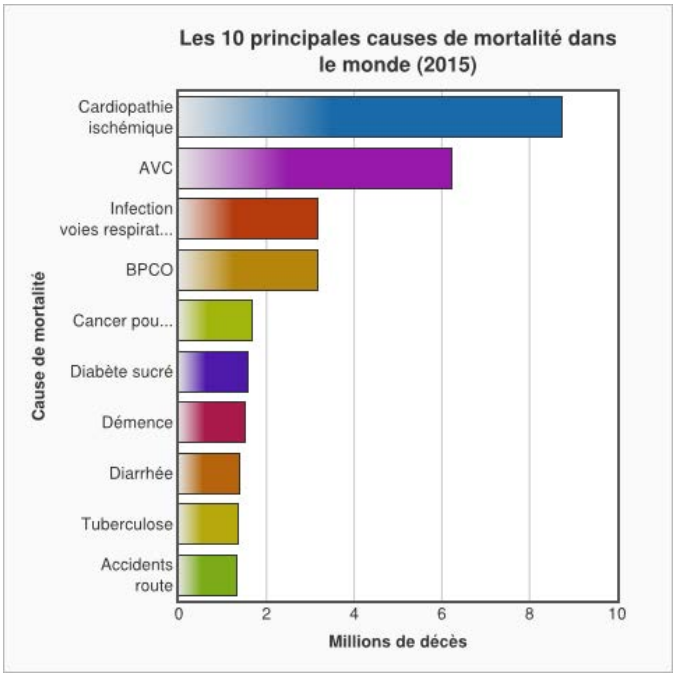

Figure 1 : Les 10 principales causes de décès dans le monde en 2015 selon l'OMS [6].

Les pathologies les plus communes sont l'angor, l'infarctus du myocarde, l'insuffisance cardiaque, les thromboses veineuses et les accidents vasculaires cérébraux (AVC). Elles représentent un coût humain et financier non négligeable. Aux Etats-Unis,

l'*Amercian Heart Association* prévoit d'ici 2030 une augmentation de la prévalence des maladies cardio-vasculaires d'au moins 10 % [7]. Cette augmentation est liée à plusieurs facteurs comme l'allongement de la durée de vie, mais aussi l'augmentation des cas d'obésités concomitante à une élévation de la pression artérielle moyenne (+8 % dans les 10 années à venir) ainsi qu'à l'apparition des cas de diabète (+100 % dans les 30 ans à venir) [8, 9].

Les facteurs de risques favorisant l'apparition de ces maladies sont bien connus. Il y a d'une part les facteurs acquis comme le sexe, l'âge, l'ethnie, les antécédents (personnels ou familiaux) et d'autre part les facteurs modulables (hypertension artérielle, hypercholestérolémie, alcoolisme, tabagisme …). Tous ces facteurs peuvent mener vers une dysfonction endothéliale et participent ainsi au développement de l'athérosclérose.

L'athérosclérose est une maladie vasculaire chronique de la paroi artérielle conduisant à l'obstruction progressive des vaisseaux. Différents acteurs sont impliqués : cellules endothéliales, cellules spumeuses, métalloprotéines … dont les actions et implications sont de mieux en mieux décrites [10, 11]. Parmi tous ces différents paramètres, les cellules endothéliales jouent un rôle clé.

1.2. Endothélium vasculaire

La monocouche cellulaire qui constitue l'endothélium occupe une place primordiale à l'interface entre le sang et les tissus environnants (Figure 2). Il joue un rôle majeur dans le maintien de l'homéostasie vasculaire.

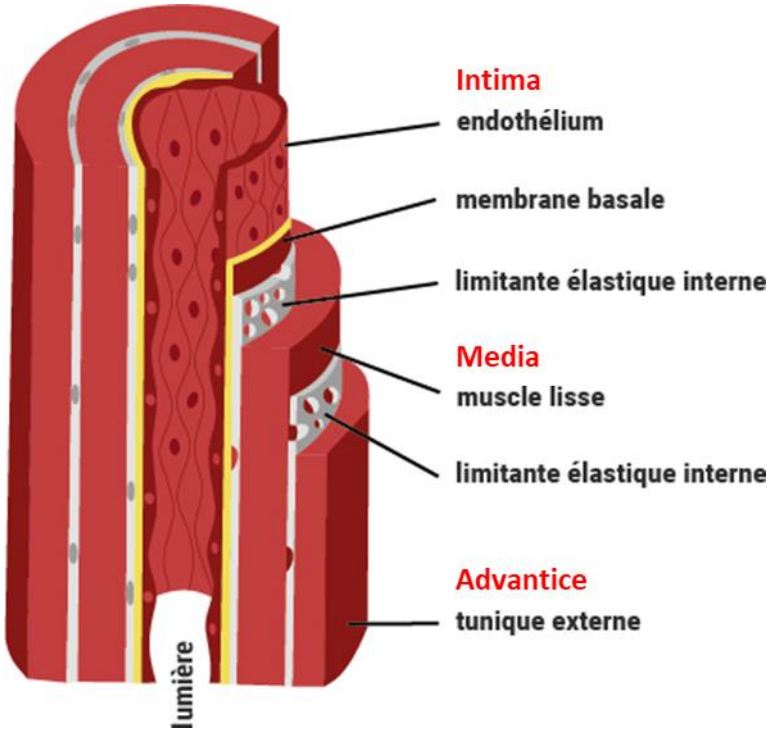

Figure 2 : Représentation schématique des différentes tuniques d'une artère de gros ou moyen calibre (selon la Fédération Française de Cardiologie)

Les cellules endothéliales sont constamment exposées à des stimuli chimiques (hormones, neurotransmetteurs …) et mécaniques (contrainte de cisaillement). En réponse à ces stimuli, elles sécrètent des substances modulant la vasomotricité, l'angiogenèse, la perméabilité vasculaire, l'hémostase et l'inflammation. En condition physiologique, la libération de facteurs de relaxation des cellules musculaires lisses (*via* le monoxyde d'azote, NO) prédomine sur celle des facteurs de contraction. Cependant, un déséquilibre dans la synthèse de ces facteurs peut rapidement amener le vaisseau vers une vasoconstriction ou relaxation trop importante.

1.3. Le monoxyde d'azote

Le NO est une espèce radicalaire, gazeuse et soluble possédant une très faible demi-vie [12]. Il est produit en continu au niveau des cellules endothéliales par une enzyme, la *nitric oxide synthase* (NOS) à partir de la L-arginine. Cette enzyme est active de façon constitutive mais peut être stimulée par différents agonistes comme par exemple la thrombine [13], l'adénosine 5'-diphosphate (ADP) [14] ou les kinines [15]. Néanmoins, le principal stimulus de la production basale de NO semble être la contrainte de cisaillement exercée par le flux sanguin [16-18]. Hecker *et al.* ont observé une diminution du taux basal de NO lorsque des cellules endothéliales sont cultivées *ex vivo* sans contrainte mécanique [19].

Le monoxyde d'azote exerce de multiples effets au niveau vasculaire (Figure 3).

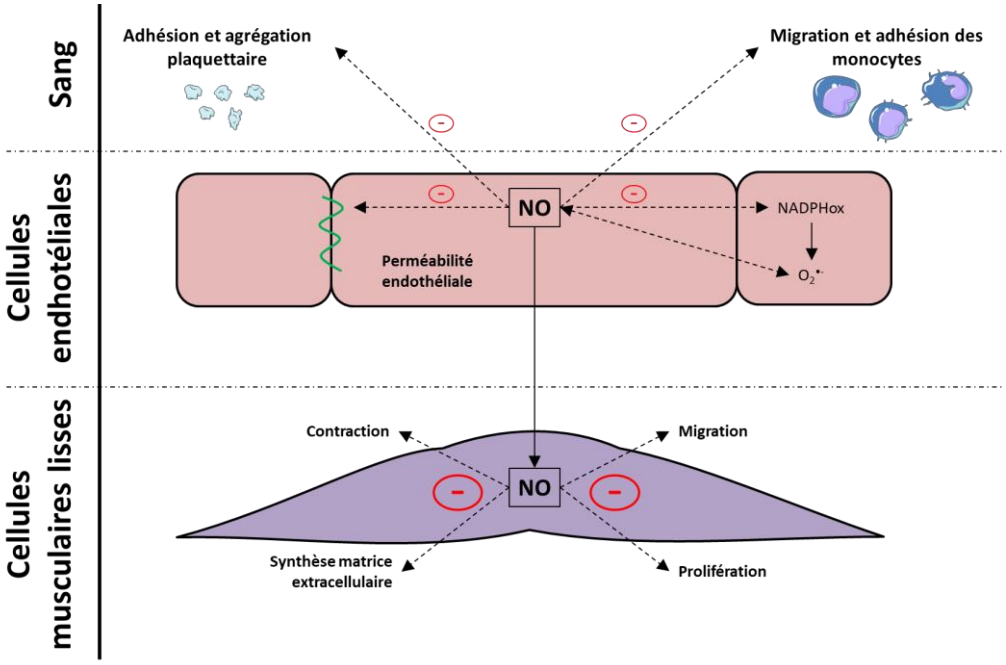

Figure 3 : Représentation des différents effets du monoxyde d'azote sur les éléments du sang et sur la paroi vasculaire (selon [20]). NADPHox : NADPH oxydase, $O_2^{\bullet-}$: anion superoxyde.

Comme évoqué précédemment, NO intervient dans le maintien du tonus basal en relaxant les cellules musculaires lisses vasculaires [21]. Il possède, de plus, des propriétés anti-athérogéniques : il agit par exemple sur les plaquettes, non seulement en inhibant l'adhésion, l'activation, la sécrétion du contenu des granules et l'agrégation des plaquettes, mais également en facilitant leur désagrégation [22]. NO prévient aussi le chimiotactisme des monocytes [23], inhibe l'adhésion des leucocytes à l'endothélium [24] ainsi que la migration [25] et la prolifération [26] des cellules musculaires lisses. Ceci limite la prolifération néointimale survenant après un traumatisme vasculaire. Combiné à son effet stimulant sur la migration et la prolifération des cellules endothéliales [27], ceci suggère un rôle de NO dans la réparation des vaisseaux. Par ailleurs, ce radical, à concentration physiologique (de l'ordre du nanomolaire), présente des propriétés anti-inflammatoires, notamment en diminuant la perméabilité vasculaire [28], en inhibant la dégranulation des neutrophiles [29] et des mastocytes [30], ou encore en inhibant la production de cytokines immuno-modulatrices (interleukines IL-12 et IL-1) par les macrophages [31].

Il existe 3 isoformes de NOS qui sont nommées en fonction de leur localisation ou de leur principale caractéristique : la NOS neuronale (nNOS), la NOS inductible (iNOS) et la NOS endothéliale (eNOS). La eNOS et la nNOS produisent de faibles quantités de NO (de l'ordre du nanomolaire) alors que la iNOS, elle, est généralement induite suite à une réaction allergique ou inflammatoire et produit de fortes quantités de NO (de l'ordre du micromolaire). La production massive de NO au niveau des macrophages permet la génération d'espèces réactives de l'oxygène et de l'azote (peroxynitrite) qui conduisent à la destruction de l'agent responsable de la réaction.

1.3.1. Implications physiopathologiques

Les iNOS sont activées et produisent du NO de façons massive et continue. Ceci entraine la formation d'un grand nombre d'espèces réactives (de l'oxygène ou de l'azote) qui permettent la destruction des agents pathogènes. Un déséquilibre de ce système (NOS constitutives *vs* inductible) entraine donc des situations pathologiques variées (Figure 4).

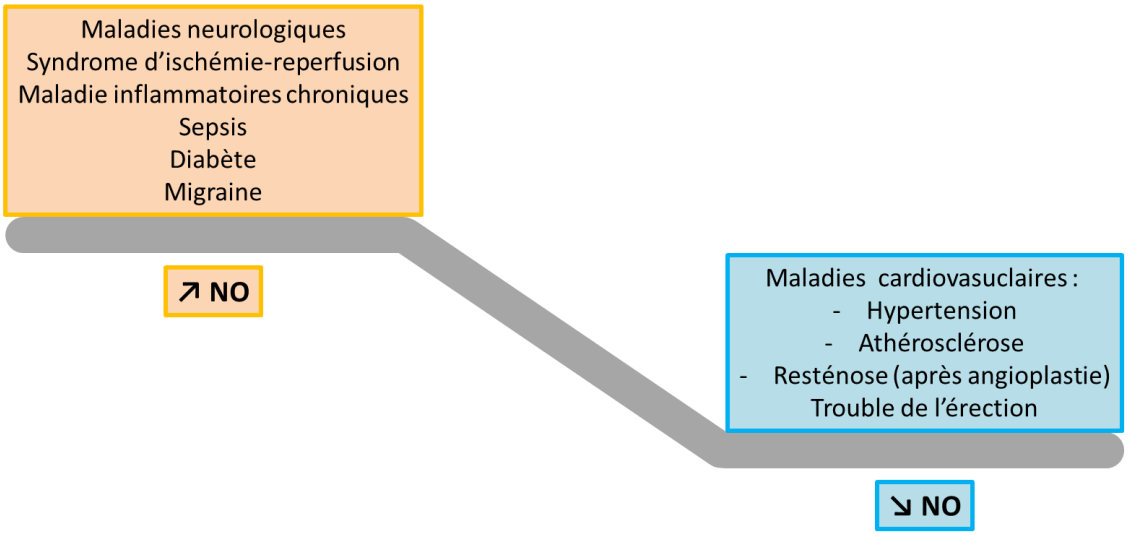

Figure 4 : Principales conséquences de la diminution ou de l'augmentation de la biodisponibilité de NO

1.3.1.1. NO et système nerveux central

Les NOS du cerveau sont principalement situées dans les neurones de la couche granuleuse du *cerebellum* et dans les bulbes olfactifs accessoires [32]. Il a été suggéré que NO pouvait intervenir également dans la plasticité synaptique et influencer certains phénomènes neurophysiologiques de mémorisation, comme la potentialisation ou la dépression à long terme [33].

Par ailleurs, NO est un médiateur de la destruction neuronale lors de l'ischémie-reperfusion. En effet, les modèles expérimentaux de neurotoxicité suggèrent une libération massive de glutamate après ischémie-reperfusion entraînant une stimulation intense des

récepteurs au *N*-méthyl-*D*-aspartate (NMDA), une augmentation du calcium intracellulaire et une libération prolongée de NO [34]. L'administration d'antagonistes des récepteurs NMDA ou d'inhibiteurs de NOS réduit la destruction neuronale observée dans ces modèles [35].

1.3.1.2. NO et système vasculaire

L'endothélium vasculaire est la couche cellulaire qui compose la paroi interne des vaisseaux. Il agit de façon indépendante pour permettre une vasorelaxation constante des vaisseaux et ainsi assurer le flux sanguin. Il empêche aussi l'adhésion des plaquettes et des leucocytes. L'homéostasie vasculaire est assurée par différents acteurs, comme le NO, la prostaglandine I2, le thromboxane A2 … chacun ayant une action vasorelaxante ou constrictrice.

Les effets vasculaires du NO sont la relaxation du muscle lisse, l'inhibition de l'adhésion et de l'agrégation des plaquettes [36, 37] et des leucocytes [24], l'inhibition de la génération d'endothéline (un facteur vasoconstricteur) [38] ainsi que l'inhibition de la prolifération des cellules musculaires lisses (CML) [39]. De plus, NO agit au niveau du rein et a une action sur l'homéostasie du volume sanguin intravasculaire et donc la pression sanguine [40].

Les défauts de régulation des effets vasculaires de NO peuvent donc contribuer au développement de diverses pathologies : hypertension artérielle, dysfonction endothéliale induite par l'hypercholestérolémie et l'hypertension artérielle pulmonaire chronique. Il faut aussi préciser que les produits de glycosylation avancés [41] et les lipoprotéines oxydées [42], qui réduisent également la biodisponibilité de NO, contribuent donc à une vasorelaxation défectueuse, retrouvée notamment chez les patients présentant un diabète ou de l'athérosclérose. Enfin, une production massive de NO en réponse à des stimuli

inflammatoires (stimulation des iNOS des cellules endothéliales et CML par les lipopolysaccharides ou certaines cytokines) entraine une hypotension massive lors d'un choc septique [43].

1.4. Les maladies occlusives artérielles

1.4.1. Définition

Les maladies occlusives artérielles se définissent comme un blocage partiel ou total d'une artère causé par une accumulation de lipides dans la paroi vasculaire (aux niveaux des artères coronaires, des membres supérieurs et inférieurs ainsi que celles du cerveau…). Le blocage d'une artère entraînera une diminution de la circulation du sang vers les organes et les muscles en périphérie, diminuant ainsi l'apport en nutriments et en oxygène.

Les principales conséquences sont la survenue d'infarctus ou bien d'AVC, mais il faut aussi mentionner les risques d'amputation (atteinte périphérique) ou d'infarctus mésentériques ou rénaux. Toutes ces pathologies sont d'urgence vitale en engagent dans 90 % des cas la survie du patient.

1.4.2. Survenue de l'ischémie

L'ischémie, aussi appelée sténose vasculaire, est un phénomène multifactoriel se développant sur le long terme. Comme expliqué précédemment, le développement des plaques d'athérosclérose, favorisé par des facteurs précédemment cités, entraine une diminution de la lumière vasculaire et donc une perturbation du flux sanguin (Figure 5).

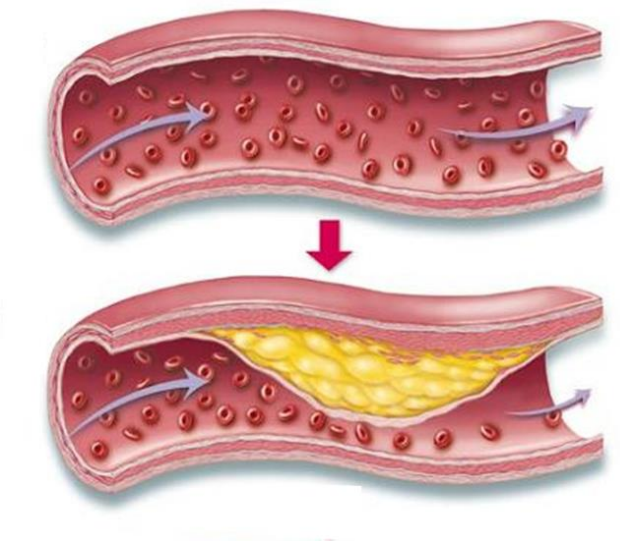

Figure 5 : Conséquence du développement d'une plaque d'athérome sur le flux sanguin

Le risque principal engendré par la présence d'une telle plaque est sa rupture. En effet, en se rompant, la plaque d'athérome entraine la formation de caillots qui peuvent bloquer les vaisseaux (artères de plus petits calibres). La plupart du temps, ce blocage intervient au niveau des artères coronaires (infarctus) ou de la circulation cérébrale (AVC). Ils peuvent aussi venir se loger dans les artères pulmonaires (embolie pulmonaire), au niveau rénal (infarctus rénal) ou digestif (infarctus mésentérique).

1.4.3. Traitements

Parmi les solutions proposées pour traiter les maladies artérielles occlusives, on trouve en prévention primaire une prise en charge préventive des facteurs de risque (règles hygiéno-diététiques), puis un traitement médicamenteux associés ou non à des traitements chirurgicaux dits invasifs ou mini-invasifs.

1.4.3.1. Prophylaxie et recommandations

Selon la Haute Autorité de Santé, il est recommandé en prévention primaire d'appliquer des modifications du mode de vie, quel que soit le risque cardio-vasculaire du patient [44]. Une prise en charge diététique individualisée, associée à la pratique d'une activité physique régulière, permet de renforcer l'efficacité d'un éventuel traitement médicamenteux. Les conseils sur l'hygiène de vie sont d'autant plus importants que le risque cardio-vasculaire est élevé. Il est bien évidement indispensable d'arrêter de fumer ainsi que de limiter la consommation d'alcool. Dans le cas où une chirurgie est nécessaire, des séances de kinésithérapie de réadaptation à l'effort sont prescrites pour encadrer le patient dans sa reprise d'une activité physique.

1.4.3.1. Traitements médicamenteux préventifs et complémentaires

Lorsque les règles hygiéno-diététiques ne sont plus suffisantes ou après une chirurgie, un traitement médicamenteux est mis en place. Il a pour but de réguler les principaux phénomènes responsables de l'apparition des maladies cardiovasculaires.

Parmi les spécialités médicales prescrites on retrouve l'aspirine ou les antiagrégants plaquettaires (clopidogrel, ticagrelor …). Inhiber l'agrégation des plaquettes permet de limiter la formation de caillots et donc le risque de développer un accident ischémique.

Le deuxième facteur cible des traitements sont les hyperlipidémies. Réduire le taux de lipides circulant revient à diminuer l'accroissement de plaques d'athérome. Les statines sont la classe thérapeutique la plus utilisée (simvastatine, atorvastatine …). Ce sont des inhibiteurs de l'hydroxyméthylglutaryl-CoA réductase, une enzyme clé dans la synthèse du cholestérol endogène.

Enfin, l'hypertension artérielle étant un facteur de risque majeur de l'apparition des maladies cardiovasculaires, la mise en place d'un traitement régulateur de la tension artérielle est nécessaire. Pour cela plusieurs classes thérapeutiques sont disponibles, mais les recommandations préconisent l'utilisation d'inhibiteurs de l'enzyme de conversion (IEC) de l'angiotensine (énalapril, captopril …). Les IEC sont préférés aux autres antihypertenseurs grâce à leur action néphroprotectrice.

Il est à noter que dans certains cas spécifiques (infarctus mésentériques) un traitement antibiotique (métronidazole + gentamicine) est mis en place pour éviter l'apparition d'une septicémie à la suite de l'opération. Il est aussi courant d'y associer une héparinothérapie à la place des traitements antiplaquettaires.

1.4.3.2. Chirurgie invasive

Lorsque plusieurs artères (notamment coronaires) sont touchées par des problèmes d'athérosclérose, il devient nécessaire d'effectuer un geste chirurgical appelé « pontage ».

Le principe est de dériver le sang provenant de l'aorte ou d'une de ses branches pour contourner la partie sténosée d'une artère coronaire (Figure 6). Pour créer cette dérivation, on utilise un pontage (ou greffon), qui peut être :

- Une artère ou une veine du patient (autogreffe), quasiment toujours utilisées.
- Un tube prothétique en dacron (fibres textiles de polyester), actuellement en cours d'études pré-cliniques.

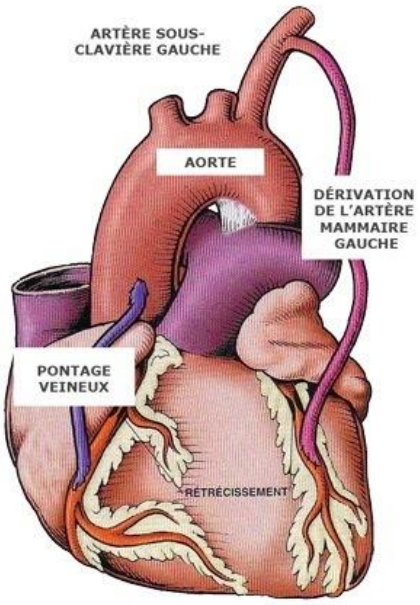

Figure 6 : Exemple de pontage coronarien.

Selon le nombre de sténoses, un ou plusieurs pontages peuvent être effectués, on parle alors de double, triple, quadruple voire même quintuple pontage.

Il existe deux types principaux de pontage :

- A l'aide des artères mammaires internes : moins de risques de thrombose mais opération plus compliquée et longueur limitée.
- A l'aide des veines saphènes : prélèvement facile (face interne de la jambe), mais non utilisable en cas de varices ou fibrose et taux de thromboses plus important.

1.4.3.3. Chirurgie mini-invasive

Si la sténose est trop importante pour être traitée seulement par des médicaments et qu'elle ne touche qu'une ou deux artères simultanément, le traitement par angioplastie percutanée est mis en place.

Ce traitement est réalisé par les cardiologues ou les chirurgiens vasculaires, sous anesthésie locale et consiste à dilater la partie sténosée de l'artère coronaire. On introduit au niveau d'une artère du bras (radiale) un cathéter sur le bout duquel est placé un ballonnet. Ce dernier est remonté jusqu'au rétrécissement de la coronaire grâce à un contrôle radiologique (coronarographie), puis dilaté. Ceci va écraser la plaque d'athérome et reformer le vaisseau. Le cathéter avec le ballonnet est ensuite retiré. L'angioplastie est actuellement très souvent associée à la mise en place d'une endoprothèse ou stent. C'est une sorte de petit ressort entourant le ballonnet et restant en place à l'intérieur du vaisseau quand on dilate le ballonnet. Cette technique (Figure 7) améliore le résultat initial et diminue le risque de resténose (reformation de la sténose).

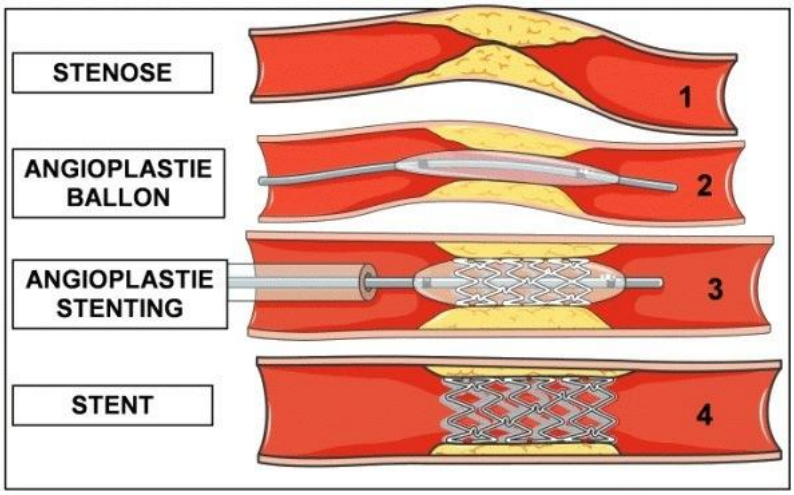

Figure 7 : Etape d'une angioplastie avec pose de stent.

Les stents nus

Les premiers modèles implantés chez l'Homme étaient initialement constitués d'acier ou de Nitinol®, un alliage nickel/titane, le titane pur présentant une trop faible résistance

mécanique. Le Nitinol® se comporte à la fois comme un matériau à mémoire de forme et un alliage super-élastique. Cette dernière caractéristique lui permet d'avoir une excellente résistance à la fatigue ainsi qu'une grand déformabilité, ce qui en fait le matériau de choix pour la fabrication de stents auto-expansibles [45]. Cependant, il est relativement peu efficace sur des lésions très calcifiées (donc très rigides).

L'acier 316LM, lui, comprend des taux de Chrome, Nickel et Molybdène plus élevé qu'un acier normal. Ce métal possède des qualités remarquables en termes de résistance mécanique et de biocompatibilité. Cependant, ses propriétés ferromagnétiques le rendent incompatible avec l'imagerie par résonnance magnétique (IRM). De plus, sa capacité élastique étant limitée, l'acier 316LM n'est plus le matériau de choix pour la fabrication de stents.

Enfin, on trouve actuellement des stents en alliages Cobalt/Chrome. Ces alliages sont largement utilisés dans le domaine biomédical. Concernant les performances mécaniques et élastiques, ils sont supérieurs aux aciers. Ces stents ont une densité supérieure à l'acier, ce qui les rend radio-opaques. De plus, étant amagnétiques, ils n'interfèrent pas avec les acquisitions en IRM.

Depuis quelques années, l'amélioration des techniques de fabrication des stents (rugosité diminuée, découpe laser plus précise …) ont permis d'améliorer la biocompatibilité de ces derniers sans distinction de l'alliage utilisé.

Les stents actifs

Aussi qualifiés de « stent à élution de médicaments », les premiers stents actifs étaient recouverts d'un polymère libérant de l'héparine [46].

Aujourd'hui, on implante ces stents actifs dans 70 % des cas [47]. Ils sont dans la grande majorité des cas recouverts d'une matrice polymérique biodégradable (acide poly(lactique) [48], acide poly(vynilique) [49], phosphorylcholine [50]…) ou non (polyvinyle pyrolidone [51], polyéthylène téréphtalate (PET) [52]…) capable de libérer des principes actifs. Récemment, le stent ADSORB (AbbottVascular, Santa Clara, CA, USA) a vu le jour. Il est constitué d'un support non métallique en polymère résorbable (acides poly(L-lactique) et poly(D,L-lactique)) permettant l'élution dans le temps de médicaments et aboutit à sa dégradation [53]. Cependant, le corps médical reste encore divisé sur la nécessité ou non d'avoir un support rigide à long terme pour favoriser la cicatrisation du vaisseau.

Parmi les principes actifs libérés, la majorité sont des drogues anti-tumorales agissant à différents niveaux du cycle cellulaire. On peut citer : le paclitaxel, le sirolimus, tacrolimus (et autres macrolides du genre « -limus ») ou la cytochalasine D.

Malgré ces évolutions, le coût des stents à libération de molécules thérapeutiques semble élevé par rapport aux services rendus au patient [54]. L'incidence des thromboses tardives, ou resténoses, induites par les dispositifs actuels, à l'origine d'une morbi-mortalité importante, rentre également dans le débat sur la légitimité de leur utilisation. La fréquence d'apparition de resténose est supérieure à celle constatée pour les stents nus. On estime entre 0,6 et 1,8 % son incidence et tous les stents actifs ne semblent pas égaux face à cette complication [55-58].

1.5. NO et resténose

La resténose est définie comme la perte d'au moins 50 % du diamètre de la lumière artérielle par rapport au diamètre artériel post-pose du stent [59]. Contrairement à la thrombose qui est un phénomène de survenue brutale, la resténose est un phénomène

d'apparition plus progressive. Elle débute dès l'agression mécanique de la paroi artérielle et se prolonge pendant plusieurs semaines [60]. Le diagnostic est posé suite à une exploration par angiographie. Il s'agit d'un phénomène multifactoriel (Figure 8) dont les principales étapes sont décrites ci-dessous par ordre chronologique [61, 62] :

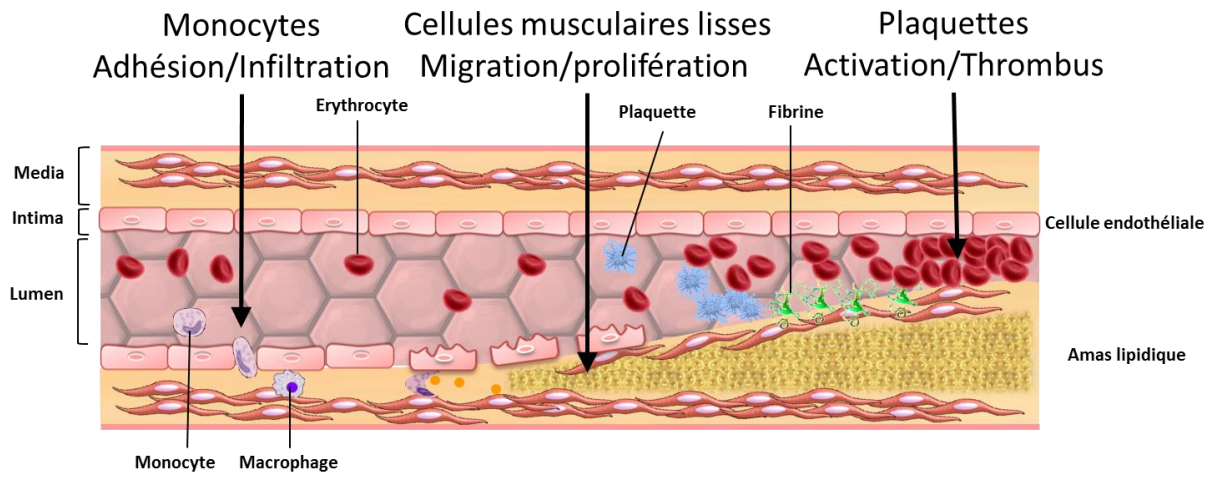

Figure 8 : Schématisation des différentes étapes conduisant à la resténose.

- A court terme :
    - Dommages au niveau de l'endothélium : inévitablement lié à l'acte chirurgical et garant de sa bonne qualité. Mais celui-ci entraine une détérioration des trois couches du vaisseau (intima, media et adventice).
    - Formation d'un thrombus :
        - En raison des dommages occasionnés sur l'endothélium, des protéines plasmatiques (dont le facteur von Willebrand et le fibrinogène) adhèrent sur la media. De plus, le sous-endothélium est directement mis en contact avec le sang exposant différentes protéines (dont la fibronectine et la laminine) provoquant activation, adhésion et agrégation plaquettaire.

- En parallèle l'endothélium endommagé, les plaquettes et le stent recrutent et activent les polynucléaires neutrophiles, monocytes et macrophages.
- Le thrombus apparait rapidement après la pose d'un stent et il va agir comme une matrice qui sécrète des facteurs visant à recruter les CML issues de la media, entrainant ainsi la formation d'une hyperplasie néointimale.

- A moyen et long termes
  - Activation des CML en réponse aux facteurs de croissance et cytokines produits par les plaquettes, les cellules endothéliales, les monocytes/macrophages ainsi que par les polynucléaires neutrophiles.
  - Formation néo-intimale : en parallèle d'une migration et d'une prolifération incontrôlée, les CML recrutées vont, à leur tour, synthétiser une matrice et du collagène.
  - Remodelage : la formation néo-intimale croît pendant les trois premiers mois suivants la pose du stent puis elle se stabilise et une réduction de cette structure est observée après 6 mois.
  - Résolution de l'inflammation : elle est retrouvée à toutes les étapes du processus en raison du traumatisme causé et de la présence d'un corps étranger. Il en résulte la mise en place d'une fibrose cicatricielle au niveau de la media et de l'adventice.

Dans cette pathologie, l'utilisation de principes actifs en administration systémique a conduit à des échecs en raison de l'insuffisance de ciblage de la zone lésée et l'induction d'effets secondaires [63]. Comme mentionné précédemment, les premières endoprothèses vasculaires développées étaient constituées d'alliages à base de titane ou d'acier inoxydable.

Des stents capables de libérer des principes actifs ont été développés dans le but de limiter la prolifération des CML. Cependant, ils sont sans effet, à long terme, sur la diminution du nombre de décès ou des infarctus du myocarde d'après la Haute Autorité de Santé [47]. En effet, ils sont associés à un risque augmenté de thrombose tardive notamment lorsque le traitement antiagrégant plaquettaire est arrêté. Cette complication serait en relation avec une cicatrisation incomplète ou retardée de la paroi artérielle et également avec une réaction d'hypersensibilité induite par le(s) polymère(s) (copolymères d'acide lactique et glycolique, poly-ε-caprolactone et polyéthylène glycol) [64]. Partant de ce constat, un cahier des charges du principe actif le plus adapté a été établi et ses propriétés sont les suivantes [61] :

- Lipophilie de la molécule avec une bonne rétention tissulaire.
- Elution « douce » mais prolongée à partir du stent.
- Propriétés spécifiques de ce principe actif évitant les risques de thrombose et de resténose :
    - Effet antiprolifératif vis-à-vis des CML (sans induction de la mort cellulaire).
    - Effet de recrutement des cellules endothéliales afin de reformer l'endothélium.
    - Effet anti-inflammatoire.
    - Effet antiagrégant plaquettaire.

Ainsi le NO, possède des propriétés similaires, qui, à la concentration de l'ordre du nanomolaire, concordent avec le cahier des charges défini. Des donneurs de NO, les RSNO, dont certains naturellement présents dans l'organisme, ont déjà été utilisés sur des stents [3, 65, 66]. Dans ces études, l'incorporation du RSNO a été réalisée dans un système monolithique : la matrice de polymère contenant le principe actif étant solidifiée autour du dispositif. Un maximum de 28 j de libération a été obtenu [65]. Des propriétés anti-thrombogéniques ainsi que de non adhésion/non activation plaquettaires ont aussi été mises en évidence [3, 65, 66].

Ceci prouve l'intérêt des RSNO dans cette indication même si la période couverte par la libération de NO reste toutefois insuffisante pour favoriser la ré-endothélialisation de la zone lésée (> 6 semaines) et limiter le risque de resténose [3, 67]. Cela signifie qu'il faut une formulation adaptée à un réservoir de RSNO capable d'être libéré sur de plus longues périodes.

Pour réussir ce défi, deux points cruciaux ont été mis en évidence :

1) L'obtention d'un profil de libération adapté à la pathologie : contrôlé en termes de concentrations (*i.e.* nanomolaire) et de durée d'au moins 6 semaines. Pour cela, des films multicouches de polyélectrolytes dit « *layer-by-layer* » (LbL) seront développés.
2) La nécessité d'avoir un réservoir de donneurs de NO suffisant pour couvrir les besoins de la libération : ceci sera achevé par une nanostructuration des films *via* l'utilisation de nanoparticules d'or pouvant être fonctionnalisées facilement par des principes actifs avec un rendement de greffage important comme l'ont prouvé des travaux précédents dans l'équipe [4]. Les différents donneurs de NO seront comparés dans le chapitre 2.

2. Nanostructuration de surface

2.1. Dispositifs médicaux et législation

Les DM sont définis par la Directive Européenne ; directive 93/42/CEE [68] comme étant « tout instrument, appareil, équipement, logiciel, matière ou autre article, utilisé seul ou en association, y compris le logiciel destiné par le fabriquant à être utilisé spécifiquement à des fins diagnostique et /ou thérapeutique, et nécessaire au bon fonctionnement de celui-ci. Le dispositif médical est destiné par le fabriquant à être utilisé chez l'Homme à des fins de :

- Diagnostic, prévention contrôle, traitement ou atténuation d'une maladie,
- Diagnostic, contrôle, traitement d'atténuation ou de compensation d'une blessure ou d'un handicap,
- D'étude ou de remplacement ou modification de l'anatomie ou d'un processus physiologique,
- Maîtrise de la conception,
- Et dont l'action principale voulue dans ou sur le corps humain n'est pas obtenue par des moyens pharmacologiques ou immunologiques ni par métabolisme, mais dont la fonction peut être assistée par de tels moyens. » [68, 69].

Ils sont classés en quatre catégories selon leur niveau de risque potentiel pour la santé :

- Classe I (risque le plus faible) : lunettes, véhicules pour personnes handicapées…
- Classe IIa (risque potentiel modéré) : lentilles de contact, appareils d'échographie…
- Classe IIb (risque potentiel élevé) : préservatifs, produits désinfectants…
- Classe III (risque élevé) : prothèses mammaires, endoprothèses vasculaires ou stents, prothèses de hanche…

2.2. Fonctionnalisation de surface

La fonctionnalisation de surface est un domaine promettant un large champ d'applications. Les matériaux dont la surface a été modifiée sont utilisés dans beaucoup de domaines : électronique, énergie, industrie textile,… En ce qui concerne le domaine biomédical, ils sont utilisés comme biocapteurs, réservoirs de principes actifs ainsi que sur des dispositifs médicaux [70], implantables ou non. Il existe différents moyens pour introduire des modifications en surface. Par exemple, la fabrication de films multicouches,

décrite par Decher [71], consiste en un dépôt alternatif de polyélectrolytes de charges opposées à la surface d'un matériau. Cette adsorption successive de polycations/polyanions sur un matériau entraine l'apparition d'une nouvelle surface, possédant une charge (théoriquement correspondante au dernier polyélectrolyte déposé) due à une surcompensation des charges de surface. (Figure 9). Ce changement confère de nouvelles propriétés à la surface traitée [70]. Les matériaux les plus utilisés pour la construction des films multicouches sont principalement des polymères synthétiques cationiques ou anioniques.

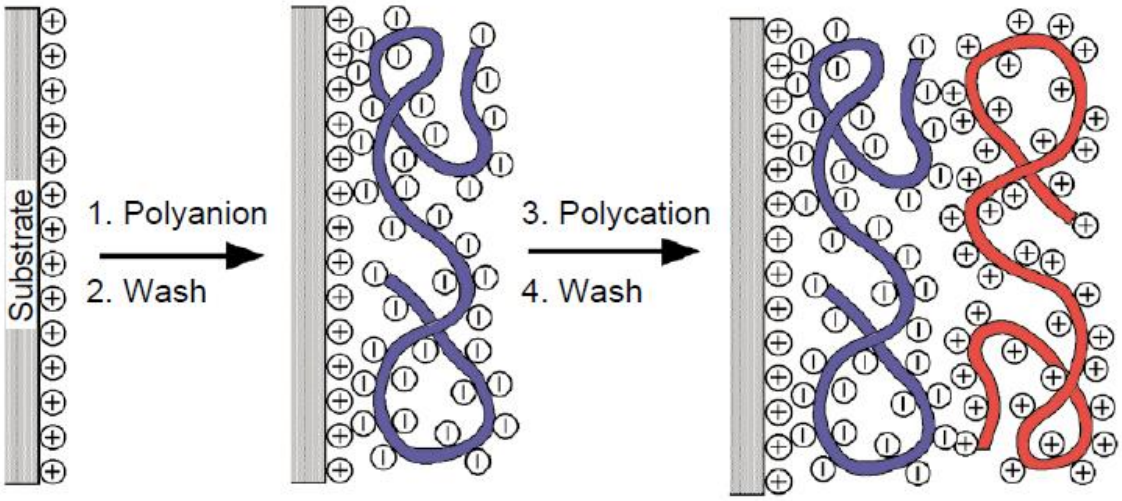

Figure 9 : Schématisation de la méthode de fabrication d'un film multicouche (selon [71]).

Un des avantages des films LbL est le large choix de matériaux sur lesquels peuvent être déposés ces films (verre, céramique, polymères, métaux, …). Un deuxième avantage repose sur la possibilité de piéger au sein des couches de polymères des principes actifs (PA) [72] qui pourront être libérés de manière contrôlée et prolongée dans le temps soit par diffusion du principe actif hors de la matrice soit par destruction du film (Figure 10). Ainsi, une libération contrôlée sur cinq semaines a été obtenue à partir de films multicouches piégeant des molécules modèles (kétoprofène et cytochalasine D) [73]. Cependant, la couche la plus externe composée de polymères cationiques peut présenter un inconvénient non

négligeable car peu biocompatible en raison d'une éventuelle interaction électrostatique entre les charges positives du polymère et les membranes cellulaires majoritairement négatives [74].

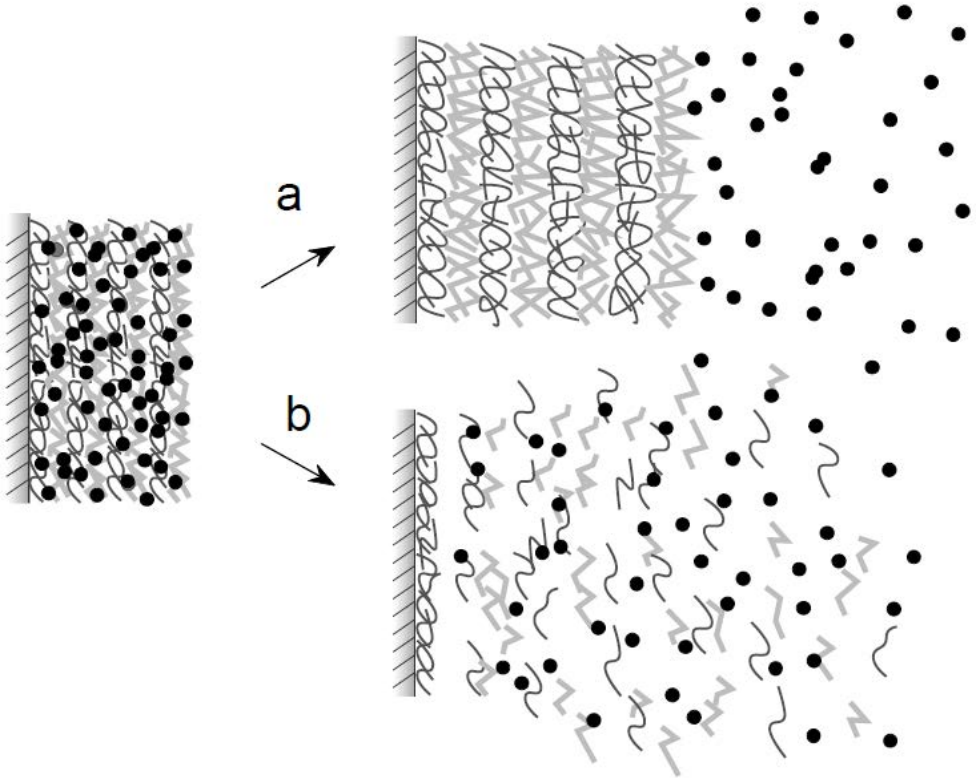

Figure 10 : Schéma de la libération d'un principe actif piégé dans un film multicouche. (selon [72]). Les points noirs représentent ici des molécules de PA libérées

L'article suivant propose une revue de la littérature concernant les DM intégrant des nanotechnologies. Le but est de mettre en évidence l'intérêt croissant de ces dernières pour le développement de nouvelles solutions. Nous nous sommes uniquement focalisés sur les nanotechnologies immobilisées (surfaces nanostructurées, nanoparticules immobilisées, surfaces nanoporeuses …) et n'avons pas pris en considération l'utilisation des nanoparticules colloïdales comme principe actif car elles font déjà l'objet de nombreuses revues dans la littérature [75-80].

2.3. Article 1 : Are nanotechnologies the future of medical devices

Are nanotechnologies the future for medical devices?

Arnaud PALLOTTA[1], Igor CLAROT[1], Jonathan SOBOCINSKI[2], Ariane BOUDIER[1]

[1]Université de Lorraine, CITHEFOR EA 3452, Nancy, France

[2]Université de Lille, CHU Lille, Lille, France

Phone +33 372 747 349

ariane.boudier@univ-lorraine.fr

Abstract

Numerous medical devices (implantable or not) are including nanomaterials either by nano-objects decorating their surface or by a surface nanostructuration. This paper gives an overview of the products currently on the market in various health domains (wound healing, infectious diseases (prevention or treatment), cardio-vascular diseases, organ or joint replacement, or as a mean to administer drugs). Then, the main parameters for physicochemical characterization are described. Keys to understand their possible interaction with the organism (positive or negative *via* toxicity) are given. As a conclusion, a discussion emphasizes on their quality control as well as on the regulatory issues especially because of a lack of specificity towards nanomaterial combining medical devices.

Key-words: surface nanostructuration; nano-objects; nanoparticles; pharmacokinetics; implants; quality control; regulatory issues.

Table of content

1. Introduction

Pharmaceutical companies register two main kinds of products: medicines and medical devices (MD). Today, there are an estimated 2 million different kinds of medical devices on the world market, categorized into more than 22 000 generic devices groups [1] (see Box 1 for the definition and classification of MD). They are classified in a wide range of references from the simplest (bandage, wheelchair…) to the more hyphenated that can be sterile and/or implantable such as needles, surgery cements, bone implants….

Up to now, new technologies are devoted to MD in order for example to get more personalized, less invasive, miniaturized devices sometimes with a pharmacological effect through drug elution [2-4]. Some of them have already reached the market. Nanotechnologies (definitions of the International Standard of Harmonization are given in Box 2) are nowadays more and more included into the development of MD. Under the prefix "nano-", in 2014 around 230 products were registered: 165 medicines and 65 MD [5]. As illustrated in Figure 1A, there is a growing interest in the field for both the scientific academic community and the industrial companies. Nanomaterial combining products are applied to MD as well as implantable MD (IMD) (Figure 1B). Surface of medical devices are including nanoparticles or nanocrystals with or without a matrix, or the surface it-self is nanostructured (Figure 1B). A quick look of the marketed devices (Table 1) indicates that inorganic particles or materials are the most studied. They are mainly based on silver, zirconium, steel, magnesium, silicium, titanium, hydroxyapatite and its derivatives, iron and iridium. These innovative designs are developed to achieve for example:

- Lighter materials but also reinforced from a mechanical point-of-view (by the inclusion of carbon nanotubes [6])

- Materials able to mimic biological systems so as to increase the biocompatibility [7-10]
- Materials being bio-resorbable [11, 12]
- Materials able to have an intrinsic pharmacological activity (inclusion of silver nanoparticles [13]) or to release an active drug [14].

Some of nanostructured MD or nanoparticle included MD are applied for patient care. The use of such devices, parallel to the actual debate on nanoparticle toxicity especially the inorganic ones [15], raises questions about the benefit/risk balance.

This review deals with MD (implantable or not) including nanoparticles or that are nanostructured and will emphasize on the advantages and drawbacks of these nanomaterials. A report [16] was published few years ago but since then no up to date was performed on the subject which is the purpose of the present article. Indeed, this review will not focus on colloidal nanoparticles used as drugs or drug candidates (in cancer for example) which was already extensively reviewed in the literature [17-22]. In the same way, even if the inclusion of nanoparticles into the development of diagnostic devices was crucial (gene bio-array or lab-on-a-chip characterized by a nearly molecular precision [23], nanostructured surfaces or miniaturized valves [24] or nanosensors [25]), this is not the topic of the present paper. Herein, after an overview of the devices already on the market or under clinical trials, the physicochemical characterization of the materials will be described. Then, the biocompatibility in relationship to the surface phenomena that are closely linked to the nanoscale will be detailed. The possible toxicity induced by the nanoparticles entrapped into a nanostructured material or a nanomaterial will be described. As a conclusion, the article will give outlooks on the requirement of a pharmaceutical quality control and on regulatory

issues. Thus, the existing obstacles to ease new nanostructured MD or nanoparticles included into MD to reach bedside will be deeply discussed.

2. Nanostructured devices and their evolution

2.1. Marketed nanostructured devices

Nanotechnologies either as nanoparticles entrapped into a MD or as a nanostructured material are used in a wide range of clinical applications (Tables 1 and 2, and Figure 1B). Included into non-implantable or implantable MD, they are applied into wound healing, infectious diseases (prevention and treatment), cardio-vascular diseases, organ or joint replacement, or as a drug administration tool.

2.1.1. Non implantable medical devices

Nanostructuration is already used into needles, bandages, catheters, scalpels and diagnostic devices (Table 1 and Figure 1B). Since the Antiquity, silver, as a nitrate salt or under its colloidal form, is used in bandages for its antimicrobial properties thanks to its broad spectrum activity. If mechanisms of action remain unclear, hypotheses rely on a synergistic action of both nanoparticles (through catalytic and Fenton-like reactions) and silver ions. They result from nano-objects dissolution/corrosion due to a contact between extracellular water and patient exudates [26-28]. The colloidal form allows a prolonged and enhanced effect compared to the salt [29, 30]. This strategy is used both in surgical masks to prevent infections and in catheters coating to prevent nosocomial infections [31]. Further work on catheters tries to include a polymeric matrix made of clay or ceramic nanoparticles or even carbon nanotubes in order to reinforce the conventional material and to improve its mechanical and physical properties [32].

Scalpels are also nanostructured by a diamond nanometric coating allowing a more precise and tinier incision and a less invasive surgery thanks to a low friction coefficient [33]. The developed coating also decreases tissue adhesion on the scalpel surface and ease its penetration.

2.1.2. Implantable medical devices

Among implantable MD, synthetic grafts, stents, implants for various organs as well as artificial organs that contain NP are currently developed (Table 1 and Figure 1B).

Synthetic grafts are mainly applied to vessel replacement in order to develop *in silico* organs. In this way, nanofibers are created for example by electrospinning [34, 35]. These nanofibers are tunable in terms of form (by the support and template), density and fiber size (as a function of the polymer used). Their major parameters are able to create extracellular matrices very similar to the biological environment.

Coronary failure due to vessel stenosis is treated by angioplasty usually followed by stent implantation. These medical devices are generally composed by a metallic (stainless steel, titanium, chromium/cobalt or nickel/titanium alloys) or a polymeric (polylactic acid) structure. Some of them can release drugs such as immunosuppressive or antiproliferative agents. However, intra-stent restenosis which is a common side effect can occur, implying a new surgery. As a result, nanometric coatings made of nanoporous ceramic or polymers were applied to stent surface. For example, Polyzene-F® (a polyphosphazene derivative) as a stent coating proved a satisfying hemocompatibility, a fast and complete vessel healing thanks to an antiplatelet effect at the site of implantation [36, 37]. However, after clinical evaluation, the benefit/risk balance of such coating was not sufficient face to similar devices (drug eluting stent).

Apart from the vascular domain, a wide range of implants are on the market to be applied to bones, joints, teeth, and eyes. These implants are placed for a long time (10 to 15 years [9]) and the chosen metallic alloys are characterized by good mechanical properties and a good resistance *versus* corrosion. Implant surface nanostructuration as well as the nano-object nature (*e.g.* hydroxyapatite or calcium phosphate for bone) enhance cell adhesion and differentiation improving the long-term biocompatibility [38].

Nanoparticles offer innovation into artificial organ: heart, kidney, and retina. The first totally artificial heart (Carmat Company) was implanted in 2013. Up to now, six patients benefited from this innovative heart. In this technology, the internal surfaces which are in contact with the bloodstream are coated by synthetic or biological hydrophobic biomaterials (near valves in order to avoid any coagulation and blood cell adhesion) or nanoporous surfaces (at the interface of veins and arteries) in addition to other miniaturized captors for the heart adaptation to physical activity. Artificial kidneys were also developed. They are composed of thousands of nanoporous structures able to selectively adsorb toxins [39]. The principle relies on a combination between an ultrafiltration membrane and a bioreactor made of human kidney tubule cells to reproduce the metabolic, endocrine and immunological functions of the organ. Cells are cultivated on a nanoporous silicon film [40, 41] in order to mimic renal activity avoiding protein deposition and limiting a loss of blood proteins. Three artificial retinas using nano-electrodes able to transmit information recorded by a camera to the optical nerve are currently marketed or under evaluation. These implants (3 × 3 mm) are composed by up to 1500 miniaturized electrodes.

2.2. *Nanostructured medical devices at early stages*

Although a lot of marketed MD are including nanoparticles or are nanostructured, an intensive research focuses on this axis. Thus, some projects study implantable active MD at

the nanometric size: *e.g.* ultra-sensitive captor [42], molecular computers [43]. The components are described as biocompatible and bioresorbable [44]. According to the studies, these nanorobots could in a future be able to specifically diagnose one cell for a disease and kill it, preserving the healthy ones. Translating to the nanoscopic scale can widen the range towards new surgery perspectives by the development of nano-electromechanic systems assisted by a computer. These technologies could supply biological data while performing less invasive surgeries such as "nano-manipulation" controlled by the surgeon [45].

3. Nanomaterials physicochemical characterization

Physicochemical characterization of nanomaterials is essential to define the material and to predict the behavior in an organism. The unique knowledge of the nanoparticle size or chemical composition is needed but not sufficient. Nowadays, a thorough overview of the literature highlights the measurement of 8 fundamental physicochemical parameters which are considered as relevant for the biological evaluation. These parameters are the size and the size distribution, the form, the possible aggregation and agglomeration, the specific surface, the composition, the surface charge and the surface chemistry. Physical parameters (size and size distribution, form, aggregation/agglomeration linked to a thermodynamical instability and specific surface) are usually measured by microscopic (transmission/scanning electron microscopies, atomic force microscopy) and/or spectroscopic (light scattering) techniques and physisorption (Brunauer, Emmett and Teller (BET) method). These characteristics greatly impact the potential stability and reactivity of the surface. Chemical parameters (composition, surface charge and surface chemistry) are explored by various complementary techniques (*e.g.* spectroscopies (Xray diffraction, NMR, infrared…[46]), thermal analysis, spectrometries (Mass, elemental analysis…[46, 47] and electrophoresis [47, 48]). The

chemical composition should quantify active substances (if relevant) as well as impurities (see dedicated paragraph) which are called related substances when referred to pharmaceutical products. While the levels are well-defined for a drug by Pharmacopoeias, it is not the case for nanomaterials at the moment as no monographs exist. However it seems to be of main importance when nanomaterials are combined to MD since the impurities can come from degradation products, synthesis intermediates, solvents, catalyzers… Surface chemistry and surface charge are key points since they govern the direct interactions between a nanomaterial and its biological environment through catalytic properties, molecule adsorption/desorption [49, 50] or diffusion [51].

4. Nanostructured devices and their interaction with the organism

It is obvious that nanostructured devices develop an important contact surface interacting with the organism. This can lead to increased surface effects with either beneficial events or toxicological issues.

4.1. Biocompatibility tests

Biocompatibility is defined by ISO 10-993 as the ability of a material to perform an appropriate host response in a specific situation [52]. Biocompatibility is therefore different from inertness since it suggests a beneficial interaction, as examples: the depot of a hydroxyapatite film on the implant surface improves its affinity towards osteoblasts [53] and the implant microstructuration of titanium surface modifies its interaction with blood proteins and favors cell adhesion [54]. The tests employed to demonstrate it are described in a general manner into this standard. As a function of medical device classification (I, IIa, IIb and III, Box I), the tests are different. They are organized into:

- Primary tests: *in vitro* assays of cytotoxicity, genotoxicity, and hemolysis and *in vivo* assays of cancerogenicity, reproduction, and systemic toxicity;
- Secondary tests: mucosal or cutaneous irritation test, sensitization, and implantation;
- Test on animals according to the future use of the medical device;
- Clinical trials.

4.2. Importance of surface effects

Biocompatibility depends not only on the material nature but also on its interaction with the organism *i.e.* at the material/tissue interface: its superficial composition and organization are key factors influencing it. Due to their specific properties (chemical, physical, magnetic, electric, optic, mechanic…), nanotechnology can improve or at least modify the MD properties. However, the main cause of interaction with the organism is based on the increase of surface over volume ratio. As an example, if one considers a microcrystal of iron (1 µm of diameter) less than 1% of its atoms are localized at the surface; on the contrary, 90% of the atoms are present at the surface of a nanocrystal (1 nm of diameter) [55]. As a consequence, the specific surface (external surface over mass ratio) which is the exchange surface is a lot more important at the nano-scale compared to the micro- one.

4.3. Consideration on beneficial aspects and possible toxicity

4.3.1. Interaction with proteins

4.3.1.1. Kinetic considerations

When a nanomaterial is exposed into a biological environment, it is covered very rapidly by a protein layer in a dynamic equilibrium creating a corona. The affinity of a protein towards a material surface highly depends on its state, bulk or nanometric, in relationship to its structuration, specific surface, surface reactivity… Moreover, the "material/protein" complex evolves as a function of the time. The phenomenon, called the Vroman's effect [56], explains a biphasic kinetic: firstly the proteins present at a high concentration adsorb and are progressively replaced by other proteins characterized both by a higher affinity and a lower concentration (Figure 2). Thus, albumin (40 g/L) is usually the first interacting element before other such as fibrinogen (2-3 g/L), complement protein (C3 (1.6g/L [57]), C4, and C5), immunoglobulins (IgA 2.5 g/L, IgG 11.0 g/L, IgM 1.3 g/L [58]). Protein adsorption tends to increase with a positive surface charge (this is explained by the isoelectric point value of blood proteins which confers to them a global negative charge at the physiological pH) and with a hydrophobic surface [59]. Even though surface properties of a material are of main importance in this phenomenon, its composition may influence protein adsorption. Indeed, when core/corona nanoparticles are included into a material, a re-organization may be described and the core components may migrate at the surface, implying a modification of the reactivity [60]. On the contrary, protein adsorption can be limited by a direct grafting of polymers such as *N,N*-dimethylacrylamide (PDMA) [61], polyethylene oxide (PEO) nanobrushes or even using poly(lactic-*co*-glycolic) acid (PLGA) grafted by PEO [62].

4.3.1.2. Consequences of this phenomenon

Protein adsorption at the surface of nanomaterials implies either negative or beneficial consequences. As example, as a function of the polymeric brush grafting density on a nanomaterial, a modulation of hemostasis is observed. Thus, a poor PDMA density of

grafting implies an initiation of the coagulation whereas a high density of grafting inhibits platelet aggregation [61, 63]. Moreover, nanostructured materials using poly(alkylcyanoacrylate) (PACA) nanoparticles can induce a different immunologic response as a function of the geometry (brush or loop) of the polymers grafted onto the nanoparticles [64]. For nanostructured materials, the quantity and the nature of adsorbed proteins are essential to modulate adhesion, migration, and cell differentiation. Yang *et al*., showed that a titanium nanostructured surface adsorbed in a more specific pathway fibronectin compared to albumin [65]. As a consequence, osteoblasts adhesion and in parallel osteointegration is easier, helping tissue reparation.

4.3.2. Pharmacokinetic aspects of potential degradation products

The pharmacokinetic aspects described in this part concerns the degradation products coming from the nanomaterial combining MD (Figure 3). The pharmacokinetic profile of colloidal nanoparticles (administered *per se*) will not be described and can be found in other papers [66, 67]. Degradation products from these materials can be:

- Colloidal nanoparticles included or not into the matrix which entrapped them;
- Aggregated or agglomerated nanoparticles included or not into the matrix;
- Nanoparticle fragments;
- Metallic ions coming from the nanoparticle dissolution [26, 28] or from the metallic device surface corrosion [68]

Based on this, all the pharmacokinetic steps will be further detailed.

Absorption

With the use of nanomaterial combining MD, degradations products can be absorbed by various pathways whose cutaneous route, and oral/respiratory routes.

Topical medical devices such as silver nanoparticles entrapped into bandages imply an important exposure to these particles or degradation product originating from them. Healthy skin represents an efficient physical barrier against environment attacks and its physiological organization prevents the absorption of chemical products which is also the case for silver nanoparticles [69]. However, in the case of a damaged skin, a nanoparticle penetration from bandage was possible and quite important: high serum silver concentrations were quantified in patients suffering from severe burns. Concentrations returned close to 0 only 3 months after treatment end [69].

Nanostructured dental products (such as some prostheses) and nanostructured MD applied to the upper aero-digestive pathways can provide degradation products that penetrate the body through the digestive tract. As an example, one study proved that nanoparticle fragments derivate from dental prosthesis were absorbed by the intestine and led to side effects: fever, liver and spleen inflammation, acute renal failure… All these symptoms were observed one year after dental prosthesis implantation. At the implant withdrawal, all the symptomatology disappeared [70].

Distribution and metabolism

After being in the blood stream, degradation products can be opsonized by opsonins (components of the complement system such as C3, C4, and C5) and other proteins (laminin, fibronectin, C-reactive protein, type I collagen and many others) in order to be easily recognized by the reticuloendothelial system and phagocyte by monocytes and macrophages

such as what can be observed with colloidal nanoparticles [66]. They are then orientated to the spleen, liver and kidneys where they can undergo metabolism and/or accumulate [71]. They are potentially detectable in the long term in the heart, the lungs, the bone marrow and a migration into the central nervous system can also be envisaged.

Excretion

Degradation product elimination is not well-described. It mainly depends on the exposure pathway and on the physicochemical of the considered fragment. The ones present in the digestive tract may be eliminated by feces. The ones that are inhaled may be absorbed into the blood stream or eliminated by the muco-ciliary system. When they are present into the blood, degradation products can either be filtered by the kidney to be excreted into the urine or be excreted by the biliary after liver metabolism [72]. This last pathway is classically described for drugs but remain to be confirmed for nanoparticles or degradation products coming from nanomaterial combining MD.

Toxicity

The possible persistence of products of degradation coming from nanostructured MD in the human body may induce acute, chronic toxicities and even the development of tumorous processes.

The wear of MD leads to the formation of fragments which is particularly the case for joint prostheses due to friction forces between articular surfaces, bone interaction, corrosion phenomenon… Metallic fragments generate particles (*ca.* 10^{12} particles/year) with a size of *ca.* 50 nm [73]. However, it is possible that particles characterized by a diameter of less than

50 nm can be underestimated due to the limitation imposed by the detection techniques in a biological medium. Generated fragments can be endocyted by macrophages before being transported to the lymph nodes for excretion [74]. Macrophages can be locally retained implying a tissue inflammation. That explains why an inflammatory response can often be observed but degradation fragments can also induce immunity disturbance [75].

The antimicrobial properties of silver nanoparticles are due not only to their inherent properties but also to their dissolution into ions (Ag^+) *via* a corrosion phenomenon [26, 28, 76-78]. These agents can be absorbed by the cutaneous route because of a damaged skin as previously explained. A hepatotoxicity, appearing one week after the beginning of the treatment, was described in a patient presenting burns and treated by silver nanoparticles containing bandage. A total regression of the symptoms was observed when the bandages were taken off [79]. When these particles are associated to catheters, the antimicrobial properties were maintained but an initiation of the coagulation was noticed with a possible associated risk of thrombosis [80]. In parallel, the clinical trials AVERT which tested the efficiency of heart valves containing silver nanoparticles was prematurely stopped because in particular of side effects appearance such as thrombosis. The coating made of nano-objects was called into question even though the collected data were not significant from a statistical point of view [81, 82].

Conclusion and outlook

As a conclusion, nanomaterials used into MD and implantable MD are already on the market and they proved numerous beneficial aspects and further research on this axis may open new perspectives in therapy or diagnostic or even theranostic. This wide pharmaceutical domain is indeed characterized by an important dynamism in terms of innovation (Figure 1A).

However, in spite of the great potential offered by the domain, it seems that there is a lack of dedicated pharmaceutical quality control and regulatory issues are not totally well addressed. In the literature, even though eight criteria are usually used to describe nanomaterials combining products, there remain not sufficient to define them from a pharmaceutical point of view. It is obvious that the quality control of such product is much more complicated than the one of bulk materials. There is, indeed, a wide variety of products that are nanostructured or that include nano-objects (Figure 1B) and maybe new properties have to be taken into consideration in a case-by-case approach. This suggests the development or at least the transposition of analytical methods that may provide information in a complementary manner. This really represents a new multidisciplinary challenge not only for analysts but also for scientists of other disciplines. At that time, in the regulatory texts, there are no standard guidelines for nano-product manufacturing and their control, so they must follow the current Good Manufacturing Practices (cGMP). Moreover, there is no monograph on any nanomaterial in the Pharmacopoeias (US or European). This situation is the same than the one observed few years ago for raw materials coming from medicinal plants and vegetal drugs. A lot of impurities can be generated from nanomaterials combining products from which a potential toxicity may originate: impurities coming from the synthesis and the storage or even the degradation products (as cited above and illustrated into Figure 3). These elements must be defined and their amount should be normalized into assay values and corresponding calculated standard deviations. It is obvious that a better characterization and quality control of such products would lead to better understanding of potential interaction with biological elements as well as possible related toxicity and the way to avoid it.

Even though there is an international definition of nanomaterials given by the ISO (Box 2), the regulatory Authorities of countries possess their own definition which was recently highlighted in a review [83]. This induces an important lack of clarity. In parallel, the

classification of a product as either a drug or a MD may be different as a function of the concerned regulatory Authorities from one country to another. Altogether, these Agencies started to discuss about nanomedicine as an example, there was a first joint workshop between the Food and Drug Administration (FDA) and the European Medicines Agency (EMA) in 2010[5]. This may help for further normalization of regulatory issues.

Moreover, as nanomaterials can easily be functionalized by drugs with high yields, one can easily imagine new devices combining three partners: a device, nano-objects or a nanostructuration and an active molecule. Some lab works [84-87] are currently developing such products showing an important axis of innovation and dynamism in the design, the architecture and in the adopted medical strategy. This idea can lead to a new family of combination compound. This class of medicine already combines two or three single-regulated entities: drug, biological and/or medical device (with as examples transdermal patches or drug-eluting stents [2]). This definition may need to be broadened in order to include product containing drug(s), MD and nanomaterials. These hyphenated technologies might also trigger new regulatory aspects. According to the FDA definition of the MD (Box 1) and of the drug, the difference is set as "if the primary intended use of the product is achieved through chemical action or by being metabolized by the body, the product is usually a drug". Although this statement clearly separates MD from drug, the approval of such drug and nanomaterial combining products ought to be more defined by new regulatory issues. To go further, with the development of such products, the regulatory barriers between drug, nanomaterials and MD may fade away.

Acknowledgements: UL pour corrections,

Conflict of interest: none

Box 1. Definition of a medical device according to a Food and Drug Administration.
Extracted form www.fda.gov (MD: Medical Device, IMD: Implantable Medical Device)

A **medical device** is "A device is an instrument, apparatus, implement, machine, contrivance, implant, *in vitro* reagent, or other similar or related article, including a component part, or accessory which is:

- Recognized in the official National Formulary, or the United States Pharmacopoeia, or any supplement to them,
- Intended for use in the diagnosis of disease or other conditions, or in the cure, mitigation, treatment, or prevention of disease, in man or other animals, or
- Intended to affect the structure or any function of the body of man or other animals, and which does not achieve its primary intended purposes through chemical action within or on the body of man or other animals and which is not dependent upon being metabolized for the achievement of any of its primary intended purposes."

"This definition provides a clear distinction between a medical device and other FDA regulated products such as drugs. If the primary intended use of the product is achieved through chemical action or by being metabolized by the body, the product is usually a drug."

"**Medical implants** are devices or tissues that are placed inside or on the surface of the body. Many implants are prosthetics, intended to replace missing body parts. Other implants deliver medication, monitor body functions, or provide support to organs and tissues." Some implants are made from skin, bone or other body tissues. Others are made from metal, plastic, ceramic or other materials.

Implants can be placed permanently or they can be removed once they are no longer needed. For example, stents or hip implants are intended to be permanent. But chemotherapy ports or screws to repair broken bones can be removed when they no longer needed."

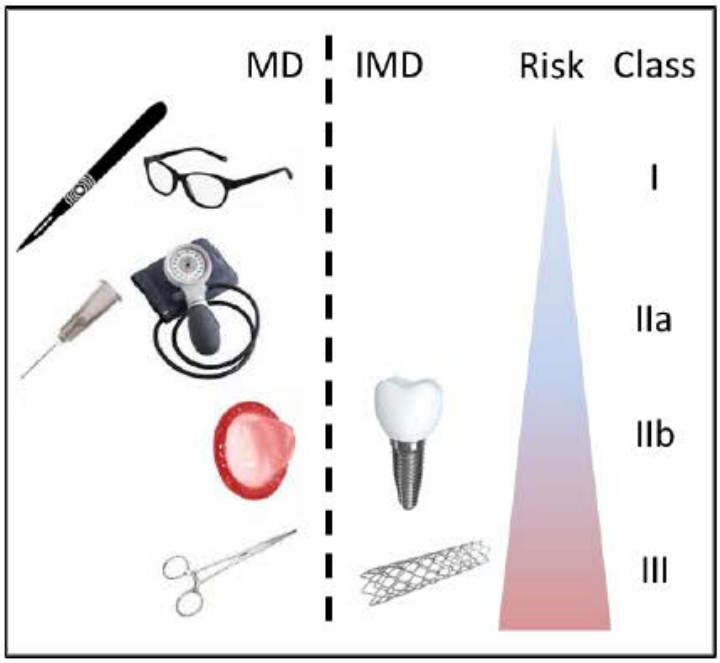

Box 2. ISO definition of words containing "nano-".

The International Organization for Standardization (ISO) has defined "nanomaterial" as a "material with any external dimension in the nanoscale or having internal structure or surface structure in the nanoscale" [52] and "nanoparticle" as a "nano-object with all three external dimensions in the nanoscale" where nanoscale is defined as the size range from approximately 1–100 nm [88].

The ISO defines the relevant terms as follows[88-90]:

Nanoscale (or nano range): Size range from approximately 1 nm to 100 nm.

Nanomaterial: Material with any external dimension in the nanoscale (**nano-objects**) or having internal structure or surface structure in the nanoscale (**nanostructured materials**).

Nano-object: Material confined in one, two, or three dimensions at the nanoscale. This includes **nanoparticles** (all three dimensions in the nanoscale), **nanofibres** (two dimensions in the nanoscale) and **nanoplates** (one dimension in the nanoscale). Nanofibres are further divided into nanotubes (hollow nanofibre), nanorods (solid nanofibre) and nanowire (electrically conducting or semiconducting nanofibre).

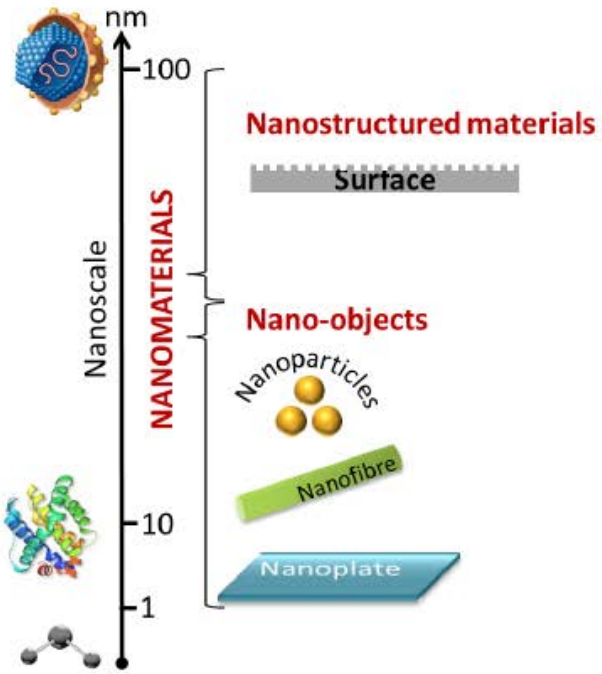

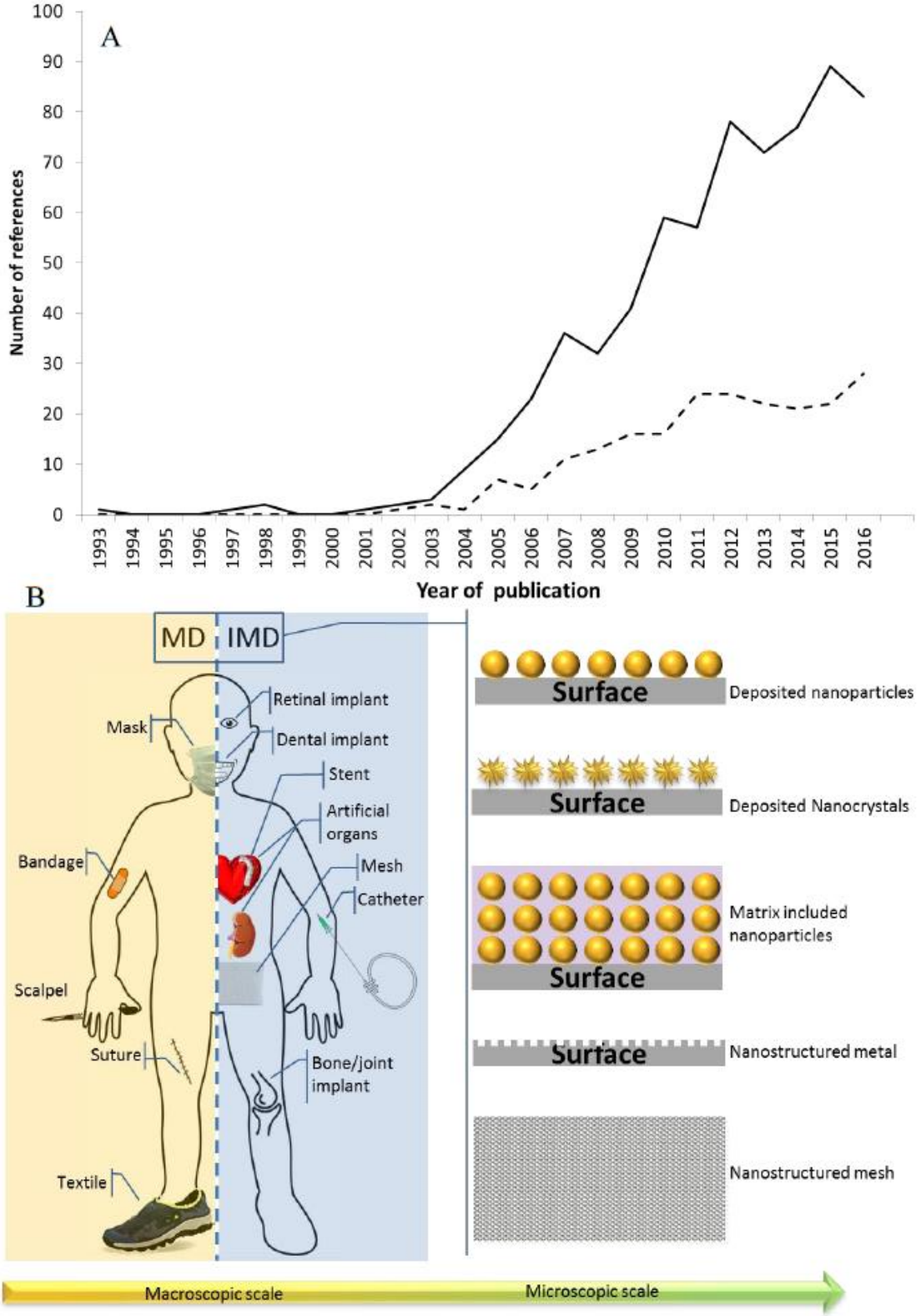

Figure 1. Overview of the marketed nanostructured medical devices: A infatuation of the community extracted from Web of Sciences website with keywords nanoparticles, nanotechnologies, nanomaterials combined with medical device (academic publications in solid line; patents in dash line) and B classical medical devices (MD) and implanted medical devices (IMD) and their microscopic organization.

21

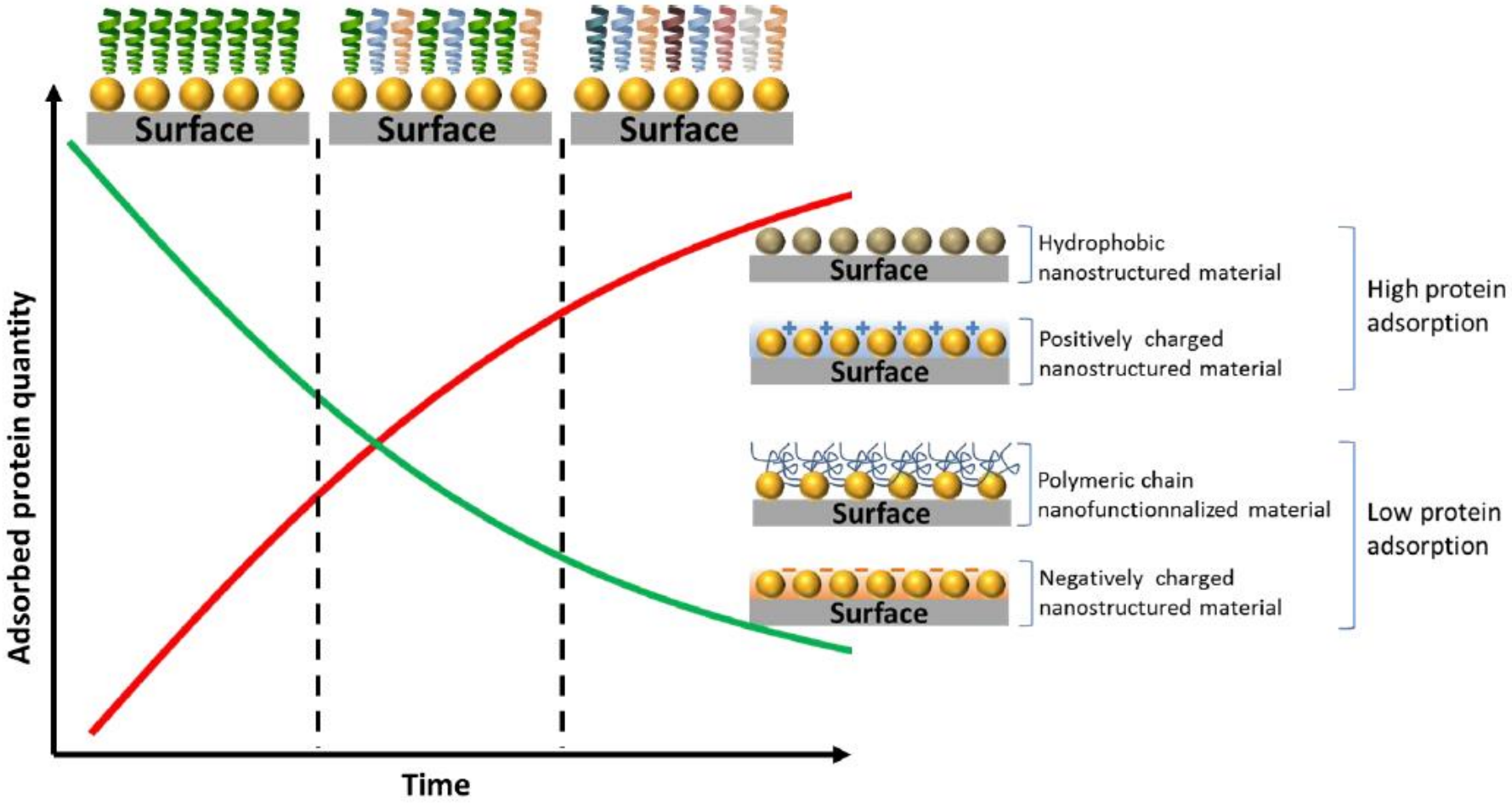

Figure 2. Kinetic of interaction of nanostructured materials with plasmatic proteins and their affinity for protein adsorption. Three phases can be observed: highly concentrated protein with low affinity are first adsorbed (green curve) and this equilibrium is progressively modified towards protein less concentrated with better affinity for material surface (red curve).

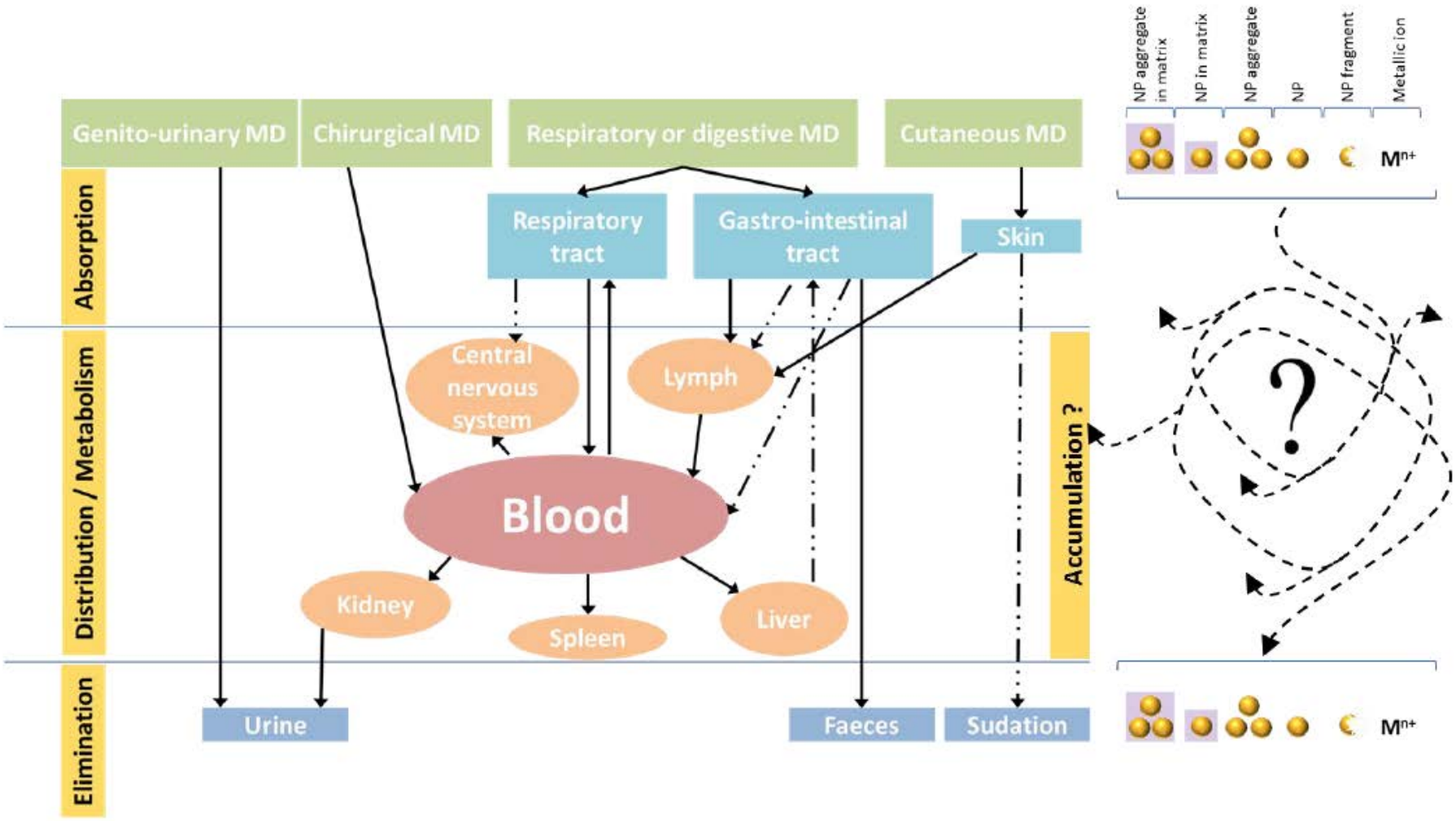

Figure 3. Potential degradation products coming from nanostructured medical devices and their possible journey into the organism (modified from 30). Confirmed pharmacokinetic pathways are indicated in plain arrows and hypothesized ones in dotted arrows.

Table 1: List of the marketed devices which is either nanostructured or which includes nanotechnologies. The medical indication of the device is indicated. The size of the nanotechnology is indicated when the information is available.

Organ	Medical device	Name of the marketed device	Nanotechnology	Name of the compagny (Country)
Skin	Bandage	Acticoat®	Silver NP (> 15 nm) Silcryst™	SMITH & NEPHEW (United Kingdom)
	Adhesive system	Adper™ Scotchbond™ SE	Silanized zirconium NP	3M ESPE (USA)
	Antimicrobial textile	Mipan® Magic Silver Nano	Silver NP	HYOSUNG (Corea)
	Suture needle	Sandvik Bioline 1RK91™	Steel nanocrystals (1-10 nm)	AB SANDVIK MATERIALS TECHNOLOGY (Sweden)
Eye	Retinal implant	Argus™	Nano-electronic component	SECOND SIGHT MEDICAL PRODUCTS (USA)
Mouth	Surgical mask	NanoMask®	Magnesium oxide NP	EMERGENCY FILTRATION PRODUCTS (USA)

24

	Surgical mask filtering influenza virus	NanoFenseTM	Silver NP	APPLIED NANOSCIENCES
Tooth	Dental restoration composite	Aerosil®	Silicium oxide NP (7-40nm)	DEGUSSA (Germany)
		Ketac™ N100	Nano-ionomer	3M ESPE (USA)
		Grandio®	Hybrid nanocomposite	VOCO (Germany)
	Photopolymerisable dental restoration composite	Filtek™ Supreme	Silicium NP	3M ESPE (USA)
		Optiglaze	Silicium NP	GC CORPORATION (Japan)
	Dental restoration product based on synthetic resin	Kappalux Nano	Silicium dioxide and zirconium oxide NP (10-100 nm)	PRODUITS DENTAIRES PIERRE ROLLAND (France)
	Metallic dental implant	NanoImplant®	Nanostructured titanium	TIMPLANT (Czech republic)
Bone	Product for injectable bone filling	Nanogel®	Hydroxyapatite NP (100-200 nm)	TEKNIMED (France)
		NanostimTM / Ostim®	Hydroxyapatite NP	AAP BIOMATIERALS (Germany) / MEDTRONIC (France)

25

		PerOssal®	Hydroxyapatite NP	AAP BIOMATERIALS (Germany)
		FortrOss®	Hydroxyapatite NP (NanOss®) combined to osteoconductive E-Matrix	PIONEER SURGICAL TECHNOLOGY (USA)
		Vitoss® Scaffold	Nanoporous calcium phosphate	ORTHOVITA (USA)
	Nanostructured metallic orthopedic implant	Puretex®	Nanostructured titanium surface	SYBRON IMPLANT SOLUTIONS (USA)
Bone/joint	Orthopedic or joint prosthesis	Nanos™ Symax™	Microporous coating (Bonit®) with hydroxyapatite nanocrystals (made by DOT (Allemagne))	SMITH&NEPHEW (United Kingdom) STRYKER (France)
	Orthopedic or teeth prosthesis	NanoTite™	Calcium phosphate nanocrystals (20-100 nm) deposited on a surface	BIOMET *3i*
	External knee prosthesis	Rheo Knee	Iron NP (100 nm)	OSSUR (Iceland)
	Surgical device delivering data on custom	Mako	Nanosensors	ORTHOSENSOR (USA)

26

	orthopedic knee implantation			
Vessel	Stent coating	Debiostent™	Ceramic (TiO_2, ZrO_2, SiO_2, IrO_2, Al_2O_3, CaP) nanostructured coating (thikness from 100 nm to 10 µm)	DEBIOTECH (Switzerland)
	Naked coronary stent	Catania™	Polyzene®-F coating (thickness of 40-50 nm)	CELONOVA BIOSCIENCES (Canada)
	Drug-eluting stent	VestaSync™	Nanoporous hydroxyapatite coating (100 nm)	MIV THERAPEUTICS (Canada)
	Vascular graft		Nanocages of UCL-NanoBio™	Royal Free Hospital of London (United Kingdom)
	Catheter for anesthesia	ON-Q® SilverSoaker™	Coating including silver NP (SilvaGard™ made by ACRYMED (USA))	I-FLOW CORP. (USA)
Abdomen	Ventral Hernia Mesh	NovaMesh™	Nanofiber integrated into a tissue	NICAST (Israel)

27

Table 2. List of the nanostructured devices currently under clinical trial evaluation. Extracted from https://clinicaltrials.gov/ (keywords: nanoparticles, nanotechnologies and nanomaterials)

Study name Official title ClinicalTrials.gov Identifier:	Medical device nanoparticles	Status	Purpose
IABN Clinical Study: the Antibacterial Effect of Insoluble Antibacterial Nanoparticles (IABN) Incorporated in Dental Materials for Root Canal Treatment NCT01167985	Dental restoration Polyethyleneimine nanoparticles	Unknown	Effect of Antibacterial Nanoparticles, Incorporated in root canal sealer material and in provisional restoration
Clinical Study: the Effect of Addition of Insoluble Antibacterial Nanoparticles(IABN) in Resin Base Provisional Cement NCT00502606			Effect of Antibacterial Nanoparticles, Incorporated in cement, on *S. mutans* in the margins of provisional restorations
Clinical Evaluation of Esthetic Restorations Placed in Primary Molars With Composite Resin Enriched With Insoluble Anti Bacterial Nano-Particles			Effect of Antibacterial Nanoparticles

(IABN) NCT00389714			
Clinical Study of Antibacterial Nanoparticles Incorporated in Composite Restorations NCT00299598	Alkylated polyethyleni mine nanoparticles	Completed	Resin composites withholding antibacterial properties useful in preventing recurrent caries
Altrazeal Range of Motion Study Comparing With Typical Carboxymethyl (ROM) NCT01062191	Hydrogel bandage Nanoflex® NP	Terminated due to a lack of enrollment	Difference in joint range of motion of a new flexible hydrogel nanoparticle wound dressing compared to typical sodium carboxymethylcellulose dressing Aquacel AG for treatment of partial thickness burns
SNOOPY2 Exhaled Breath Olfactory Signature of Pulmonary Arterial Hypertension NCT02782026	Electronic nose (E-nose) Gold-nanoparticles coated with organic ligands	Currently recruiting	Evaluate the diagnostic performance of a novel electronic nose (E-nose) for the detection of Pulmonary Arterial Hypertension (PAH)
Wear Characteristics of Denture	Denture teeth	Terminated	To evaluate the wear

Teeth NCT01188226	Nano hybrid composite		characteristics of new resin denture teeth (nano particles - hybrid composite) made by an injection technique

References

[1] World Health Organization, WHO Global Model Regulatory Framework for Medical Devices including in vitro diagnostic medical devices, (2017).
[2] D.S. Couto, L. Perez-Breva, P. Saraiva, C.L. Cooney, Lessons from innovation in drug-device combination products, Adv Drug Deliv Rev, 64 (2012) 69-77.
[3] P.-Y. Li, J. Shih, R. Lo, S. Saati, R. Agrawal, M.S. Humayun, Y.-C. Tai, E. Meng, An electrochemical intraocular drug delivery device, Sensors and Actuators A: Physical, 143 (2008) 41-48.
[4] T. Betancourt, L. Brannon-Peppas, Micro- and nanofabrication methods in nanotechnological medical and pharmaceutical devices, International journal of nanomedicine, 1 (2006) 483-495.
[5] LEEM, Applications des nanotechnologies à la médecine (2014).
[6] M.A. Meyers, A. Mishra, D.J. Benson, Mechanical properties of nanocrystalline materials, Progress in Materials Science, 51 (2006).
[7] Y. Liu, H. Wang, Nanomedicine: Nanotechnology tackles tumours, Nature nanotechnology, 2 (2007) 20-21.
[8] M. Jager, C. Zilkens, K. Zanger, R. Krauspe, Significance of nano- and microtopography for cell-surface interactions in orthopaedic implants, Journal of biomedicine & biotechnology, 2007 (2007) 69036.
[9] M. Sato, T.J. Webster, Nanobiotechnology: implications for the future of nanotechnology in orthopedic applications, Expert review of medical devices, 1 (2004) 105-114.
[10] T.J. Webster, J.U. Ejiofor, Increased osteoblast adhesion on nanophase metals: Ti, Ti6Al4V, and CoCrMo, Biomaterials, 25 (2004) 4731-4739.
[11] S.V. Dorozhkin, Nanosized and nanocrystalline calcium orthophosphates, Acta Biomater, 6 (2010) 715-734.
[12] F. Watari, N. Takashi, A. Yokoyama, M. Uo, T. Akasaka, Y. Sato, S. Abe, Y. Totsuka, K. Tohji, Material nanosizing effect on living organisms: non-specific, biointeractive, physical size effects, Journal of the Royal Society, Interface, 6 Suppl 3 (2009) S371-388.
[13] M.L. Knetsch, L.H. Koole, New Strategies in the Development of Antimicrobial Coatings: The Example of Increasing Usage of Silver and Silver Nanoparticles, Polymers, 3 (2011) 340-366.
[14] H. Kim, B.H. Kim, B.K. Huh, Y.C. Yoo, C.Y. Heo, Y.B. Choy, J.H. Park, Surgical suture releasing macrophage-targeted drug-loaded nanoparticles for an enhanced anti-inflammatory effect, Biomaterials science, 5 (2017) 1670-1677.
[15] D.J. McClements, H. Xiao, P. Demokritou, Physicochemical and colloidal aspects of food matrix effects on gastrointestinal fate of ingested inorganic nanoparticles, Advances in colloid and interface science, 246 (2017) 165-180.
[16] ANSM, Evaluation biologique des dipositifs médicaux contenant des nanomatériaux, (2011).
[17] Y. Yi, H.J. Kim, P. Mi, M. Zheng, H. Takemoto, K. Toh, B.S. Kim, K. Hayashi, M. Naito, Y. Matsumoto, K. Miyata, K. Kataoka, Targeted systemic delivery of siRNA to cervical cancer model using cyclic RGD-installed unimer polyion complex-assembled gold nanoparticles, Journal of controlled release : official journal of the Controlled Release Society, 244 (2016) 247-256.
[18] R. Taniguchi, Y. Miura, H. Koyama, T. Chida, Y. Anraku, A. Kishimura, K. Shigematsu, K. Kataoka, T. Watanabe, Adequately-Sized Nanocarriers Allow Sustained Targeted Drug Delivery to Neointimal Lesions in Rat Arteries, Molecular pharmaceutics, 13 (2016) 2108-2116.

[19] I. Brigger, C. Dubernet, P. Couvreur, Nanoparticles in cancer therapy and diagnosis, Adv Drug Deliv Rev, 54 (2002) 631-651.
[20] E. Roger, J.C. Gimel, C. Bensley, A.S. Klymchenko, J.P. Benoit, Lipid nanocapsules maintain full integrity after crossing a human intestinal epithelium model, Journal of controlled release : official journal of the Controlled Release Society, 253 (2017) 11-18.
[21] J. Hardie, Y. Jiang, E.R. Tetrault, P.C. Ghazi, G.Y. Tonga, M.E. Farkas, V.M. Rotello, Simultaneous cytosolic delivery of a chemotherapeutic and siRNA using nanoparticle-stabilized nanocapsules, Nanotechnology, 27 (2016) 374001.
[22] M.E. Davis, Z.G. Chen, D.M. Shin, Nanoparticle therapeutics: an emerging treatment modality for cancer, Nature reviews. Drug discovery, 7 (2008) 771-782.
[23] X. Li, M. Soler, C.I. Ozdemir, A. Belushkin, F. Yesilkoy, H. Altug, Plasmonic nanohole array biosensor for label-free and real-time analysis of live cell secretion, Lab on a chip, 17 (2017) 2208-2217.
[24] H.A. Stone, A.D. Stroock, A. Ajdari, Microfluidics Towards a Lab-on-a-Chip, Annual Review of Fluid Mechanics, 36 (2004) 381-411.
[25] G.M. Whitesides, The origins and the future of microfluidics, Nature, 442 (2006) 368-373.
[26] J. Tournebize, A. Sapin-Minet, G. Bartosz, P. Leroy, A. Boudier, Pitfalls of assays devoted to evaluation of oxidative stress induced by inorganic nanoparticles, Talanta, 116 (2013) 753-763.
[27] M. Rai, A. Yadav, A. Gade, Silver nanoparticles as a new generation of antimicrobials, Biotechnology advances, 27 (2009) 76-83.
[28] S. Prabhu, E.K. Poulose, Silver nanoparticles: mechanism of antimicrobial action, synthesis, medical applications, and toxicity effects, International Nano Letters, 2 (2012) 32.
[29] H.Q. Yin, R. Langford, R.E. Burrell, Comparative evaluation of the antimicrobial activity of ACTICOAT antimicrobial barrier dressing, The Journal of burn care & rehabilitation, 20 (1999) 195-200.
[30] K. Dunn, V. Edwards-Jones, The role of Acticoat with nanocrystalline silver in the management of burns, Burns : journal of the International Society for Burn Injuries, 30 Suppl 1 (2004) S1-9.
[31] V. Alt, T. Bechert, P. Steinrucke, M. Wagener, P. Seidel, E. Dingeldein, E. Domann, R. Schnettler, An in vitro assessment of the antibacterial properties and cytotoxicity of nanoparticulate silver bone cement, Biomaterials, 25 (2004) 4383-4391.
[32] V. Kumar, D.-J. Lee, Studies of nanocomposites based on carbon nanomaterials and RTV silicone rubber, Journal of Applied Polymer Science, 134 (2017) n/a-n/a.
[33] A. Erdemir, C. Donnet, Tribology of diamond-like carbon films: recent progress and future prospects, J. Phys. D: Appl. Phys, 39 (2006) R311-R327.
[34] S. Nedjari, A. Hébraud, S. Eap, S. Siegwald, C. Mélart, N. Benkirane-Jessel, G. Schlatter, Electrostatic Template-Assisted Deposition of Microparticles on Electrospun Nanofibers: Towards Microstructured Functional Biochips for Screening Applications, Rsc Adv, 5 (2015) 83600-83607.
[35] R.K. Poduval, S. Noimark, R.J. Colchester, T.J. Macdonald, I.P. Parkin, A.E. Desjardins, I. Papakonstantinou, Optical fiber ultrasound transmitter with electrospun carbon nanotube-polymer composite, Applied Physics Letters, 110 (2017) 223701.
[36] C. Mrowietz, R.P. Franke, U.T. Seyfert, J.W. Park, F. Jung, Haemocompatibility of polymer-coated stainless steel stents as compared to uncoated stents, Clinical hemorheology and microcirculation, 32 (2005) 89-103.
[37] C. Henn, S. Satzl, P. Christoph, P. Kurz, B. Radeleff, U. Stampfl, S. Stampfl, I. Berger, G.M. Richter, Efficacy of a polyphosphazene nanocoat in reducing thrombogenicity, in-stent

stenosis, and inflammatory response in porcine renal and iliac artery stents, Journal of vascular and interventional radiology : JVIR, 19 (2008) 427-437.
[38] V.V. Rani, L. Vinoth-Kumar, V.C. Anitha, K. Manzoor, M. Deepthy, V.N. Shantikumar, Osteointegration of titanium implant is sensitive to specific nanostructure morphology, Acta Biomater, 8 (2012) 1976-1989.
[39] W.H. Fissell, A.J. Fleischman, H.D. Humes, S. Roy, Development of continuous implantable renal replacement: past and future, Translational research : the journal of laboratory and clinical medicine, 150 (2007) 327-336.
[40] W.H. Fissell, S. Manley, A. Westover, H.D. Humes, A.J. Fleischman, S. Roy, Differentiated growth of human renal tubule cells on thin-film and nanostructured materials, ASAIO journal, 52 (2006) 221-227.
[41] L. Muthusubramaniam, R. Lowe, W.H. Fissell, L. Li, R.E. Marchant, T.A. Desai, S. Roy, Hemocompatibility of silicon-based substrates for biomedical implant applications, Annals of biomedical engineering, 39 (2011) 1296-1305.
[42] S.C. Mannsfeld, B.C. Tee, R.M. Stoltenberg, C.V. Chen, S. Barman, B.V. Muir, A.N. Sokolov, C. Reese, Z. Bao, Highly sensitive flexible pressure sensors with microstructured rubber dielectric layers, Nature materials, 9 (2010) 859-864.
[43] Z. Li, G. Zhu, R. Yang, A.C. Wang, Z.L. Wang, Muscle-driven in vivo nanogenerator, Advanced materials, 22 (2010) 2534-2537.
[44] D.H. Kim, J. Viventi, J.J. Amsden, J. Xiao, L. Vigeland, Y.S. Kim, J.A. Blanco, B. Panilaitis, E.S. Frechette, D. Contreras, D.L. Kaplan, F.G. Omenetto, Y. Huang, K.C. Hwang, M.R. Zakin, B. Litt, J.A. Rogers, Dissolvable films of silk fibroin for ultrathin conformal bio-integrated electronics, Nature materials, 9 (2010) 511-517.
[45] R.K. Jha, P.K. Jha, K. Chaudhury, S.V. Rana, S.K. Guha, An emerging interface between life science and nanotechnology: present status and prospects of reproductive healthcare aided by nano-biotechnology, Nano reviews, 5 (2014).
[46] M. Sengupta, S. Das, A. Bordoloi, Cu/Cu2O nanoparticle interface: Rational designing of a heterogeneous catalyst system for selective hydroamination, Molecular Catalysis, 440 (2017) 57-65.
[47] D. Mozhayeva, C. Engelhard, Separation of Silver Nanoparticles with Different Coatings by Capillary Electrophoresis Coupled to ICP-MS in Single Particle Mode, Analytical chemistry, (2017).
[48] A. Pallotta, A. Boudier, P. Leroy, I. Clarot, Characterization and stability of gold nanoparticles depending on their surface chemistry: Contribution of capillary zone electrophoresis to a quality control, J Chromatogr A, 1461 (2016) 179-184.
[49] S. Takagi, T. Shimada, Y. Ishida, T. Fujimura, D. Masui, H. Tachibana, M. Eguchi, H. Inoue, Size-matching effect on inorganic nanosheets: control of distance, alignment, and orientation of molecular adsorption as a bottom-up methodology for nanomaterials, Langmuir, 29 (2013) 2108-2119.
[50] J.M. Dennison, J.M. Zupancic, W. Lin, J.H. Dwyer, C.J. Murphy, Protein Adsorption to Charged Gold Nanospheres as a Function of Protein Deformability, Langmuir, 33 (2017) 7751-7761.
[51] J.-X. Wang, X.-Z. Yang, Near infrared light-activated super-sensitive drug release using nanoparticles with a flow core, Journal of Controlled Release, 259 (2017) e145.
[52] ISO/TS, Norme ISO 10-993 "Evaluation biologique des dispositifs médicaux", (2010).
[53] A.P. Serro, A.C. Fernandes, B. Saramago, J. Lima, M.A. Barbosa, Apatite deposition on titanium surfaces--the role of albumin adsorption, Biomaterials, 18 (1997) 963-968.
[54] F. Rupp, L. Scheideler, D. Rehbein, D. Axmann, J. Geis-Gerstorfer, Roughness induced dynamic changes of wettability of acid etched titanium implant modifications, Biomaterials, 25 (2004) 1429-1438.

[55] C. Wang, L. Wang, W. Yang, Preparation and characterization of functional inorganic/organic composite microspheres via electrostatic interaction, J Colloid Interface Sci, 333 (2009) 749-756.
[56] L. Vroman, A.L. Adams, G.C. Fischer, P.C. Munoz, Interaction of high molecular weight kininogen, factor XII, and fibrinogen in plasma at interfaces, Blood, 55 (1980) 156-159.
[57] A.S. Silva, A.G. Teixeira, L. Bavia, F. Lin, R. Velletri, R. Belfort, L. Isaac, Plasma levels of complement proteins from the alternative pathway in patients with age-related macular degeneration are independent of Complement Factor H Tyr(402)His polymorphism, Molecular Vision, 18 (2012) 2288-2299.
[58] A. Gonzalez-Quintela, R. Alende, F. Gude, J. Campos, J. Rey, L.M. Meijide, C. Fernandez-Merino, C. Vidal, Serum levels of immunoglobulins (IgG, IgA, IgM) in a general adult population and their relationship with alcohol consumption, smoking and common metabolic abnormalities, Clinical and Experimental Immunology, 151 (2008) 42-50.
[59] Z. Sheikh, A.S. Khan, N. Roohpour, M. Glogauer, I.U. Rehman, Protein adsorption capability on polyurethane and modified-polyurethane membrane for periodontal guided tissue regeneration applications, Materials science & engineering. C, Materials for biological applications, 68 (2016) 267-275.
[60] S.R. Saptarshi, A. Duschl, A.L. Lopata, Interaction of nanoparticles with proteins: relation to bio-reactivity of the nanoparticle, Journal of nanobiotechnology, 11 (2013) 26-26.
[61] B.F. Lai, A.L. Creagh, J. Janzen, C.A. Haynes, D.E. Brooks, J.N. Kizhakkedathu, The induction of thrombus generation on nanostructured neutral polymer brush surfaces, Biomaterials, 31 (2010) 6710-6718.
[62] M.A. Rufin, M.E. Barry, P.A. Adair, M.L. Hawkins, J.E. Raymond, M.A. Grunlan, Protein resistance efficacy of PEO-silane amphiphiles: Dependence on PEO-segment length and concentration, Acta Biomater, 41 (2016) 247-252.
[63] Y. Zou, B.F.L. Lai, J.N. Kizhakkedathu, D.E. Brooks, Inhibitory Effect of Hydrophilic Polymer Brushes on Surface-Induced Platelet Activation and Adhesion, Macromolecular bioscience, 10 (2010) 1432-1443.
[64] D. Labarre, C. Vauthier, C. Chauvierre, B. Petri, R. Muller, M.M. Chehimi, Interactions of blood proteins with poly(isobutylcyanoacrylate) nanoparticles decorated with a polysaccharidic brush, Biomaterials, 26 (2005) 5075-5084.
[65] Y. Yang, R. Cavin, J.L. Ong, Protein adsorption on titanium surfaces and their effect on osteoblast attachment, J Biomed Mater Res A, 67 (2003) 344-349.
[66] D.E. Owens, N.A. Peppas, Opsonization, biodistribution, and pharmacokinetics of polymeric nanoparticles, Int J Pharm, 307 (2006) 93-102.
[67] A. Fundarò, R. Cavalli, A. Bargoni, D. Vighetto, G.P. Zara, M.R. Gasco, Non-stealth and stealth solid lipid nanoparticles (SLN) carrying doxorubicin: pharmacokinetics and tissue distribution after i.v. administration to rats, Pharmacological research, 42 (2000) 337-343.
[68] Y.F. Zheng, X.N. Gu, F. Witte, Biodegradable metals, Materials Science and Engineering: R: Reports, 77 (2014) 1-34.
[69] E. Vlachou, E. Chipp, E. Shale, Y.T. Wilson, R. Papini, N.S. Moiemen, The safety of nanocrystalline silver dressings on burns: a study of systemic silver absorption, Burns : journal of the International Society for Burn Injuries, 33 (2007) 979-985.
[70] M. Ballestri, A. Baraldi, A.M. Gatti, L. Furci, A. Bagni, P. Loria, R.M. Rapana, N. Carulli, A. Albertazzi, Liver and kidney foreign bodies granulomatosis in a patient with malocclusion, bruxism, and worn dental prostheses, Gastroenterology, 121 (2001) 1234-1238.
[71] W.H. De Jong, W.I. Hagens, P. Krystek, M.C. Burger, A.J. Sips, R.E. Geertsma, Particle size-dependent organ distribution of gold nanoparticles after intravenous administration, Biomaterials, 29 (2008) 1912-1919.

[72] N. Naghavi, A. de Mel, O.S. Alavijeh, B.G. Cousins, A.M. Seifalian, Nitric oxide donors for cardiovascular implant applications, Small, 9 (2013) 22-35.
[73] P.F. Doorn, P.A. Campbell, J. Worrall, P.D. Benya, H.A. McKellop, H.C. Amstutz, Metal wear particle characterization from metal on metal total hip replacements: transmission electron microscopy study of periprosthetic tissues and isolated particles, Journal of biomedical materials research, 42 (1998) 103-111.
[74] P.A. Revell, The combined role of wear particles, macrophages and lymphocytes in the loosening of total joint prostheses, Journal of the Royal Society, Interface, 5 (2008) 1263-1278.
[75] F. Billi, P. Campbell, Nanotoxicology of metal wear particles in total joint arthroplasty: a review of current concepts, Journal of applied biomaterials & biomechanics : JABB, 8 (2010) 1-6.
[76] K. Chaloupka, Y. Malam, A.M. Seifalian, Nanosilver as a new generation of nanoproduct in biomedical applications, Trends in biotechnology, 28 (2010) 580-588.
[77] S. Pal, Y.K. Tak, J.M. Song, Does the antibacterial activity of silver nanoparticles depend on the shape of the nanoparticle? A study of the Gram-negative bacterium Escherichia coli, Applied and environmental microbiology, 73 (2007) 1712-1720.
[78] J.R. Morones, J.L. Elechiguerra, A. Camacho, K. Holt, J.B. Kouri, J.T. Ramirez, M.J. Yacaman, The bactericidal effect of silver nanoparticles, Nanotechnology, 16 (2005) 2346-2353.
[79] M. Trop, M. Novak, S. Rodl, B. Hellbom, W. Kroell, W. Goessler, Silver-coated dressing acticoat caused raised liver enzymes and argyria-like symptoms in burn patient, The Journal of trauma, 60 (2006) 648-652.
[80] K.N. Stevens, O. Crespo-Biel, E.E. van den Bosch, A.A. Dias, M.L. Knetsch, Y.B. Aldenhoff, F.H. van der Veen, J.G. Maessen, E.E. Stobberingh, L.H. Koole, The relationship between the antimicrobial effect of catheter coatings containing silver nanoparticles and the coagulation of contacting blood, Biomaterials, 30 (2009) 3682-3690.
[81] L. Englberger, H.V. Schaff, W.R. Jamieson, E.D. Kennard, K.A. Im, R. Holubkov, T.P. Carrel, A. Investigators, Importance of implant technique on risk of major paravalvular leak (PVL) after St. Jude mechanical heart valve replacement: a report from the Artificial Valve Endocarditis Reduction Trial (AVERT), European journal of cardio-thoracic surgery : official journal of the European Association for Cardio-thoracic Surgery, 28 (2005) 838-843.
[82] G.L. Grunkemeier, R. Jin, K. Im, R. Holubkov, E.D. Kennard, H.V. Schaff, Time-related risk of the St. Jude Silzone heart valve, European journal of cardio-thoracic surgery : official journal of the European Association for Cardio-thoracic Surgery, 30 (2006) 20-27.
[83] D.R. Boverhof, C.M. Bramante, J.H. Butala, S.F. Clancy, M. Lafranconi, J. West, S.C. Gordon, Comparative assessment of nanomaterial definitions and safety evaluation considerations, Regulatory Toxicology and Pharmacology, 73 (2015) 137-150.
[84] S. Heid, H. Unterweger, R. Tietze, R. Friedrich, B. Weigel, I. Cicha, D. Eberbeck, A. Boccaccini, C. Alexiou, S. Lyer, Synthesis and Characterization of Tissue Plasminogen Activator—Functionalized Superparamagnetic Iron Oxide Nanoparticles for Targeted Fibrin Clot Dissolution, International journal of molecular sciences, 18 (2017) 1837.
[85] J. Varshosaz, M.A. Davoudi, S. Rasoul-Amini, Docetaxel loaded nanostructured lipid carriers functionalized with Trastuzumab (Herceptin) for HER2-positive breast cancer cells, Journal of Liposome Research, (2017) 1-36.
[86] L. Pascual, C. Cerqueira-Coutinho, A. García-Fernández, B. de Luis, E.S. Bernardes, M.S. Albernaz, S. Missailidis, R. Martínez-Máñez, R. Santos-Oliveira, M. Orzaez, F. Sancenón, MUC1 aptamer-capped mesoporous silica nanoparticles for controlled drug delivery and radio-imaging applications, Nanomedicine: Nanotechnology, Biology and Medicine.

[87] A. Jafarizad, A. Aghanejad, M. Sevim, Ö. Metin, J. Barar, Y. Omidi, D. Ekinci, Gold Nanoparticles and Reduced Graphene Oxide-Gold Nanoparticle Composite Materials as Covalent Drug Delivery Systems for Breast Cancer Treatment, ChemistrySelect, 2 (2017) 6663-6672.
[88] ISO/TS, Nanotechnologies - Terminology and definitions for nano-objects, nanoparticle, nanofibre and nanoplate., (2008).
[89] I.T. 80004-1, Nanotechnologies - Vocabulary - Part 1 : Core Terms, (2015).
[90] ISO/TS, Norme ISO/TS 80004-2 "Nanotechnologies - Vocabulaire - Partie 2 : Nano-objets", (2015).

Ainsi qu'il a été précédemment décrit, de plus en plus de nanoparticules sont intégrées dans des DM dans le but d'obtenir des surfaces nanostructurées. Les nanoparticules sont utilisées directement comme principe actif (nanoparticules d'argent et propriétés antibactériennes [81]) ou pour améliorer la biocompatibilité des DM (nanoparticules de titane [82] ou d'hydroxyapatite [83]). Dans ces travaux de recherche, nous nous sommes focalisés sur les AuNP qui serviront de réservoir de principe actif. La facilité de fonctionnalisation des AuNP avec des rendements importants [4] en font des candidats médicament de premier choix pour le développement de nouveaux DM.

2.4. Nanoparticules d'or

L'or (élément *Au*, numéro atomique Z = 79) fait partie du groupe 11 de la classification périodique des éléments. Sa couleur, son aspect brillant, son caractère inaltérable et inoxydable, (d'où le qualificatif de métal noble) ont fait de l'or un métal source de fascination et convoitise au cours des siècles. Au cours des âges, il a été utilisé principalement comme monnaie d'échange, pour la fabrication de bijoux et la réalisation d'œuvres d'art.

De nos jours, sans prendre en compte la valeur spéculative de ce métal, l'or est principalement utilisé dans la microélectronique (fabrication de connecteurs) mais aussi dans le domaine de la santé. Sa première application a été dans la fabrication de prothèses en odontologie, mais il aussi été utilisé sous forme de complexe organométallique dans le traitement des polyarthrites rhumatoïdes sous forme de comprimés (Ridauran®, retiré du marché en 2009) ou injectable (Miocrisin®, retiré du marché en 2012). Aujourd'hui, la recherche se tourne vers la fabrication et l'utilisation de l'or sous forme nanoparticulaire pour leurs propriétés physiques, optiques, chimiques et leur capacité de modification (taille,

charge, chimie de surface …) [5, 75, 84-87]. Les AuNP trouvent leurs applications dans de nombreux domaines. En physique, la capacité des AuNP à absorber l'énergie provenant de sources lumineuses ou radioactives (Rayons X) puis à restituer cette énergie sous forme de chaleur et de la transmettre au milieu dans lequel elles se trouvent, permet la création de nano-émetteurs thermiques. Cette propriété peut donner lieu à des applications, notamment dans le domaine de la biologie. Toujours en physique, les propriétés de résonnance plasmonique de l'or (oscillation collective et en phase des électrons de surface d'une NP) permettraient, lors de l'excitation par une onde électromagnétique, de transmettre des informations de proche en proche aux autres particules disposées sur une surface. Dans ce cas, les AuNP joueraient le rôle de nano-émetteurs électromagnétiques, ce qui aboutirait à la formation de nouveaux types d'ordinateurs capables de transmettre des informations à très grande vitesse.

En biologie, les applications potentielles des AuNP reposent principalement sur trois points : leur capacité à être fonctionnalisées, leur biocompatibilité et leur faible toxicité, la présence de la bande plasmon (pour certaines NP). Les AuNP sont principalement utilisées pour le diagnostic et l'imagerie notamment dans le domaine de la cancérologie. Une des techniques de détection des cellules cancéreuses consiste à greffer des AuNP avec des anticorps spécifiques aux marqueurs de ces cellules [88]. Si l'injection de ces AuNP est en plus couplée à de la radiothérapie, comme indiqué précédemment, l'énergie incidente est retransmise rapidement dans l'environnement sous forme de chaleur. Cette élévation locale de température permet une destruction quasi spécifique des cellules ayant interagi avec les AuNP. Les particules se comportent donc comme des outils non plus de diagnostic, mais de théranostique [89]. Enfin, les AuNP peuvent aussi être utilisées comme agent de vectorisation et fonctionnalisées avec des principes actifs avec des rendements élevés conférant une charge utile importante de la particule en principe actif [90]. Ces AuNP sont capables de délivrer des

molécules actives dans une zone d'intérêt (tumeur, infection profonde, ADN …). L'adressage spécifique d'un médicament permet de diminuer les doses nécessaires à son action et ainsi de diminuer les effets secondaires potentiels.

Toutes ces propriétés font des AuNP d'excellentes candidates pour le développement de thérapies innovantes. A l'heure actuelle, l'utilisation d'AuNP comme agents thérapeutiques a entrainé la mise en place de six essais cliniques aux champs d'applications variés : athérosclérose [91], diabète, hypertension pulmonaire, cancer… (Tableau 1).

Tableau 1 : Essais cliniques utilisant des AuNP (à partir de clinicaltrials.gov)

Nom de l'étude **Titre officiel** **Identifiant ClinicalTrials.gov :**	**Type d'AuNP**	**Pathologie**	**Statut**	**But**
NANOM PCI Plasmonic Photothermal and Stem Cell Therapy of Atherosclerosis Versus Stenting NCT01436123	AuNP à cœur fer-silice	Athérosclérose	Arrêtée	Améliorer le pronostic de patients atteints de plaques d'athéromes. Injection intra plaque d'AuNP combinée à de la thérapie photodynamique + pose de stent.
NANOM-FIM Plasmonic Nanophotothermal Therapy of Atherosclerosis NCT01270139			Terminée	Améliorer le pronostic de patients atteints de plaques d'athéromes. Injection intra plaque d'AuNP combinée à de la thérapie photodynamique *vs* pose de stent.
EE-ASI-1 Enhanced Epidermal Antigen Specific Immunotherapy Trial -1 NCT02837094	AuNP	Diabète (type 1)	Recrutement	Phase 1 : évaluer la toxicité AuNP injectées par voie sous cutanée (hypersensibilité, suivi sanguin et lymphatique …).
NU-0129 Treating Patients With Recurrent Glioblastoma or Gliosarcoma Undergoing Surgery NCT03020017	AuNP fonctionnalisées par des acides nucléiques sphériques	Glioblastome / Gliosarcome	Recrutement	Phase 0 : évaluation des effets secondaires, biodistribution dans les tumeurs, concentration sanguine … Cible : BCL2
SNOOPY2 Exhaled Breath Olfactory Signature of Pulmonary Arterial Hypertension NCT02782026	AuNP fonctionnalisées par des ligands organiques	Hypertension artérielle pulmonaire	Recrutement	Conception d'un nez électronique (E-nose) capable de détecter les composés volatiles exhalés lors de l'hypertension artérielle pulmonaire.
Diagnosis of Gastric Lesions With Na-nose NCT01420588	AuNP fonctionnalisées par des ligands organiques Nanotubes de carbone	Ulcères / gastrite	Recrutement	Conception d'un nez électronique (Na-nose) capable de détecter les composés volatiles exhalés lors de lésions gastriques

3. Objectif du travail de doctorat

Le projet vise à obtenir une libération prolongée de NO à une concentration de l'ordre du nanomolaire à partir d'un stent. Différents points sont à analyser pour mener à bien ce projet : le type de donneur de NO, le moyen de constituer un réservoir du principe actif et d'obtenir un profil de libération prolongée dans le temps ainsi que la création d'un revêtement stable qui n'entraine pas de dissémination d'AuNP *in vivo*.

Concernant le type de donneur de NO, comme mentionné précédemment, le radical doit être apporté par une pro-drogue. Il en existe différentes classes :

- Les nitrates organiques, dont certaines molécules sont commercialisées tels que la trinitrine (ou nitroglycérine) ou le dinitrate d'isosorbide, libèrent NO après des réactions enzymatiques impliquant une déplétion des réserves redox intracellulaires.
- Les diazeniumdiolates (ou NONOates) qui ont la capacité de se décomposer en NO sans subir de biotransformation mais qui ont l'inconvénient d'épuiser à terme le stock de thiols endogènes.
- Les RSNO qui sont, pour certains, des composés endogènes (*S*-nitrosoglutathion, *S*-nitrosocystéine, *S*-nitrosoalbumine, …) et qui sont caractérisés par une faible demi-vie (45 min [92]). Ils peuvent se décomposer pour libérer NO grâce à l'action d'enzymes (par exemple la thiorédoxine) ou par l'action de thiols de faible masse moléculaire ou de cations divalents (Cu^{2+}) (limitant ainsi le risque de déplétion des réserves redox des cellules). Les RSNO seront les pro-drogues choisies dans le présent travail.

Dans ce projet, en raison des propriétés intéressantes des AuNP exposées précédemment, et comme elles ont fait l'objet de nombreux travaux au sein de l'EA 3452

CITHEFOR [4, 5, 84, 93], elles seront fonctionnalisées en surface par une grande quantité de RSNO afin de constituer un réservoir suffisant de principe actif.

Afin d'obtenir une libération prolongée de principe actif à partir de ces AuNP (caractérisées par une charge de surface négative), celles-ci seront piégées entre des couches de polyélectrolytes au sein d'un film multicouche (Figure 11). Cette approche a déjà fait ses preuves dans la littérature pour charger de grandes quantités de principes actifs ainsi que pour les libérer à une concentration choisie sur une période prolongée dans le temps.

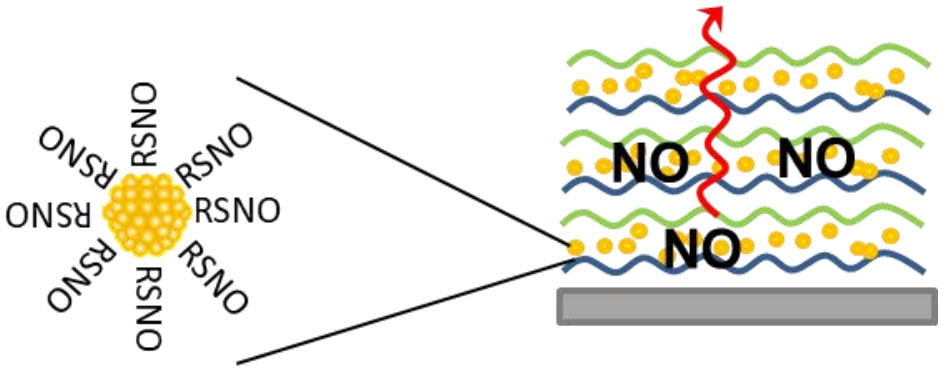

Figure 11 : Schéma représentatif de la composition de films LbL nanostructurés par des AuNP fonctionnalisées par des RSNO.

Ici, la diffusion d'espèces dénitrosantes (cations divalents, …) à travers les différentes couches entrainera la libération de NO par clivage de la liaison soufre-azote des RSNO. Enfin, afin d'éviter le relargage des AuNP dans la circulation sanguine, réduisant d'autant le réservoir en NO et pouvant entrainer des effets non désirés, des polyélectrolytes biocompatibles mais non biodégradables seront choisis.

De ce fait, ce projet propose une approche originale constituée par des dépôts multicouches de polymères successivement chargés négativement et positivement permettant

une libération prolongée, par diffusion passive de NO à partir d'un réservoir (AuNP fonctionnalisées).

Le prochain chapitre fera l'objet du développement des méthodes et techniques essentielles au bon développement des AuNP ainsi qu'à leur contrôle.

CHAPITRE II CONTROLE QUALITE ET DONNEES PRELIMINAIRES POUR LA FONCTIONNALISATION DES NANOPARTICULES D'OR

Avec le développement de nouveaux dispositifs médicaux nanostructurés, le statut même des nanoparticules est en train de changer. Doivent-elles être considérées comme des matières premières pharmaceutiques ? Si c'est le cas, des moyens analytiques permettant leur contrôle qualité, l'évaluation de leur stabilité ainsi que de leur profil de dégradation sont nécessaires. En ce qui concerne les AuNP, il n'en existe pas, à l'heure actuelle, de qualité pharmaceutique. Les bulletins analytiques des AuNP commerciales ne donnent pas d'informations précises quant à leur pureté, dispersité de population ou stabilité.

Dans ce chapitre, nous proposons deux méthodologies complémentaires permettant de contrôler la qualité d'AuNP synthétisées. La première consiste à doser l'or est capable de dissocier la part ionique (impureté provenant de la synthèse, ou de leur dégradation par dissolution) de la part nanoparticulaire (calcul de la teneur). Elle sera, par la suite appliquée pour évaluer l'absence de dissémination ou la potentielle biodistribution des AuNP après implantation du DM *in vivo*. La deuxième méthode repose sur l'utilisation de l'électrophorèse capillaire de zone (ECZ). Elle permettra de déterminer les teneurs et les profils d'impuretés de chaque lot synthétisé ainsi que d'effectuer un suivi de leur stabilité.

1. Dosage d'or

1.1. Introduction

Comme mentionné précédemment, l'utilisation d'AuNP pour des applications biomédicales est de plus en plus plébiscitée dans la littérature. Leur synthèse aisée, leur capacité à être fonctionnalisées ainsi que leurs applications multiples en font des candidats de choix. Cependant, malgré la relative absence de toxicité de l'or massique, il n'y a, actuellement, pas de consensus sur celle de l'or nanoparticulaire notamment dans les applications *in vivo* (*cf.* article 1). Même si les AuNP utilisées au cours de ce travail seront

immobilisées au sein de films multicouches (décris dans le chapitre 3), ils ne doivent pas libérer d'AuNP après leur implantation intravasculaire. La méthode de dosage de l'or développée au laboratoire [93] est simple à mettre en place, sans appareillage sophistiqué et repose sur la formation d'une paire d'ion entre un sel d'or ($AuCl_4^-$) et la Rhodamine B. Son principal point faible se trouve dans sa limite de détection (90,0 µM) beaucoup trop élevée par rapport aux concentrations d'or attendues dans les tissus ou les cellules (de l'ordre de 1,0 µM [94, 95]). Il a donc été nécessaire d'optimiser la méthode pour atteindre l'objectif de quantification.

Les améliorations se sont principalement axées sur la miniaturisation de la méthode, l'utilisation d'une chaine de chromatographie liquide haute performance (HPLC) ainsi que sur l'optimisation des paramètres expérimentaux (longueur d'onde de détection, chauffage, agitation, extraction …). Après optimisation de la méthode, celle-ci a été validée selon les critères classiques ICH et FDA [96, 97] pour le dosage de l'or sous sa forme ionique et/ou nanoparticulaire (Article 2, soumis dans *Talanta*). L'optimisation a permis de contrôler la qualité de la synthèse des AuNP *via* la quantification de l'or restant sous forme ionique après synthèse (rendement de réaction). L'absence de relargage de nanoparticules à partir d'un film de polyélectrolytes sous un flux aqueux dynamique est également prouvée. Des pistes seront aussi envisagées pour étudier la biodistribution d'AuNP *in vivo*.

1.2. Article 2 : High sensitive ion-pairing chromatography with visible detection to easily quantify gold nanoparticles in aqueous media

Graphical abstract

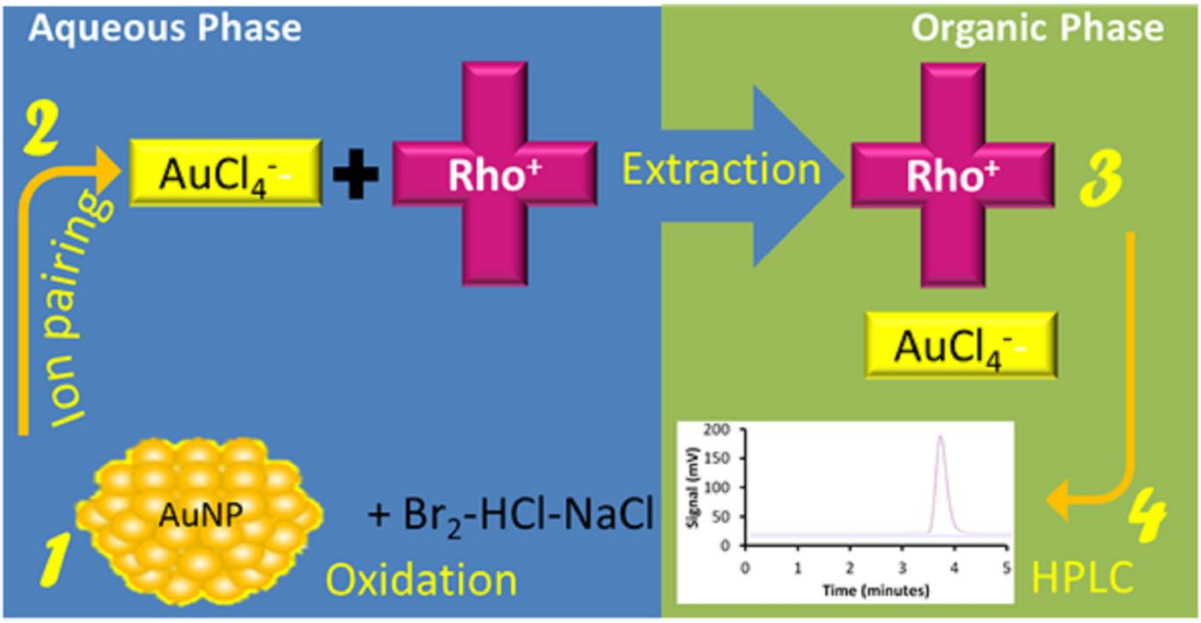

Highlights

- A simple optimized chromatographic method based on ion pairing extraction
- Quantification of gold under tetrachloroaurate or colloidal forms after oxidation
- Application to nanoparticle quality control
- Application to nanostructured film stability under shear stress

Highly sensitive and simple liquid chromatography assay with ion-pairing extraction and visible detection for quantification of gold from nanoparticles

Arnaud PALLOTTA[£], Valentin PHILIPPE[£], Ariane BOUDIER, Pierre LEROY, Igor CLAROT[*]

Université de Lorraine, CITHEFOR EA 3452, BP 80403, 54001 Nancy Cedex, France.

[£]: Equal contribution to this work.

*Corresponding author: igor.clarot@univ-lorraine.fr

Abstract

A simple isocratic HPLC method using visible detection was developed and validated for the quantification of gold in nanoparticles (AuNP). After a first step of oxidation of nanoparticles, an ion-pair between tetraurochlorate anion and the cationic dye Rhodamine B was formed and extracted from the aqueous media with the help of an organic solvent. The Rhodamine B extracted was finally quantified by reversed phase liquid chromatography using a Nucleosil C18 (150mm × 4.6mm, 3µm) column and with a mobile phase containing acetonitrile and 0.1% trifluoroacetic acid aqueous solution (25/75, V/V) at 1.0mL.min^{-1} and at a wavelength of 555nm. The method was validated using methodology described by the International Conference on Harmonization and was shown to be specific, precise (RSD < 11%), accurate and linear in the range of 0.1 – 30.0µM with a lower limit of quantification (LLOQ) of 0.1µM. This method was in a first time applied to AuNP quality control after their synthesis. In a second time, the absence of gold leakage (either as AuNP or gold salt form) from nanostructured multilayered polyelectrolyte films under shear stress was assessed.

Keywords

Gold nanoparticles; Ion-pairing extraction; Rhodamine B; HPLC; Quality control; Polyelectrolytes layer-by-layer films

1. Introduction

Gold properties, under its metallic state (Au redox state: 0), are known since the Antiquity. Its low reactivity with oxygen, sulfur or concentrated bases or acids allows its usage in human health such as prostheses and dental implants [1, 2]. On the contrary, gold reacts easily with halogens and dissolves in highly acid solutions (*aqua regia*) containing chloride ions to form tetrachloroauric acid ($HAuCl_4$, Au redox state: III). This specific reactivity leads to biologically active gold solutions. Those preparations have been used in the treatment of rheumatoid arthritis or various cancers [3]. Furthermore, $HAuCl_4$, when put in presence of a strong reducer (as sodium borohydride, $NaBH_4$) and a stabilizer (as sodium citrate), has the ability to form nanoparticles (AuNP, Au redox state: 0) [4]. Syntheses create well-defined mono-dispersed particles that can strongly bind several drugs or sensitive molecules thanks to their surface reactivity [5]. This high affinity makes them ideal candidates for biomedical purposes such as biosensors [6], diagnostic agents [7] and even drug carriers [8]. The use of AuNP as therapeutic agents led to seven clinical trials in different fields of application as atherosclerosis (NANOM FIM [9]), diabetes, pulmonary hypertension, cancer or stomach diseases (clinicaltrial.gov). AuNP can also be immobilized on surfaces (*e.g.* silica, quartz, glass …) to act as electrochemical catalysts [10] or diagnostic tools [7]. Recently, AuNP were entrapped inside multilayered polyelectrolyte films as nanostructurating agents [11]. After their functionalization with a therapeutic agent, AuNP will act as drug reservoirs able to induce a local pharmacologic effect *via* the drug release. These new uses of AuNP raise practical concerns about the health effects of long-term exposure on humans. Despite being promising, AuNP utilization in therapeutic can still lead to possible toxic effects [12]. Few studies take their biodistribution into consideration [13]. Their wide size range (from 2 to 100nm of Au core diameter) and surface functionalization (either *via* weak energy or covalent bonds) induce multiple possibilities of interaction with a variety of proteins, cells and organs.

Different methods exist to quantify gold (under its ionic or NP forms): from the most easy-to-use spectrophotometry method to the ultra-specific mass spectrometry one. Visible spectrophotometry is one of the easiest method to quantify gold [14]. Its principle is based on the measurement of a tetraurochlorate-Rhodamine B ion-pair extracted by a liquid/liquid process. The main drawback lays in its low sensitivity (LOD = 90.0µM of gold salt) which is not compatible with gold quantity usually found in cells (less than 1.0µM of gold salt). Other

2

methods used to detect and quantify gold are very sensitive and specific (Table 1) but required hyphenated dedicated apparatus such as: Inductively Coupled Plasma – Mass Spectrometry (ICP-MS), Atomic Absorption Spectrometry (AAS) or Atomic Emission Spectrometry (AES). To quantify gold concentration below the µM range, ICP-MS is the gold standard (from 0.1 to 1.0×10^{-5}µM). Despite being the reference method, it shows a lot of drawbacks such as a lack of reproducibility of results obtained in biological media, the necessity to have the dedicated platform and operator and a consequent sample preparation time. Furthermore, ICP-MS is usually coupled with different separative treatment methods such as Liquid Chromatography (LC-ICP-MS) [15] or Capillary Electrophoresis (CE-ICP-MS) [16].

Direct or indirect determinations of gold by most of these methods may lead to analytical issues due to the interferences between the matrix components of real sample and the method sensitivity. Therefore, pretreatment steps parallel to the analyte concentration in the sample are required to ensure the repeatability, reproducibility of results, and to reach the needed limit of quantification. But to the best of our knowledge, there is no easy-to-use method that ensures enough sensitivity to quantify gold in different aqueous matrices.

In this paper, we optimized a method based on the ion-paired tetraurochlorate -Rhodamine B detection [14]. Rhodamine B is commonly used to quantify gold either by visible or fluorescent detection [14, 17]. On the one hand, Tournebize *et al.* [15] were using a visible detection (565nm) with a spectrophotometer to quantify gold salt and AuNP. This method is simple but lacks of sensitivity. On the other hand, Liu *et al* [17] used fluorescence to measure the decrease of Rhodamine B signal in presence of Au(III). This technique had a low limit of detection (LOD) (1.52×10^{-2}µM), but required the synthesis of Rhodamine B coupled to chitosan nanoparticles and appears to be unsuitable for the quantification of AuNP. The optimization (incubation times, agitation, evaporation …) described in the present paper, consists mainly in miniaturizing the method to achieve the best LOD. This method was applied to quality control of AuNP synthesis and their immobilization on multilayered polyelectrolyte films [11]. We quantified gold deposition and the resulting possible leakage either as AuNP or as gold salt from films undergoing shear stress conditions.

2. Experimental

3

2.1 Reagents and standards

Ammonium chloride was purchased from VWR Chemicals. Acetonitrile (99.8%) was purchased from Biosolve Chimie, poly(allylamine hydrochloride) powder (PAH) and poly(acrylic acid, sodium salt) (PAA) solution 35% wt in water with average molecular masses of 15,000 were purchased from Sigma Aldrich. Phosphate-buffered saline (PBS) solution was prepared as follow: $[Na_2HPO_4] = 6.48 \times 10^{-3}$M, $[KH_2PO_4] = 1.47 \times 10^{-3}$M, $[NaCl] = 138 \times 10^{-3}$M and $[KCl] = 2.68 \times 10^{-3}$M, final pH was adjusted to 7.4. All other reagents were supplied by Sigma Aldrich and were of analytical grade. Ultrapure deionized water (>18.2MΩ.cm) was used for the preparation of all solutions.

2.2 HPLC analysis

HPLC analyses were carried out on a SpectraSystem system constituted by the following modules: vacuum degasser (SCM1000), quaternary pump (P1000XP), autosampler (AS300) and UV-Visible detector (UV2000). The column (Nucleosil ® C18, 150 mm × 4.6 mm, 3 µm particles size and 100Å porosity) was thermostated at 40°C using a Croco-cil (1267) oven. Data acquisition and injection control were performed by the Azur software (version 5.0, Datalys®). The mobile phase consisted on a mixture of acetonitrile and 0.1% trifluoroactic acid aqueous solution (25/75, V/V). The injection volume was 20µL. The detector was set at 555nm and the pump at a flow rate of $1.0 mL.min^{-1}$.

2.3 AuNP synthesis

Citrate stabilized gold nanoparticles were synthesized in the lab according to [4]. Briefly, a gold salt solution ($AuCl_4^-$) was added into 90mL of ultrapure water to a final concentration of 270µM and 2mL of sodium citrate (55mM) was added under inert atmosphere. The solution was stirred for 1min then 1mL of $NaBH_4$ (19.5mM) was added and the solution was stirred for 5min. The final AuNP concentration was 90nM according to the spectrophotometric method [13]. The resulting suspension was immediately stored in the dark at 4°C during 20 days [23]. AuNP obtained were completely described in [11, 14] and their gold core diameter was measured at 5.3±1.1nm.

All concentrations reported in this paper will be expressed as gold salt concentrations.

2.4 AuNP sample preparation

Samples preparation was adapted from [14]. Briefly, AuNP suspension (400µL) was mixed with an HCl-NaCl-Br_2 solution (400µL, 1.0M-0.3M-0.025M respectively) for 20min protected from light in LoBind Eppendorf microtubes (1.5mL). The mixture was then partially evaporated using a Turbovap (Biotage) at 40°C under inert gas (N_2, 4psi) for 20min. 200µL of NH_4Cl solution (30% m/V), 100µL of 6M HCl and 100µL of Rhodamine B solution (0.084µM) were then added. To extract the ion-pair formed between tetraurochlorate anion and Rhodamine B, 200µL of diisopropyl ether was finally added. Tubes were agitated on a Vibramax 100 (Heidolf Instruments) for 3min at 1500rpm, then centrifuged (Mini Spin Plus, Eppendorf) 3min at 12100×*g*. 150µL of the supernatant (organic phase) were withdrawn, completely evaporated (Turbovap, 5min, N_2 3psi) and the dried residue was dissolved in mobile phase (150µL) before injection into the HPLC system.

2.5 Method validation

The method was validated according to the ICH guidelines [25] and FDA recommendations [26].

2.6 Nanoparticle immobilization on glass and shear stress experiments

Layer-by-layer polyelectrolyte films were built as described elsewhere in details [11]. Briefly, cover glasses (75×38mm, Menzel-Glaser), were totally immersed in different solutions: PAH (0.1M in PBS), citrate stabilized AuNP suspension and PAA (0.1M in PBS), for 10min each. This cycle was repeated 3 times.

For shear stress experiments, parallel-plate culture flow chambers, designated 2D chambers, were used as illustrated in Figure 1.

Experimentations were carried out at 37°C on an incubator for 48h. The PBS flow rate applied to the glasses was measured at 16mL.min^{-1}. Gold released from the film was quantified in the media after 12, 24 and 48h with and without HCl-NaCl-Br_2 treatment. After 48h of incubation glasses were crushed, rinsed in 1.0mL of HCl-NaCl-Br_2 solution, and stirred during 20min (600rpm) to evaluate the total gold content.

3. Results and discussion

5

3.1 Method development

The initial parameters of the extraction method were based on that previously developed with colorimetric detection [14]. The direct use of this method with AuNP leads to recoveries of around 65% which were not adequate to achieve the targeted sensitivity (0.1µM). Thus, an important optimization step was required.

First, we sought to miniaturize the method (used volume) to allow better sensitivity by significantly increasing the ratio of sample volume versus organic solvent one. Very similar results were obtained but residues appeared when Eppendorf tubes were used. The replacement by Lobind tubes eliminated this problem and achieved a significant increase of 20% in the signal-to-noise (S/N) ratio. However, the increase in the proportion of the sample volume (initially 2.5% of total volume against 50.0% after miniaturization) caused a problem due to the high oxidizing power of Br_2. Its action on Rhodamine B caused a notable loss of its effectiveness in forming the ion pair with the gold salt (which is essential to its proper extraction). Since the boiling temperature of Br_2 is relatively low (59°C), the solution consisted in evaporating the Br_2 by simple heating to 60°C. The first tests were not very conclusive, even after 48h of heating; therefore, an evaporation of Br_2 under nitrogen flow at 40°C was envisaged. In the laboratory, we previously used this type of evaporation for a fragile peptide [27] and we observed a notable improvement using partial and not total evaporation in a highly aqueous sample. The results showed that a partial evaporation (20min, 4psi, 40°C) led to a S/N ratio 4 times higher than the one obtained with total evaporation (1h, 4psi, 40°C). Finally, it is perfectly described in the literature that agitation time is a key point in a liquid-liquid extraction process [21]. Then, different stirring times (0.5 to 5min) were tested and the results are illustrated in Figure 2. An extraction rate close to 100% was measured when stirring is performed for 5min. However, long agitation led to an increased difficulty of separation of the diphasic system parallel to S/N ratio decrease. An additional step of centrifugation (3min at 12100×*g*) solved this problem by obtaining the maximum extraction rate as well as the best sensitivity.

These various optimizations allowed us to reach the target quantification limit (0.1µM), examples of chromatograms resulting from the final method (fully described in part 2.4) are given as in Figure 3.

3.2 Quality control of synthesized AuNP

Optimized method was first used to control the quality of AuNP synthesized in the laboratory. To ensure the complete conversion of gold salt into AuNP, a suspension of freshly made AuNP was analyzed with (quantification of AuNP and gold salt) or without (quantification of gold salt only) the Br_2 oxidation step. Reaction yield was calculated as 99.6±0.4% of gold salt converted into AuNP. To confirm this result, when a fresh AuNP suspension was centrifuged at 620,000×g for 20min and total gold was quantified into the supernatant, only 0.2±0.1% of gold under its salt form was found. The developed method was demonstrated to be specific of gold either as a salt or under its colloidal state.

3.3 Method validation

3.3.1 Linearity and limit of quantification

Linearity was evaluated for calibration curves using gold salt solutions and AuNP suspensions. Both were diluted in the range of 0.1 – 30.0µM using PBS. The Lower Limit of Quantification (LLOQ) was mathematically determined through the lowest concentration point with a relative standard deviation (RSD) inferior to 20% according to the FDA recommendations [26], and it was determined equal to 0.1µM in accordance with the targeted value. Results are summarized in Table 2 and indicate a good linearity for both gold states ($R > 0.997$). Slopes and intercepts were demonstrated statistically identical (at risk $\alpha = 5\%$) leading to the simple use of a gold salt standard solution to quantify AuNP after oxidation.

3.3.2 Accuracy

The recovery percentage of the method was measured through analyzing a standard solution (in triplicate) at three different concentrations (quality control samples at 0.2, 10.0 and 30.0µM). As described in Table 3, the accuracy remained satisfactory in the whole domain of linearity.

3.3.3 Precision

Repeatability (intra-day) and intermediate precision (inter-day) were determined through analysis (triplicate) of the sample (either gold salt or AuNP) at three different concentrations (0.2, 10.0 and 30.0µM). The RSD of each point was determined. The intermediate precision

was determined over a period of 3 days with 3 injections per day. Results are illustrated in Table 3 and it can be noticed a good precision of the method even at the lower concentration of 0.2µM (RSD < 11%).

3.4 Nanostructured film stability

Nanoparticles were immobilized into polymeric layer-by-layer films which were reported as interesting candidates for medical device coatings [11]. However, to complete the obtained data on their cyto/hemocompatibility, the proof of neither AuNP leakage from the coating nor the AuNP dissolution (resulting in gold salt) should be brought. As a direct application of the validated method, film stability was assessed under shear stress conditions. Shear stress (1.5Pa) was chosen to mimic forces applied on a medical device implanted inside an artery. This value (between 1 and 2Pa) corresponds to the physiological value of shear stress in vessels having a diameter of 6mm (small arteries such as coronaries) [28]. During experiments, gold released in medium was quantified, with or without Br_2 oxidation, at 12, 24 and 48h of exposure. The quantity found was below the LLOQ (0.1µM) in each case (Table 4). According to our calculation, this value corresponded to a loss of gold of 0.5% of the total AuNP present inside films. The quantity of immobilized AuNP on films was also evaluated after 48h of shear stress condition. No significant modification was observed confirming the capacity of the film to strongly anchor AuNP.

4. Conclusion

In summary, this study showed that AuNP under colloidal state or gold salt can be quantified by a simple, sensitive (0.1µM) and robust liquid chromatographic method coupled with visible detection and using ion-pairing extraction. Its application was successfully used to evaluate the gold content of citrate stabilized AuNP (quality control) and the stability of a layer-by-layer device coating incorporating AuNP. Further work will try to extend this method to other AuNP capped with various organic compounds and to gold measurement in biological materials and matrices: cells and tissues. This could help to go insight into the understanding of the possible AuNP biodistribution.

Acknowledgments

The authors thank Professor Patrick Menu (IMOPA, UMR7365 CNRS-UL) for lending the shear stress cell.

References

[1] R. Doolabh, H.D. Dullabh, L.M. Sykes, A comparison of preload values in gold and titanium dental implant retaining screws, J. Dent. Assoc. S. Afr. 69 (2014) 316-320.

[2] M. Gjuric, S. Schagerl, Gold prostheses for ossiculoplasty, Am. J. Otol. 19 (1998) 273-276.

[3] C.J. Murphy, A.M. Gole, J.W. Stone, P.N. Sisco, A.M. Alkilany, E.C. Goldsmith, S.C. Baxter, Gold nanoparticles in biology: beyond toxicity to cellular imaging, Acc. Chem. Res. 41 (2008) 1721-1730.

[4] J. Tournebize, A. Boudier, O. Joubert, H. Eidi, G. Bartosz, P. Maincent, P. Leroy, A. Sapin-Minet, Impact of gold nanoparticle coating on redox homeostasis Int. J. Pharmaceut. 438 (2012) 107-116.

[5] M. Wang, M. Thanou, Targeting nanoparticles to cancer, Pharm. Res., 62 (2010) 90-99.

[6] S.M. Shawky, A.M. Awad, W. Allam, M.H. Alkordi, S.F. El-Khamisy, Gold aggregating gold: A novel nanoparticle biosensor approach for the direct quantification of hepatitis C virus RNA in clinical samples, Biosens. Bioelectron. 92 (2017) 349-356.

[7] F. Lu, T.L. Doane, J.J. Zhu, C. Burda, Gold nanoparticles for diagnostic sensing and therapy, Inorg. Chim. Acta 393 (2012) 142-153.

[8] D. Pooja, S. Panyaram, H. Kulhari, B. Reddy, S.S. Rachamalla, R. Sistla, Natural polysaccharide functionalized gold nanoparticles as biocompatible drug delivery carrier, Int. J. Bio. Macromol. 80 (2015) 48-56.

[9] A.N. Kharlamov, A.E. Tyurnina, V.S. Veselova, O.P. Kovtun, V.Y. Shur, J.L. Gabinsky, Silica-gold nanoparticles for atheroprotective management of plaques: results of the NANOM-FIM trial, Nanoscale 7 (2015) 8003-8015.

[10] A. Quintanilla, S. Garcia-Rodriguez, C.M. Dominguez, S. Blasco, J.A. Casas, J.J. Rodriguez, Supported gold nanoparticle catalysts for wet peroxide oxidation, App. Cat. B: Env. 111-112 (2012) 81-89.

[11] A. Pallotta, M. Parent, I. Clarot, M. Luo, V. Borr, P. Dan, V. Decot, P. Menu, R. Safar, O. Joubert, P. Leroy, A. Boudier, Blood Compatibility of Multilayered Polyelectrolyte Film Containing Immobilized Gold Nanoparticles, Part. Part. Sys. Char. 34 (2017) 1600184.

[12] M.T. Ortega, J.E. Riviere, K. Choi, N.A. Monteiro-Riviere, Biocorona formation on gold nanoparticles modulates human proximal tubule kidney cell uptake, cytotoxicity and gene expression, Toxicol. In Vitro 42 (2017) 150-160.

[13] S. Si-Mohamed, D.P. Cormode, D. Bar-Ness, M. Sigovan, P.C. Naha, J.B. Langlois, L. Chalabreysse, P. Coulon, I. Blevis, E. Roessl, K. Erhard, L. Boussel, P. Douek, Evaluation of spectral photon counting computed tomography K-edge imaging for determination of gold nanoparticle biodistribution in vivo, Nanoscale (2017) DOI: 10.1039/c7nr01153a.

[14] J. Tournebize, A. Sapin-Minet, R. Schneider, A. Boudier, P. Maincent, P. Leroy, Simple spectrophotocolorimetric method for quantitative determination of gold in nanoparticles, Talanta 83 (2011) 1780-1783.

[15] S. Lopez-Sanz, N.R. Farinas, R.S. Vargas, R.D. Martin-Doimeadios, A. Rios, Methodology for monitoring gold nanoparticles and dissolved gold species in culture medium and cells used for nanotoxicity tests by liquid chromatography hyphenated to inductively coupled plasma-mass spectrometry, Talanta 164 (2017) 451-457.

[16] M. Matczuk, K. Anecka, F. Scaletti, L. Messori, B.K. Keppler, A.R. Timerbaev, M. Jarosz, Speciation of metal-based nanomaterials in human serum characterized by capillary electrophoresis coupled to ICP-MS: a case study of gold nanoparticles, Metallomics 7 (2015) 1364-1370.

[17] J. Liu, W. Liu, M. Xu, B. Wang, Z. Zhou, L. Wang, Sensitive detection of Au(III) using regenerative rhodamine B–functionalized chitosan nanoparticles, Sensors Actuat. B-Chem. 233 (2016) 361-368.

[18] M. Wang, L.N. Zheng, B. Wang, H.Q. Chen, Y.L. Zhao, Z.F. Chai, H.J. Reid, B.L. Sharp, W.Y. Feng, Quantitative analysis of gold nanoparticles in single cells by laser ablation inductively coupled plasma-mass spectrometry, Anal. Chem. 86 (2014) 10252-10256.

[19] S.A. Pergantis, T.L. Jones-Lepp, E.M. Heithmar, Hydrodynamic chromatography online with single particle-inductively coupled plasma mass spectrometry for ultratrace detection of metal-containing nanoparticles, Anal. Chem. 84 (2012) 6454-6462.

[20] M.S. El-Shahawi, A.S. Bashammakh, S.O. Bahaffi, Chemical speciation and recovery of gold(I, III) from wastewater and silver by liquid-liquid extraction with the ion-pair reagent amiloride mono hydrochloride and AAS determination, Talanta 72 (2007) 1494-1499.

[21] A. Hol, A.A. Kartal, A. Akdogan, A. Elci, T. Arslan, L. Elci, Ion pair-dispersive liquid-liquid microextraction coupled to microsample injection system-flame atomic absorption spectrometry for determination of gold at trace level in real samples, Acta Chim. Slov. 62 (2015) 196-203.

[22] I. De La Calle, F. Pena-Pereira, N. Cabaleiro, I. Lavilla, C. Bendicho, Ion pair-based dispersive liquid-liquid microextraction for gold determination at ppb level in solid samples after ultrasound-assisted extraction and in waters by electrothermal-atomic absorption spectrometry, Talanta 84 (2011) 109-115.

[23] Y. Wu, Z. Jiang, B. Hu, J. Duan, Electrothermal vaporization inductively coupled plasma atomic emission spectrometry determination of gold, palladium, and platinum using chelating resin YPA(4) as both extractant and chemical modifier, Talanta 63 (2004) 585-592.

[24] A. Pallotta, A. Boudier, P. Leroy, I. Clarot, Characterization and stability of gold nanoparticles depending on their surface chemistry: Contribution of capillary zone electrophoresis to a quality control, J. Chrom. A 1461 (2016) 179- 184.

[25] ICH Q2(R1) Note for Guidance on Validation of Analytical Procedures: Text and Methodology Ref. CPMP/ICH/381/95.

[26] Food and Drug Administration, Guidance for Industry, Bioanalytical Method Validation, Revision 1, September 2013.

[27] M. Parent, A. Boudier, P. Maincent, S. Gibot, H. Ait-Oufella, A. Boufenzer, L. Jolly, M. Derive, M. Kouach, J.-F. Goossens, P. Leroy and I. Clarot, LR12-peptide quantitation in whole blood by RP-HPLC and intrinsic fluorescence detection: Validation and pharmacokinetic study, Biomed. Chrom. 31 (2017) e3877.

[28] D. Giddens, C. Zarins, S. Glagov, The role of fluid mechanics in the localization and detection of atherosclerosis, J. Biomech. Eng. 115 (1993) 588-594.

Table 1: Overview of different gold quantification methods and their applications.

Method	LOD (µM)	Applications/media	Ref
Spectrophotometry	90.00	AuNP in aqueous medium	[11]
Fluorescence	1.52×10^{-2}	Gold salt in tap or lake water	[14]
LA-ICP-MS	0.14	AuNP in cells	[15]
LC-ICP-MS	2.60×10^{-4}		[12]
CE-ICP-MS	5.00×10^{-2}	AuNP in human serum	[13]
HDC-ICP-MS	1.10×10^{-5}	AuNP in aqueous medium	[16]
AAS	0.61	Gold salt in water and soils	[17]
FAAS	9.20×10^{-3}		[18]
ETAAS	4.30×10^{-5}		[19]
ETV-ICP-AES	3.80×10^{-2}		[20]

AAS: atomic absorption spectrometry, AES: atomic emission spectrometry, CE: capillary electrophoresis, ETAAS: electrothermal atomic absorption spectrometry, ETV: electrothermal vaporization, FAAS: flame atomic absorption spectrometry, HDC: hydrodynamic chromatography, ICP: inductively coupled plasma, LA: laser ablation, LC: liquid chromatography, LOD: Limit of detection, MS: mass spectrometry.

Table 2: Statistical evaluation of linearity for $AuCl_4^-$ and AuNP (0.1 – 30.0µM, 10 concentrations on three days) with a linear regression model.

Linear Model		Theoretical value	$AuCl_4^-$	AuNP
Range			[0.1-30.0µM]	
Slope			744	722
Standard deviation on slope			10	8
Intercept			-64	-76
Standard deviation on intercept			125	101
Correlation coeff. R			0.997	0.998
F regression	F-value 0.01	7.636	5066.358	7377.724
F Lack of fit	F-value 0.05	2.447	1.073	2.311
Intercept comparison	t-value 0.05	2.003	1.632	
Slope comparison	t-value 0.05	2.003	0.072	

Table 3: Evaluation of precision (3 injections for repeatability per day and 9 injections on 3 days for intermediate precision inter-days) and accuracy (3 concentrations in triplicate per day on 3 days covering the entire linearity range) given as mean with $\alpha = 0.05$.

	RSD run-to-run (%)	RSD day-to-day (%)	Accuracy (%)
30.0µM	1.24	6.81	98.65±6.71
10.0µM	3.24	10.37	108.28±11.19
0.2µM	10.91	8.54	81.57 ±5.42

Table 4: Quantification of gold in the circulating medium and into films during 48h of shear stress. (N.D.: not determined)

Time (h)	Gold in medium (µM)	Gold on films ($\times 10^{11}$ AuNP/cm²)
0	<0.1	9.4±2.2
12	<0.1	N.D.
24	<0.1	N.D.
48	<0.1	9.8±3.1

Figure Captions

Figure 1: Schematic representation of the shear stress cell for film stability evaluation.

Figure 2: Signal-to-noise ratio (□) and recoveries (■) obtained for High Quality Control (30.0µM) under different extraction conditions.

Figure 3: Typical chromatograms of AuNP (corresponding to $AuCl_4^-$ 5.0µM) (A), $AuCl_4^-$ at 5.0µM (B), 0.1µM (C) and blank in PBS (D).

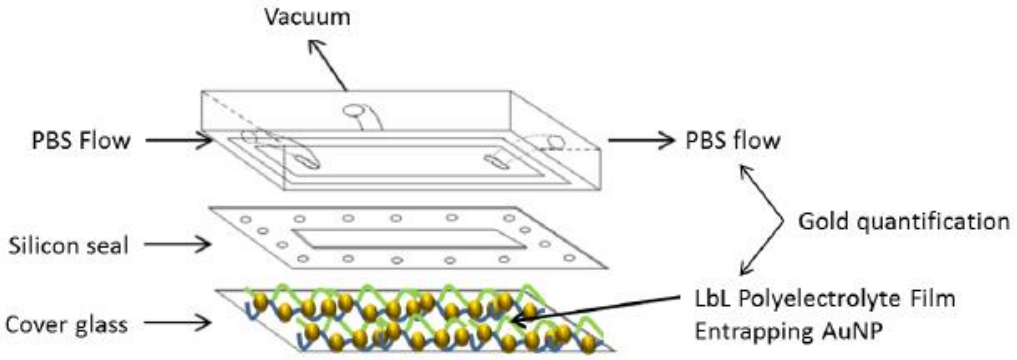

Figure 1

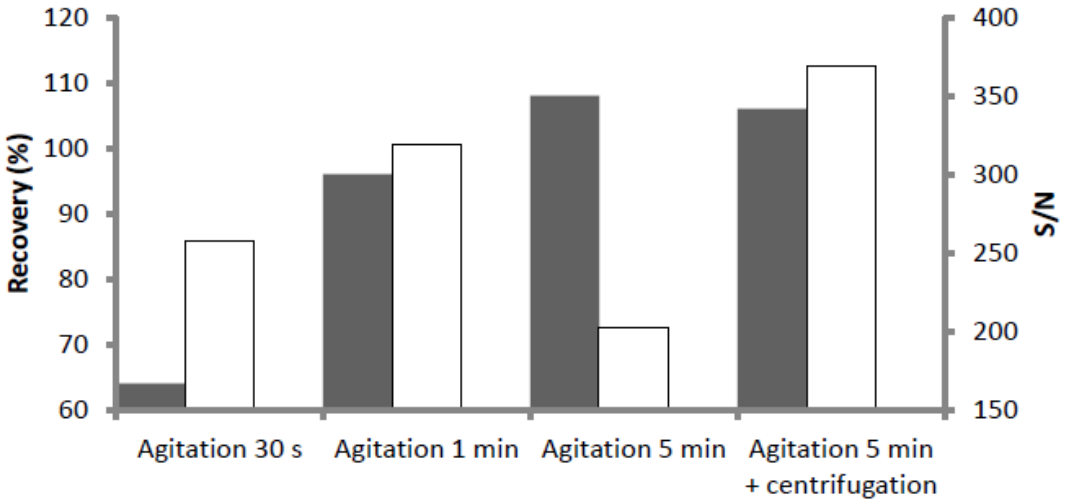

Figure 2

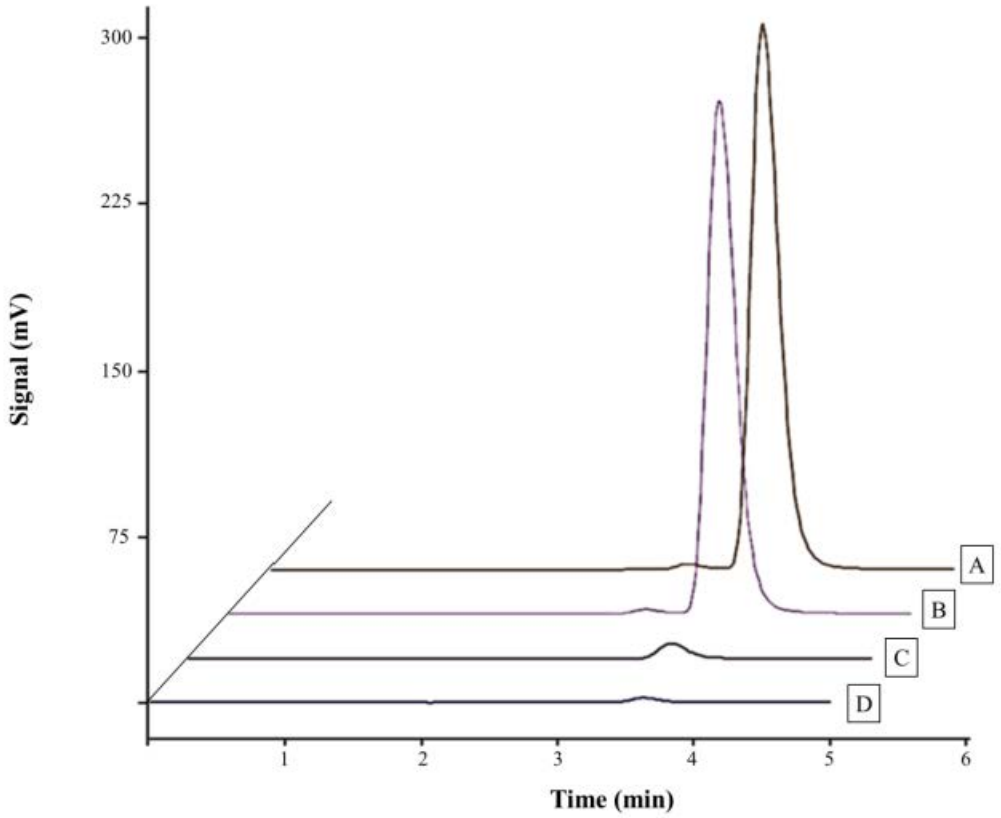

Figure 3

1.3. Conclusion

Le travail réalisé dans l'article nous a permis d'optimiser et de valider, selon des critères internationaux [96, 97], une méthode de dosage d'or précédemment initiée au laboratoire [93]. La validation a été effectuée en milieu modèle, prérequis obligatoire au dosage dans des matrices complexes telles que des milieux biologiques, cellulaires ou tissulaires en ajoutant une étape supplémentaire de prétraitement des échantillons (digestion et lyse des cellules et/ou tissus). Les résultats préliminaires obtenus après traitement des échantillons et application de la méthode décrite précédemment, sur cellules (lignée cellulaire U87 issues d'un glioblastomes et fournie par le laboratoire CRAN UMR 7039 (Centre de Recherche Automatique de Nancy)) et sur tissus (foies de rats Wistar) montrent cependant la présence d'un effet de matrice important (Figure 12). L'effet de matrice se caractérise par une réponse différente de l'analyte en fonction du milieu où la mesure est effectuée. Il est évalué par le rapport signal sur bruit (S/B) et est directement dépendant du milieu où est effectuée la mesure. En milieu aqueux, une concentration de 5 µM d'or amène un S/B égal à 400. La même concentration d'or mise en présence de cellules ou de tissus entraine une diminution du S/B à 53 et 30 respectivement, soit une diminution de plus de 86 % du rapport S/B pour une matrice composée uniquement de cellules et de 92 % lorsqu'il s'agit de tissu.

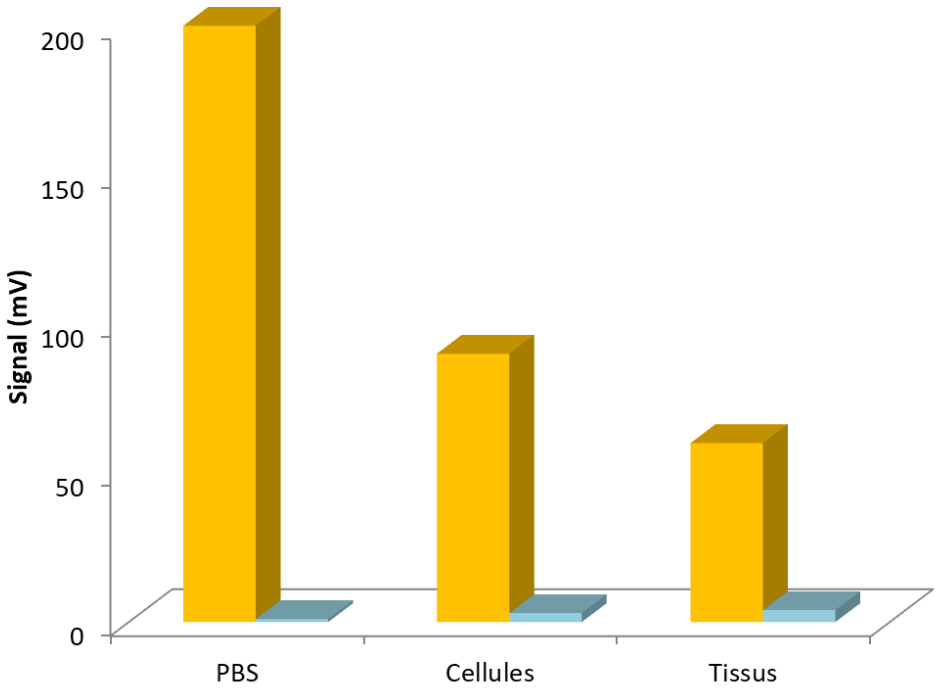

Figure 12 : Evolution du signal correspondant à 5 µM d'or (barres jaunes) ou 0 µM (barres bleues) en fonction des différentes matrices selon la méthode décrite précédemment. Avant quantification de l'or contenu dans 10^7 cellules ou 10 mg de tissus humides selon la méthode décrite dans l'article 2, une étape de digestion (HCl 6 M, 60 °C, 30 min) a été appliquée.

La première estimation des limites de détection de cette méthode dans les cellules et les tissus est respectivement de 0,5 µM et 1,7 µM. Ces valeurs, bien supérieures aux limites validées en milieu aqueux (0,1 µM), restent cependant dans les concentrations classiquement retrouvées dans la littérature lorsque des AuNP colloïdales sont utilisées comme vecteurs de médicaments [94, 95]. La prochaine étape est donc de valider la méthode dans les différents milieux biologiques d'intérêt selon les référentiels précédents.

Enfin, des études préliminaires de biodistribution d'AuNP ont été réalisées chez la souris en collaboration avec l'Institut Lumière Matière, UMR 5306 de Grenoble. 100 µL d'AuNP couplées à l'acide lipoïques (AuNP@LA, diamètre hydrodynamique de 9 ± 1 nm et potentiel zêta -36 ± 6 mV) ont été injectés chez trois souris par voie intraveineuse. Pendant l'injection et immédiatement après, aucune réaction inflammatoire locale ou générale n'a été

mise en évidence. Après la mise à mort, différents organes ont été prélevés (foie, poumons, rate). La présence d'or sous forme de sel ($AuCl_4^-$) ou de nanoparticules a ensuite été étudiée grâce à la technique du *laser induced breakdown spectroscopy* (LIBS). Le LIBS consiste à balayer la surface d'un échantillon avec un laser d'intensité modérée pour générer un plasma lumineux à sa surface. La lumière émise par le plasma est ensuite analysée pour en déterminer la composition chimique. Il s'agit d'une méthode très sensible car l'or est généralement absent des milieux biologiques (limite de détection de l'ordre du µg d'or par g de tissus). L'analyse des différents organes prélevés n'a révélé aucune accumulation d'or (sel ou nanoparticules) à 3, 6 et 24 h après l'injection (valeurs inférieures aux limites de détection). L'hypothèse avancée est que ces AuNP sont rapidement éliminées par le rein ou le foie. Ceci est probable compte tenu des travaux précédents de l'équipe qui ont montré leur inertie vis-à-vis de protéines (absence d'adsorption) de cellules immunitaires (absence d'initiation d'une réaction immunitaire) grâce à leur couronne d'acide lipoïque. L'hypothèse, sera confirmée par l'utilisation d'une cage métabolique et l'analyse des urines et des fèces. Cependant, l'absence d'accumulation *in vivo* de ces AuNP est une première preuve importante de la biocompatibilité des AuNP utilisées. Il faudra également s'assurer que ces résultats ne sont pas fonction de la couronne (AuNP@LA-GSH).

2. Contrôle qualité des AuNP

La méthode développée précédemment est spécifique de l'or, mais n'indique en rien la qualité des AuNP utilisées (indice de polydispersité, taille, charge, fonctionnalisation…). Peu d'études s'intéressent à la mise en place d'un contrôle qualité (CQ) rigoureux des nanoparticules lors de leur synthèse [98] et aucune quant à celle des AuNP. De plus, les méthodologies classiquement utilisées dans la caractérisation des nanoparticules

(spectrophotométrie UV-Vis., diffusion dynamique de la lumière (*dynamic light scattering*, DLS), microscopie électronique à transmission (MET), microscopie électronique à balayage (MEB) …) ne montrent qu'une estimation globale de la population et ne prennent pas en compte la présence ou non de substances apparentées (intermédiaires de synthèse ou produits de dégradation). Enfin, la grande variabilité de greffage possible à la surface des AuNP rend leur caractérisation compliquée.

Les nanoparticules utilisées comme matière première pharmaceutique ne sont habituellement pas analysées en termes de stabilité à court ou long terme. Dans l'article suivant (Article 3 paru dans *Journal of Chromatography A*) nous proposons une méthode d'analyse et de caractérisation basée sur l'ECZ.

2.1. L'électrophorèse capillaire de zone

L'ECZ constitue le mode de séparation le plus simple à mettre en œuvre et le plus utilisé parmi les techniques d'électrophorèse capillaire. La séparation des espèces est réalisée dans un capillaire rempli par un tampon de pH et de force ionique constants. Les différentes espèces injectées migrent à des vitesses différentes selon leur charge apparente et leur rayon hydrodynamique. Dans la littérature, seules quelques études se sont concentrées sur la séparation de nanoparticules en fonction de leur taille et de leur charge de surface [99, 100].

La vitesse de migration ou vitesse apparente (μ_{APP}) est constituée de la somme algébrique de la vitesse électrophorétique (μ_{EP}) et de la vitesse du flux électroosmotique (μ_{FEO}). Le flux électroosmotique (FEO) est dépendant de l'état de charge surface du capillaire (Figure 13). Au pH de travail (7,4), un capillaire en silice non recouverte est chargé négativement par la présence de groupement silanoate à sa surface. Cette charge de surface va permettre de faire bouger les cations contenus dans le tampon de migration. Ces cations

forment une couche attirée vers la cathode et entrainent la formation du FEO par un phénomène d'électro-osmose.

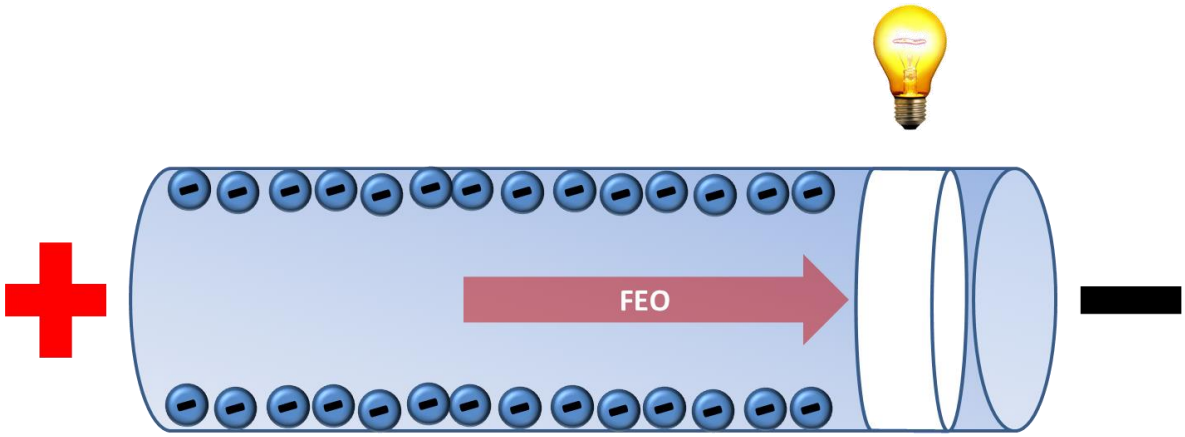

Figure 13 : Schématisation du flux électroosmotique.

Plus la surface du capillaire est chargée, plus le FEO qui en découle sera important (sans prendre en compte le sens de déplacement).

La vitesse (ou mobilité) électrophorétique est directement liée à un composé donné (rapport taille sur charge). La mobilité apparente de chaque espèce peut être calculée selon l'équation 1:

$$\mu_{app} = \mu_{ep} + \mu_{FEO} = \frac{L \times l}{T_m \times V} \quad (1)$$

avec : μ_{app}, μ_{ep} et μ_{FEO} les mobilités apparente, électrophorétique et le flux électro-osmotique respectivement ($cm^2.V^{-1}.s^{-1}$), L et l les longueurs totales et effectives du capillaire (cm), T_m le temps de migration de l'espèce considérée (s) et V le voltage appliqué (V).

Ainsi, les espèces cationiques seront accélérées et a contrario les espèces anioniques seront freinées. Les espèces neutres, quant à elles, ne seront ni attirées par l'anode ni par la cathode et migreront donc à la même vitesse que le FEO Selon le même principe, deux

populations différentes (tailles et/ou charges) d'AuNP auront donc un temps de migration différent (Figure 14).

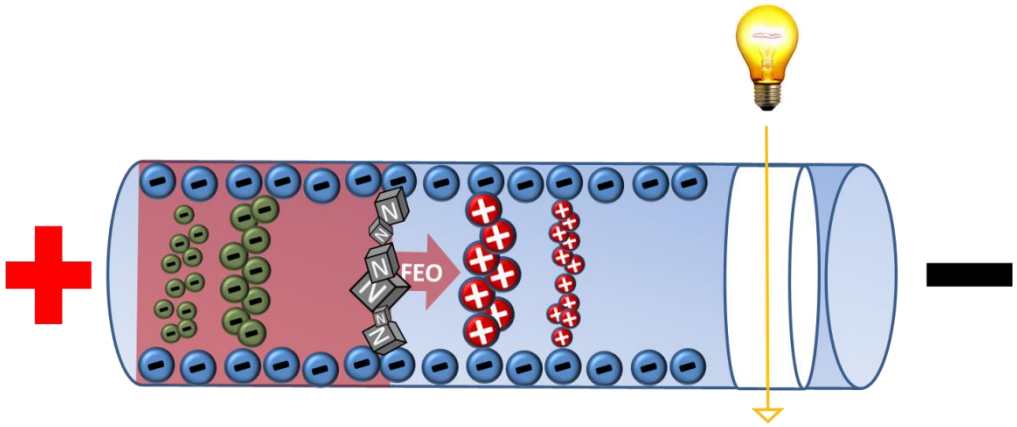

Figure 14 : Principe de séparation d'espèces chargées et neutres en ECZ.

Cette méthode séparative, nous a permis d'analyser différents lots d'AuNP et de confronter les résultats à ceux obtenus par les méthodes classiques. Le point principal mis en avant est la complémentarité des résultats obtenus par les différentes méthodes qui s'intègrent dans la mise en place d'un CQ des AuNP qui serait potentiellement applicable à d'autres types de NP.

2.2. Article 3 : Characterization and stability of gold nanoparticles depending on their surface chemistry : Contribution of capillary zone electrophoresis to a quality control.

Journal of Chromatography A, 1461 (2016) 179–184

Contents lists available at ScienceDirect

Journal of Chromatography A

journal homepage: www.elsevier.com/locate/chroma

Characterization and stability of gold nanoparticles depending on their surface chemistry: Contribution of capillary zone electrophoresis to a quality control☆

Arnaud Pallotta, Ariane Boudier, Pierre Leroy, Igor Clarot*

Université de Lorraine—CITHEFOR EA 3452, BP 80403, 54001 Nancy Cedex, France

ARTICLE INFO

Article history:
Received 27 April 2016
Received in revised form 11 July 2016
Accepted 12 July 2016
Available online 12 July 2016

Keywords:
Inorganic nanoparticles
Surface chemistry
Batch-to-batch survey
Conformity
Capillary zone electrophoresis
Photodiode array detection

ABSTRACT

Four kinds of gold nanoparticles (AuNP) quite similar in terms of gold core size (*ca.* 5 nm) and shape (spherical) but differing by their surface chemistry (either negatively, or positively charged, or neutral) were synthesized. They were analyzed using both the classical physicochemical approach (spectrophotometry, dynamic light scattering coupled or not to electrophoresis and transmission electron microscopy) and capillary zone electrophoresis equipped with photodiode array detection. The results obtained by both methodologies (related to Surface Plasmon Band-maximal absorbance wavelength-, and zeta potential and electrophoretic mobilities) were well correlated. Moreover, taking advantage of the separation method, the sample heterogeneity was evaluated and an impurity profile was extracted. This allowed setting some specifications which were then applied on the one hand to a batch-to-batch survey to declare NP as conform or not after production and on the other hand to a stability study.

1. Introduction

Nanoparticle development is an extensively growing research field especially for cancer diagnosis and treatment and among them gold nanoparticles (AuNP) are widely studied [1]. Indeed, they are characterized by several properties that have led two products to enter clinical trials (CYT-6091 [2] and Auroshell (ClinicalTrials.gov identifier: NCT01679470)). They are biocompatible, easily synthesized and can be functionalized by a wide range of active pharmaceutical ingredients, and their specific optical properties (Surface Plasmon Band) confer an interesting capacity to behave as biosensors or diagnostic agents [1,3].

However, now that they are translated from bench to bedside and in order to ensure patient safety, a rigorous quality control to frame minimal batch-to-batch variation should be defined. A physicochemical characterization is always performed using classical methodologies to define the nano-objects in terms of size, shape (light scattering, electron or atomic force microscopies, ...) and chemical composition (atomic spectroscopies, electroanalytical techniques, ...), but this approach does not take into account the profile of impurities and population polydispersity and still suffers from some limitations [4]. As a result, various separative methods have already been applied to NP analyzes: size exclusion chromatography [5], high performance liquid chromatography [6], flow field fractionation [7], and gel electrophoresis [8]. Capillary electrophoresis is also suitable for nanoparticle analyzes [9]. Focusing on AuNP, they were separated according to their size [10–12] and shape [13] with a high performance level obtained in separation resolution as well as in number of theoretical plates [14]. This method was also used to investigate their surface chemistry [10,15] and as a tool to monitor the nano-object stability (flocculation or aggregation) [16]. Therefore, capillary zone electrophoresis (CZE) has already been suggested as an appropriate method devoted to the quality control [9,13] of inorganic nanoparticles.

In this study, four kinds of AuNP were synthesized varying their surface chemistry in terms of charge (negatively charged using citrate ions, AuNP-Cit, neutral using a triblock copolymer polyethylene oxide-*b*-polypropylene oxide-*b*-polyethylene oxide, AuNP-COP, and positively charged using cetyltrimethylammonium, AuNP-CTA), as well as in terms of ligand binding energy (low energy with the previous cited ones *vs.* covalent binding using dihydrolipoic acid AuNP@DHLA). These AuNP were quite similar in terms of size (*ca.* 5 nm for the gold core) and shape (spherical). The aim of this work was to establish a quality control devoted to batch-to-batch NP production and to study their stability using the classical physicochemical approach usually applied

☆ Selected paper from 14th International Symposium on Hyphenated Techniques in Chromatography and Separation Technology, 27-29 January 2016, Ghent, Belgium.

* Corresponding author.
E-mail address: igor.clarot@univ-lorraine.fr (I. Clarot).

http://dx.doi.org/10.1016/j.chroma.2016.07.031
0021-9673/

to nanomedicines (*i.e.* UV–vis spectral properties, dynamic light scattering (DLS) coupled or not to electrophoresis (zeta potential, ζ), and transmission electron microscopy (TEM)) in parallel to CZE equipped with a diode array detection (DAD). As these nano-objects represent the mostly AuNP used in the literature, this work is the first, to the best of our knowledge, to evaluate a wide panel of quite similar AuNP only differing by their surface charge, and using the same methodology.

2. Materials and methods

2.1. Chemicals

All reagents and solvents were of analytical grade and used without further purification. Sodium borohydride, sodium citrate, α-dihydrolipoic acid, tetrachloroauric acid trihydrate ($HAuCl_4 \cdot 3H_2O$), Pluronic F-127, HCl 1 M and NaOH 1 M were supplied by Sigma Aldrich; boric acid and NaOH were purchased from Riedel-de-Haën and cetyltrimethylammonium bromide (CTAB) came from Prolabo. Phosphate-buffered saline (PBS) was prepared as follows: $[Na_2HPO_4] = 6.48 \times 10^{-3}$ M, $[KH_2PO_4] = 1.47 \times 10^{-3}$ M, $[NaCl] = 137.93 \times 10^{-3}$ M, and $[KCl] = 2.68 \times 10^{-3}$ M, final pH was adjusted to 7.4. Ultrapure water (>18.2 mΩcm) was used for the preparation of all solutions.

2.2. Gold nanoparticle synthesis and surface chemistry modification

Citrate stabilized AuNP (AuNP-Cit) and α-dihydrolipoic acid capped AuNP (AuNP@DHLA) were synthetized in aqueous solution according to previous works [17–19]. Briefly, 1 mL of $AuCl_4^-$ solution (10 mg/mL) was added into 90 mL of water and 2 mL of sodium citrate 55 mM was added. The solution was stirred for 1 min then 1 mL of $NaBH_4$ 19.5 mM was added and the solution was stirred for 5 min under nitrogen. The resulting suspension was immediately stored in the dark at 4 °C. Based on AuNP-Cit, three kinds of NP were prepared varying their surface chemistry.

Alpha-dihydrolipoic acid capped AuNP [20] (AuNP@DHLA) were prepared using 600 μmol of α-dihydrolipoic acid in 10 mL of 0.5 M NaOH solution added to 25 mL of freshly prepared AuNP-Cit. The reaction mixture was stirred under inert atmosphere for 24 h at room temperature (20–23 °C). A dialysis against PBS for 48 h using a bag (regenerated cellulose with a cut-off of 6–8 kDa (Roth® France)) was performed. The dialysis medium was changed to fresh PBS after 24 h.

Pluronic F-127 stabilized AuNP (AuNP-COP) were prepared by mixing 5 mL of 90 nM AuNP-Cit with 5 mL 0.4 μM Pluronic F-127 in water. The reaction mixture was stirred under inert atmosphere at room temperature for 4 h to perform the ligand exchange.

Cetyltrimethylammonium stabilized AuNP (AuNP-CTA) were prepared by mixing 5 mL of 90 nM AuNP-Cit with 5 mL 10 mM CTAB in water. The reaction mixture was stirred under inert atmosphere at room temperature for 4 h.

The final concentration reaches 90 nM for each kind of AuNP obtained and they were stored in the dark at 4 °C.

2.3. AuNP characterization

A UV–vis spectrophotometer (UV-1800 Shimadzu) was used for spectra recordings and absorbance measurements. The hydrodynamic diameter (Dh) and ζ of AuNP were measured at 20 ± 1 °C using a Zetasizer Nano ZS (Malvern Instruments, UK). All Dh values are volume averaged, based on three independent measurements realized on at least three AuNP batches. Zeta potential measurements were carried out in ultrapure water (implying preliminary dialysis of AuNP@DHLA for 4 h). All surface charges are mean values based on three independent measurements realized on three AuNP batches. Transmission electron microscopy images were recorded using a Philips CM 200 instrument with a LaB6 cathode operating at 200 kV. Gold NP suspensions were deposited onto a 400 mesh carbon film copper grids. The average diameter of the gold core (Dc) was calculated for each AuNP sample by counting *ca.* 200 individual particles from the TEM images.

2.4. Capillary zone electrophoresis

Capillary Zone Electrophoresis measurements were carried out using a P/ACE MDQ CE system (Beckman Coulter) equipped with a diode array detector (DAD, λ from 200 to 600 nm). Measurements were performed at 25 ± 1 °C using a 40 cm bare silica capillary (effective length: 34 cm). For anionic and neutral AuNP species, the background electrolyte (BGE) was a 25 mM boric acid/sodium borate buffer pH 8.5 adjusted with 40% (m/V) NaOH. AuNP detection was performed under 12 kV (normal polarity, cathodic electroosmotic flow, EOF). For the cationic AuNP-CTA, a reverse polarity method was used (−12 kV), the BGE was changed to 25 mM sodium borate buffer pH 8.5 containing 0.5 mM of CTAB (below critical micellar concentration (CMC) *i.e.* 1.0 mM). 90 nM of AuNP were injected hydrodynamically (20 mbar for 20 s). The capillary was rinsed with NaOH 1.0 M (2 min), ultrapure water (2 min) and BGE (2 min) before each injection. The EOF was determined using the neutral marker, benzyl alcohol, (migration time = 2.06 ± 0.03 min, EOF = $9.1 \pm 0.1 \times 10^{-4}$ cm^2 V^{-1} s^{-1} (n = 5)). AuNP@DHLA suspensions were dialyzed against water for 4 h before injection.

Each injection was made in triplicate and the obtained peaks were identified by their relative migration time (RMT):

$$RMT = T_m / T_{mneutralmarker}$$

in which T_m is the migration time of the peak of interest and $T_{mneutralmarker}$ is the migration time of the neutral species.

3. Results and discussion

3.1. Gold nanoparticle characterization

3.1.1. Classical approach

Results of AuNP characterization performed by the classical physicochemical approach as well as by CZE are presented in Table 1, Figs. 1 and 2. Visible spectra of AuNP (Fig. 1 and Table 1) highlighted the Surface Plasmon Band (λ_{max}) which is specific of these nano-objects. Surface Plasmon Band of AuNP is due to "the collective oscillation of the conducting electrons of metal NP when their frequency matches that of the incident electro-magnetic radiations" [21]. It mainly depends on NP size and aggregation, shape, core/corona composition and suspension medium (interparticle distance, dielectric constant) [21]. After ligand exchange or grafting from AuNP-Cit to prepare to other kinds of particles, a red shift was observed (increase of λ_{max}), which reflected the surface chemistry modification. The images obtained by TEM (Fig. 1) showed well-individualized AuNP whatever the considered surface chemistry without the presence of any aggregate. The values of Dc (corresponding to the gold core) for AuNP-Cit, AuNP@DHLA, AuNP-COP and AuNP-CTA were similar (5.0 ± 0.8, 4.9 ± 0.7, 5.2 ± 0.7 and 6.4 ± 1.2 nm, respectively). The values of Dh (including gold core, surface chemistry and some hydration layers) were larger than Dc (Table 1), as expected. The overall results (λ_{max}, Dh and Dc) were in accordance with previously reported studies [18,22,23]. Surface potential values of prepared AuNP corresponded well to the charge conferred by capping of citrate anions or cetyltrimethylammonium cations or neutral copolymer or by grafting of dihydrolipoate anion (Table 1). Concerning AuNP-CTA, ligand exchange may not be fully

Table 1
Physicochemical characterization of AuNP using the classical approach and CZE after synthesis (D0) and 20 days of storage (D20). Results are expressed as mean ± standard deviation of at least three independent batches. D0 values are used as specifications to compare with D20. Values out of specifications after 20 days are marked in grey.
Physicochemical characterization of AuNP using the classical approach and CZE after synthesis (D0) and 20 days of storage (D20). Results are expressed as mean ± standard deviation of at least three independent batches. D0 values are used as specifications to compare with D20. Values out of specifications after 20 days are marked in grey.

AuNP		Classical approach			CZE		
	Batch	λ_{max} (nm)	Dh (nm)	ζ potential (mV)	μ_{EP} ($\times 10^{-4}$ cm^2 V^{-1} s^{-1})	λ_{max} (nm)	Assay (%)
D0							
Cit		514 ± 1	6.5 ± 0.9	−32.6 ± 0.7	−1.75 ± 0.44	521 ± 3	88.7 ± 2.5
DHLA		521 ± 1	9.0 ± 0.3	−36.8 ± 3.7	−2.83 ± 0.30	518 ± 3	82.4 ± 5.0
COP		519 ± 3	6.2 ± 0.8	−2.6 ± 2.0	−0.27 ± 0.10	521 ± 8	100.0 ± 0.0
CTA		522 ± 1	16.2 ± 1.2	45.4 ± 2.9	14.77 ± 1.70	521 ± 9	100.0 ± 0.0
D20							
Cit	1	517	6.6	−29.8	−5.01	525	82.2
	2	515	6.5	−16.0	−4.88	528	63.7
	3	518	7.9	−13.6	−1.68	520	100.0
DHLA	1	521	8.8	−37.4	−3.14	522	93.3
	2	521	7.7	−40.3	−4.71	514	89.2
	3	521	8.7	−38.9	−3.19	516	76.5

completed with some remaining citrate ions even if the global charge of the prepared AuNP shifted from negative to positive.

3.1.2. Capillary zone electrophoresis

Electrophoregrams of synthesized AuNP are presented in Fig. 1 and Table 1. Detection was performed from 200 to 600 nm in order to monitor in the same experiment AuNP migration (Surface Plasmon Band, *ca.* 520 nm) and impurity profile (214 nm). The Surface Plasmon Band was determined on each major peak and assessed the presence of AuNP. Their electrophoretic mobilities (μ_{EP}) were in accordance with their surface chemistry: negative values for AuNP-Cit (in relation of previously reported values [11]) and AuNP@DHLA, value near zero for AuNP-COP and positive value for AuNP-CTA. These results were well correlated to the ones found by the classical physicochemical approach (on the one hand values of λ_{max} collected by UV–vis spectrophotometer and DAD, and on the other hand ζ and electrophoretic mobilities) as illustrated in Fig. 2.

From electrophoregrams obtained at day 0, as far as AuNP-Cit, AuNP@DHLA are concerned, an impurity profile was collected. As no certified standard with known purity exists, in a first approximation and to compare the different batches, the assay corresponding to the main product percentage was determined by a classical normalization process (corrected area of the main peak versus the total corrected area). From these data, the main product assay was calculated; a minimum of 80% was obtained for each kind of AuNP (Table 1). According to ICH Q2(R1) recommendations [24], the limit of detection was calculated as a Signal on Noise Ration equal to 3. This value represents 2.6 ± 0.5% of the product main peak. Some impurities, which may origin from either the raw materials and/or degradation products, were pointed out: uncoupled ligands, AuNP-Cit (they were the first step of the other AuNP synthesis), uncapped or ungrafted gold core leading to AuNP aggregation, and heterogeneous surface coating. The latter case represents the most problematic one since their physicochemical properties depend on time storage (size and charge related to gold atom number and loss of surface functionalization, and molar absorbance coefficient). As an example, in the case of AuNP-Cit, only neutral impurities were detected representing 11.3 ± 2.5% of the sample (mean of the three batches recorded at D0 in Table 2).

However, CZE was not suitable for AuNP-COP and AuNP-CTA analyzes. Concerning AuNP-COP, as their surface charge is neutral, they migrate only with the EOF and at the same RMT than the one corresponding to all neutral species (even neutral impurities). For the cationic AuNP-CTA, the methodology previously described was not well-adapted as the main peak obtained corresponded to an anionic one (migration after neutral species) indicating the loss of CTA capping. So, the migration was performed in presence of CTAB in BGE (concentration under the surfactant CMC) in order to annihilate EOF and to maintain the gold core functionalization. A positive electrophoretic mobility was indeed measured but this modification limited the possibility to screen the whole profile of impurities.

From this characterization study, specifications (Table 1) were set in order to establish the conformity or the rejection of each newly synthesized AuNP batch (Table 3), as well as to monitor their stability (Tables 1 and 2).

Table 2
Impurity profile of AuNP-Cit by CZE analyzes after synthesis (D0) and after 20 days of storage (D20) recorded at 214 nm.

AuNP-Cit	Batch #	1	2	3
D0				
Main peak	RMT	1.19 ± 0.08	1.24 ± 0.05	1.06 ± 0.03
	CA	14730 ± 1855	14710 ± 2354	9300 ± 2892
	CA%	91.6 ± 2.2	87.2 ± 1.0	87.3 ± 2.5
Neutral Species	RMT	1.00	1.00	1.00
	CA	1354 ± 210	2167 ± 248	1357 ± 123
	CA%	8.4 ± 2.2	12.8 ± 1.0	12.7 ± 2.5
D20				
Main peak	RMT	1.38 ± 0.07	1.37 ± 0.02	1.00
	CA	31152 ± 4142	16328 ± 1948	94147 ± 19916
	CA%	82.2 ± 1.1	63.7	100.0
Neutral Species	RMT	1.00	1.00	
	CA	625 ± 180	207 ± 43	
	CA%	1.6 ± 0.3	0.8 ± 0.1	
Impurity A	RMT	1.52 ± 0.04	1.52 ± 0.03	ND
	CA	1062 ± 149	1222 ± 108	ND
	CA%	2.8 ± 0.1	4.8 ± 0.1	ND
Impurity B	RMT	ND	1.56 ± 0.02	ND
	CA	ND	7857 ± 338	ND
	CA%	ND	30.7 ± 1.6	ND
Impurity C	RMT	1.80 ± 0.09	ND	ND
	CA	5062 ± 192	ND	ND
	CA%	13.4 ± 1.3	ND	ND

CA: Corrected Area; CA%: Corrected Area (%); ND: Not Detected.

3.2. Batch-to-batch survey

The analysis of each newly synthesized batch was performed both by the classical physicochemical approach and by CZE. Results are presented in Table 3. For some batches, values out of specifications were obtained by both the classical physicochemical approach and CZE (batch # 6 for AuNP-Cit, AuNP-COP and AuNP-CTA). However, as far as AuNP@DHLA is concerned, only CZE rejected batch # 4 proving that this methodology may be complementary to the

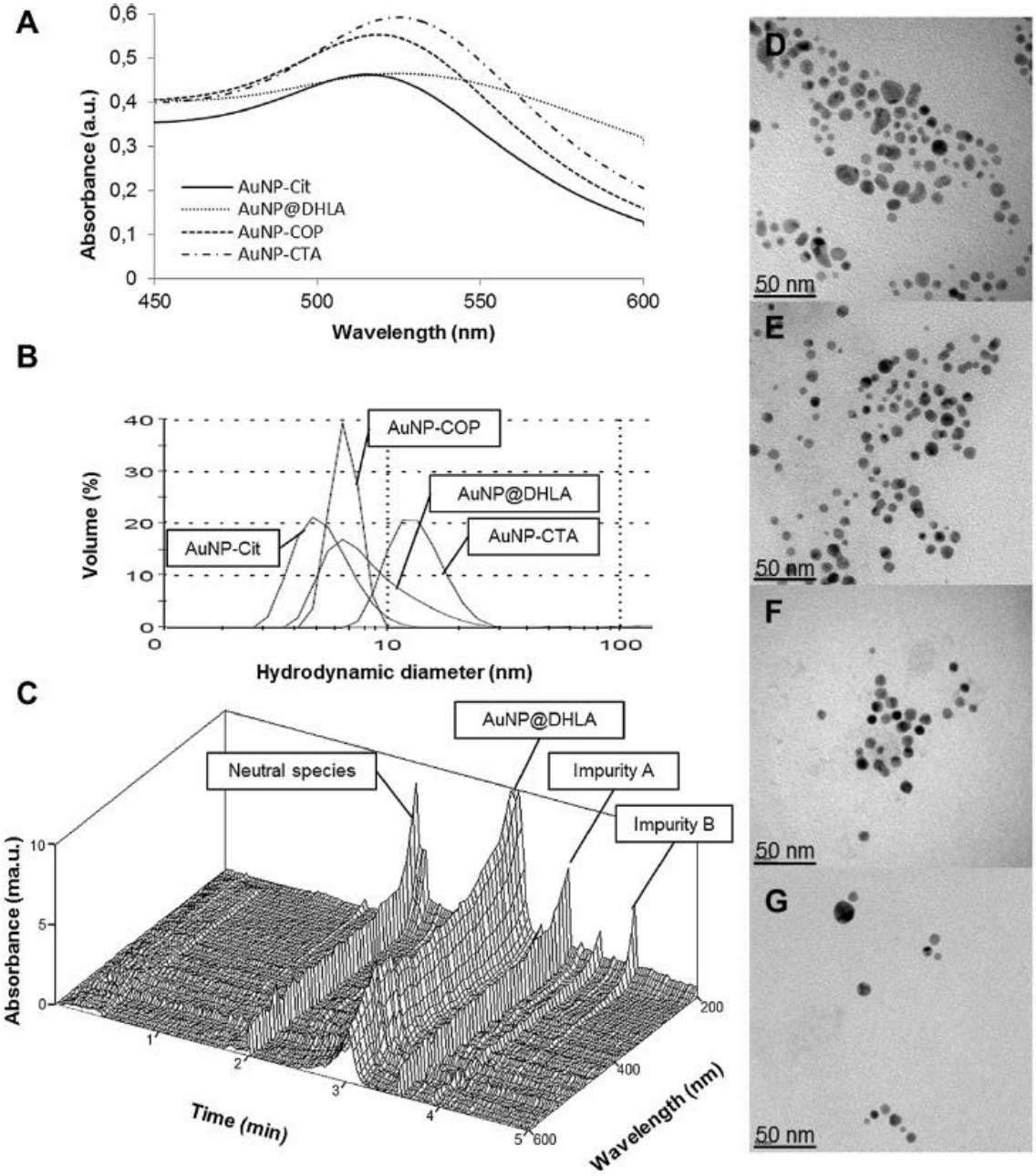

Fig. 1. Physicochemical characterization of AuNP by spectrophotometry (A), dynamic light scattering (B), CZE (C: performed on AuNP@DHLA) and TEM analyzes on AuNP-Cit (D), AuNP@DHLA (E), AuNP-COP (F) and AuNP-CTA (G).

physicochemical approach to survey the NP production. We can conclude that the use of a separation method which focuses on the major population (main peak) is more discriminant than the classical global approach. This conclusion shows the complementarity of the two methodologies used in this work and demonstrates the usefulness of capillary electrophoresis in the field of pharmaceutical quality process.

3.3. Stability study

A stability study was conducted between day 0 and day 20, AuNP being stored at 4 °C, in the dark. Day 20 was chosen as it corresponded to half the time of the reported AuNP@DHLA stability (monitored by the classical physicochemical approach) [18]. In our study, these NP should be the most stable ones due to the covalent bonds between the gold core and the sulfur atoms of DHLA. After this storage period, AuNP-Cit (Tables 1 and 2), AuNP-COP and AuNP-CTA were not stable (data not shown), being out of specifications determined by both the classical physicochemical approach and CZE. Moreover, if one focus on AuNP-Cit batch # 3, it was excluded by the value of the assay (100.0%) measured by CZE, since its related impurity profile was not in accordance with the one recorded at day 0: the main peak overlaid the one of the neutral species (Table 2). Therefore, hypothesis concerning the batch #3 in Table 2 could be a neutralization of AuNP (loss of functionalization), or a possible aggregation leading to an increase of the particle size. Such particles migrate too fast (anionic species with a higher size) with our method which is not dedicated to this size range (migration time similar than neutral species). This fact proved that a good agreement exists between the two method-

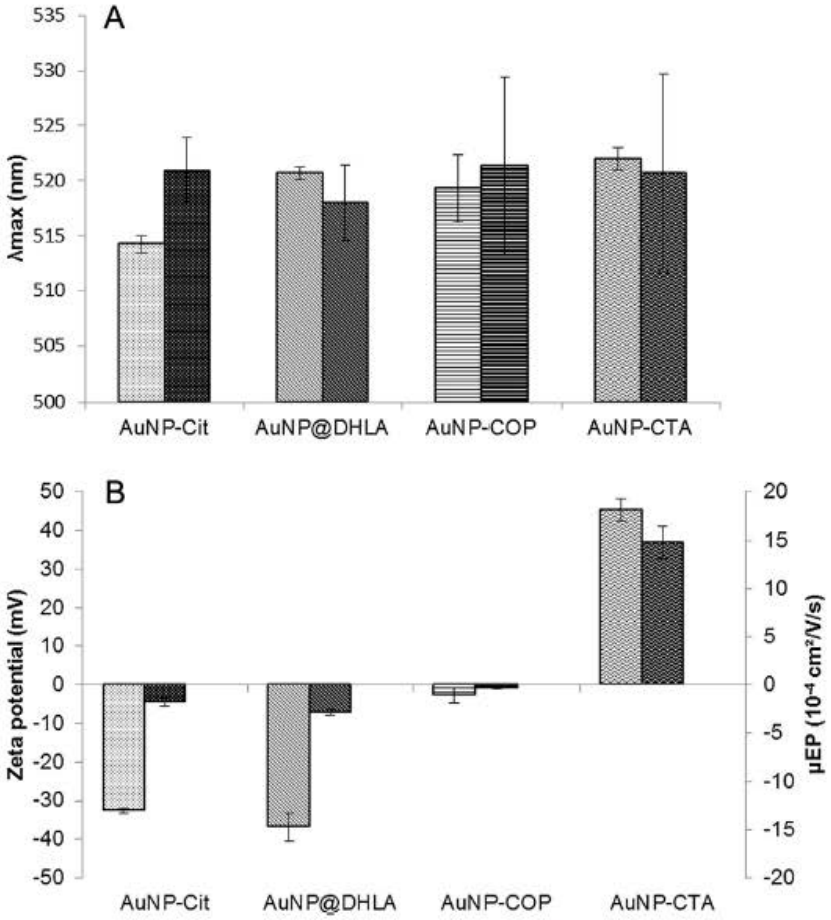

Fig. 2. Correlation of results obtained by the classical physicochemical approach (open bars) and CZE (close bars) according to on the one hand Surface Plasmon Band and on the other hand surface charge (ζ) and electrophoretic mobilities.

Table 3
Batch-to-batch survey of the three kinds of AuNP (for each batch the obtained result and the criterion of conformity (C) or rejection (R) is indicated).

	Classical approach			CZE		
	λ_{max} (nm)	Dh (nm)	ζ potential (mV)	μ_{EP} ($_x 10^{-4}.cm^2.V^{-1}.s^{-1}$)	λ_{max} (nm)	Assay (%)
AuNP-Cit						
Specifications	514 ± 1	6.5 ± 0.9	−32.6 ± 0.7	−1.75 ± 0.44	521 ± 3	>86.0
Batch # 4	514 (C)	6.8 (C)	−32.3 (C)	−2.19 (C)	524 (C)	91.6 (C)
Batch # 5	515 (C)	7.1 (C)	−32.1 (C)	−1.39 (C)	520 (C)	87.2 (C)
Batch # 6	518 (R)	7.2 (C)	−13.3 (R)	−1.23 (R)	526 (R)	87.3 (C)
AuNP@DHLA						
Specifications	521 ± 1	9.0 ± 0.3	−36.8 ± 3.7	−2.83 ± 0.30	518 ± 3	>77.0
Batch # 4	521 (C)	9.3 (C)	−33.4 (C)	−2.48 (R)	522 (R)	78.0 (C)
Batch # 5	520 (C)	8.8 (C)	−40.5 (C)	−3.00 (C)	516 (C)	81.4 (C)
Batch # 6	521 (C)	9.1 (C)	−36.4 (C)	−3.00 (C)	516 (C)	87.8 (C)
AuNP-COP						
Specifications	519 ± 3	6.2 ± 0.8	−2.6 ± 2.0	−0.27 ± 0.10	521 ± 8	NA
Batch # 4	516 (C)	6.7 (C)	−1.4 (C)	−0.23 (C)	520 (C)	–
Batch # 5	520 (C)	6.7 (C)	−4.6 (C)	−0.20 (C)	514 (C)	–
Batch # 6	522 (C)	5.3 (R)	−10.6 (R)	−0.38 (R)	530 (R)	–
AuNP-CTA						
Specifications	522 ± 1	16.2 ± 1.2	45.4 ± 2.9	14.77 ± 1.70	521 ± 9	NA
Batch # 4	522 (C)	16.8 (C)	43.5 (C)	13.21 (C)	512 (C)	
Batch # 5	522 (C)	16.9 (C)	48.3 (C)	14.51 (C)	530 (C)	
Batch # 6	522 (C)	14.9 (R)	44.0 (C)	16.59 (R)	520 (C)	

NA: Not Applicable.

ologies. As far as AuNP@DHLA are concerned, only one batch (# 2) was rejected by both approaches after 20 days in accordance with previously reported results [18]. This highlighted the fact that AuNP@DHLA are the most stable ones, as expected, since the ligand is linked to the gold core through covalent bonds, on the contrary to low energy bonds for three other ligands [16,25]. However, the

two other batches were out of specifications only according to CZE analysis because of either λ_{max} or assay deviations emphasizing the complementarity aspect of this technique compared to the classical approach.

4. Conclusion

In this study, four kinds of AuNP only differing by their surface chemistry were analyzed by the classical physicochemical approach and CZE. The results obtained by both methodologies proving a good agreement and some advantages and drawbacks can be cited:

- Classical physicochemical approach:

1 Advantages: evaluation of an average population and possibility to reuse the samples.
2 Drawbacks: at least two different devices used with a large volume of sample (1 mL which corresponds to 4000.10^9 AuNP).

- CZE:

1 Advantages: population heterogeneity spotting and assay determination in a small volume of sample (150 nL which corresponds to $0.6.10^9$ AuNP).
2 Drawbacks: DAD specific to NP possessing optical properties (or modification of detection mode) with no possibility to reuse samples.

As a conclusion, this work demonstrates that CZE is an efficient tool to frame batch-to-batch variations in order to set a quality control as well as to evaluate NP stability in a complementary manner to the classical approach.

Acknowledgement

This work was financially supported by Université de Lorraine (project 2015- AAP-002-100, supervisor: Dr A. Boudier).

References

[1] H.C. Huang, S. Barua, G. Sharma, S.K. Dey, K. Rege, Inorganic nanoparticles for cancer imaging and therapy, J. Control. Release 155 (2011) 344–357.
[2] S.K. Libutti, G.F. Paciotti, A.A. Byrnes, H.R. Alexander Jr., W.E. Gannon, M. Walker, G.D. Seidel, N. Yuldasheva, L. Tamarkin, Phase I and pharmacokinetic studies of CYT-6091, a novel PEGylated colloidal gold-rhTNF nanomedicine, Clin. Cancer Res. 24 (2010) 6139–6149.
[3] P. Ghosh, G. Han, M. De, C.K. Kim, V.M. Rotello, Gold nanoparticles in delivery applications, Adv. Drug. Deliv. Rev. 60 (2008) 1307–1315.
[4] F. Laborda, E. Bolea, G. Cepria, M.T. Gomez, M.S. Jimenez, J. Perez-Arantegui, Detection, characterization and quantification of inorganic engineered nanomaterials: a review of techniques and methodological approaches for the analysis of complex samples, Anal. Chim. Acta 904 (2016) 10–32.
[5] G.S. Duesberg, J. Muster, V. Krstic, M. Burghard, S. Roth, Chromatographic size separation of single-wall carbon nanotubes, Appl. Phys.–Mater. Sci. Process 67 (1998) 117–119.
[6] V.L. Jimenez, M.C. Leopold, C. Mazzitelli, J.W. Jorgenson, R.W. Murray, HPLC of monolayer-protected gold nanoclusters, Anal. Chem. 75 (2003) 199–207.
[7] A. Zattoni, D.C. Rambaldi, P. Reschiglian, M. Melucci, S. Krol, A.M. Coto Garcia, Asymmetrical flow field-flow fractionation with multi-angle light scattering detection for the analysis of structured nanoparticles, J. Chromatogr. A. 1216 (2009) 9106–9112.
[8] J.Y. Kim, H.B. Kim, D.J. Jang, Electrophoretic separation of gold nanoparticles according to bifunctional molecules-induced charge and size, Electrophoresis 34 (2013) 911–916.
[9] I. Clarot, C. Wolpert, V. Morosini, R. Schneider, L. Balan, L. Diez, Optimization of CDTE quantum dots synthesis using capillary zone electrophoresis curr, Nanosci 5 (2009) 154–159.
[10] E. Ban, Y.S. Yoo, E.J. Song, Analysis and applications of nanoparticles in capillary electrophoresis, Talanta 141 (2015) 15–20.
[11] F.K. Liu, A high-efficiency capillary electrophoresis-based method for characterizing the sizes of Au nanoparticles, J. Chromatogr. A 1167 (2007) 231–235.
[12] F.K. Liu, M.H. Tsai, Y.C. Hsu, T.C. Chu, Analytical separation of Au/Ag core/shell nanoparticles by capillary electrophoresis, J. Chromatogr. A 1133 (2006) 340–346.
[13] N. Surugau, P.L. Urban, Electrophoretic methods for separation of nanoparticles, J. Sep. Sci. 32 (2009) 1889–1906.
[14] F.K. Liu, Extremely highly efficient on-line concentration and separation of gold nanoparticles using the reversed electrode polarity stacking mode and surfactant-modified capillary electrophoresis, Anal. Chim. Acta 694 (2011) 167–173.
[15] A.I. Lopez-Lorente, M. Laura Soriano, M. Valcarcel, Analysis of citrate-capped gold and silver nanoparticles by thiol ligand exchange capillary electrophoresis, Microchim. Acta. 181 (2014) 1789–1796.
[16] M.R. Ivanov, H.R. Bednar, Investigations of the mechanism of gold nanoparticle stability and surface functionalization in capillary electrophoresis, A.J. Haes Acs. Nano 3 (2009) 386–394.
[17] J. Tournebize, A. Boudier, O. Joubert, H. Eidi, G. Bartosz, P. Maincent, Impact of gold nanoparticle coating on redox homeostasis, Int. J. Pharm. 438 (2012) 107–116.
[18] J. Tournebize, A. Boudier, A. Sapin-Minet, P. Maincent, P. Leroy, R. Schneider, Role of gold nanoparticles capping density on stability and surface reactivity to design drug delivery platforms, ACS. Appl. Mater. Interfaces 4 (2012) 5790–5799.
[19] J. Tournebize, A. Sapin-Minet, R. Schneider, A. Boudier, P. Maincent, P. Leroy, Simple spectrophotocolorimetric method for quantitative determination of gold in nanoparticles, Talanta 83 (2011) 1780–1783.
[20] S. Roux, B. Garcia, J.-L. Bridot, M. Salom&#x00E9, C. Marquette, L. Lemelle, P. Gillet, L. Blum, P.I Perriat, O. Tillement, Characterization of dihydrolipoic acid capped gold nanoparticles, and functionalization by the electroluminescent luminol, Langmuir 21 (2005) (2005) 2526–2536.
[21] D. Vilela, M. Cristina Gonzalez, A. Escarpa, Sensing colorimetric approaches based on gold and silver nanoparticles aggregation: chemical creativity behind the assay. A review, Anal. Chim. Acta 751 (2012) 24–43.
[22] T. Sakai, P. Alexandridis, Single-step synthesis and stabilization of metal nanoparticles in aqueous pluronic block copolymer solutions at ambient temperature, Langmuir 20 (2004) 8426–8430.
[23] J. Tang, J. Huang, S.Q. Man, Preparation of gold nanoparticles by surfactant-promoted reductive reaction without extra reducing agent, Spectrochim. Acta A. Mol. Biomol. Spectrosc. 103 (2013) 349–355.
[24] ICH Q2(R1) Note for Guidance on Validation of Analytical Procedures: Text and Methodology Ref. CPMP/ICH/381/95.
[25] E. Pensa, E. Cortes, G. Corthey, P. Carro, C. Vericat, M.H. Fonticelli, The chemistry of the sulfur–gold interface: in search of a unified model, Acc. Chem. Res. 45 (2012) 1183–1192.

2.2.1. Conclusion

Dans l'article 3, la complémentarité entre les méthodes classiquement utilisées pour l'étude des nanoparticules et l'électrophorèse capillaire de zone a été démontrée. Avant le développement du contrôle en ECZ, la stabilité des lots était évaluée par un contrôle de la bande plasmon de résonnance, une mesure du diamètre hydrodynamique et du potentiel zéta. Lorsqu'une valeur sortait des spécifications (*i.e.* 514 ± 1 nm, 6 ± 1 nm et -36 ± 4 mV pour les AuNP stabilisées par des ions citrate), le lot était considéré comme non conforme. Avec les méthodes classiques, la stabilité des AuNP était évaluée à environ 40 jours. L'ECZ a mis en évidence qu'un lot présentant une bande plasmon spécifique dans l'intervalle défini pouvait présenter des non-conformités en termes de dispersité de population ou de charge de surface. A titre d'exemple, au bout de 20 jours, 61 % des lots synthétisés était déclarés conformes par les méthodes classiques et seulement 28 % par l'ECZ (sur 18 lots indépendants). Ces résultats ont eu pour principale conséquence d'améliorer l'appréciation de la stabilité des lots grâce à la méthode développée.

3. Fonctionnalisation et nitrosation des AuNP

3.1. Introduction

La fonctionnalisation des nanoparticules peut être envisagée selon deux principales stratégies : directe ou indirecte (Figure 15).

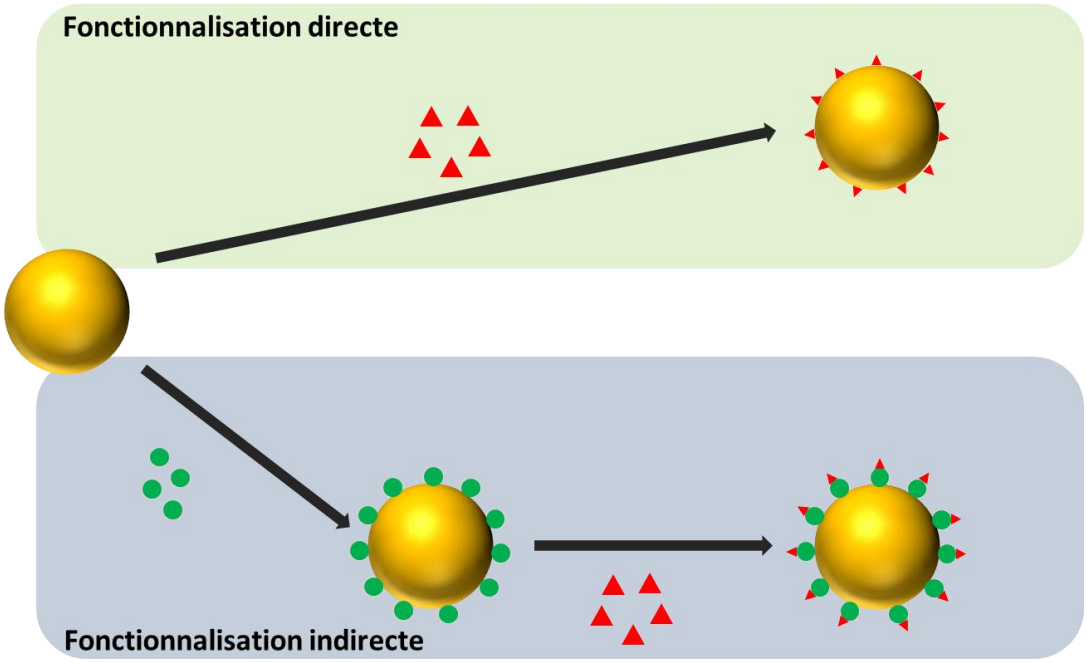

Figure 15 : Les deux voies de fonctionnalisation principale d'une nanoparticule.
▲ : principe actif d'intérêt. ● : bras d'ancrage.

La première stratégie consiste à fonctionnaliser directement la particule avec le principe actif d'intérêt (▲). La fonctionnalisation directe est simple car elle ne requiert qu'une seule étape. La principale limite de cette méthode peut être l'incompatibilité entre le groupement fonctionnel du principe actif et la méthode de couplage. Dans notre cas, la fonctionnalisation directe par du *S*-nitrosoglutathion (GSNO) (Figure 16) entrainerait le clivage de la liaison S-NO [101] et donc une perte de la fonction d'intérêt. La fonctionnalisation directe par du glutathion (GSH) suivie de sa nitrosation n'est également pas envisageable [4].

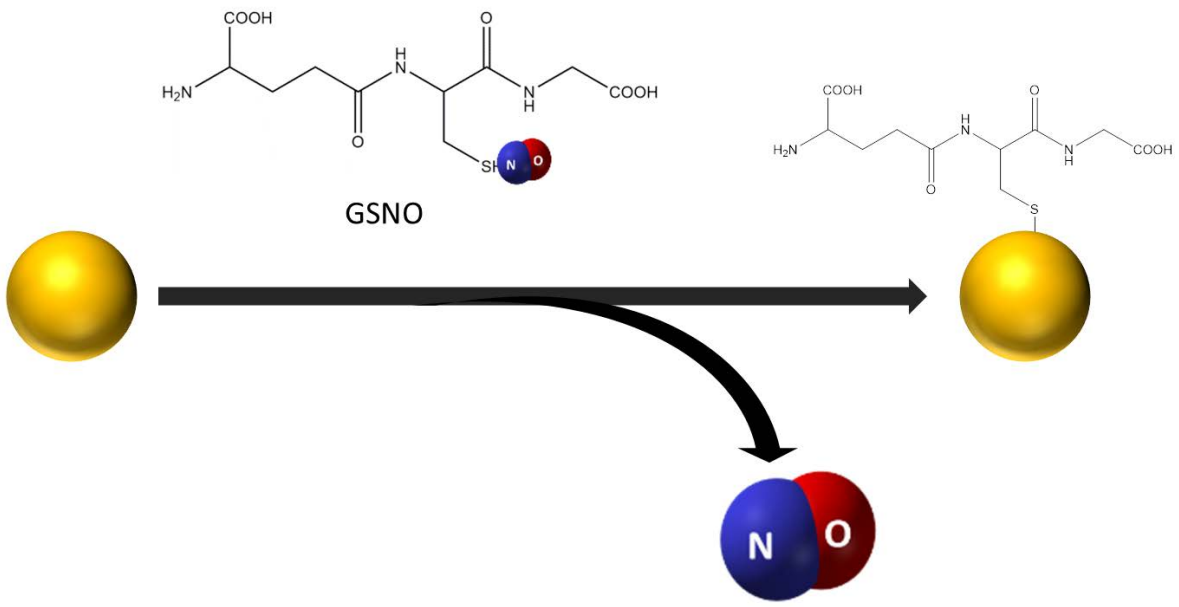

Figure 16 : Fonctionnalisation directe d'une AuNP par une molécule de GSNO.

La solution repose sur la fonctionnalisation indirecte. Elle nécessite une étape de greffage supplémentaire au cours de laquelle un bras d'ancrage (un *spacer*, ●) est greffé à la surface de la nanoparticule avant d'y ajouter le principe actif d'intérêt. Le *spacer* utilisé dans notre protocole est l'acide lipoïque (LA) dont la fonction acide carboxylique pourra être couplée pour former une liaison amide avec le GSH (**Figure 17**) [5]. Ceci a déjà été réalisé au laboratoire lors de travaux précédents et a montré la possibilité de greffer 7500 ± 2500 molécules de GSH par AuNP avec une fonction -SH préservée (AuNP@LA-GSH) [4].

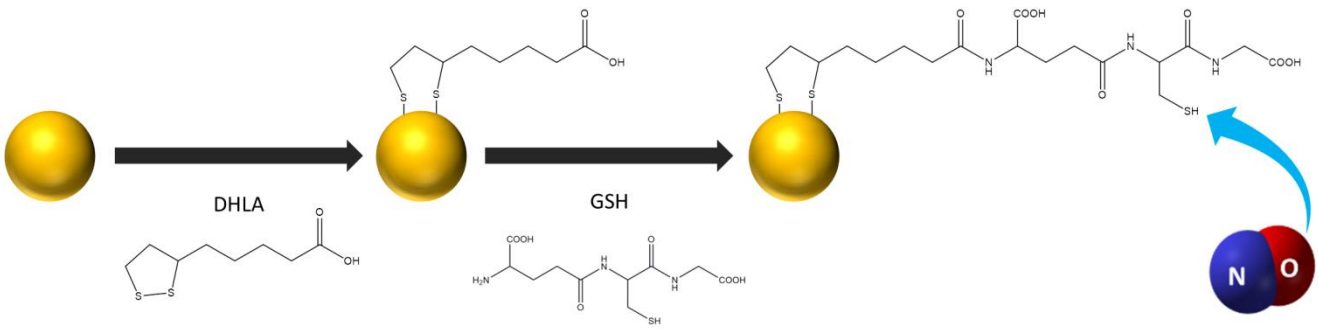

Figure 17 : Fonctionnalisation indirecte d'une AuNP par du GSH *via* un greffage à l'acide lipoïque.

Cependant, la fonctionnalisation des AuNP@LA-GSH par NO, selon le protocole classiquement utilisé au laboratoire, nécessite des conditions incompatibles avec les particules (1 h à 4 °C dans HCl 0,5 M). En effet, la modification de pH, de force ionique, ainsi que la dilution des AuNP entraine systématiquement leur précipitation. Il n'est donc pas possible de nitroser directement des AuNP fonctionnalisées par GSH.

Pour pallier à ce problème, le phénomène de transnitrosation a été étudié. La transnitrosation est une réaction chimique spécifique entre un thiol (R-SH) et un RSNO qui consiste en l'échange d'un groupement NO d'un donneur vers un receveur (Figure 18).

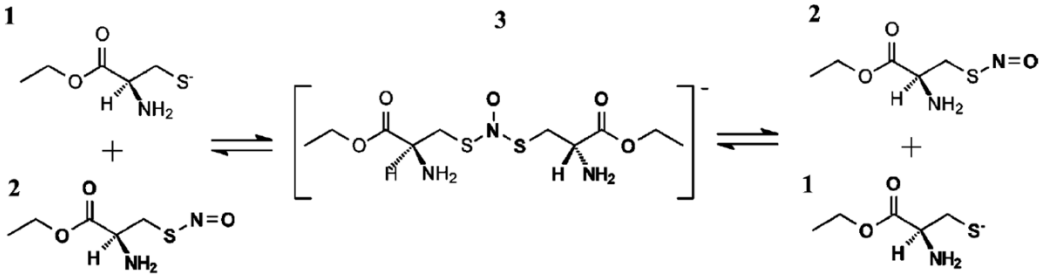

Figure 18 : Réaction de transnitrosation entre une (1) cystéine ester et une (2) *S*-nitrosocystéine ester, et (3) l'intermédiaire réactionnel selon [102].

Pour mimer le transfert d'un groupement NO d'un RSNO vers une AuNP@LA-GSH, l'albumine sérique de bœuf a été utilisée. L'albumine est une protéine majoritairement présente dans la circulation sanguine (40 g/L). Son diamètre hydrodynamique (7 nm) proche de celui des AuNP synthétisées et son groupement thiol disponible (résidu cystéine 34) en font un modèle simple pour étudier les phénomènes de transitrosation entre un RSNO et une NP. Les conditions de transnitrosation sont celles du plasma (pH, force ionique et température physiologiques) ce qui est parfaitement toléré par les AuNP [84], Enfin, les différences de masse molaire entre un RSNO de faible masse molaire (le donneur de NO) et l'albumine (l'entité receveuse) sont intéressantes pour permettre leur séparation et la purification de l'albumine nitrosée en fin de réaction. Ces éléments sont explorés dans l'article suivant. Le taux de nitrosation de l'albumine sera évalué en fonction de l'espèce utilisée pour la nitrosation. Trois familles différentes seront testées : le nitrite de sodium en milieu acide comme substance de référence, trois RSNO (GSNO, *S*-nitrosocystéine et *S*,*S*-dinitrosobucillamine) et enfin du diéthylamine NONOate (donneur de nitrate organiques).

3.2. Article 4 : Albumin as a carrier for NO delivery preparation physicochemical characterization and interaction with gold nanoparticles

DRUG DEVELOPMENT AND INDUSTRIAL PHARMACY, 2016
VOL. 42, NO. 12, 1928–1937
http://dx.doi.org/10.1080/03639045.2016.1182546

Taylor & Francis
Taylor & Francis Group

RESEARCH ARTICLE

Albumin as a carrier for NO delivery: preparation, physicochemical characterization, and interaction with gold nanoparticles

Ming Luo[a], Ariane Boudier[a], Arnaud Pallotta[a], Philippe Maincent[a], Jean-Baptiste Vincourt[b,c] and Pierre Leroy[a]

[a]Université de Lorraine – CITHEFOR EA 3452, Nancy Cedex, France; [b]Université de Lorraine – IMoPA, UMR 7365 CNRS, Vandœuvre-lès-Nancy Cedex, France; [c]Proteomics Platform of Fédération de Recherche 3209, Biopole de la Faculté de Médecine de Nancy, Vandœuvre-lès-Nancy Cedex, France

ABSTRACT

Background: Nitric oxide (NO) is a gaseous transmitter playing numerous physiological roles and characterized by a short half-life. Its binding to endogenous thiols increases its stability, facilitating its storage and transport. The purpose of this study was to investigate the nitrosated serum albumin (SA-SNO) and to provide a reference for its easy preparation for further use in *in vitro* studies.

Methods: Serum albumin (SA) was *S*-nitrosated by reacting with (i) $NaNO_2$ in acidic medium; (ii) different low-molecular weight *S*-nitrosothiols (RSNO) (*S*-nitrosocysteine (CysNO), *S*-nitrosoglutathione (GSNO), and *S,S'*-dinitrosobucillamine ($Buc(NO)_2$)); and (iii) diethylamine NONOate (DEA/NO). SA-SNO was purified by size exclusion chromatography and the *S*-nitrosation site and the rate were studied by mass spectrometry and Griess–Saville assay, respectively. Then, SA-SNO was characterized by spectrofluorimetry, dynamic light scattering, and circular dichroism. Finally, SA-SNO reactivity with citrate stabilized gold nanoparticles (AuNP-citrate) was investigated *via* determination of NO release.

Results: *S*-nitrosation rates of SA were 90.1 ± 3.3, 76.8 ± 2.7, 80.3 ± 3.2, 84.8 ± 5.0, and $15.4 \pm 1.9\%$ ($n = 5$), when SA was reacted with acidified $NaNO_2$, CysNO, GSNO, $Buc(NO)_2$, and DEA/NO, respectively. The physicochemical characterization indicated that the resulting product corresponded to a mono-*S*-nitrosothiol (on cysteine-34), and the conformational construction remained unchanged. Stability studies showed that the NO content was preserved over 1 week. AuNP-citrate reacted with SA-SNO with increase of its hydrodynamic diameter but preservation of SNO bond.

Conclusions: SA-SNO prepared and stored under the reported conditions affords a well-defined reference suitable for *in vitro* studies.

ARTICLE HISTORY
Received 10 September 2015
Revised 20 April 2016
Accepted 20 April 2016
Published online 17 May 2016

KEYWORDS
Citrate-stabilized gold nanoparticles; conformational study; serum albumin; S-nitrosation processes; stability

Introduction

Serum albumin (SA) occupies a pivotal position as it is the most abundant circulatory protein in mammals. It displays an extraordinary affinity for a wide range of ligands, plays key physiological roles in transport, distribution, and metabolism of many endogenous and exogenous compounds[1]. As a versatile protein carrier, SA is biocompatible and biodegradable, non-toxic as well as non-immunogenic, which makes it an ideal material for drug delivery[2]. Over the last decades, SA derivatives have emerged as functional carriers available on the market, mainly for diagnosing and treating cancer, rheumatoid arthritis, diabetes, and infectious diseases among others[3].

Nitric oxide (NO), first known as the endothelium-derived relaxing factor, is biosynthesized from L-arginine, dioxygen, and NADPH by catalysis of three NO synthase isoforms[4]. In mammals, NO is an important cellular signaling molecule involved in many physiological and pathological processes, especially in the cardiovascular system. They include vascular smooth muscle cell relaxation, antiplatelet effect, immune and blood pressure regulation[5]. *S*-nitrosation of the free thiol groups found in endogenous compounds including proteins and low-molecular weight compounds leads to *S*-nitrosothiols (RSNO), the most important ones in the body being *S*-nitrosoglutathione (GSNO) and *S*-nitrosated serum albumin (SA-SNO). The latter corresponds to the storage and transport of NO, exhibiting a long half-life in the range of several hours compared with a few seconds for the gaseous radical NO. Thus SA-SNO plays an important role in maintaining NO pool, especially in pathological states.

S-nitrosation of SA operated *in vitro* has been widely investigated but so far very few works regard the preservation of its native form during the process. Indeed, SA is frequently denaturated before *S*-nitrosation to increase the number of available reactive thiol groups by reducing disulfide bonds. At the same time, an additional chemical reaction with Traut's reagent (2-iminothiolane) was often operated to increase more considerably this number. A codification of the various SA-SNO forms resulting from those different approaches has been published[6], and we have summarized here the different pathways used in the literature to *S*-nitrosate native SA (bovine (BSA) as well as human (HSA) SA) (Table 1).

Based on the literature overview of *S*-nitrosation processes, the most frequently methods used to *S*-nitrosate native SA are the reaction with either NO gas or $NaNO_2$ in acidic medium (nitrous acid), or *S*-transnitrosation by reacting with low-molecular weight RSNO or with 1-substituted diazen-1-ium-1,2-diolates, also called NONOates. From a physicochemical point-of-view, there is a need to easily and quickly obtain native SA-SNO as a well-defined product for various biochemical, pharmacological, and bioanalytical assays included in preclinical studies. In the present work, three kinds of processes to obtain SA-SNO were compared: (i) reaction

CONTACT Pierre Leroy pierre.leroy@univ-lorraine.fr Université de Lorraine – CITHEFOR EA 3452, BP 80403, Nancy Cedex 54001, France

Table 1. Literature overview of methods for *S*-nitrosation of native serum albumin.

SA type	Nitrosation reagents and molar equivalent (eq.)	Purification method	Quantification method	*S*-nitrosation rate	Ref.
BSA	200, 500, and 1000 eq. $NaNO_2$/HCl	Ultrafiltration	Saville–Griess assay	73.9–65.8%[a]	7
BSA	1 eq. $NaNO_2$/HCl	None	Saville–Griess assay	0.85 SA-SNO/BSA[b]	8
BSA, HSA	$NaNO_2$/HCl	None	UV–vis at 345 and 545 nm	Not indicated	9
BSA	1 eq. $NaNO_2$/H_2SO_4	None	UV–vis at 334 nm and Saville–Griess assay	100%[a]	10
BSA	NO gas in anaerobic conditions	None	Ellman's assay	No SA-SNO obtained	11
HSA in human plasma	Butylnitrite	Centrifugation and chromatography (HiTrapBlue Sepharose affinity column)	GC-MS *via* Saville–Griess assay	90.9%[a]	12
BSA	3 eq. GSNO	SEC (PD10 column)	Saville-Griess assay	0.35 SA-SNO/BSA[b]	13
BSA	10, and 40 eq. low molecular weight RSNO[c]	None	Ellman's assay	Not indicated	14
BSA	20 eq. CysNO	SEC (Sephadex G-25)	NO electrode	Not indicated	15
BSA	SNO-4B[d]	Gravity precipitation	Saville–Griess assay	No SA-SNO obtained	16

[a]*S*-nitrosation rate based on thiol content within SA.
[b]*S*-nitrosation rate based on SA.
[c]Low molecular weight *S*-nitrosated thiol (L-cysteine ethyl ester, dimethylaminoethanethiol, L-cysteine, GSH, mercaptoethylamine, 2-mercaptoethanol).
[d]*S*-nitroso-glutathionyl-sepharose 4B beads.

with $NaNO_2$ in acidic medium by initially mixing the same molar equivalent of nitrite ions and free thiol; (ii) *S*-transnitrosation by reacting with an excess of low molecular weight RSNO at pH 7.4, and (iii) reaction with diethylamine NONOate (DEA/NO) at pH 7.4 (Figure 1). The *S*-nitrosation site was studied by mass spectrometry (MS) and the *S*-nitrosation rates were measured by Saville–Griess assay. The possible conformational changes were investigated by different physicochemical methods. Stability studies of purified SA-SNO were performed to define optimal storage conditions. Lastly, the prepared SA-SNO, used as a model of endogenous RSNO, was incubated with citrate stabilized gold nanoparticles (AuNP-citrate) to study their reactivity and to estimate further biocompatibility of AuNP-citrate in blood.

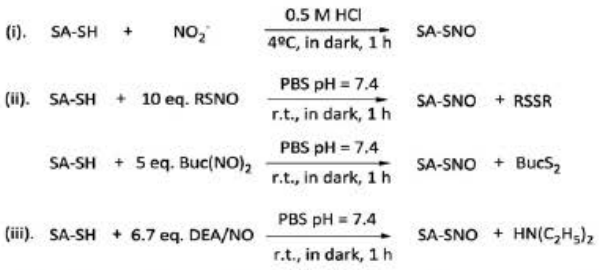

Figure 1. Reaction scheme of the three pathways used for mono-*S*-nitrosated serum albumin (SA-SNO) synthesis: (i) reaction with nitrite ions in acidic medium; (ii) *S*-transnitrosation with low-molecular weight *S*-nitrosothiols (CysNO, GSNO or Buc(NO)$_2$); $BucS_2$ is 8,8-dimethyl-6-oxo-1,2,5-dithiazocane-4-carboxylic acid; (iii) reaction with NO released from diethylamine NONOate (DEA/NO).

Materials and methods

Chemicals and reagents

All chemicals and solvents were of analytical reagent grade and used without further purification. All solutions and experiments were prepared in deionized ultrapure water (>18.2 MΩ cm). SA (BSA Cohn fraction V, powder), DEA/NO, iodoacetic acid (IAA), *N*-ethylmaleimide (NEM), ascorbic acid, and trichloroacetic acid (TCA) were purchased from Sigma-Aldrich (St. Louis, MO), and Sephadex® G-25 (Fine) was provided by GE Healthcare Company (Chicago, IL). Bucillamine (2-[(2-methyl-2-sulfanylpropanoyl)amino]-3-sulfanylpropanoic acid; Buc) was purchased from Fine Chemicals Discovery (San Diego, CA). Phosphate buffer saline solution (PBS pH 7.4, 0.148 M) was prepared as follows: 8 g NaCl, 0.2 g KCl, 0.2 g KH_2PO_4, 0.92 g Na_2HPO_4 were dissolved in 1 L of water.

S-nitrosoglutathione and *S,S'*-dinitrosobucillamine (Buc(NO)$_2$) were synthesized and quantified as previously described[17,18]; *S*-nitrosocysteine (CysNO) was obtained according to the same protocol. Briefly, 9 ml of reduced glutathione (GSH), cysteine, or Buc solution prepared at a free thiol concentration of 20 mM in 0.5 M HCl were added to 1 ml of 200 mM $NaNO_2$ solution. After 1 h incubation at 4 °C in the dark, the reaction was stopped by neutralization with 0.5 ml of a 40% (w/v) NaOH solution and the volume was finally completed to 20.0 ml with 0.5 M phosphate buffer pH 7.4. The concentration of prepared low molecular weight RSNO solutions was assayed by measuring absorbance at 334 nm and using their molar absorbance: $\varepsilon = 922\ M^{-1}\ cm^{-1}$ for GSNO, $\varepsilon = 900\ M^{-1}\ cm^{-1}$ for CysNO, and $\varepsilon = 1720\ M^{-1}\ cm^{-1}$ for Buc(NO)$_2$ (UV–vis spectrophotometer model UV-1800, Shimadzu Corporation, Kyoto, Japan). As an example, residual amount of nitrite ions in GSNO was 0.57% (w/w). All low molecular weight RSNO solutions were stored at 4 °C before further use. A Clark electrode (Hansatech, Hansatech Instruments Ltd., King's Lynn, UK) was used to measure the O_2 concentration in the reaction medium. Calibration was operated with deionized water oxygenated by exposing to air with intense magnetic stirring (100% O_2, 260 nmol/ml) and an addition of sodium dithionite (0% O_2).

Ellman's assay

The free thiol content in SA was determined by using Ellman's assay. Briefly, 5,5'-dithiobis-(2-nitrobenzoic acid) at 1 mM was reacted with SA in 0.1 M phosphate buffer pH 7.4 at room temperature (rt) in the dark for 10 min. The absorbance of the released 5-thio-2-nitrobenzoic acid was measured at 412 nm and a calibration curve built with GSH as the standard in the range 3–30 μM.

Serum albumin S-nitrosation and reaction with N-ethylmaleimide

Serum albumin (final protein concentration: 176 μM, thiol concentration measured by Ellman's assay: 100 μM) was *S*-nitrosated by

three different synthetic pathways (excess of *S*-nitrosation reagents were based on thiol concentration), as follows:

(i) *S*-nitrosation of SA with nitrous acid was realized as previously reported[8]. A 10 mM $NaNO_2$ solution was prepared in degassed water, and SA (116.5 mg) was dissolved in ca. 3.5 ml of water in a 10.0 ml volumetric flask. Then, 5 ml of 1 M HCl and 1 ml of 1 mM $NaNO_2$ solution were added, and the volume was filled up to 10.0 ml with water. The resulting mixture was sealed and kept in the dark at 4 °C for 1 h. At last, 0.5 ml of 40% (w/v) NaOH solution was added and the volume was completed to 20.0 ml with 0.5 M phosphate buffer pH 7.4.

(ii) *S*-transnitrosation was operated by mixing SA and a 10-fold molar excess of GSNO, CysNO or a five-fold molar excess of $Buc(NO)_2$ in PBS, and incubating in a sealed 10.0 ml volumetric flask in the dark at rt for 1 h.

(iii) *S*-nitrosation by NO released from DEA/NO was acted by mixing SA and a 6.7-fold molar excess of DEA/NO in PBS and incubating in a sealed 10.0 ml volumetric flask in the dark at rt for 1 h.

Each protocol was performed on 5 independent replicates and on two different SA batches. In some experiments, thiol function of SA was blocked using *N*-ethylmaleimide (NEM). A 10-fold excess of NEM (a final concentration of 1.76 mM) was reacted on SA (a final concentration of 0.176 mM) in PBS pH 7.4, 0.148 M. Then, SA-NEM was purified using the size exclusion chromatography described below. After purification, according to Ellman's assay, no thiol content in SA-NEM (a protein content of 65 µM) was measured (below the limit of quantification which is equal to 3 µM).

Griess and Saville–Griess assays

Nitrite ion and RSNO concentrations were determined by using Griess and Saville–Griess assays, respectively, as previously described[19]. Briefly, samples were diluted with 1.75 M acetoacetic buffer pH 2.5, in order to obtain a final volume of 200 µl. Calibration curves were performed in the range 1.0–10.0 µM, using $NaNO_2$ and GSNO (exact concentration determined using molar absorbance at 334 nm) as the standards for Griess and Saville–Griess assays, respectively. As concerned the Griess assay, 40 µl of sulfanilamide solution (0.6% (w/v) prepared in 0.4 M HCl) were added to the previously diluted sample. After a 3 min incubation in the dark at rt, 10 µl of *N*-1-(naphthyl)ethylenediamine solution (0.6% (w/v) prepared in 0.4 M HCl) were added and another 5 min incubation period at rt was acted before the measurement. The same operating conditions were used for the Saville–Griess method, but the sulfanilamide solution was added with $HgCl_2$ (0.2% w/v). The quantification of RSNO was performed using Saville–Griess result compensated by Griess result in parallel. The absorbance was measured by using a 96-well microplate reader equipped with a 570 nm filter (Bio-TEK Instrument, INC®, Winooski, VT). The methods were validated according to Food and Drug Administration guidelines[20]. The linearity for Griess and Saville–Griess methods was checked in the range 1.0–10.0 µM, with corresponding equations of the regression lines: A (absorbance at 570 nm) = 0.0161 × [NO_2^-] (±0.0010) + 0.0384 (±0.0037); coefficient of determination, $r^2 = 0.995$ (6 points, $n = 5$) and A = 0.0180 × [GSNO] (±0.0017) + 0.0367 (±0.0063); $r^2 = 0.995$ (6 points, $n = 5$) for Griess and Saville–Griess assays, respectively. Limits of detection and quantification were calculated based on blank deviation and the values were found to be 0.2 and 0.7 µM and 0.2 and 0.8 µM for Griess and Saville–Griess assays, respectively. Finally, repeatability, intermediate precision, and accuracy were evaluated. The relative standard deviations for Griess and Saville–Griess assays, respectively, were equal to 3.0 and 1.4% for repeatability (six determinations at 100% of the test concentration, 5 µM) and 4.1 and 2.2% for intermediate precision (five determinations on 5 d). Accuracy was evaluated at 101.7 ± 14.4 and 104.3 ± 8.9% for Griess and Saville–Griess assays, respectively (five points, $n = 5$).

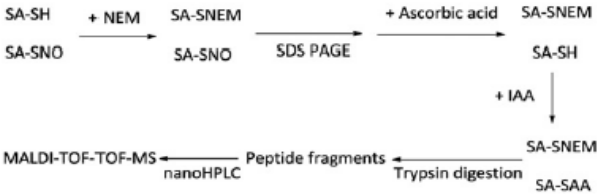

Figure 2. Experimental procedures of matrix-assisted laser desorption/ionization time-of-flight mass spectrometry (MALDI-TOF/TOF-MS) for determination of SA *S*-nitrosation site.

Purification by size exclusion chromatography

S-nitrosated SA was separated from other components of the reaction medium by size exclusion chromatography (SEC) with PBS as the eluent. A polypropylene column (20 × 1.5 cm) was filled up with Sephadex® G-25 (10 ml) and eluted with PBS at a flow rate of 250 µl min^{-1}. The column was equilibrated with the eluent for 10 min and 0.5 ml of the reaction medium resulting from different *S*-nitrosation processes was deposited at the top of the column; the eluate was collected (0.5 ml fractions). The absorbance of eluate fractions was measured at 278 nm for protein content (linear range: 1–10 µM), and by Griess and Saville–Griess assays for nitrite and SA-NO content, respectively. The *S*-nitrosation rate of SA was calculated using the following equation:

$$(\mathrm{SA-SNO})\mathrm{rate} = \frac{n_{\mathrm{SA-SNO}}}{n_{\mathrm{SA}} \times \mathrm{thiol\ content}} \times 100 \qquad (1)$$

where $n_{SA\text{-}SNO}$ is the quantity measured by Saville–Griess assay, n_{SA} is the quantity of protein, and thiol content is determined by Ellman's assay.

Spectroscopic analyses

Mass spectrometry

The procedure is summarized in Figure 2. A 1 µl aliquot of SA or SA-SNO at 60 µM was reacted with 40 mM NEM in sodium dodecyl sulfate (SDS) solution for 30 min to block free thiols. Then the samples were purified by a SDS polyacrylamide gel electrophoresis (SDS-PAGE) to remove the NEM excess. The gels were then stained with Coomassie blue and visible bands were cut and reduced for 15 min by a 40 mM ascorbic acid solution, and the resulting free thiols were alkylated by the addition of a 40 mM IAA solution. Gel bands were destained through two successive cycles of washes in 100 µl of 50 mM ammonium bicarbonate and 25 mM ammonium bicarbonate, 50% acetonitrile (ACN). Proteins were digested in 25 µl of 25 mM ammonium bicarbonate, containing 1 ng trypsin (Promega, Fitchburg, WI, sequencing grade), at 37 °C overnight. Peptides were extracted twice by sonication in a water bath sonicator in 25 µl 80% ACN, 1% trifluoroacetic acid (TFA). Extracts were dried, resuspended in 2% ACN, 0.1% TFA, and fractionated/analyzed based on Riffault et al.[21]. Fractionation was performed by nanoHPLC (Ultimate3000 system) on a pepMap 100 C18 desalting precolumn and a 15 cm pepMap RSLC C18 fractionation column (all from Dionex, Sunnyvale, CA). Five µl were injected using the µlpickup mode and eluted by a 2–45% ACN gradient over 30 min

at a flow rate of 300 nl min^{-1}. The resulting fractions were collected on a ProteineerFcII (Bruker, Billerica, MA) and were directly mixed on MTP-1536 TF target (Bruker, Billerica, MA) spots with α-cyano-4-hydroxycinnamic acid (Bruker). Matrix-Assisted Laser Desorption/Ionisation coupled with time-of-flight (MALDI-TOF/TOF) MS runs were processed according to Ref. [21].

Spectrofluorimetry

The fluorescence spectra were recorded on a spectrofluorimeter (JASCO FP-8300iRM, JASCO Incorporated, Portland, OR) with a 1.0 cm quartz cuvette in the range of 200–500 nm for emission and excitation wavelengths (bandwidth =5 nm; sensitivity: medium); the samples were prepared in PBS at a final protein concentration of 0.7 μM.

Dynamic light scattering

The hydrodynamic diameters (Dh) of SA and SA-SNO were measured by dynamic light scattering (DLS) using a Zetasizer Nano ZS (Malvern Instruments, Malvern, UK) at 25 °C with an angle detection of 173° backscatter (NIBS default). All Dh values reported were volume average values, based on three independent measurements of three SA and SA-SNO batches.

Circular dichroism

The circular dichroism (CD) spectra were recorded on a Chirascan™ CD spectrometer (Applied Photophysics Ltd, Leatherhead, UK) with a 0.1 mm quartz cuvette in the range of 180–260 nm for far-UV and with 1.0 cm quartz cuvette in the range of 260–320 nm for near-UV. The samples were prepared and diluted in chloride-free solvents to keep the final protein concentration at 12 μM for far-UV recording, and the initial concentration (60 μM) was used for near-UV recording. The data were collected with an interval of 1 nm and with a scan speed of 100 nm min^{-1} at 25 °C. PBS was used for baseline correction.

Stability studies

The purified SA-SNO was stored in PBS in the dark at 37, 4, −20, and −80 °C at a concentration of 60 μM (vials were completely filled with the solution). The remaining SA-SNO concentration was measured by Saville–Griess assay every day during the first week and every week till 1 month.

Interaction of S-nitrosated serum albumin with citrate-stabilized gold nanoparticles

Citrate-stabilized gold nanoparticles were prepared and characterized as previously reported[22] by using spectrophotometry and transmission electronic microscopy (Philips CM20 instrument with a LaB6 cathode operating at 200 kV, Philips Inc, Amsterdam, UK). The AuNP-citrate suspension (550 μl) at a final concentration of 10, 20, 40 and 60 nM were added to either SA-SNO or GSNO solution (60 μl) in PBS at a final concentration of 5 μM (corresponding to SNO concentration). The resulting samples were incubated at rt for 2 h, and centrifuged at 42,000 × *g* for 10 min at 4 °C. Then 100 μl of 10% (v/v) TCA solution were mixed with 550 μl of supernatant and centrifuged at 42,000 × *g* for 10 min at 4 °C. For the measurement of NO release, 600 μl of each diluted supernatant (1–10 times) in PBS were mixed with 60 μl of 105 μM 2,3-diaminonaphthalene (DAN) prepared in 0.6 M HCl; the resulting mixture was incubated for 10 min at 37 °C followed by the addition of 40 μl of 2.4 M NaOH. Fluorescence intensity was read by using a spectrofluorimeter at λ_{exc} = 375 nm and λ_{em} = 415 nm. Concentrations of NO were calculated by using a calibration curve of $NaNO_2$ in the range of 0.05–0.50 μM. Besides, AuNP-citrate suspension (1100 μl) at a final concentration of 60 nM were incubated with GSH, GSNO, SA, and SA-SNO (120 μl) in PBS at a final concentration of 5 μM (corresponding to SNO concentration) in the dark at rt for 2 h. Then their visible spectra were recorded, and the Dh values were measured by DLS. Controls (AuNP concentration of 60 nM) were performed with SA-NEM (5 μM) using DLS and visible spectrophotometry characterization and $NaNO_2$ (5 μM) using DAN method quantification.

Statistical analysis

Where appropriate, results are shown as mean ± standard deviation (SD). Statistical significance between groups was determined by a one-way analysis of variance. All statistical analyses were done using GraphPad Prism® (GraphPad Inc., San Diego, CA) version 5.0. In all cases, $p < 0.05$ denoted significance.

Results and discussion

S-Nitrosation of serum albumin and product purification

Bovine SA which is 88% homologous with HSA is constituted by a single chain of 583 amino acid residues which contains 35 cysteine residues forming 17 disulfide bridges; the free cysteine residue is located at position 34 (Cys-34). The asymmetrically assembled secondary structure results in the package of Cys-34 residue, which is located in a sterically hindered anionic and hydrophobic crevice, resulting in limited access to the solvent[23]. In agreement with this opinion, a commercial mature BSA, which is derived from cow plasma proteins purified by Edwin Cohn's methodology with retained biological activity, used in the present study possessed only 56.8 ± 1.3% (n = 3) of free thiol content determined by Ellman's assay.

After realizing *S*-nitrosation of SA with different nitrosating reagents (reagent equivalents are defined according to the measured thiol content), the excess of chemical reagents and their possible decomposition compounds were removed by SEC. SA-SNO and unreacted SA were eluted under the same peak, due to their similar physicochemical properties (Figure 3). However, using a well-defined mixture of SA-SNO and SA in preclinical studies and further clinical investigation is convenient because SA-SNO and SA naturally co-exist in the blood. In chromatogram ii, SA-SNO was separated from low molecular weight RSNO with an acceptable baseline-resolution (R_S) between peaks (R_S = 1.8), measured according to European Pharmacopeia. However, another impurity (3-nitrotyrosin-SA[24]) may occur in all the *S*-nitrosation protocols as previously described with the use of nitrite ions in acidic medium[25,26] as well as with transnitrosation processes[27].

Then, the nitrosated site was checked by using LC-MALDI-TOF/TOF MS analysis. The reference commonly used in MS studies is a BSA precursor which contains 607 amino acids, while the mature protein contains 583 amino acids. Thus, the mature BSA starts from amino acid residue 25–607, and as a result, the free cysteine residue is located at position 58 instead of 34. When examining peptide fragments ranging from amino acids 45–65 and according to our sample preparation (Table 2), only *N*-ethylmaleimide coupling was observed for native SA on cysteine 58 (indicated C_{58} in Table 2). On the contrary, both carbamidomethylation and *N*-ethylmaleimide addition were observed at this site for SA-SNO.

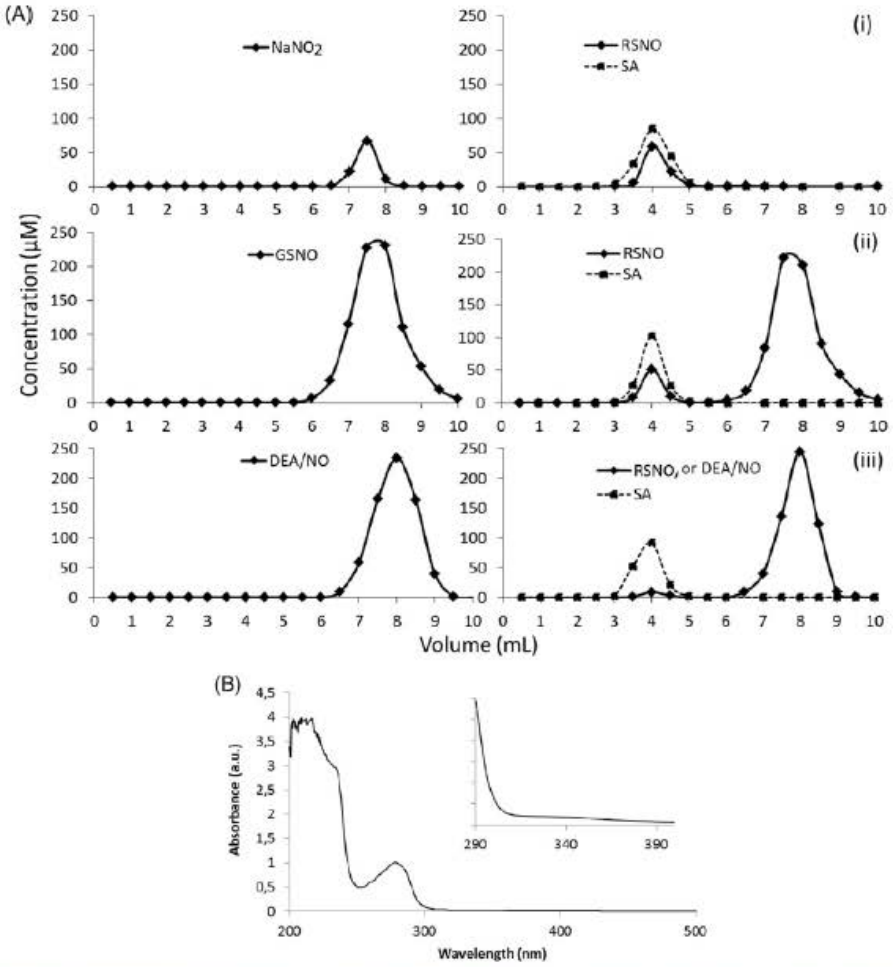

Figure 3. (A) Typical chromatograms corresponding to blank (left) and the purification of SA-SNO (right) by SEC: (i) *S*-nitrosation with $NaNO_2$ in acidic medium, (ii) *S*-transnitrosation with low-molecular weight RSNO (GSNO in this graph), and (iii) *S*-nitrosation by NO released from DEA/NO. The SA content in collected fractions was monitored by absorbance measurement at 278 nm, the NO_2^- and RSNO were measured by Griess and Saville–Griess assay, respectively. (B) Typical UV–visible spectra obtained on SA-SNO after *S*-nitrosation process.

Table 2. Determination of *S*-nitrosation site by LC-MALDI-TOF/TOF analyses of SA-SNO fragment peptides (mass of *N*-ethylmaleimide and carboxymethyl fragments are 126 and 59 a.m.u., respectively).

Sample name	SA content	Rt (min)	Obtained *m/z* ratio (molecular peak)	Peptide sequence (letter codified amino acids with sequence number underscript)
				Theoretical sequence:
Native SA	SA-SH	–	Expected value: 2434	K.G_{45}LVLIAFSQYLQQC_{58}PFDEHVK$_{65}$.L
Native SA	SA-SH	42.3	2560.282	K.G_{45}LVLIAFSQYLQQC_{58}PFDEHVK$_{65}$.L | *N*-ethylmaleimide
S-nitrosated-SA	SA-SNO	40.9	2492.248	K.G_{45}LVLIAFSQYLQQC_{58}PFDEHVK$_{65}$.L | *S*-carboxymethyl
	SA-SH	42.3	2560.282	K.G_{45}LVLIAFSQYLQQC_{58}PFDEHVK$_{65}$.L | *N*-ethylmaleimide

This analysis proved that the *S*-nitrosated site was located on the free cysteine residue, as expected, and that SA-SNO contains also a non-*S*-nitrosated fraction, as previously explained.

Based on various *S*-nitrosation pathways, different *S*-nitrosation rates were obtained (Table 3). The use of nitrite ions in acidic medium afforded the highest yield of SA-SNO (90%, expressed *versus* the free content of thiol in SA determined by Ellman's assay), followed by transnitrosation with low molecular weight RSNO which yielded lower *S*-nitrosation rates (85–76%) in the following order: $Buc(NO)_2$ > GSNO > CysNO, while DEA/NO produced low yield of SA-SNO (15%). The *S*-nitrosation yield was also confirmed by UV-visible spectrophotometry at 334 nm (typical UV–visible spectrum is shown in Figure 3). Indeed, taking into account (i) the additivity of Beer Lambert's law, (ii) molar absorbances at this wavelength of SA (606 ± 7 M^{-1}. cm^{-1}) and GSNO (922 M^{-1}. cm^{-1})[17], and (iii) 56.8% of free thiol in SA, the theoretical molar absorbance value of SA-SNO is 1067 versus 1130 M^{-1}. cm^{-1} calculated or measured in our study.

Table 3. Rates of albumin *S*-nitrosation (%) obtained by the three pathways.

S-nitrosation pathway	$NaNO_2$ in acidic medium	*S*-transnitrosation			DEA/NO
		CysNO	GSNO	$Buc(NO)_2$	
S-nitrosation rate (%)	$90.1 \pm 3.0^{a,b,c}$	76.2 ± 4.9^{a}	78.8 ± 1.6^{a}	$84.8 \pm 6.5^{a,b}$	$15.4 \pm 1.9^{b,c}$

Percentages of RSNO obtained (mean ± SD; $n = 5$) are expressed versus free thiol content measured by Ellman's assay.
[a] $p < 0.05$ versus DEA/NO.
[b] $p < 0.05$ versus CysNO.
[c] $p < 0.05$ versus GSNO.

Table 4. Nitrosation rate of SA by acidified $NaNO_2$ under different oxygenation conditions.

Oxygenation condition	$[O_2]^a$ (nmol/ml)	Nitrosation rate (%)
Degassing in an ultrasonic bath for 3 min	260	89.4 ± 2.7^{b}
Exposing the reaction medium to air with intense magnetic stirring	260	91.7 ± 2.6^{b}
Bubbling with nitrogen for 3 min	0	84.6 ± 3.9^{b}

[a] Measured with Clark electrode.
[b] $p < 0.05$ versus our operating conditions ($NaNO_2$ in acidic medium).

S-Nitrosation by acidified $NaNO_2$ involves several mechanisms: resulting nitrous acid efficiently reacts with thiol groups either directly or by the way of tightly related oxidized derivatives such as N_2O_3 or N_2O_4 and this phenomenon may be catalyzed by ClNO[9]. The influence of dissolved O_2 in the medium on synthesis yield was studied (Table 4). Whatever the tested condition (degassing with ultrasonic bath or N_2 bubbling or saturated 0_2 using intense stirring), no difference in term of *S*-nitrosation rate was observed. Moreover, the excess of nitrite ions in acidic medium can oxidize the free thiol of SA, but can also react with the indole nitrogen atom of a tryptophan residue, inducing polynitrosation[8] and a lower *S*-nitrosation conversion. For example, 200 and 1000 equivalents of NO_2^- yield 71 and 60% of SA-SNO, respectively[7]. As a consequence, it is of main importance to operate with exactly the same equivalent amounts of NO_2^- and SA (considering its thiol content). In our operating conditions, NO_2^- is fully consumed, as demonstrated by no NO_2^- detection after reaction (see chromatogram i of Figure 3). Two batches of SA were tested in the present study and both give rise to the same *S*-nitrosation rate (ca. 90%) when considering their initial amount of free thiol measured by Ellman's assay (data not shown). At the same time, *S*-nitrosated HSA was prepared with a yield of 79.7%, based on 14.6% thiol content, by using acidified $NaNO_2$.

S-transnitrosation should appear as a softer process than direct *S*-nitrosation, because it is operated at physiological pH. The NO exchange between low molecular weight RSNO and SA thiol group occurs mainly *via* nitrosonium ion (NO^+) and thiolate form[28] which is more abundant at physiological pH. SA-SNO obtained by transnitrosation presents a molar absorbance at 334 nm equal to 947 ± 21 M^{-1} cm^{-1} ($n = 3$), which is in accordance with the calculated nitrosation rate.

A factor which may also promote the formation of SA-SNO is the stability of low molecular weight RSNO or the NO^+ releasing rate. In our study, three RSNO with different half-lives ($Buc(NO)_2$ > GSNO > CysNO) were tested: resulting *S*-nitrosation rates increased with their stability. The dinitrosothiol, $Buc(NO)_2$, appears as the most interesting *S*-transnitrosation reagent when compared to GSNO and CysNO. A 10-fold excess of low molecular weight RSNO was presently used, according to previous literature reports[14]. Accordingly, a nine-fold ratio of GSNO peak area to SA-SNO peak area was obtained by using Excel® calculation (chromatogram ii in Figure 3). Increasing this excess (up to 20 and 50 equivalents of low molecular weight RSNO for one thiol equivalent of SA) or extending reaction time (2 and 4 h), or even using inert atmosphere did not yield significantly higher *S*-nitrosation rates (data not shown). As a consequence, whatever the considered RSNO, SA was not totally transnitrosated. This may be due to the formation of an intermolecular disulfide derivative (RS-SA) which can be a by-product of this reaction[29].

At rt and pH 7.4, one mole of DEA/NO releases 1.5 mole of NO and its congeneric nitroxyl from every parent compound. The protonation of $[NN(O)NO]^-$ functional group releases NO[30], which can attack Cys-34 in water, thus forming an *N*-centered radical, e.g., $RSN^{\bullet}OH$. This radical mutually combines and leads to disulfide[31] but not to RSNO formation. In our case, the O_2 level (260 mmol/ml) produced the oxidized derivatives and it resulted in low SA-SNO amounts (15%).

Influence of S-nitrosation on conformational and structural changes

Serum albumin may undergo reversible conformational transitions in its three-dimensional structure at different pH values and under drug binding[1]. *S*-nitrosation of SA on Cys-34 was hypothesized to induce secondary reactions leading to *C*-, *N*-, and *O*-nitrosoalbumin[12], which in turn may cause conformational changes altering original biological activities of SA. Several physicochemical techniques were used to investigate this possibility: spectrofluorimetry, DLS, and CD.

Serum albumin possesses intrinsic fluorescence due to aromatic amino acid residues. Compared with tyrosine and phenylalanine residues, tryptophan residues play the main role as fluorescence probes in optical studies of proteins to monitor conformational changes[32]. In this study, the excitation spectra of SA-SNO prepared by different *S*-nitrosation processes, standard SA, and positive control (SA treated with NaCl in 0.5 M HCl solution but without NO_2^- at rt for 1 h followed with SEC purification) exhibited similar maximum emission wavelength located at 284 nm and fluorescence intensity. The excitation spectra of all samples were also located at 340 nm with almost the same intensity (Figure 4A). No change was observed in the fluorescence of aromatic amino acid residues, which means that their environment was not affected by the different *S*-nitrosation processes.

Dynamic light scattering is a tool to determine size distribution, polydispersity, and aggregation phenomena in solution. The change of SA size demonstrates the thermal denaturation of SA. As shown in Figure 4(B), the Dh values of SA-SNO (whatever the process), SA standard, and SA treated in HCl-NaCl were centered at 7 nm, these results being consistent with literature data[33]. Furthermore, it illustrated the absence of aggregates.

Circular dichroism is interesting to investigate protein structure, especially for analysis of conformational changes. SA-SNO, SA

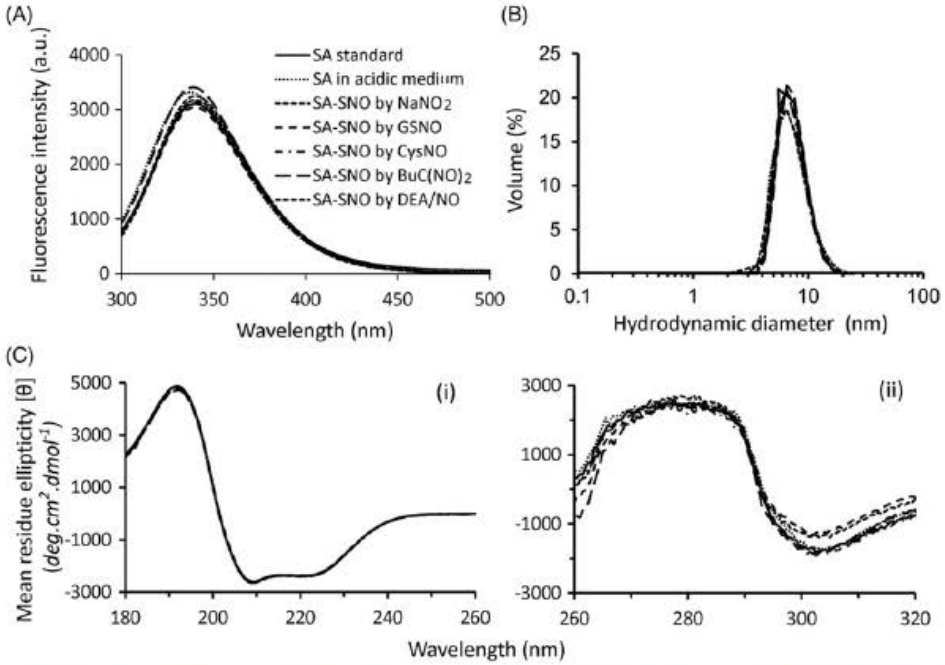

Figure 4. Physicochemical characterization of SA-SNO as a function of the three *S*-nitrosation processes studied by (A) fluorescence, (B) DLS, and (C) far UV (I) and near UV (II) CD.

standard, and positive control were monitored by CD in the far and near UV for getting secondary and tertiary structure information. For the far UV CD analysis (Figure 4(C), (i), the shape of curves, in the entire window 180–260 nm, is identical whatever the treatment, which revealed that the helical structure of SA remained unchanged after the different *S*-nitrosation processes. SA kept most part of its peptide bonds and secondary structure under all *S*-nitrosation modes. The literature reported that the ellipticities of SA[34] at 220 nm decreased markedly with pH drop from 5 to 2. SA nitrosated by acidified $NaNO_2$ underwent the conformational changes but its ellipticity recovered its original level with pH readjustment, mainly due to the reversible conformational transitions. The near UV spectrum of a protein is related to a specific signature. Moreover, small perturbations in the tertiary structure can be observed in this range. The near UV data (Figure 4(C), (ii) showed that there was no significant difference between SA-SNO obtained by the different processes and SA standard. As the signals recorded in the range 260–320 nm are related to the aromatic amino acids environment, the obtained near UV data confirmed the fluorescence results.

Based on the results obtained with the various physicochemical methods reported above, the conclusion can be drawn that no conformational changes in SA occur as a function of *S*-nitrosation methods used, even when using very low pH values (direct *S*-nitrosation) or excess of low molecular weight RSNO (*S*-transnitrosation).

Storage conditions

The *in vitro* stability of purified SA-SNO in PBS was studied by storing at 37 °C, 4 °C, −20 °C, and −80 °C (vials were completely filled with the solution to match more closely to usual experimental conditions) in the dark, and monitored by Saville–Griess assay. Table 5 revealed that ca. 5% of SA-SNO obtained by different *S*-nitrosation methods was lost when kept at different temperatures after 1 week. The purified SA-SNO degraded when the storage time increased in all temperatures, indicating that conservation of the SA-SNO did not rely on the temperature, but probably on other storage conditions, as superoxide anion and metallic ions presence[35]. Besides, metal ion chelators, e.g., ethylene diamino tetraacetic acid and diethylene triamine pentaacetic acid, can stabilize RSNO but they were not used during synthesis and purification to avoid any disagreement in further biological experiments.

Table 5. The residual percentages of *S*-nitrosated albumin stored in PBS at different temperatures. Data shown are mean ± SD ($n = 3$).

	Days						
	0	1	2	3	4	7	30
4 °C	100 ± 0	99 ± 2	98 ± 2	97 ± 2	97 ± 3	95 ± 3	86 ± 6
37 °C	100 ± 0	98 ± 1	97 ± 1	96 ± 3	95 ± 3	93 ± 3	83 ± 3
−20 °C	100 ± 0	98 ± 3	98 ± 3	96 ± 4	96 ± 2	93 ± 1	85 ± 3
−80 °C	100 ± 0	98 ± 1	97 ± 4	96 ± 3	94 ± 5	92 ± 4	85 ± 3

Interaction of S-nitrosated serum albumin with citrate-stabilized gold nanoparticles

Gold nanoparticles (AuNP) have drawn extensive attention over the last decade for their potential applications in biology, diagnostics, and medicine[36]. However, due to their small size and high reactivity, they can interact with biological components causing serious adverse effects, predominantly via induction of an oxidative stress (defined as an imbalance between protective antioxidants and damaging oxidants such as reactive oxygen and nitrogen species)[37]. The endogenous antioxidants (e.g., thiols and related RSNO) are considered to be the first line against AuNP[22], thus the reactivity between these antioxidants and AuNP in cell-free conditions should be studied for predicting the fate of AuNP in the human body and for the stability of SA-SNO when reacted with highly active particles. Very few interaction studies between RSNO and AuNP were already reported in the literature: Jia et al.[38] and Tournebize et al.[22] observed that AuNP-citrate catalyzes the decomposition of endogenous low molecular weight RSNO, by the formation of Au-thiolate on the surface of AuNP, inducing a linear

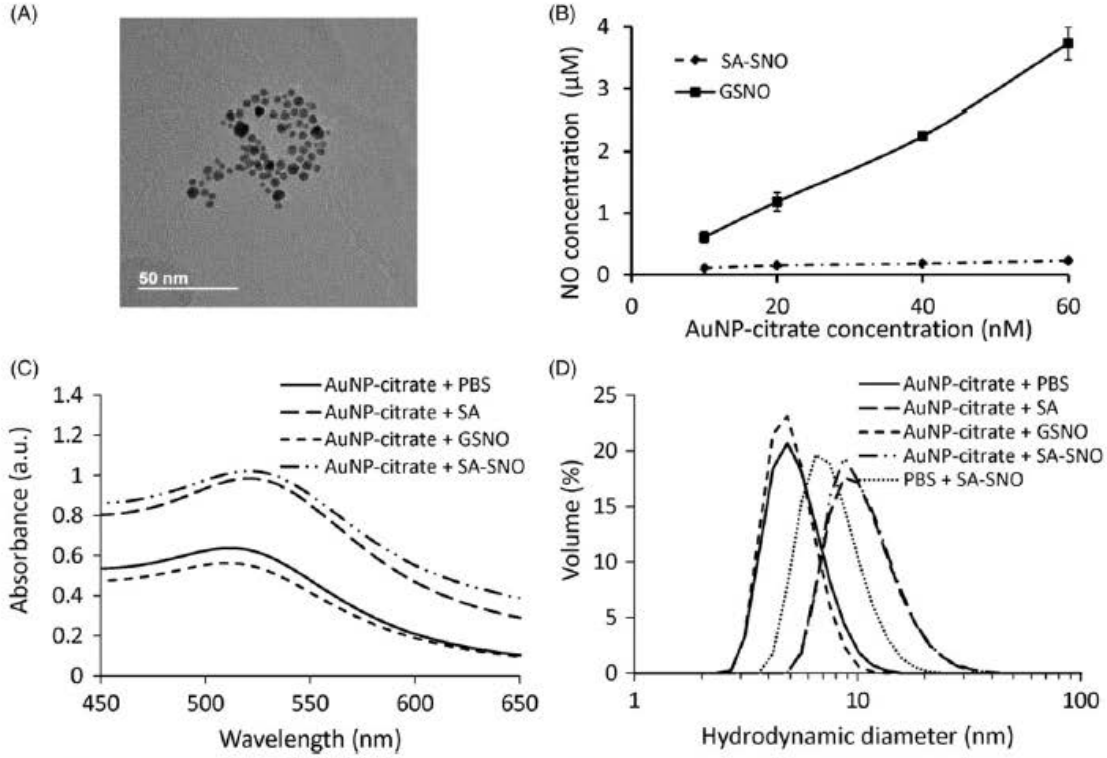

Figure 5. Citrate-stabilized gold nanoparticles (AuNP-citrate) interaction between SA-SNO and GSNO: (A) transmission electronic microscopy picture of AuNP-citrate, and (B) concentration of nitric oxide (NO) released from SA-SNO and GSNO (50 µM) when incubating with different concentrations of AuNP-citrate in PBS at room temperature for 2 h. Data shown correspond to the mean ± SD ($n = 3$); (C) visible spectrum of AuNP-citrate when incubated with PBS, SA, GSNO and SA-SNO; (D) hydrodynamic diameter of SA-SNO, AuNP-citrate, and AuNP-citrate incubated with SA, GSNO, and SA-SNO.

dose-dependent NO release. At that time, the reactivity between AuNP-citrate, the most commonly used AuNP in the literature, and SA-SNO has not yet been tested *in vitro*. Herein, AuNP-citrate (5.3 ± 1.1 nm and 5.5 ± 1.1 nm for core diameters (Dc) and Dh, respectively and 512 nm for maximum absorbance wavelength; see Figure 5) was incubated with either SA-SNO or GSNO. Due to spectroscopic interferences in the visible range, a spectrofluorimetric method (based on DAN assay) was used instead of the classical spectrophotometric Griess assay, and protein and AuNP were precipitated before measurement. The results demonstrated that the high molecular weight RSNO (i.e., SA-SNO) was much less reactive than the low molecular weight one (i.e., GSNO). Indeed, a very low level of released NO was monitored when incubating with SA-SNO, while a linear profile of NO release was observed in the case of GSNO. A control incubating nitrite ions with the particles showed a total recovery of this species (4.96 ± 0.26 µM parallel to a NP precipitation; maximal wavelength = 550 nm and Dh = 254 ± 36 nm). Moreover, after SA-SNO incubation, AuNP showed modified physicochemical properties (Dh of 11.4 ± 0.2 and 10.7 ± 0.4 nm and maximal wavelengths of 522 and 521 nm for SA-SNO and SA incubated with AuNP, respectively). Their incubation with SA-NEM demonstrated similar results: Dh = 9.5 ± 1.2 nm and maximal wavelength = 521 nm. On the contrary, particles incubated with GSNO were not deeply different from native objects (Dh of 6.2 ± 0.9 and 5.5 ± 0.1 nm and maximal wavelengths of 513 and 512 nm for GSNO incubated with AuNP and native particles, respectively). These modifications were mainly attributed to the interaction between AuNP and serum albumin, which would result in a protein corona[39] and an enhanced electron density on the particle surface (modified surface plasmon resonance band)[40]. Moreover, this study highlighted, for the first time, that serum albumin/AuNP interaction was not driven through gold-sulfur binding because of steric hindrance between AuNP and SA which may limit the access to the packed SNO group (but through hydrogen and electrostatic bond as previously reported[41]). It can be concluded that AuNP-citrate does not modify NO pool stored by albumin.

Conclusion

To our knowledge, this study is the first comprehensive description about SA *S*-nitrosation and related physicochemical characterization. It leads to a well-defined reference for further biological investigation and preclinical studies of SA-SNO, such as application as a NO donor. Meanwhile, the described *S*-nitrosation methods provide a referable template for applying to other macromolecules possessing free thiols.

Acknowledgements

Authors would like to acknowledge Miss Agnieszka Lyczykowska for her support.

Disclosure statement

The authors report that they have no conflicts of interest.

Funding information

This work was financially supported by *Région Lorraine* (CPER) and *Université de Lorraine*. Authors are grateful to the program of China Scholarships Council for its financial support of Ming Luo's PhD thesis; to Dr Alexandre Kriznik (*Service Commun de Biophysicochimie des Interactions Moléculaires (SCBIM) de l'Université de Lorraine*) for

CD measurements, and to Pr Jolivet Yves and Mrs Gérard Joelle (*UMR 1137, Ecologie et Ecophysiologie Forestières de l'Université de Lorraine*) for providing Clark electrode.

References

1. Fanali G, Masi A, Trezza V, et al. Human serum albumin: from bench to bedside. Mol Aspects Med 2012;33:209–90.
2. Yang F, Liang H. Editorial: HSA-based drug development and drug delivery systems. Curr Pharm Des 2015;21:1784.
3. Elsadek B, Kratz F. Impact of albumin on drug delivery – new applications on the horizon. J Control Release 2012;157:4–28.
4. Förstermann U, Sessa WC. Nitric oxide synthases: regulation and function. Eur Heart J 2012;33:829–37.
5. Lei J, Vodovotz Y, Tzeng E, Billiar TR. Nitric oxide, a protective molecule in the cardiovascular system. Nitric Oxide 2013;35:175–85.
6. Tsikas D. Comments on the article "Nitrosylated human serum albumin (SNO-HSA) induces apoptosis in tumor cells (nitric oxide 22 (2010)259–265)". Nitric Oxide 2011;24:123–4.
7. Katsumi H, Nishikawa M, Ma SF, et al. Physicochemical, tissue distribution, and vasodilatation characteristics of nitrosated serum albumin: delivery of nitric oxide in vivo. J Pharm Sci 2004;93:2343–52.
8. Stamler JS, Simon DI, Osborne JA, et al. S-Nitrosylation of proteins with nitric oxide: synthesis and characterization of biologically active compounds. Proc Natl Acad Sci USA 1992;89:444–8.
9. Noble R, Williams D. Formation and reactions of S-nitroso proteins. J Chem Soc, Perkin Trans 2001;2:13–17.
10. Boese M, Mordvintcev PI, Vanin AF, et al. S-nitrosation of serum albumin by dinitrosyl-iron complex. J Biol Chem 1995;270:29244–9.
11. Charuvila TA, Jan C, Marc DL. Steric effect and effect of metal coordination on the reactivity of nitric oxide with cysteine-containing proteins under anaerobic conditions. Biophys Chem 2000;85:1–16.
12. Tsikas D, Sandmann J, Rossa S, et al. Measurement of *S*-nitrosoalbumin by gas chromatography–mass spectrometry I. preparation, purification, isolation, characterization and metabolism of S-[^{15}N]nitrosoalbumin in human blood *in vitro*. J Chromatogr B 1999;726:1–12.
13. Giustarini D, Tsikas D, Rossi R. Study of the effect of thiols on the vasodilatory potency of S-nitrosothiols by using a modified aortic ring assay. Toxicol Appl Pharmacol 2011;256:95–102.
14. Hao Z, Gary EM. S-*nitrosation of serum albumin: spectrophotometric determination of its nitrosation by simple S-nitrosothiols. Anal Biochem 1996;237:141–4.
15. Shah C, Bell S, Locke I, et al. Interactions between cell surface protein disulphide isomerase and S-nitrosoglutathione during nitric oxide delivery. Nitric Oxide 2007;16:135–42.
16. Liu Z, Rudd M, Freedman J, Loscalzo J. S-Transnitrosation reactions are involved in the metabolic fate and biological actions of nitric oxide. J Pharmacol Exp Ther 1998;284:526–34.
17. Parent M, Dahboul F, Schneider R, et al. A complete physicochemical identity card of S-nitrosoglutathione. Curr Pharm Anal 2013;9:31–42.
18. Dahboul F, Perrin-Sarrado C, Boudier A, et al. S,S'-dinitrosobucillamine, a new nitric oxide donor, induces a better vasorelaxation than other *S*-nitrosothiols. Eur J Pharmacol 2014;2:34–42.
19. Bryan N, Grisham M. Methods to detect nitric oxide and its metabolites in biological samples. Free Radic Biol Med 2007;43:645–57.
20. Food and Drug Administration, Guidance for Industry, Bioanalytical Method Validation, Revision 1, September 2013.
21. Riffault M, Moulin D, Grossin L, et al. Label-free relative quantification applied to LC-MALDI acquisition for rapid analysis of chondrocyte secretion modulation. J Proteomics 2015;114:263–73.
22. Tournebize J, Boudier A, Joubert O, et al. Impact of gold nanoparticle coating on redox homeostasis. Int J Pharm 2012;438:107–16.
23. Taguchi K, Chuang VT, Maruyama T, Otagiri M. Pharmaceutical aspects of there combinant human serum albumin dimer: structural characteristics, biological properties, and medical applications. J Pharm Sci 2012;101:3033–46.
24. Knight TR, Kurtz A, Bajt ML, et al. Vascular and hepatocellular peroxynitrite formation during acetaminophen toxicity: role of mitochondrial oxidant stress. Toxicol Sci 2001;62:212–20.
25. d'Ischia M, Napolitano A, Manini P, Panzella L. Secondary targets of nitrite-derived reactive nitrogen species: nitrosation/nitration pathways, antioxidant defense mechanisms and toxicological implications. Chem Res Toxicol 2011;24:2071–92.
26. Oldreive C, Zhao K, Paganga G, et al. Inhibition of nitrous acid-dependent tyrosine nitration and DNA base deamination by flavonoids and other phenolic compounds. Chem Res Toxicol 1998;11:1574–9.
27. Daiber A, Bachschmid M, Kavakli C, et al. A new pitfall in detecting biological end products of nitric oxide-nitration, nitros(yl)ation and nitrite/nitrate artefacts during freezing. Nitric Oxide 2003;9:44–52.
28. Inami K, Kondo S, Ono Y, et al. Transnitrosation of alicyclic N-nitrosamines containing a sulfur atom. Bioorg Med Chem 2013;21:7853–7.
29. Dalle-Donne I, Rossi R, Giustarini D, et al. *S-glutathionylation in protein redox regulation. Free Radic Biol Med 2007;43:883–98.
30. Valiev M, Lymar SV. Decomposition of amino diazeniumdiolates (NONOates): molecular mechanisms. J Inorg Biochem 2014;141:28–35.
31. Jourd'heuil D, Jourd'heuil FL, Feelisch M. Oxidation and nitrosation of thiols at low micromolar exposure to nitric oxide. Evidence for a free radical mechanism. J Biol Chem 2003;278:15720–6.
32. Gao D, Tian Y, Bi S, et al. Studies on the interaction of colloidal gold and serum albumins by spectral methods. Spectrochim Acta a Mol Biomol Spectrosc 2005;62:1203–8.
33. Jachimska B, Wasilewska M, Adamczyk Z. Characterization of globular protein solutions by dynamic light scattering, electrophoretic mobility, and viscosity measurements. Langmuir 2008;24:6866–72.
34. Muzammil S, Kumar Y, Tayyab S. Molten globule-like state of human serum albumin at low pH. Eur J Biochem 1999;266:26–2.
35. Gaucher C, Boudier A, Dahboul F, et al. S-Nitrosation/denitrosation in cardiovascular pathologies: facts and concepts for the rational design of *S*-nitrosothiols. Curr Pharm Des 2013;19:458–72.

36. Shah M, Badwaik VD, Dakshinamurthy R. Biological applications of gold nanoparticles. J Nanosci Nanotechnol 2014;14:344–62.
37. Tournebize J, Sapin-Minet A, Bartosz G, et al. Pitfalls of assays devoted to evaluation of oxidative stress induced by inorganic nanoparticles. Talanta 2013;116:753–63.
38. Jia H, Liu Y, Zhang X, et al. Potential oxidative stress of gold nanoparticles by induced-NO releasing in serum. J Am Chem Soc 2009;131:40–1.
39. Shannahan JH, Podila R, Brown JM. A hyperspectral and toxicological analysis of protein corona impact on silver nanoparticle properties, intracellular modifications, and macrophage activation. Int J Nanomed 2015;10:6509–21.
40. Bhan C, Brower TL, Raghavan D. SPR studies of the adsorption of silver/bovine serum albumin nanoparticles (Ag/BSA NPs) onto the model biological substrates. J Colloid Interface Sci 2013;402:40–9.
41. Wang Y, Ni Y. Combination of UV–vis spectroscopy and chemometrics to understand protein-nanomaterial conjugate: a case study on human serum albumin and gold nanoparticles. Talanta 2014;119:320–30.

3.3. Conclusion

Le modèle d'albumine utilisé comme accepteur de NO valide l'hypothèse qu'une transnitrosation entre un RSNO en solution et une particule colloïdale est possible. L'obtention d'AuNP pouvant libérer du NO et d'un réservoir conséquent est donc envisageable en ayant recours à cette technique.

Nous avons développé des méthodes permettant une évaluation stricte des AuNP (synthèse, caractérisation, stabilité), leur fonctionnalisation ainsi que leur nitrosation. La prochaine étape comprend leur inclusion dans des films multicouches afin de former la couverture de DM recherché. Le chapitre suivant décrit l'immobilisation des AuNP modèles au sein de films multicouches de polyélectrolytes.

CHAPITRE III : FILMS POLYMERIQUES MULTICOUCHES FONCTIONNALISES PAR DES NANOPARTICULES D'OR

Dans la littérature, les films nanostructurés sont, la plupart du temps, constitués par deux partenaires : un polyélectrolyte et des nanoparticules de charge opposée [103]. Dans notre étude, un système à trois partenaires est étudié, constitué par un polycation, des AuNP et un polyanion. En effet, alors que les AuNP sont chargées négativement, l'ajout d'un polyanion pourrait sembler superflu ; cependant, ce dernier peut contribuer à l'inertie des films créés. Il est possible que les AuNP ne recouvrent pas complètement le polycation, ce qui serait à l'origine d'interactions électrostatiques voire de réactions (dont des réactions redox) avec différentes protéines. De plus, les AuNP (colloïdales ou immobilisées) présentent une réactivité importante vis-à-vis d'une grande majorité des molécules biologiques (en raison, par exemple, de la présence de fonctions thiols). Ceci pourrait être défavorable à la bonne tolérance d'un DM recouvert et conduire à d'éventuels effets secondaires comme une initiation de la coagulation. De plus, l'ajout du polyanion favorisera le confinement des AuNP au sein de films multicouches de polyélectrolytes stables et non biodégradables et permettrait ainsi d'annuler ou de réduire leur réactivité. Ce système tripartite a été développé, d'une part, pour diminuer la réactivité des AuNP et empêcher leur dissémination et d'autre part pour améliorer la biocompatibilité du film créé. Ce montage constitue une approche originale par rapport à la littérature.

Pour étudier et évaluer la construction de tels films, des « prototypes » sont utilisés. Ces films multicouches, composés de couches de polyélectrolytes alternativement cationiques et anioniques entre lesquelles sont enchâssées des AuNP modèles (AuNP non fonctionnalisées), ont été déposés sur plusieurs types de supports.

Le premier support, constitué d'une lamelle de verre, permettra d'évaluer la faisabilité de la méthode et de caractériser les films dans des conditions statiques. Ce système offre l'avantage d'un montage simple (méthode de trempage [104]) et permet de réaliser

rapidement la caractérisation du film. Un modèle de contraintes de cisaillement, sur des lames de verre, mimant les forces présentes dans les vaisseaux sanguins a aussi été utilisé pour vérifier la résistance des films face à flux. Le deuxième modèle fait intervenir l'ECZ. Les films seront déposés sur la paroi interne d'un capillaire en verre. Ceci mène à la formation de films soumis à des flux et mime donc plus précisément les différents mécanismes influant sur leur stabilité. Le dernier fait appel à la microbalance à cristal de quartz (QCM) qui permet de visualiser en temps réel le dépôt des différentes couches ainsi que les quantités (notamment d'AuNP) déposées.

1. Biocompatibilité des films

1.1. Introduction

Les polymères retenus dans un premier temps pour la construction des films sont le chlorhydrate de polyallylamine (PAH) comme polymère cationique et l'acide polyacrylique (PAA) comme polymère anionique (Figure 19).

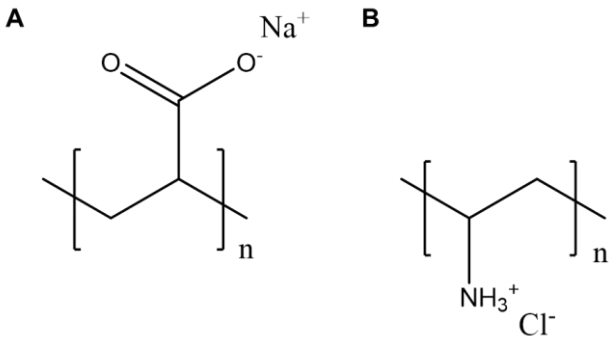

Figure 19 : Formules chimiques (A) du polyacrylate de sodium (PAA) et (B) du chlorhydrate de polyallylamine (PAH)

Ce choix est motivé par l'utilisation de polymères simples (une seule charge par monomère, pas de chaine alkyl longue), classiquement utilisés dans la construction de LbL et aussi parce que l'utilisation humaine du PAA et du PAH ont déjà été validées par la FDA [105, 106]. Les nanoparticules sont des AuNP stabilisées par des ions citrate utilisées comme modèles préliminaires à l'obtention d'AuNP fonctionnalisées par des RSNO. Ces AuNP sont très réactives, ce qui les rend « défavorables » à une application biologique en cas de mauvaise inclusion au sein du film.

Dans un premier temps, après formation des films, ceux-ci ont été caractérisés grâce à différentes méthodes telles que la spectrophotométrie UV-Vis., la MEB et MET, l'ECZ et la microscopie à force atomique (AFM) … L'ECZ permet de suivre la formation des films multicouches. Comme décrit dans le chapitre 2, le FEO est dépendant de la charge de surface du capillaire. Le dépôt des différentes couches des films entraine une modification de cette charge et donc du FEO. Une molécule neutre ne présentant aucune charge, sa mobilité électrophorétique sera nulle et son temps de migration dépendra uniquement de l'état de charge de surface du capillaire. L'injection d'une molécule neutre est donc un moyen d'évaluer l'état de surface d'un capillaire notamment dans le cadre du dépôt de films polymériques (Figure 20).

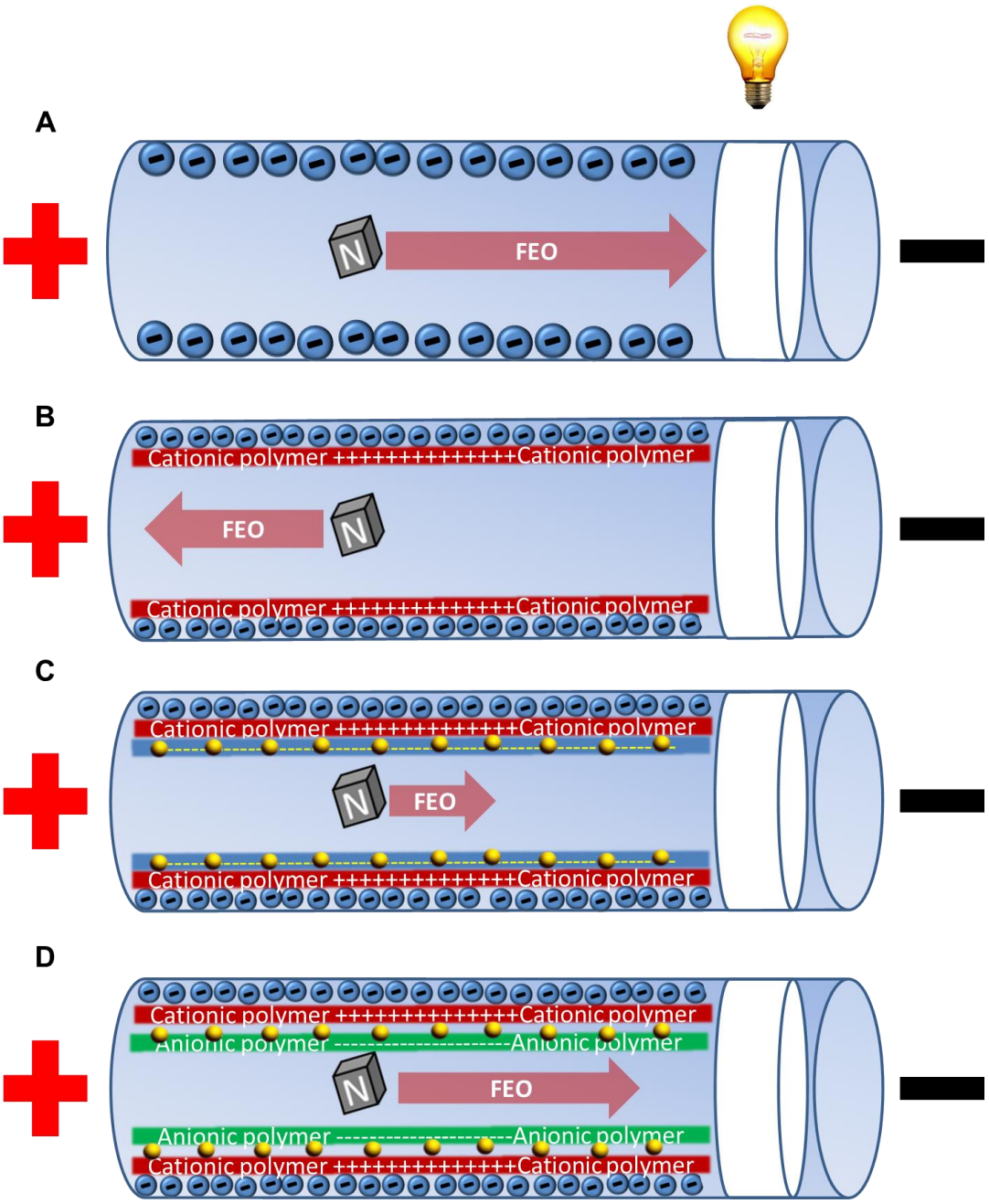

Figure 20 : Evolution du FEO dans un capillaire nu (A) puis lors de l'ajout du polymère cationique (B), des AuNP (C) et du polymère anionique (D).

Au pH de travail (7,4), un capillaire nu est chargé négativement par la présence de groupement silanoate à sa surface. Cette charge de surface va permettre aux cations contenus dans le tampon de migration de se déplacer vers la cathode et ainsi créer le FEO (Figure 20 A). Après le dépôt de la première couche de polymère (cationique), la surface devient

cationique et le flux inversé se dirige donc vers l'anode (Figure 20 B). L'ajout d'une couche nanoparticulaire chargée négativement permet à nouveau de renverser le flux vers la cathode. Cependant, si toutes les charges positives n'ont pas été compensées, il sera moins important que la valeur initiale du flux (Figure 20 C). Enfin, l'ajout d'une dernière couche polyanionique permet de retrouver un flux normalisé par l'apport d'un grand nombre de charges négatives (Figure 20 D). La mesure des valeurs de mobilité du FEO en fonction de la couche déposée permettent d'évaluer la construction du film ainsi que sa charge de surface globale.

Enfin, leur inertie a été évaluée. La charge de surface influe sur la réactivité et la biocompatibilité d'un objet. Pour trouver le meilleur candidat, des films dont la dernière couche variait (polycation ou AuNP ou polyanion) ont été fabriqués. Ils ont ensuite été placés en présence de diverses molécules biologiques (protéines, antioxydants …), puis de cellules (monocytes) pour être finalement mis en contact de sang total. Tous ces résultats ont fait l'objet d'un article paru dans *Particle & Particle Systems Characterization* (Article 5).

1.2. Article 5 : Blood compatibility of multilayered polyelectrolyte films containing immobilized gold nanoparticles

Graphical abstract:

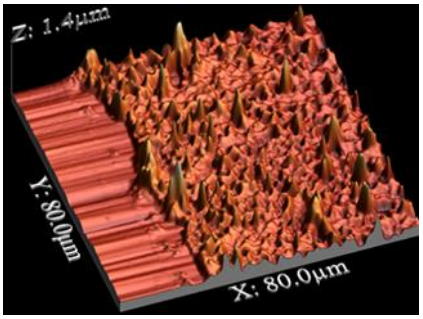

ADVANCED SCIENCE NEWS
www.advancedsciencenews.com

Particle & Particle Systems Characterization
www.particle-journal.com

Blood Compatibility of Multilayered Polyelectrolyte Films Containing Immobilized Gold Nanoparticles

*Arnaud Pallotta, Marianne Parent, Igor Clarot, Ming Luo, Vincent Borr, Pan Dan, Véronique Decot, Patrick Menu, Ramia Safar, Olivier Joubert, Pierre Leroy, and Ariane Boudier**

Surface material functionalization including layer-by-layer (LbL) polyelectrolyte films with incorporated nanoparticles is a growing field with a wide range of biomedical applications: drug reservoirs, medical devices, or tissue engineering. In parallel, gold nanoparticles (AuNPs) can be grafted by drugs and sensitive molecules using simple protocols. This study shows that AuNP behavior is modified when they are entrapped into three partner LbL films in comparison to the colloidal solution. A polycationic (polyallylamine hydrochloride (PAH)) and a polyanionic (polyacrylic acid (PAA)) polymer is used to build films based on three cycles ($(PAH/AuNP/PAA)_3$). To investigate the interaction with biomolecules and cells, three different films are developed changing the outer layer (either PAH or AuNP or PAA) with the same number of AuNP deposit. The best biocompatibility is observed with a polyacrylic acid outer layer. Due to the high capacity of drug grafting on gold nanoparticles, the results seem promising for the development of nanostructured biomedical devices.

1. Introduction

Surface material functionalization is a growing field with a wide range of possible applications. It is usually achieved using various techniques including layer-by-layer (LbL) assemblies.[1] This means of deposition has attracted an increasing interest since it is a low-cost method able to produce reproducible surfaces through simple protocols in order to confer new properties to the material.[1] Thin films based on LbL assemblies find new applications in electronics, energy, photonics, textile, and paper industry.[2] In the biomedical domain, they are used as biosensors, drug reservoirs, implantable or not biomedical devices, as well as for tissue engineering.[1,3–5] These last years, micro- or nanoparticles were included into LbL assemblies for surface modification to afford high drug loading, stabilization of sensitive molecules (proteins, peptides, or nucleic acids), and also the ability to trigger drug release in response to stimuli (pH, temperature, ionic strength, and light).[4,6–8] Among all the existing nanoparticles, a lot of them have already been incorporated into LbL films including polymeric as well as inorganic nanoparticles.[4,7,8]

Gold nanoparticles (AuNP) are one of the most studied nano-objects and some of them are currently evaluated through clinical trials. They possess the advantages of an easy synthesis, creating well-defined mono-dispersed particles. They can also be grafted by drugs and sensitive molecules using simple protocols.[9] As a result, they can be considered as ideal candidates to functionalize material surface for biomedical purposes. Only few reports related to the development of bioreactive supports focus on their entrapment into LbL films.[10–13] However, to the best of our knowledge, no report has been published yet on the biocompatibility of assemblies entrapping AuNP for a future application as a drug reservoir inside medical devices. Herein, LbL assemblies including AuNP were prepared and characterized, and their stability and behavior after incubation with biomolecules, plasma-like media, immunocompetent cells, and whole blood were studied. Citrate-capped AuNPs were chosen to be entrapped since they are the most frequently used particles, as they often represent a first step of synthesis before being grafted.[14] Moreover, they are interesting in the present study as their gold core is characterized by a residual catalytic activity which induces a poor bio- and cytocompatibility.[15,16] Thus, after a physicochemical characterization of the prepared LbL films based on polyelectrolytes containing three layers of AuNP, the last component deposited at the surface was varied and the effect of such films on the biological materials was evaluated.

2. Results and Discussion

The LbL films, based on polyacrylic acid (PAA), a weak acid (pKa = 4.3) and polyallylamine (PAH), a weak base (pKa = 10.0), were prepared using the classical dipping protocol.[17,18]

A. Pallotta, Dr. M. Parent, Dr. I. Clarot, Dr. M. Luo, V. Borr, Dr. R. Safar, Dr. O. Joubert, Prof. P. Leroy, Dr. A. Boudier
Université de Lorraine
CITHEFOR EA 3452, BP 80403
Nancy Cedex F-54001, France
E-mail: ariane.boudier@univ-lorraine.fr
P. Dan, Dr. V. Decot, Prof. P. Menu
Department of Cell and Tissue Engineering
Vectorization, Imaging, UMR 7365 CNRS Université de Lorraine
Ingénierie Moléculaire et Physiopathologie Articulaire
Biopôle de l'Université de Lorraine
Avenue de la forêt de Haye, C.S. 50184
Vandœuvre-lès-Nancy Cedex F-54505, France

DOI: 10.1002/ppsc.201600184

Particle
Particle Systems Characterization
www.particle-journal.com

ADVANCED SCIENCE NEWS
www.advancedsciencenews.com

Glassware (cover glasses) were successively put into the polycation solution, then into the AuNP suspension (as they present a negative zeta potential value),[15] and finally into the polyanion solution. This cycle was repeated three times. On the contrary to other published works (usually a polyelectrolyte and oppositely charged AuNP),[10–13] herein, films based on three partners $(PAH/AuNP/PAA)_x$ were developed: indeed, PAA was added in order to improve the biocompatibility of the film, as it will be later explained. Phosphate buffer solution (PBS) (at the physiological pH and ionic strength) was chosen to solubilize the polyelectrolytes. Its pH allowed the polymers to be mostly under their ionized form. This should create a film characterized by a dense electrostatic binding network,[5] able to anchor the nano-object and to avoid any release of particles into the external medium (that might induce toxicity).[19] Moreover, for a biomedical application, an inert surface is required; therefore, we hypothesized that a last negatively charged layer ($(PAH/AuNP/PAA)_3$), would be less reactive toward biological environment than both AuNP ($(PAH/AuNP/PAA)_2$-PAH/AuNP) or positively charged ($(PAH/AuNP/PAA)_3$-PAH) layers.

2.1. Film Characterization and Stability

After one cycle deposited, a red shift of the plasmon band of AuNP was observed between the colloidal solution and the film (509 ± 1 to 544 ± 3 nm, respectively) (**Figure 1**A).

This phenomenon was already observed and is attributed to differences between nanoparticle environments. Indeed, this is due to modification into the dielectric environment as well as the decrease of interparticle distance in the film compared to the colloidal solution.[12,13] However, no significant difference in plasmon band values with the increasing number of cycles was observed. As the absorbance of the nanostructured films was increasing according to a linear profile (Figure 1B), the amount of adsorbed AuNP was proportional to the gold layer number. After gold quantification, the amount of gold after three cycles was equal to $2.7 \pm 0.5 \times 10^{12}$ AuNP cm^{-2}, which was comparable to other published work.[10] Then, transmission electron microscopy (TEM) images (Figure 1C,D) were recorded to compare object size and dispersity of colloidal solution and films. The repartition of the particles on the films obtained by TEM pictures (based on a three cycle film, i.e., $(PAH/AuNP/PAA)_3$) showed a low density of coverage. This can be explained because of the choice of PAH which presents one basic group per monomer in comparison to previous results reported with polyethylenimine (four basic groups per unit).[11] However, the particles looked well-individualized in the films with core diameters of 5.2 ± 0.9 nm (vs 5.3 ± 1.1 nm for the colloidal solution). Therefore, the nanoparticles did not aggregate during film formation.

The stability of the films $(PAH/AuNP/PAA)_3$ was studied under various conditions. A long-term study was led: the films were stored either dried at 4 °C or immersed in PBS at 37 °C. In both situations, even after one year, neither modification in maximal wavelength nor in absorbance was observed showing an important stability. On the contrary, the colloidal solution was less stable: at 37 °C, particle aggregation was noticed after one month for the pure suspension and only after 1 h when

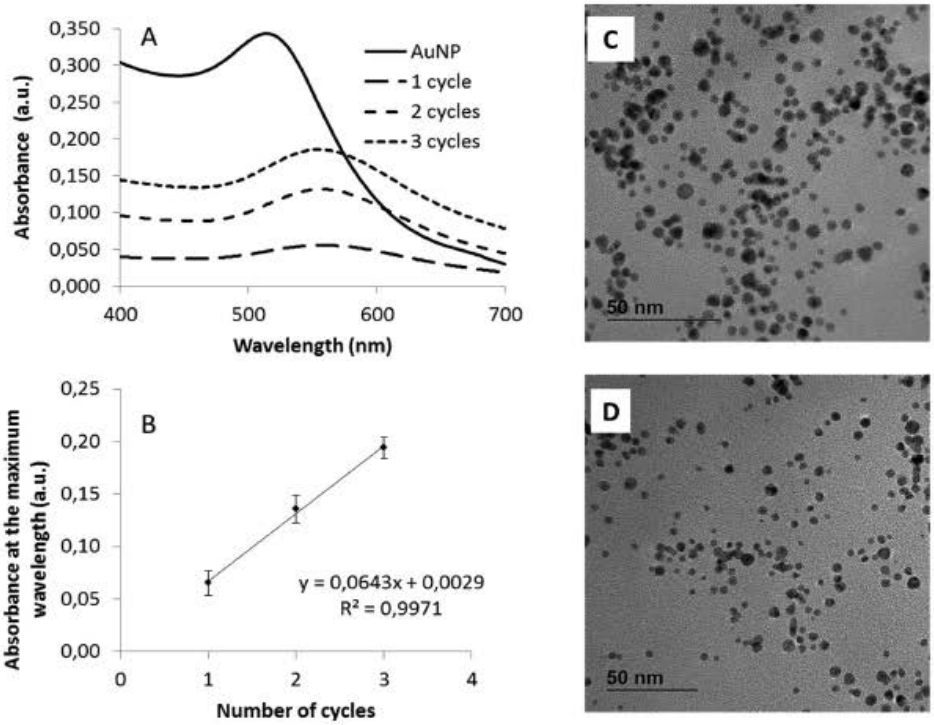

Figure 1. A) Visible spectra of the colloidal solution and the films and B) variation of maximal absorbance of the plasmon band plotted as a function of the number of coating cycles ($n = 9$, for each condition). TEM pictures of C) AuNP suspension and D) AuNP entrapped films $(PAH/AuNP/PAA)_3$.

ADVANCED SCIENCE NEWS
www.advancedsciencenews.com

Particle & Particle Systems Characterization
www.particle-journal.com

diluted in PBS. Although the enhanced stability brought by the polyelectrolyte film was already published,[10] for the first time, a long-term storage of such nanostructured films was studied either dried at 4 °C or under physiological-like conditions which is of particular importance for a future biomedical application. Moreover, degrading conditions (i.e., pH = 1 and 12 or 4 M NaCl) were also tested. Whatever the tested condition, no significant spectral modification was observed (e.g., maximal wavelength 548 ± 2, 546 ± 2, and 546 ± 3 nm for the acidic, basic, and salt conditions, respectively). This result highlighted again an enhanced stability of the nanostructured films compared to the colloidal solution (for which each condition induced a precipitation of the objects), which may be explained by a tightly interconnected network between the three partners. At last, the stability of the films was tested after being exposed to a shear stress during 2 and 6 h mimicking blood flow (1.5 Pa). This value (between 1 and 2 Pa) corresponds to the physiological value of shear stress in vessels having a diameter of 6 mm (small arteries such as coronaries).[20] In our experiment, no significant modification in AuNP spectral properties as well as in deposited nanoparticle quantity was observed (**Figure 2**).

2.2. Biocompatibility of Nanostructured Films

In order to evaluate the biocompatibility of the AuNP-structured films, the last deposited layer (either polycation or AuNP or polyanion) was varied to study its influence on biological materials. Thus, $(PAH/AuNP/PAA)_3$-PAH, $(PAH/AuNP/PAA)_3$, and $(PAH/AuNP/PAA)_2$-PAH/AuNP films were studied according to their surface topography and charge surface using atomic force microscopy (AFM) and capillary zone electrophoresis (CZE), respectively. Analyses in AFM (**Figure 3**A–C) revealed that no significant difference in film thickness was noticed whatever the outer layer: 284, 244, and 275 nm for $(PAH/AuNP/PAA)_3$-PAH, $(PAH/AuNP/PAA)_3$, and $(PAH/AuNP/PAA)_2$-PAH/AuNP, respectively.

However, the roughness was more important than previously reported results obtained without AuNP[21] (few nanometers compared to 39 and 31 nm for $(PAH/AuNP/PAA)_3$-PAH and $(PAH/AuNP/PAA)_3$). Finally, when the outer layer was AuNP, an important roughness (65 nm) was measured and no nanoparticle was observed at the surface of the film even at higher magnification (Figure 3C) but rather, a rugged surface was obtained. This fact can be explained by the tight electrostatic interactions developed between PAH and AuNP. Then, CZE which is an interesting separation tool (charged or neutral species migrate inside a fused silica capillary under an applied electric field) was used to assess the surface charge modification of $(PAH/AuNP/PAA)_3$-PAH, $(PAH/AuNP/PAA)_3$, and $(PAH/AuNP/PAA)_2$-PAH/AuNP films. In CZE, the apparent mobilities rely on both charge/mass ratio of the species under investigation and the electroosmotic flow (EOF) resulting from the capillary inner wall charge surface (negatively charged surface due to the ionized silanol groups). For a neutral compound, i.e., benzyl alcohol, the observed migration time comes only from the EOF and therefore it is directly in relation to charges of the silica capillary wall surface (sign and magnitude). As an example, a typical electrophoregram is shown in **Figure 4**A.

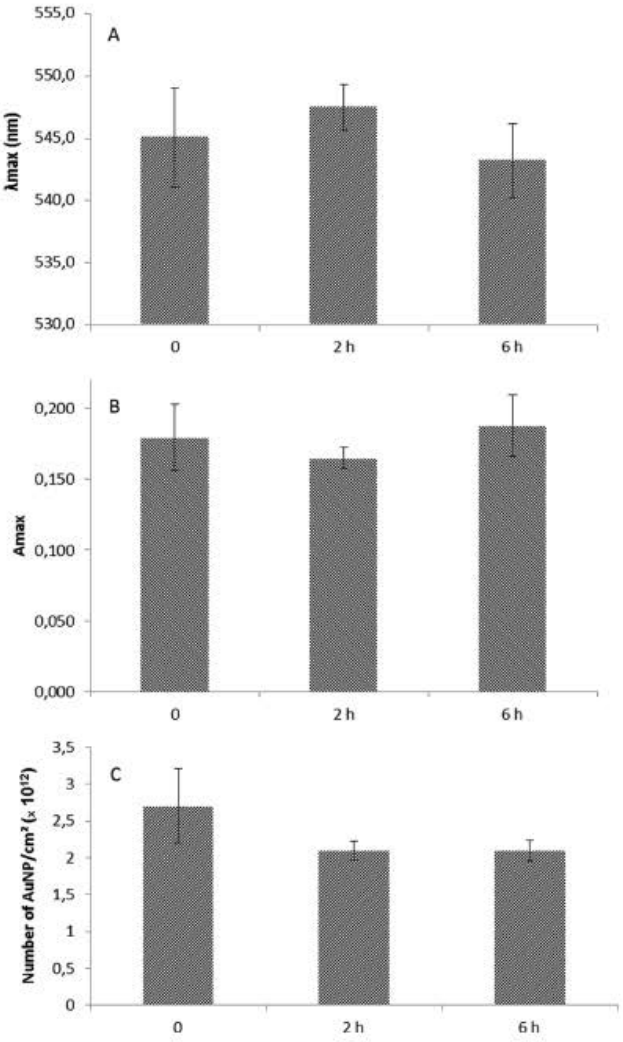

Figure 2. Behavior of films $(PAH/AuNP/PAA)_3$ after 2 or 6 h exposure to shear stress. The stability was monitored by the spectral properties of the entrapped AuNP [A) plasmon band value and B) absorbance] as well as their C) quantification ($n = 3$). Statistical analyses were performed with the Tukey–Kramer test.

The neutral marker migration time (NMT) as a function of the last deposited layer inside the capillary is monitored. After one PAH layer (layer 1), the NMT drastically increased (from 5 to 24 min) due to positive charges of polycation in tight interaction with bare silica leading to EOF neutralization. Then, the AuNP layer induced a small decrease in NMT (layer 2: NMT = 16 min) due to negative charge deposition. At last, the PAA layer brought an NMT close to bare silica (layer 3: NMT = 9 min) indicating an important anionic surface. The first cycle (PAH/AuNP/PAA) was then repeated twice and EOF obtained for each layer is described in Figure 4B. Similar results were measured for each cycle demonstrating the predominant role of the last layer coating. These results showed that $(PAH/AuNP/PAA)_3$-PAH, $(PAH/AuNP/PAA)_3$, and $(PAH/AuNP/PAA)_2$-PAH/AuNP films in which the outer layer was varied were different in

Particle & Particle Systems Characterization
www.particle-journal.com

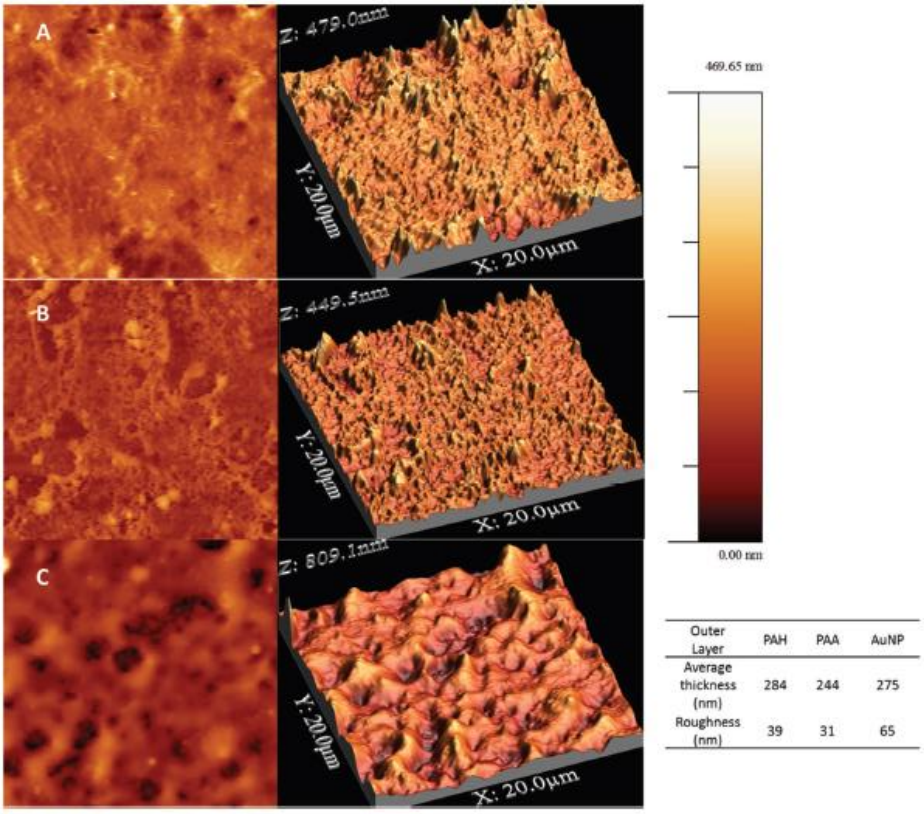

Outer Layer	PAH	PAA	AuNP
Average thickness (nm)	284	244	275
Roughness (nm)	39	31	65

Figure 3. AFM analyses and surface topography of A) $(PAH/AuNP/PAA)_3$-PAH, B) $(PAH/AuNP/PAA)_3$, and C) $(PAH/AuNP/PAA)_2$-PAH/AuNP films shown in 2D (left) or 3D (right).

terms of surface roughness and charge which may impact the interaction with biological materials.

In parallel to these physicochemical results, three main biological key points were assessed: biomolecule and protein adsorption, monocyte activation, and using rat blood: plasma protein interaction and hemolysis of whole blood. First, nanostructured film interaction with biomolecules and proteins is considered as a pivotal parameter that will assess its compatibility.[21] Therefore, a redox molecule and two proteins presently used at their plasmatic concentrations were selected: reduced glutathione (GSH; 10×10^{-6} M) as it easily reacts with AuNP,[9] albumin since it is quantitatively the most important

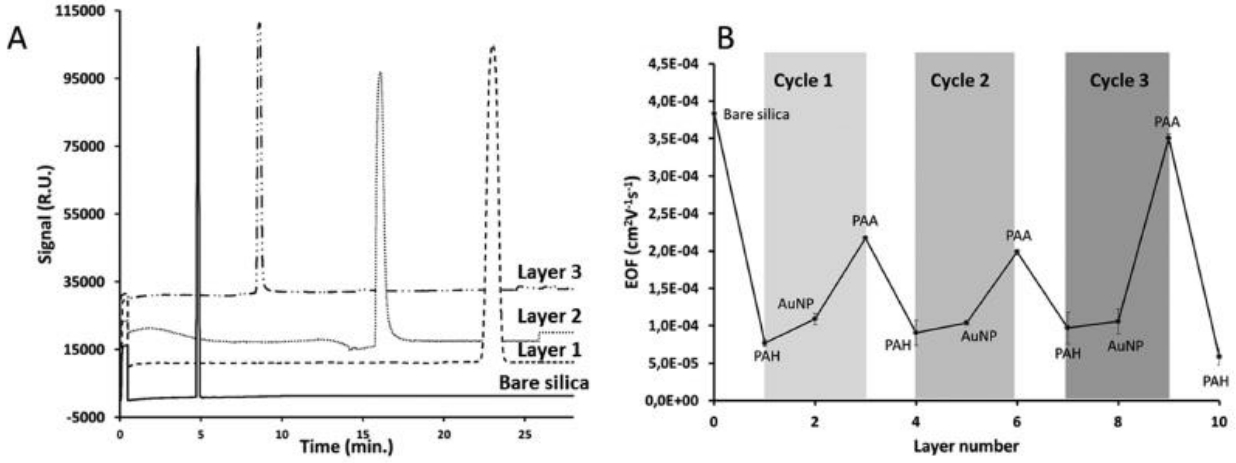

Figure 4. A) Electrophoregrams obtained by CZE for the deposition of the first cycle and B) the calculated EOF as a function of the layer number.

ADVANCED SCIENCE NEWS
www.advancedsciencenews.com

Particle & Particle Systems Characterization
www.particle-journal.com

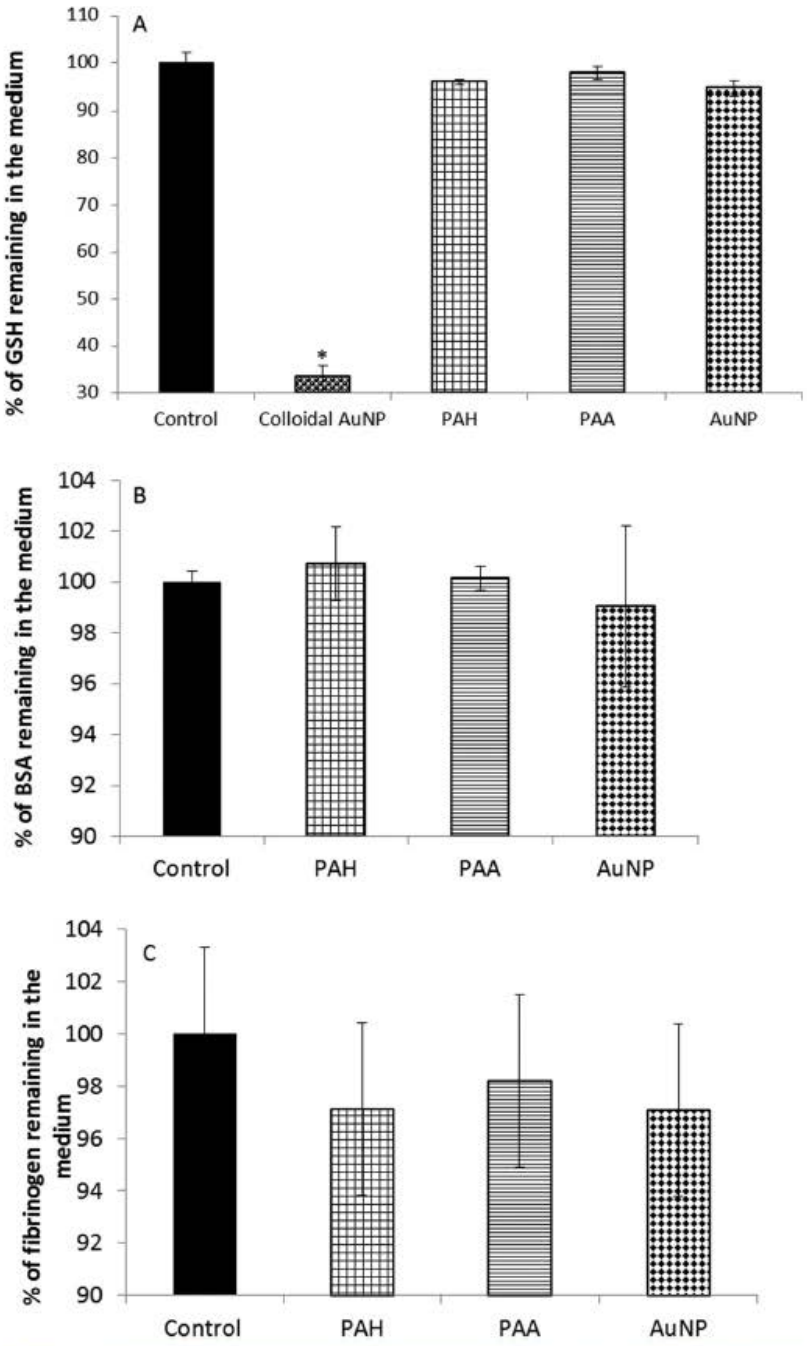

Figure 5. Biological tests realized onto AuNP either colloidal (5×10^{12} AuNP corresponding to the amount of immobilized NP on the $[PAH/AuNP/PAA]_3$ film) or entrapped polyelectrolytes films as a function of the outer layer either $((PAH/AuNP/PAA)_3\text{-}PAH)$ or $(PAH/AuNP/PAA)_3$ or AuNP $((PAH/AuNP/PAA)_2\text{-}PAH/AuNP)$ noted in the figure PAH, PAA, and AuNP, respectively, or using colloidal AuNP ($n = 3$). Biomolecule adsorption was realized using A) reduced glutathione, B) bovine serum albumin, and C) fibrinogen. Controls correspond to the same concentration of glutathione or proteins incubated without film. Statistical analyses were performed with the Tukey–Kramer test (* $p < 0.0001$ vs control).

protein in human blood (38–48 g L^{-1}) and fibrinogen (2–4 g L^{-1}) which plays a critical role in platelet adhesion and activation (**Figure 5**A–C).[21]

For all biomolecules, no significant adsorption was noticed after incubation with the films whatever the last layer. However, a 70% decrease of initial concentration of GSH was measured after incubation with colloidal AuNP. This highlighted the low AuNP reactivity when immobilized into the films.

Second, monocyte activation was studied after a 48 h incubation of the films with THP-1 cells. Indeed, monocytes are immunocompetent cells able to initiate immune responses as a function of their activation level. Based on two different tests (i.e., membrane permeation by trypan blue and mitochondrial metabolic activity by 4-[3-(4-iodophenyl)-2-(4-nitrophenyl)-2H-5-tetrazolio]-1,3-benzene disulfonate (WST-1)), no toxicity was found (viability superior to 80%). Then, real-time quantitative reverse transcription-polymerase chain reaction (qRT-PCR) analysis was performed to evaluate NCF1 (neutrophil cytosolic factor 1) and IL-1β (interleukine-1β) expression levels. Those genes are considered as classical marker genes of monocyte activation.[22] Our results (**Figure 6**A,B) showed that the monocyte phenotype was not orientated toward activation since NCF1 and IL-1β expression was not modified, whatever the last layer, which proved a great cytocompatibility.

Third, rat plasma was injected into the CZE system with LbL-coated capillaries, and after rinsing, the NMT was monitored as a function of the outer deposited layer (PAH or AuNP or PAA) (Figure 6C,D). When comparing the effect of plasma on a bare silica capillary, a protein adsorption inducing a neutralization of the charge surface was noticed; this implied a modification in NMT (10 vs 5 min when comparing Figures 6C and 4A) and a decrease in EOF. After PAH and PAH/AuNP coating (Figure 6D), the results proved an important surface neutralization (no EOF in normal and reverse polarity) and a lack of stability of the created films (multiple peaks detected), respectively, which may not match the biocompatibility criteria. Using PAA as the outer layer showed the presence of a unique NM peak, revealing a stabilization of the previous layers (PAH/AuNP) (Figure 6C). Nevertheless, PAH/AuNP/PAA films proved a more important protein adsorption than PAH/PAA (NMT of ≈15 vs 6 min, respectively).

At last, films were incubated with rat whole blood to evaluate their capacity to induce hemolysis. In this experiment (Figure 6E), the outer layer affected the obtained results. Indeed, only in the case of PAA, the hemocompatibility was proven. The other kinds of

Particle & Particle Systems Characterization
www.particle-journal.com

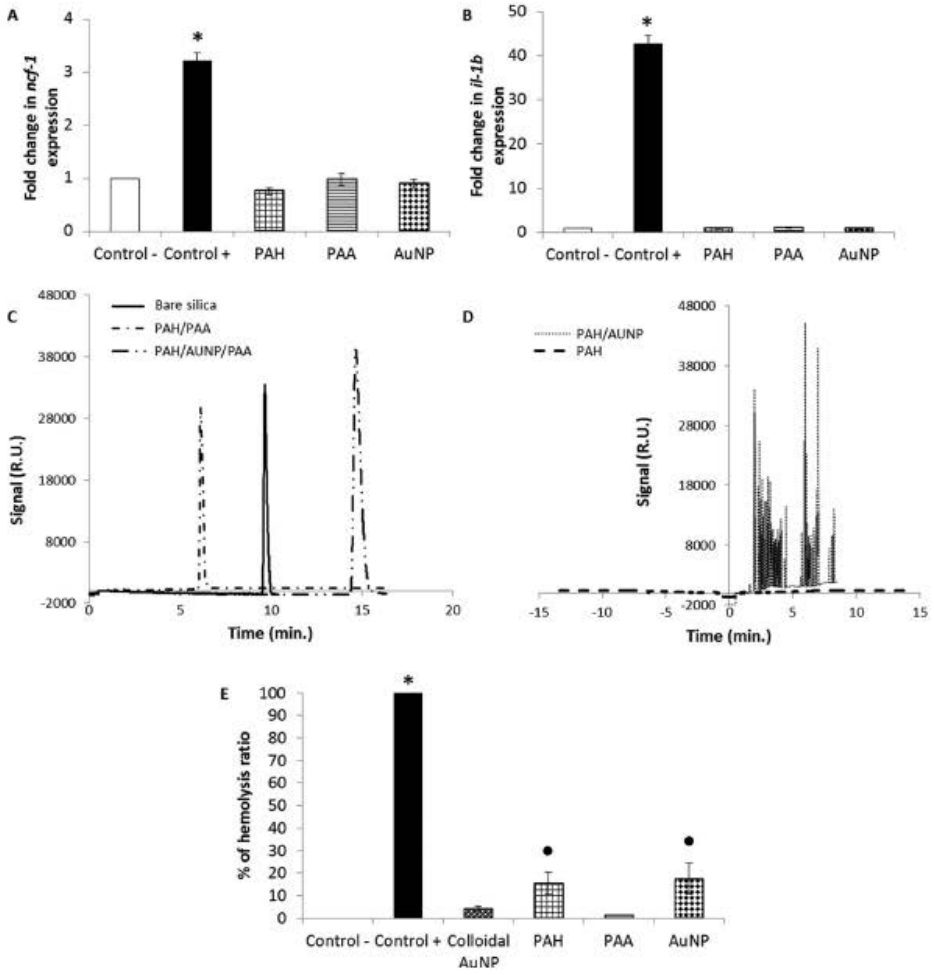

Figure 6. Biological tests realized onto AuNP either colloidal (5×10^{12} AuNP corresponding to the amount of immobilized NP on the [PAH/AuNP/PAA]$_3$ film) or entrapped polyelectrolyte films as a function of the outer layer either ((PAH/AuNP/PAA)$_3$-PAH) or (PAH/AuNP/PAA)$_3$ or AuNP ((PAH/AuNP/PAA)$_2$-PAH/AuNP) noted in the figure PAH, PAA, and AuNP, respectively, or using colloidal AuNP ($n = 3$). Monocyte activation (control −: 10 mL of cell suspension; control +: 10 ng mL^{-1} of phorbol 12-myristate 13-acetate added to cells) was checked using real-time qRT-PCR through gene expression rise of A) NCF-1 and B) IL-1β. C,D) Rat plasma interaction with pre-coated capillary was studied after 5 min injection into CZE monitoring the NMT. E) Percentage of hemolysis of rat whole blood following the absorbance of hemoglobin after covered slide incubation (control +: 10 mL of water + 0.2 mL of diluted blood; control −: 10 mL of NaCl + 0.2 mL of diluted blood). Statistical analyses were performed with the Tukey–Kramer test (* $p < 0.0001$ vs control − and • $p < 0.0002$ vs control −).

films ((PAH/AuNP/PAA)$_3$-PAH or (PAH/AuNP/PAA)$_2$-PAH/AuNP) showed a significant hemolysis. In order to investigate the effect of AuNP, some films based on one layer of PAH, or (PAH/PAA)$_1$ and (PAH/PAA)$_3$ were tested according to the same protocol. The results showed no significant hemolysis (2.5 ± 0.3%, 0.5 ± 0.2%, and 1.2 ± 0.3%, respectively) when PAA was placed on the outer layer, emphasizing the best hemocompatibility of films terminated by PAA. Such results were in accordance with the ones obtained on rat plasma. Colloidal AuNP incubated with blood induced a residual hemolysis (4.1 ± 1.1%) which was, however, not significant.

Taken together, these results highlighted main points. The nature of the outer layer influenced the biocompatibility of the prepared LbL films: when using a polyanion, PAA, better results were obtained with overall good biocompatibility. Indeed, a polycation such as PAH easily interacts with biological materials through electrostatic interactions and AuNP through redox activity or gold–sulfur bond.[5,15,16,23] Herein, the outer PAA anionic layer was essential to improve the inertness of the developed three partner-based "sandwich system."

3. Conclusion

In summary, this study showed that AuNP can be entrapped into such three partners LbL films. No modification of these entrapped particles was highlighted from a physicochemical point of view. Particles also showed an improved stability after long-term storage and also under degrading conditions compared to the colloidal solution. The interaction with biological

ADVANCED SCIENCE NEWS
www.advancedsciencenews.com

Particle & Particle Systems Characterization
www.particle-journal.com

materials was studied as a function of the outer deposited layer (either PAA or PAH or AuNP). The better cyto/hemocompatibility was obtained using the polyanion as the last depot. This report is the first one to show the behavior and inertness of AuNP immobilized films under biological conditions compared to the colloidal state and the possibility to use them for further biomedical applications. Indeed, these particles can be easily grafted by drugs or biomolecules and then being entrapped into LbL films to act as smart medical devices.

4. Experimental Section

Materials: PAH powder and PAA sodium salt solution in 35% wt in water with average molecular masses of 15 000, penicillin, streptomycin, amphotericin B, and trypan blue solution were purchased from Sigma Aldrich. Solutions of 1 M HCl from Fluka were used for pH adjustments. RPMI medium was purchased from GIBCO (In vitrogen). Dodecyl sulfate sodium salt (SDS) and fetal bovine serum were supplied by Eurobio. WST-1 was purchased from Roche Applied Sciences. PBS solution was prepared as follows: $[Na_2HPO_4] = 6.48 \times 10^{-3}$ M, $[KH_2PO_4] = 1.47 \times 10^{-3}$ M, $[NaCl] = 138 \times 10^{-3}$ M, and $[KCl] = 2.68 \times 10^{-3}$ M, final pH was adjusted to 7.4. All other reagents were supplied by Sigma Aldrich and were of analytical grade. Ultrapure deionized water (>18.2 MΩ cm) was used for the preparation of all solutions. Citrate capped gold nanoparticles were synthesized according to ref. [15].

Animals and Blood Sampling Protocol: All experiments were performed in accordance with the European Community guidelines (2010/63/EU) for the use of experimental animals. Male Wistar rats between 280 and 350 g (Charles River, France) were used in this study. To obtain arterial blood samples, rats were anesthetized (starting 15 min before sample time) with isoflurane (4% in oxygen 2 L min^{-1}). After anticoagulation (500 UI of heparin sodium, intravenous administration), a laparotomy was performed in order to access the abdominal artery. Blood was obtained directly from the artery through a short PTFE catheter (Intraflon 2, Vygon, France) and collected in Vacutainer (Becton Dickinson, USA) tubes containing heparin lithium.

Plasma was obtained after centrifugation (10000 × *g*, 15 min, 4 °C) and keep at −20 °C.

Film Preparation: The glass substrates used for the deposition (24 × 36 × 0.145 mm, Menzel-Glaser) were cleaned with SDS 0.1 M at 100 °C for 15 min, followed by extensive rinsing with water. They were then immersed in HCl 0.1 M at 100 °C for 15 min, extensively rinsed and finally dried.

Polyelectrolyte solutions (0.1 M according to monomers molecular masses) were prepared freshly before each experiment in PBS. Addition of 1 M HCl in the PAA solution was required to adjust pH to 7.4. The fabrication of AuNPs/polymer multilayer film was carried out as follows. A pre-treated glass slide was dipped in the solution of PAH for 10 min, and then rinsed with two successive baths of PBS (2 and 1 min, respectively). Subsequently, the slide was immersed in the AuNPs suspension for 10 min, then rinsed as previously described, and finally dipped in the PAA solution for 10 min, rinsed and at the end dried. The AuNPs-incorporating polymer multilayer film was obtained by the repetition of this simple three-step process in a cyclic fashion leading to $(PAH/AuNP/PAA)_3$. In some experiments, the last bath was either PAH ($(PAH/AuNP/PAA)_3$-PAH) or AuNP ($(PAH/AuNP/PAA)_2$-PAH/AuNP).

Film Characterization: Absorbance spectra (400–700 nm) of the coated slides (vs an uncoated pre-cleaned slide) were recorded on a UV-1800 apparatus (Shimadzu). For stability studies, slides were kept dried at 4 ± 4 °C or in an incubator at 37 ± 1 °C in 10 mL of PBS filtered on 0.22 µm. At predetermined time, absorbance spectrum of each slide was recorded. As controls, 10 mL of AuNP (pure and diluted 1/3 in PBS) were kept in the same conditions and their spectra recorded against PBS. Experiments were run in triplicate.

Additional stability studies were performed on slides versus pH 1 and 12 (using 1 M HCl, 1 M NaOH, and 4 M NaCl). Slides were dipped in the solution for 15 min and an absorbance spectrum was recorded.

For TEM, the films were deposited on carbon covered copper grids (Agar) using the previous protocol but decreasing the incubation time from 10 to 3 min and a last washing of 1 min in water. Then, images were recorded using a Philips CM20 instrument with a LaB6 cathode operating at 200 kV. The average diameter of the gold core was calculated for each AuNP sample by counting ≈200 individual particles from the TEM images. For AFM, films were prepared on glassware slides and immersed into PBS for analysis using a MFP3D-BIO instrument (Asylum Research Technology, Atomic Force F & E GmbH, Mannheim, Germany). Gold quantification was performed according to ref. [24] with some slight modifications. Three slides were crushed with a glass rod and carefully transferred into a vial and 1 mL of an oxidant solution (1 M HCl, 2.6 M NaCl, and 0.035 M Br_2) was added. After an incubation of 20 min under stirring at 20 °C and 1 h at 60 °C, gold was quantified using the protocol of Tournebize et al.[24]

For shear stress experiments, a parallel-chamber flow system (Masterflex, USA) was used. Briefly, shear stress experiments were carried out at 37 °C in a 5% CO_2 incubator, 7.5 × 3.8 cm glass coverslips coated with $(PAH/AuNP/PAA)_3$ were placed on the top of the flow chamber allowing fluid flux to pass though the coated surface. The shear stress was gradually increased to 1.5 Pa and lasted for 2 or 6 h.[25] Glass coverslips were then disassembled for the stability test.

Capillary Zone Electrophoresis: All experiments were performed on a Beckman P/ACE 5500 model (Beckman, Fullerton, USA) equipped with a UV detector set at $\lambda = 200$ nm in normal polarity mode, anodic injection (negative times indicate a reverse polarity). Capillary temperature was controlled by coolant at 25.0 °C. An untreated fused-silica capillary, 50 µm internal diameter with a total length of 37 cm (effective length: 30 cm) was employed. The neutral marker benzyl alcohol (0.1 mg mL^{-1} in background electrolyte, BGE) was injected in the hydrodynamic mode (10 s under pressure) at 10 kV. The experimental setup, data acquisition, and processing were governed using Beckman P/ACE Station software. The BGE was tenfold diluted PBS. For the first experiment, the capillary was rinsed with 1.0 M sodium hydroxide (20 min) and ultrapure water (20 min). Each injection was realized in triplicate, results were indicated as a mean and residual standard deviations were always lower than 3.0%. Polyelectrolyte solutions used to coat the capillary were those described in the film preparation section. Rapidly, for each layer, the capillary was first filled with the coating solution (PAH or AuNP or PAA) at 20 psi for 3 min and rinsed with the same solution at 0.5 psi (low pressure mode) for 30 min. Between each layer, benzyl alcohol was injected three times and before each injection, the capillary was successively rinsed with ultrapure water (2 min) and BGE (3 min). The EOF mobility was determined using the migration time (NMT) of the EOF marker and Equation (1)

$$EOF = \frac{L \times l}{NMT \times V} \quad (1)$$

where L and l are the total and the apparent lengths of the capillary (length to detection) and V the applied voltage.

In a second set of experiments, plasma samples were diluted in 20% BGE and injected during 5 min under a pressure of 20 psi. Then, BGE was used to rinse the capillary and the surface charge was evaluated by three NM injections. The capillary was rinsed with 1.0 M NaOH (20 min) and H_2O (20 min) to recover the initial silanol surface.

Reactivity with Reduced Glutathione: In a water bath at 37 ± 1 °C, slides were equilibrated for 1 h in PBS and then incubated for 2 h in 10 mL of 10×10^{-6} M GSH in PBS. The remaining GSH concentration in the dipping solution was determined using Ellman's method. Briefly, 200 µL of 5,5′-dithio-bis(2-nitrobenzoic) acid solution (1×10^{-3} M in 1.0 M Na_2HPO_4 and 2×10^{-3} M EDTA buffer, pH 7.5) were added to 1 mL of sample. The resulting mixture was incubated for 10 min at room temperature protected from light, before its absorbance was measured

Particle
Particle Systems Characterization
www.particle-journal.com

ADVANCED SCIENCE NEWS
www.advancedsciencenews.com

at 412 nm. Calibration curve was obtained with a standard GSH solution (3.25×10^{-3} M in 1.0 M HCl) diluted in Na_2HPO_4/EDTA buffer, in the range of $3.25–32.5 \times 10^{-6}$ M. As a control, colloidal AuNPs were diluted in PBS to obtain a final amount of 5×10^{12} NP and the resulting suspension was centrifuged at 40 000 × *g* at 4 ± 1 °C for 30 min before performing Ellman's reaction.

Reactivity with Proteins: To evaluate the adsorption of proteins, slides were equilibrated for 1 h at 37 ± 1 °C in PBS, then incubated for 2 h in a solution of bovine serum albumin (BSA, 40 g L^{-1} in PBS) or fibrinogen (2 g L^{-1} in PBS). After experiment, slides were rinsed carefully with PBS and dried. Remaining BSA and fibrinogen in the dipping solution were evaluated by spectrofluorimetry (278/340 nm, excitation and emission bandwidth 5 nm, response 0.5 s, sensitivity low, linearity range 50–1000 µg mL^{-1}, spectrofluorimeter FP-8300, Jasco).

Interaction with Monocytes: Each experiment was done with three independent biological replicates. Human THP-1 monocytes (ATCC TIB-202, Manassas, VA, USA) were grown according to ATCC recommendations in order to obtain three independent cultures. 10 mL of cell suspension were put into polypropylene tubes at 150×10^3 cells mL^{-1}. After 1 d, slides were soaked in the tubes. A negative control (10 mL of cell suspension) was realized. As a positive control, cells were exposed to 10 ng mL^{-1} of phorbol 12-myristate 13-acetate. Cell viability was assessed after 24 and 48 h exposure performing trypan blue and WST-1 methods. Variation of expression of NCF1 and IL-1 β was followed. After 24 h of exposure, cells were washed twice with sterile PBS and total RNA was extracted by TRIzol reagent (Invitrogen, La Jolla, CA) following manufacturer's protocol. Real-time quantitative reverse transcription-polymerase chain reaction analyses were performed according to the conditions of a previous work.[22]

Interaction with Blood: Hemolysis ratio (HR) of the coated cover glasses was measured using a method described previously with slight modifications.[26] Briefly, the cover glasses were pre-incubated for 1 h in 10 mL of sterile NaCl 0.9% (B-Braun) into flat-bottom bottles kept at 37 ± 1 °C in a shaking water bath. Whole arterial blood from a male Wistar rat was diluted (2 mL of blood for 2.5 mL of NaCl 0.9%) ($n = 3$). Immediately, 0.2 mL of diluted blood was added into each bottle containing 10 mL of sterile NaCl 0.9% or water for the positive control. Cover glasses were soaked in the blood solution for another 1 h. Finally, solutions were centrifuged at 1000 × *g* for 5 min and absorbance of the supernatant was measured at 576 nm. Colloidal AuNPs were diluted into blood to obtain a final amount of 5×10^{12} NP, and the resulting suspension was centrifuged at 40 000 × *g* at 4 ± 1 °C for 30 min before absorbance measurements. HR was obtained by Equation (2)

$$HR = 100 \times \frac{(AS - AN)}{(AP - AN)} \quad (2)$$

where AS is the absorbance of sample supernatant, AP and AN are the absorbance of positive (10 mL of water + 0.2 mL of diluted blood) and negative controls (10 mL of NaCl + 0.2 mL of diluted blood), respectively.

Acknowledgements

A.P. and M.P. contributed equally to this work. The authors want to thank Prof. R. Schneider, Prof. D. Rouxel, and Dr. G. Francius for AuNP synthesis, TEM and AFM facilities. This work was financially supported by Université de Lorraine (Project No. 2015, supervisor Dr. A. Boudier, Project No. AAP-002-100).

Received: July 13, 2016
Revised: September 12, 2016
Published online: October 28, 2016

[1] R. R. Costa, J. F. Mano, *Chem. Soc. Rev.* **2014**, *43*, 3453.
[2] J.-F. Chapel, J.-F. Berret, *Curr. Opin. Colloid Interface Sci.* **2012**, *17*, 97.
[3] K. Sato, S. Takahashi, J. Anzai, *Anal. Sci.* **2012**, *28*, 929.
[4] S. Pavlukhina, S. Sukhishvili, *Adv. Drug Delivery Rev.* **2011**, *63*, 822.
[5] Z. Tang, Y. Wang, P. Podsiadlo, N. A. Kotov, *Adv. Mater.* **2006**, *18*, 3203.
[6] X. Liu, P. K. Chu, C. Ding, *Mater. Sci. Eng., R* **2010**, *70*, 275.
[7] S. Srivastava, N. A. Kotov, *Acc. Chem. Res.* **2008**, *41*, 1831.
[8] H. Takahashi, D. Letourneur, D. W. Grainger, *Biomacromolecules* **2007**, *8*, 3281.
[9] B. Duncan, C. Kim, V. M. Rotello, *J. Controlled Release* **2010**, *148*, 122.
[10] D. M. Dotzauer, J. Dai, L. Sun, M. L. Bruening, *Nano Lett.* **2006**, *6*, 2268.
[11] T. Placido, E. Fanizza, P. Cosma, M. Striccoli, M. L. Curri, R. Comparelli, A. Agostiano, *Langmuir* **2014**, *30*, 2608.
[12] Z. M. Qi, I. Honma, M. Ichihara, H. S. Zhou, *Adv. Funct. Mater.* **2006**, *16*, 377.
[13] M. M. O. Thotiyl, H. Basit, J. A. Sanchez, C. Goyer, L. Coche-Guerente, P. Dumy, S. Sampath, P. Labbé, J. C. Moutet, *J. Colloid Interface Sci.* **2012**, *383*, 130.
[14] E. C. Dreaden, A. M. Alkilany, X. Huang, C. J. Murphy, M. A. El-Sayed, *Chem. Soc. Rev.* **2012**, *41*, 2740.
[15] J. Tournebize, A. Boudier, O. Joubert, H. Eidi, G. Bartosz, P. Maincent, P. Leroy, A. Sapin-Minet, *Int. J. Pharm.* **2012**, *438*, 107.
[16] J. Tournebize, A. Boudier, A. Sapin-Minet, P. Maincent, P. Leroy, R. Schneider, *ACS Appl. Mater. Interfaces* **2012**, *4*, 5790.
[17] A. I. Petrov, A. A. Antipov, G. B. Sukhorukov, *Macromolecules* **2003**, *36*, 10079.
[18] G. Decher, *Science* **1997**, *277*, 1232.
[19] N. Khlebtsov, L. Dykman, *Chem. Soc. Rev.* **2011**, *40*, 1647.
[20] D. Giddens, C. Zarins, S. Glagov, *J. Biomech. Eng.* **1993**, *115*, 588.
[21] H.-W. Chien, S.-F. Tan, K.-L. Wei, W.-B. Tsai, *Colloids Surf., B* **2011**, *88*, 297.
[22] C. Ronzani, R. Safar, R. Diab, J. Chevrier, J. Paoli, M. A. Abdel-Wahhab, A. Le Faou, B. H. Rihn, O. Joubert, *Cell Biol. Toxicol.* **2014**, *30*, 137.
[23] J. Tournebize, A. Sapin-Minet, G. Bartosz, P. Leroy, A. Boudier, *Talanta* **2013**, *116*, 753.
[24] J. Tournebize, A. Sapin-Minet, R. Schneider, A. Boudier, P. Maincent, P. Leroy, *Talanta* **2011**, *83*, 1780.
[25] C. Gaucher-Di Stasio, E. Paternotte, C. Prin-Mathieu, B. J. Reeder, G. Poitevin, P. Labrude, J. F. Stoltz, C. E. Cooper, P. Menu, *Biomaterials* **2009**, *30*, 445.
[26] X. Ye, X. Hu, H. Wang, J. Liu, Q. Zhao, *Acta Biomater.* **2012**, *8*, 1057.

1.3. Conclusion

Nos films ont montré la capacité à piéger des AuNP en grande quantité et possèdent aussi une bonne biocompatibilité. Ils ont également démontré une très bonne stabilité dans différentes conditions (à sec ou en solution, à 4 °C ou 37 °C, en milieu acide ou basique …)

Les films ont été déposés à la surface des stents (en alliage Nickel-Titane, NiTinol®, achetés auprès de Nimesys) selon la méthode de trempage décrite dans l'article 5. Vingt cycles ont été réalisés sur chaque stent. Le dosage de l'or déposé ainsi que des observations en AFM et MEB (Figure 21) ont été réalisés.

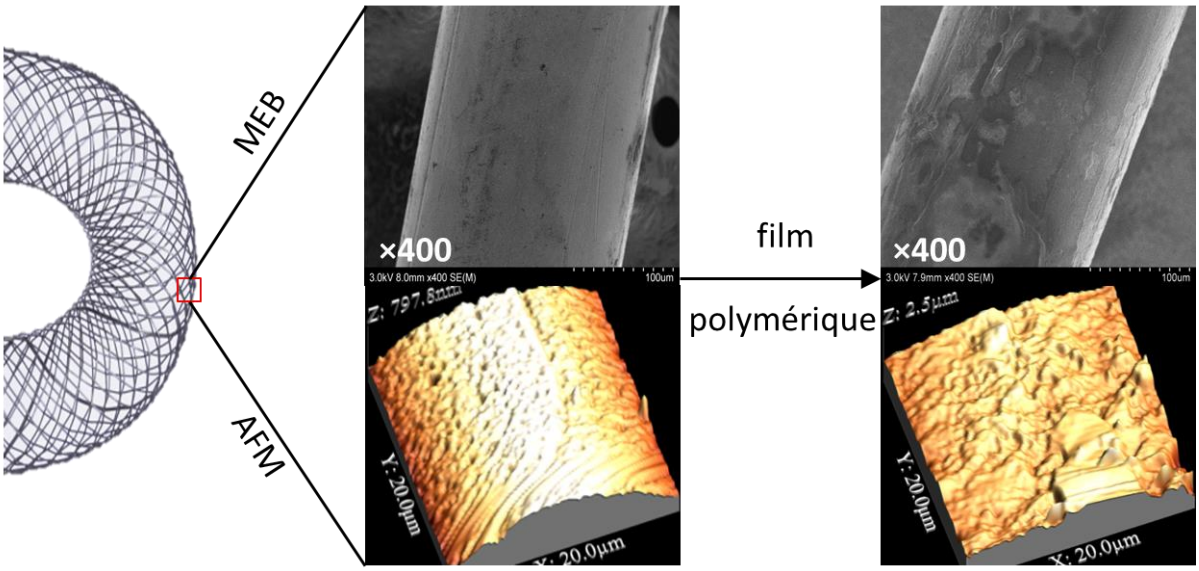

Figure 21 : Observations réalisées en MEB et AFM d'un stent nu et puis d'un stent recouvert de 20 cycles de polymères et AuNP.

Le dosage d'or montre un nombre d'AuNP égal à 2,3 ± 1,1 × 10^{11} NP/cm²/cycle (n = 3). Ce nombre est cohérent avec le résultat déterminé sur les films composés de 3 cycles et déposés sur les lamelles (moyenne à 6,3 ± 2,3 × 10^{11} NP/cm²/cycle). La méthode utilisée pour le dépôt des films est donc reproductible et répétable sur différentes surfaces.

L'épaisseur des films déposés sur stent est de 296 ± 49 nm pour une rugosité de 65 ± 21 nm (n = 3). Ces mesures, issues des observations en AFM, ont été réalisées à sec dans le cas des stents ce qui explique la faible différence d'épaisseur avec les films déposés sur des lames. Les observations sur ces derniers avaient été réalisées dans du PBS ce qui peut induire un gonflement du film sous l'effet de l'écrantage des charges entre les polyélectrolytes par les ions en solution. Dans notre étude, les quantités très importantes d'AuNP incorporées dans les films ainsi que la possibilité pour chaque particule d'être fonctionnalisée avec de forts rendements, permettront de constituer par la suite le réservoir délivrant NO. Les observations réalisées en MEB montrent un dépôt des films en forme d'îlots (Figure 21). Ce phénomène peut être expliqué par un nombre de cycles insuffisant déposé à la surface du stent. Il est probablement nécessaire d'augmenter le nombre de cycles pour aboutir à un revêtement homogène, plus adapté à une implantation *in vivo*.

2. Optimisation de la capacité du réservoir

Les résultats précédents démontrent bien la preuve de concept de la fabrication de telles décorations de surfaces pour des DM. Maintenant, en prenant en compte les données préliminaires sur la fonctionnalisation des AuNP (7500 molécules de GSH par AuNP) ainsi que le nombre d'AuNP immobilisées dans les films à chaque cycle (10^{12}) ; le nombre de cycles nécessaire pour atteindre la taille de réservoir visée serait d'environ 1500. Un tel nombre successif de cycles n'est pas envisageable et une optimisation du taux de chargement en AuNP doit être effectuée. Pour cela, la littérature montre que les conditions de formation du film sont des paramètres à optimiser. Dans notre étude, le PAH a été comparé à deux autres polycations aux propriétés différentes (constante d'ionisation (pKa), hydrophilie, nombre de charges par monomère …) lors de la construction des films. Puis, deux tampons

différents ont été étudiés : le PBS (référence) et une solution de Tris (même pH et concentration). Enfin, des surcharges d'AuNP ont été réalisées sur des films composés de 3 cycles, pour optimiser leur chargement. Les modèles précédemment cités (lamelle de verre, capillaire de l'ECZ, cristal de la QCM) ont été utilisés pour étudier la construction des différents films. Le principe de la QCM repose sur l'utilisation de matériaux piézoélectriques (*i.e.* le quartz). Lorsque celui-ci est soumis à un courant électrique, il vibre à une fréquence déterminée par sa taille et son épaisseur (Figure 22 A). Si la surface du cristal est modifiée (*i.e.* dépôt d'une couche de polymère), la fréquence de vibration est modifiée (Figure 22 B).

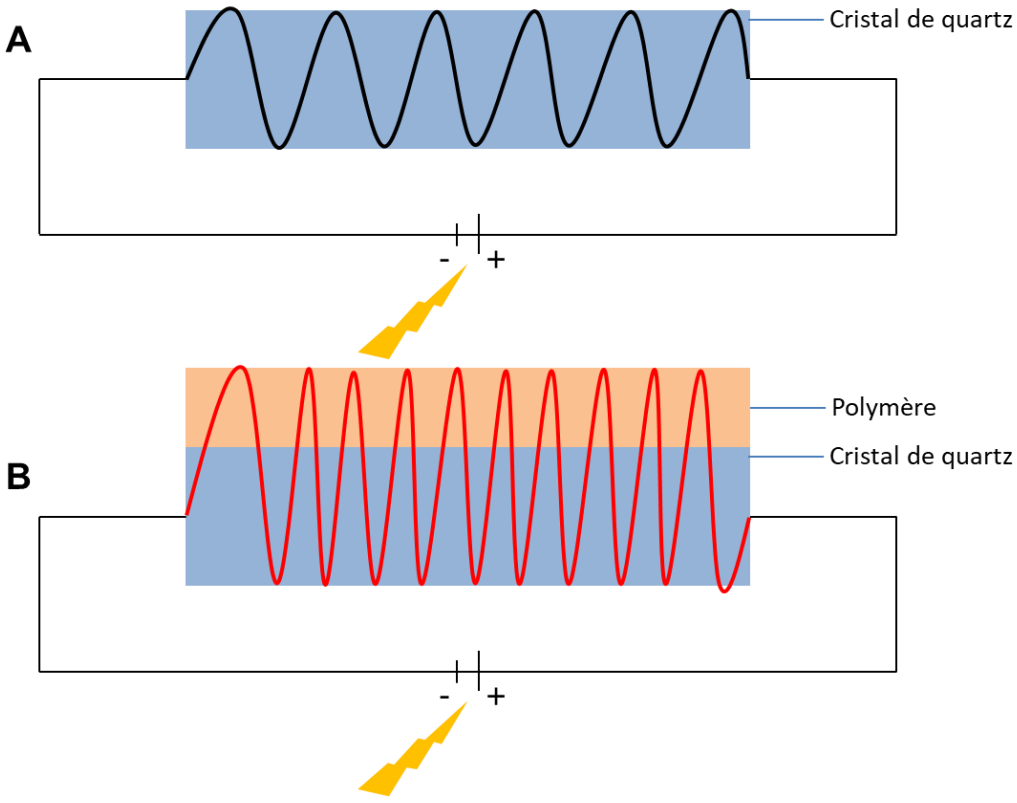

Figure 22 : Schéma de fonctionnement d'une QCM (A) avant modification de la surface du cristal et (B) après dépôt d'une couche polymérique.

En mesurant la différence des fréquences du cristal, on peut déterminer l'épaisseur ainsi que la masse de la couche déposée. Ce principe est classiquement utilisé pour visualiser

le dépôt des différentes couches des films. La quantité d'AuNP immobilisées au sein de chaque film a également été quantifiée grâce à la méthode HPLC-visible décrite dans l'article 2. Les résultats font l'objet d'une publication qui sera prochainement soumise (Article 6).

2.1. Article 6 : Some keys to enrich layer-by-layer films with nanoparticles

SOME KEYS TO ENRICH LAYER-BY-LAYER FILMS WITH NANOPARTICLES

Arnaud PALLOTTA[1], Igor CLAROT[1], Philippe LAVALLE[2], Bernard SENGER[2] and Ariane BOUDIER[*1]

1: Université de Lorraine, CITHEFOR EA 3452, « Cibles thérapeutiques, formulation et expertise préclinique du médicament », Faculty of Pharmacy, NANCY, France.

2: INSERM UMR 1121, 11 rue Humann, 67085 Strasbourg, France

[*] Contact: ariane.boudier@univ-lorraine.fr

Abstract:

The design of layer-by-layer (LbL) polyelectrolyte films including nanoparticles is a growing field of innovation in a wide range of biomedical applications. Gold nanoparticles (AuNP) are very attractive in this view. The nanostructuration of LbL films using such metallic species depends on the conditions of construction *i.e.* polymer nature and dissolution buffer. Tripartite LbL films (polycation, AuNP, polyanion) were evaluated using 3 different polycationic polymers (poly(allylamine hydrochloride) (PAH), poly(ethylene imine) (PEI) and poly(methacrylate ester) (PMAE)) and also two media (phosphate buffered saline (PBS) and Tris). The AuNP incorporation and film stability were analyzed by visible spectrophotometry, capillary zone electrophoresis, quartz crystal microbalance, and high performance liquid chromatography. The optimized AuNP enrichment conditions were obtained using PAH, best compromise between AuNP loading and film stability properties. Tris buffer allows to increase 1.7 times more AuNP than PBS in the films. As a conclusion, this work laid the bases of further development of LbL films enriched with drug functionalized AuNP for biomedical device coating.

Keywords: Polyelectrolyte films, gold, stability, nanoparticle loading, dynamic models, physicochemical evaluation

Introduction

Polyelectrolyte layer-by-layer (LbL) films are promising coatings for applications in the field of medical device. They are composed by the self-assembly of different polymers through electrostatic bonds between polyelectrolytes of opposite charge. They can include drug to induce specific therapeutic effect as well, but these films show some limitations for long term drug release [1]. To overcome this problem, two methods can be applied. The first one corresponds to hierarchically assembled films [2-3]: stratified films with barrier layers in between will lead them to gradually release the drug depending on external conditions such as pH, temperature or salt concentration… The second one deals with a mechanical increase of the reservoir capacity by its enrichment with nanoparticles (NP) that directly interact with polymers. In this case, the selected coating conditions (polyelectrolytes and media) appeared to play a major role in the film construction and stability [4-5].

Beside prolonged drug release, nanoparticle inclusion into LbL films was described to confer specific properties to the coating as antibacterial activity by the addition of silver NP [6-8], theranostic platforms using ferrous magnetic NP [9], or even sensors *via* inclusion of gold nanoparticles (AuNP) [10-11]. Recently, AuNP were entrapped inside multilayered polyelectrolyte films for the development of a biocompatible material [12]. These particles were chosen for their high capacity of active pharmaceutical ingredient grafting [13] which allowed the formation of a huge drug reservoir. But for the best of our knowledge no study took interest in maximizing the embedment of AuNP inside films.

The aim of this paper relied on the investigation of the optimization in the design of nanoparticle enriched LbL films. Based on a tripartite system (polycation + negatively-charged AuNP + polyanion), two main points were addressed: influence of the polycation and the dissolution buffer. As a hypothesis, the number of charges on the polycationic specie

should be a key parameter in the amount of immobilized AuNP loaded inside films. Herein, we tested 3 different polycations (Figure 1): two hydrophilic polymers (poly(allylamine) hydrochloride (PAH) and poly(ethylene imine) (PEI)) and one hydrophobic (poly(methacrylate ester) (PMAE)). Recent papers pointed out the important role of phosphate ions in the LbL disorganization [4-5]. Two different buffers were evaluated in this work: phosphate-buffered saline (PBS) as the reference one *vs* Tris buffer (using the same pH and salt concentration for both). To evaluate their formation, films were built under different techniques: a static one with cover glasses using a classical dip-coating method [14] and two dynamic models using capillary zone electrophoresis (CZE) and quartz crystal microbalance (QCM). The requirements to define the best conditions relied on the compromise between nanoparticle entrapment and film stability. Indeed, for future biomedical applications and taking into account mechanical constraints (blood flow, muscle contractions …) encountered by medical devices, the design of nanostructured films should lead to stable coating without any nanoparticle/film leakage.

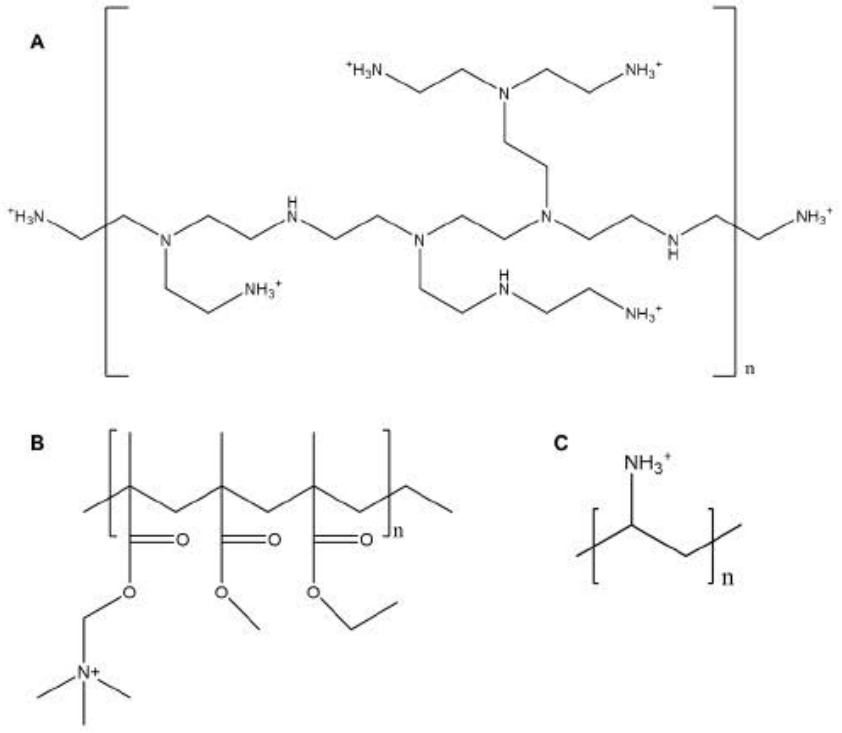

4

Figure 1: Chemical structures of (A) PEI, (B) PMAE and (C) PAH.

Experimental

1.1. Reagents

Poly(allylamine hydrochloride) powder (PAH), poly(acrylate, sodium salt) (PAA) solution 35 % wt in water with average molecular masses of 15,000 and branched poly(ethylene imine) (PEI) solution 50 % wt in water with average molecular masse of 800,000 were purchased from Sigma Aldrich. Poly(methacrylate ester) powder (PMAE) was purchased from Evonick Industries (Eudragit® RL). Solutions of HCl 1.0 M from Fluka were used for pH adjustments. Sodium dodecyl sulfate (SDS) was supplied by Eurobio. Phosphate-buffered saline (PBS 148 mM) solution was prepared as follows: $[Na_2HPO_4]$ = 6.48 mM, $[KH_2PO_4]$ = 1.47 mM, [NaCl] = 138 mM and [KCl] = 2.68 mM, final pH was adjusted to 7.4. Tris solution (148 mM) was prepared from Trizma® base (Sigma Aldrich) and final pH was adjusted to 7.4. All other reagents were supplied by Sigma Aldrich and were of analytical grade. Ultrapure deionized water (>18.2 MΩ.cm) was used for the preparation of all solutions

1.2. AuNP synthesis

Citrate stabilized AuNP were synthetized according to previous works [15-17]. Briefly, 1 mL of $AuCl_4^-$ aqueous solution (10 mg/mL) was added into 90 mL of water containing 2 mL of 55 mM sodium citrate. The solution was stirred for 1 min (500 rpm) then 1 mL of $NaBH_4$ 19.5 mM was added and the solution was stirred for 5 min under nitrogen. 5 ± 1 nm (gold core diameter) AuNP with a 514 ± 1 nm specific Plasmon band and a negative zeta potential of -

36 ± 4 mV were obtained in accordance to previous results [15, 18]. The resulting suspension was immediately stored in the dark at 4 °C for maximum 20 days.

1.3. Film fabrication

1.3.1. Cover glasses

The glass substrates used for the deposition (24 × 36 × 0.145 mm, Menzel-Glaser) were used after a strict cleaning procedure: SDS 0.1 M at 100 °C for 15 min, followed by extensive rinsing with water. They were then immersed in HCl 0.1 M at 100 °C for 15 min, extensively rinsed and finally dried.

Polyelectrolyte solutions (0.1 M either in PBS or in Tris, according to monomer molecular masses) were prepared freshly before each experiment. Addition of HCl 1.0 M in the PAA solution was required to adjust pH to 7.4. The fabrication of AuNPs/polymer LbL film was carried out as follows. A pre-treated cover glass was dipped in the solution of polycation for 10 min, and then rinsed with two successive baths of PBS (2 min and 1 min, respectively). Subsequently, the slide was immersed in the AuNP suspension for 10 min, then rinsed as previously described, and finally dipped in the PAA solution for 10 min and rinsed. The AuNP-incorporating polymer multilayer film was obtained by the repetition of this simple three-step process in a cyclic repetition. 3 different polycations were tested to build films: PAH, PEI or PMAE. For films prepared in Tris, polycation and polyanion solutions (0.1 M) and rinsing baths were realized with Tris buffer. Films constructed in PBS are defined as P-Films and in Tris as T-Films.

Absorbance spectra (400-700 nm) of the coated slides (*vs.* an uncoated pre-cleaned slide) were recorded on a UV-1800 apparatus (Shimadzu). All cover glasses presented the specific Plasmon band (λ_{max} = 535 ± 5 nm) of AuNP.

1.3.2. Capillary zone electrophoresis

All experiments were performed on a Beckman P/ACE 5500 model (Beckman, Fullerton, USA) equipped with a UV detector set at λ = 214 nm in normal polarity mode (anodic injection). Mobility negatives values indicate a reverse polarity mode. Capillary temperature was controlled by coolant at 25.0 °C. Untreated fused-silica capillaries, 75 µm internal diameter with a total length of 37 cm (effective length: 30 cm) were employed. The neutral marker benzyl alcohol solution (0.5 $mg.mL^{-1}$ in background electrolyte, BGE) was injected in the hydrodynamic mode (3 s under pressure, 0.5 psi). The experimental set-up, data acquisition, and processing were governed using Beckman P/ACE Station software. The BGE used to evaluate migration times was ten-fold diluted PBS (15 mM). For first experiments, the new capillary was rinsed with 1.0 M sodium hydroxide (20 min) and ultrapure water (20 min). Each injection was realized in triplicate, results were indicated as a mean and a residual standard deviation which was always lower than 3.0 %. Polyelectrolyte solutions (either in PBS or Tris) used to coat the capillary were those described in the cover glasses section. Deposition method was adapted from [12]. Briefly, for each layer, the capillary was first filled with the coating solution (polymers or AuNP) at 20 psi for 10 min and rinsed with nitrogen and ultrapure water after 1 h of deposition time. Between each layer, benzyl alcohol was injected three times and before each injection, the capillary was successively rinsed with ultrapure water (2 min) and BGE (3 min). The EOF mobility (μ_{EOF}) was

determined using the migration time (NMT) of the EOF marker and with the help of Equation 1:

$$\mu_{EOF} = \frac{L \times l}{NMT \times V} \qquad \text{(Equation 1)}$$

Where L and l are the total and the apparent lengths of the capillary (length to detection) and V the applied voltage.

1.3.3. Quartz crystal microbalance

QCM measurements were conducted with an E1 QCM-D at 21 °C employing SiO_2-coated (50 nm) quartz crystals (5 MHz) from Q-Sense. Initially, crystals were cleaned using a plasma cleaner (PDC-32G-2 Harris Plasma®) for 15 min. Then, LbL films were assembled inside the QCM chamber. For each layer deposition, 500 µL of polycations (either PAH or PEI or PMAE), AuNP or PAA were allowed to flow in the chamber (flow rate of 400 $\mu L.min^{-1}$) for 5 to 10 min until stable values of the frequency were attained. Every deposited layer was then rinsed with the appropriate buffer (PBS or Tris).

The deposited mass of AuNP at the surface of the crystal was calculated according to the Sauerbrey equation [19] (Equation 2):

$$\Delta m = \frac{-C}{\nu} \qquad \text{(Equation 2)}$$

where, Δm is the mass change, and C a constant characteristic of the quartz used (-17.7 $ng.cm^{-2}.Hz^{-1}$ for our crystal).

1.4. Gold quantification

Gold quantification was described elsewhere [17]. Briefly, cover glasses were crushed with a glass rod, transferred into a LoBind Eppendorf® tube and mixed with an oxidant solution (400 µL of HCl-NaCl-Br_2 solution 1.0 M-0.3 M-0.025 M respectively) for 20 min. The mixture was then partially evaporated using a Turbovap (Biotage) at 40°C under inert gas (N_2, 4 psi) for 20 min. 200 µL of NH_4Cl solution (30 % m/V), 100 µL of 6 M HCl and 100 µL of Rhodamine B solution (0.084 µM) were then added. The ion-pair formed between tetraurochlorate anion and Rhodamine B was extracted by 200 µL of diisopropyl ether. Tubes were agitated on a Vibramax 100 (Heidolf Instruments) for 3 min at 1500 rpm, then centrifuged (Mini Spin Plus, Eppendorf) 3 min at 12100 × *g*. 150 µL of the supernatant (organic phase) were withdrawn, completely evaporated (Turbovap, 5 min, N_2, 3 psi) and the dried residue was dissolved in mobile phase (150 µL) before injection into the HPLC system. HPLC analyses were carried out on a SpectraSystem system constituted by a vacuum degasser (SCM1000), a quaternary pump (P1000XP), an autosampler (AS300) and a UV-Visible detector (UV2000). The column (Nucleosil ® C18, 150 mm × 4.6 mm, 3 µm particles size and 100 Å porosity) was thermostated at 40°C using a Croco-cil (1267) oven. Data acquisition and injection control were performed by the Azur software (version 5.0, Datalys®). The mobile phase consisted on a mixture of acetonitrile and water (25/75, V/V) containing 0.1% trifluoroacetic acid. The injection volume was 20 µL. The detector was set at 555 nm and the pump at a flow rate of 1.0 $mL.min^{-1}$.

Results and discussion

1.1. Influence of the cationic polymer on film formation

The three tested polymers (PAH, PEI and PMAE) were chosen for their ability to carry positive charges through primary (PEI and PAH) or quaternary amines (PMAE) and to make electrostatic bonds with negatively charged AuNP. PAH was our reference polymer since it was characterized in our previous study [12]. Its primary amine presents an ionization constant (pKa) of 8.7. PEI, with 4 pKa (3.3, 6.7, 9.2 and 9.9 [20]), is more basic than PAH and more charged at physiological pH (*i.e.* 7.4) than PAH. With more cationic charges than PAH at physiological pH, it is hypothesized to develop greater interactions with AuNP. PAH and PEI are both water soluble and commonly used in the literature to construct LbL films. PMAE is a well-known polymer in pharmaceutical industry (used as: enteric coating, taste masking, sustain release… [21]) and is more hydrophobic than the two previous polymers. PMAE was always positively charged in studied conditions (Figure 1).

For all polycations under study, the LbL films were prepared using the classical dipping protocol [12, 14]. Depositions cycles ([polycation/AuNP/PAA]) were repeated from 3 to 5 times. PBS (at the physiological pH and ionic strength) was chosen to solubilize PAH, PEI and PAA while PMAE was dissolved into methanol due its hydrophobic characteristics. This last candidate was discarded because of its inability to form LbL films. Indeed, right after PMAE deposition on cover glasses, the layer was desorbed during the rinsing step. The alkyl chains of PMAE not soluble in water may have formed a hydrophobic layer that was unable to interact with neither AuNP nor PAA. The two remaining polymers (PAH and PEI) were successfully deposited on cover glasses and film formation were monitored using UV-Vis spectrophotometry (Figure 2)

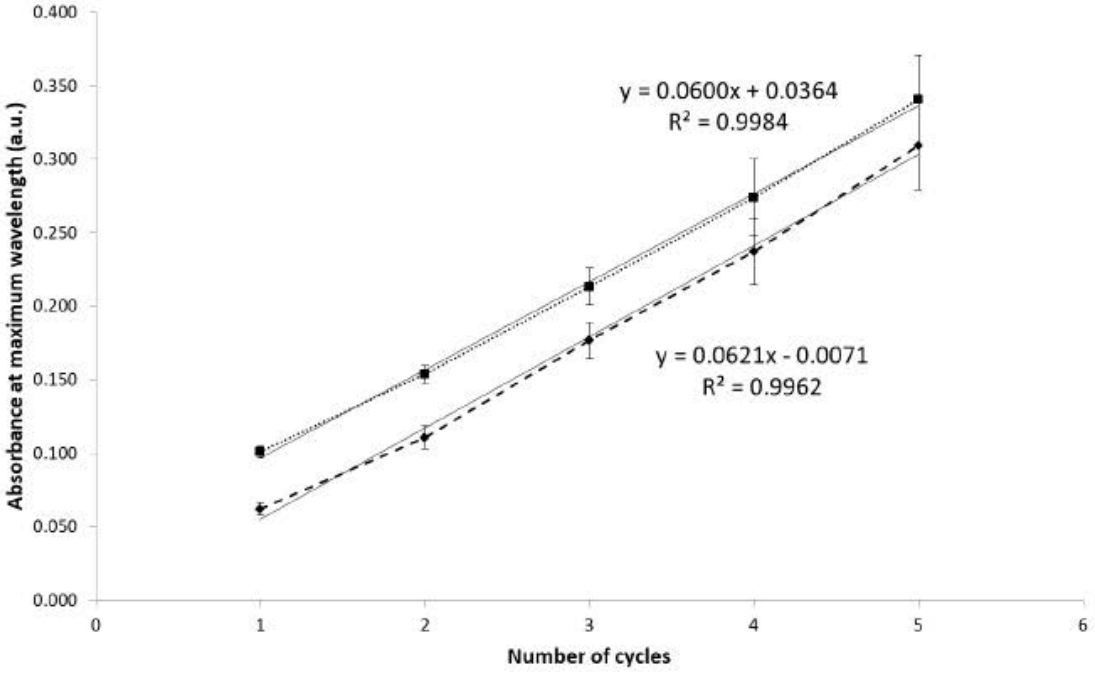

Figure 2: Variation of maximal absorbance of the Plasmon band plotted as a function of the number of coating cycles in PAH (discontinued) or PEI (dotted). 1 cycle corresponds to [polycation/AuNP/polyanion] (n = 3).

Film absorbance was directly linked to the number of AuNP embedded and, as illustrated in Figure 2, it increased linearly for both PAH and PEI films after 5 cycles ($R^2 > 0.99$ for both polymers). PEI films absorbance appeared to be more important than PAH films, certainly due to the 3 cationic groups per monomer (Figure 1). It gave the opportunity to trap more AuNP as it was already reported for previous studies with other gold particles [22]. AuNP quantification realized *via* a rhodamine B ion-pairing (electrostatic interaction between anionic gold $AuCl_4^-$ and cationic rhodamine B) and a HPLC system using UV-Vis detection (Table 1) confirmed that PEI films embedded more AuNP per cm². Spectrophotometry and AuNP quantification inside PAH films gave similar results than those previously obtained [12].

Table 1: Number of AuNP/cm² deposited per cycle and maximal absorbance after 3 cycles of films built under different conditions (n = 3).

	PAH	PEI
AuNP/cm²/cycle ($\times 10^{11}$)	9.8 ± 0.5	12.1 ± 0.7
Amax	0.177 ± 0.012	0.213 ± 0.018

Thanks to the higher number of cationic charges of PEI at pH 7.4, PEI films were able to include 1.2 times more AuNP than PAH films. This confirmed that PEI appeared to be a better candidate than PAH to optimize the use of the film as a AuNP reservoir. Then, film constructions and stability was assessed using CZE. CZE is an interesting separation tool and can be used to evaluate the global surface charge in accordance with the last deposited layer. In CZE, the mobility of a neutral compound relies only on the electro-osmotic flow (EOF) resulting from the capillary inner wall charge surface state. EOF is monitored as a function of the last deposited layer inside the capillary wall (Table 2). CZE also can provide interesting information on film stability as they are submitted to a hydrodynamic flow.

Table 2: Evolution of the electroosmotic flow mobility in accordance to the last layer deposited inside the capillary (n = 3).

		μ_{EOF} (10^{-5} cm²/V/s)	
	Nude capillary	52.8 ± 1.5	
	Deposited layer	**PAH**	**PEI**
Cycle 1	Polycation	-7.5 ± 2.7	-27.4 ± 1.6
	AuNP	9.6 ± 1.2	34.4 ± 3.2
	PAA	31.1 ± 5.6	36.5 ± 0.4
Cycle 2	Polycation	-20.1 ± 2.3	-22.6 ± 0.6
	AuNP	11.8 ± 0.8	29.4 ± 0.9
	PAA	36.4 ± 1.4	N.D.
Cycle 3	Polycation	-17.8 ± 4.0	N.D.
	AuNP	27.9 ± 0.2	N.D.
	PAA	38.9 ± 1.0	N.D.

N.D.: Not determined

The EOF mobility determined at the first step for bare capillary corresponded to negatively charged silanoate groups composing the silica material. When the polycation layer was deposited, a shift in the EOF was observed ($-7.5 \pm 2.7\times10^{-5}$ cm²/V/s for PAH and $-27.4 \pm 1.6\times10^{-5}$ cm²/V/s for PEI). These negative mobilities indicated a reversed EOF caused by cationic charges deposited on the inner capillary wall. The difference between μ_{EOF} values showed that PEI deposition created a more positively charged capillary than PAH deposition as expected by their chemical groups. Then, the AuNP layer deposition led to a positive value of EOF as cationic charges were compensated by the addition of negatively charged AuNP. However, μ_{EOF} values showed that more AuNP were embedded inside PEI films ($9.6 \pm 1.2\times10^{-5}$ cm²/V/s for PAH *vs* $34.4 \pm 3.2\times10^{-5}$ cm²/V/s for PEI). Finally, the last deposition layer (PAA) increased drastically the μ_{EOF} due to the addition of corresponding anionic charges.

Even if PEI emerged as the better candidate in terms of AuNP inclusion, PEI-built films showed an evident lack of stability highlighted by the trend to collapse inside the capillary after the first cycle deposition; this led to the definitive obstruction capillaries (as observed for 10 independent experiments). Only one cycle and a half can eventually be achieved with this technic of deposition. On the contrary, PAH-built films never clogged the capillary. This film desorption was explained by the conformation taken by the PEI in presence of high concentrated phosphate solution. Phosphate ions can diffuse inside films and interact with primary amines to destabilize the films. In this sense, Gu *et al.* [23] already showed in their work that LbL films made of PEI/PAA gradually lose mass in QCM in presence of PBS buffer. In their study, this mass loss was linked to a desorption/dissolution of the film and was not observed with the other tested solutions (Tris or NaCl).

Despite being promising in terms of AuNP inclusion, PEI-based films appeared to lack of stability under dynamic conditions. As the final purpose of those films is to be placed on

medical devices, stability is one of the major specifications that have to be reached. From the three starting polymer candidates, only PAH-built films proved to have enough stability to be used in our targeted applications. To maximize AuNP inclusion and obtain the best drug reservoir, some papers suggest that film deposition can be improved by a dissolution buffer modification [4-5].

1.2. Influence of the dissolution buffer on film formation

The second specification for LbL concerns the biological compatibility of the dissolution medium to avoid any side effect caused by the remaining buffer. Organic solvents or acetate buffers were voluntary avoided and experiments first focused on classical PBS buffer with physiological pH and salt concentration (7.4 and 0.148 M). To improve AuNP incorporation inside films, PBS buffer (pKa = 2.1, 7.2 and 12.3) was replaced by Tris buffer (pKa = 8.3) with same pH and concentration. As PAH was previously designated as the best candidate, it remained the reference for the evaluation of PBS films (P-films) and Tris films (T-films). Their behavior was first evaluated using CZE (Figure 3A) with three cycles of deposition as described in the previous part.

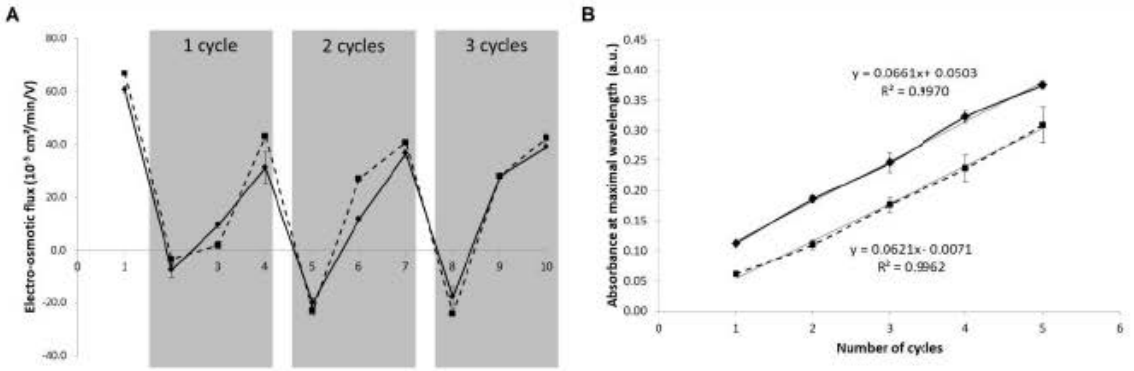

Figure 3: (A): Graphical representation of the variation of the electro-osmotic flux in accordance to the last layer deposited. (B): Variation of maximal absorbance of the Plasmon

band plotted as a function of the number of coating cycles. Films were built with either Tris buffer (plain line) or PBS (discontinuous line) (n = 3).

Values of EOF were very similar for both T-films and P-films and reproducible from one cycle to another. During construction, no collapse occurred for both conditions, on the contrary of PEI films. Though no influence of buffer can be highlighted here, CZE showed that P-films and T-films were at least equivalent in terms of stability. The comparison was also performed on films deposited on cover glasses (Figure 3B) with the dipping protocol. As explained previously, film absorbance is directly related to the number of AuNP embedded. Maximal absorbance of T-films appeared to be 1.4 times higher than P-films. This result was confirmed by the quantification of AuNP entrapped in P-films entrapped ($9.8 \pm 0.5 \times 10^{11}$ AuNP/cm²/cycle) compared to T-films ($14.3 \pm 0.8 \times 10^{11}$ AuNP/cm²/cycle which represented 1.5 times more).

For further investigation, films were built on SiO_2 coated quartz crystals in QCM. Crystal frequencies were monitored as a function of the deposition of the different layers. For P-films, the obtained patterns illustrated in Figure 4A were unusual. After PAH injection, the frequency decreased, showing the deposition of the polymer on the crystal. However, when rinsing with PBS, important decrease in frequency values was also observed (from -30 to -210 Hz for the first cycle). This may indicate water diffusion in the deposited layer leading to a swelling. Then, AuNP deposition led to a frequency decrease and PBS rinsing to a slight increase. This should indicate that AuNP have been deposited on the surface of the crystal and all elements interacting weakly with the surface have been removed during the rinsing phase. Finally, after the following PAA layer deposition show a huge increase of frequency values (respectively from -500 to -300 Hz). The obtained film after 3 cycles was 100 nm

thick. On the contrary, the profile obtained with T-films corresponds to a classical one expected during a LbL fabrication process (Figure 4 B). Each polymer or AuNP deposition led to a decrease of frequency and thus corresponds to a deposition of mass on the surface. Rinsing phases with buffer led to a small increase in frequency indicating that few weakly attached polymeric chains or AuNP desorbs from the surface. The overall building of the film followed the same pattern for each deposited layer. T-film was 70 nm thick. The very high resistance values (2.1 and 1.4 MPa) were explained by the incorporation of AuNP inside films (usually around 100 kPa for similar LbL films [24-25]). Those metallic elements greatly increased film resistance and viscosity. Altogether, those results highlighted that phosphate ions can induce film disorganization. Due to their small size and their two anionic charges, phosphate anions can easily diffuse through the different film layers, strongly interact with cationic charges, and prevent the polyanion binding. This led to an increase in film thickness (70 nm for T-films *vs* 100 nm for P-films) in relationship with the massive desorption noticed in P-films. This phenomenon was not observed with Tris.

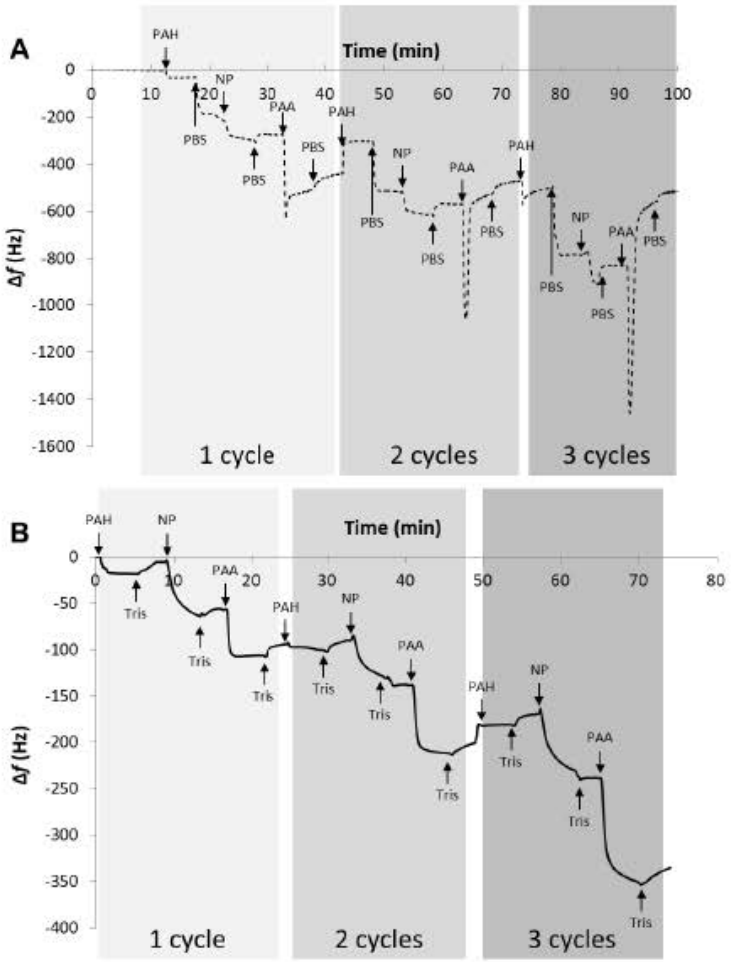

Figure 4: QCM curves of frequencies obtained by the deposition of (A) PBS-built films and (B) Tris buffer-built films.

1.3. Optimization of AuNP reservoir

The last part of this work was devoted to improve the capacity of the reservoir (film enrichment) to embed AuNP. Two strategies could be employed: more deposited cycles or more AuNP embedded on one polycation layer. The less time-consuming was preferred *i.e.* the second one. Films were constructed with the pattern: $[PAH/AuNP/PAA]_2$-[PAH/AuNP], and then AuNP were added several times. Nanoparticle deposition was monitored using

QCM and CZE (Figure 5), for both P-films and T-films. QCM curves (Figure 5A and B) showed surprisingly that AuNP can be charged without adding new cycles. After each AuNP deposition, an internal reorganization occurred and a plateau was observed. We hypothesized that it was due to a saturation of the film outer layers. A rinsing phase was required before adding more AuNP. Final thicknesses of 135 nm and 90 nm were obtained for P-film and T-film, respectively, with resistance values close to those previously measured. Densities of deposited AuNP calculated from QCM results are shown in Figure 5C and indicated that T-films embedded 1.7 times more AuNP than P-films ($10.3 \pm 2.9 \times 10^{11}$ AuNP/cm²/cycle *vs* $5.9 \pm 0.6 \times 10^{11}$ AuNP/cm²/cycle). Such calculated ratio was similar to the ones determined by UV-Vis absorption and HPLC gold quantification. Finally, CZE (Figure 5D) showed that the overloading reached a plateau after the fifth AuNP deposition for both films. The ratio between T-films and P-films EOF was 1.3 which confirmed all collected data.

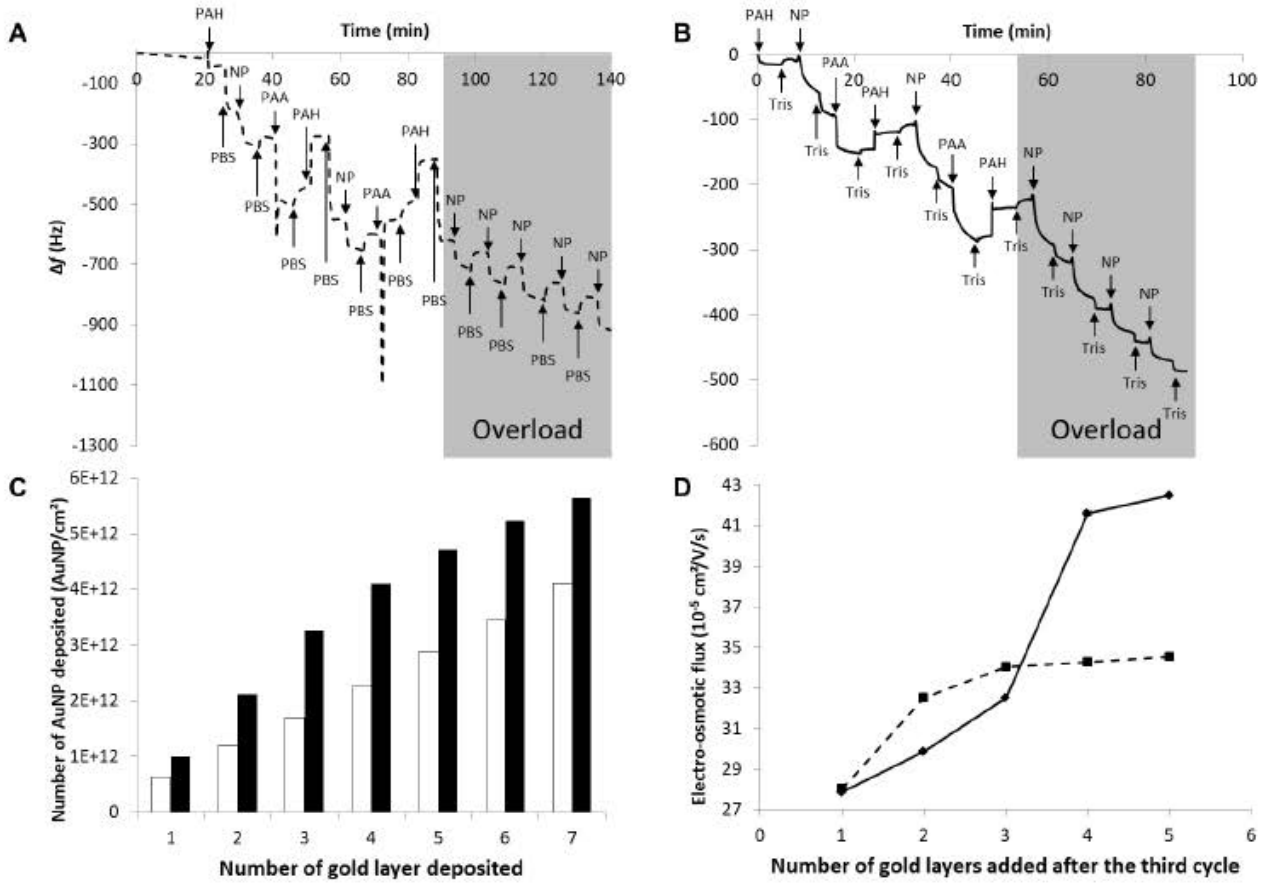

Figure 5: (A and B): QCM curves of frequencies obtained by the deposition of films in PBS (discontinuous line) and Tris buffer (plain line). (C): Number of AuNP per cm² embedded inside films in PBS (open bars) and Tris buffer (plain bars). (D) Graphical representation of the variation of the electro-osmotic flux after overloading of AuNP of films in PBS (discontinuous line) and Tris buffer (plain line).

Conclusion

This study demonstrated that two key parameters for the construction of AuNP LbL film are concerned. The nature of the polycation was important to obtain stable films with high incorporation rates of AuNP. But in our case, it appeared that PAH was the best compromise

in terms of both AuNP inclusion and film stability. The nature of the buffer also played an important role as phosphate ions (in PBS) were demonstrated to negatively impact the film formation. These anions prevented the inclusion of AuNP by their electrostatic interaction with polymer cationic functional groups and at the end creating less organized films. Tris ions were demonstrated to allow a greater drug reservoir for biomedical application.

Acknowledgments

Authors would like to thank Aurelien Renaudin and Valentin Philippe from Université de Lorraine for their help on CZE and HPLC, and Annie Tu from INSERM U1121 for her supervision on QCM.

References

(1) Acharya, G.; Lee, C. H.; Lee, Y., Optimization of Cardiovascular Stent against Restenosis: Factorial Design-Based Statistical Analysis of Polymer Coating Conditions. *Plos One* **2012,** *7*, e43100.
(2) Kim, B.-S.; Smith, R. C.; Poon, Z.; Hammond, P. T., MAD (Multiagent Delivery) Nanolayer: Delivering Multiple Therapeutics from Hierarchically Assembled Surface Coatings. *Langmuir* **2009,** *25*, 14086-14092.
(3) Pavlukhina, S.; Sukhishvili, S., Polymer assemblies for controlled delivery of bioactive molecules from surfaces. *Adv. Drug Deliv. Rev.* **2011,** *63*, 822-36.
(4) Diamanti, E.; Andreozzi, P.; Kirby, C.; Anguiano, R.; Yate, L.; Heinz, H.; Ziolo, R. F.; Donath, E.; Moya, S. E., Study of the Impact of Polyanions on the Formation of Lipid Bilayers on Top of Polyelectrolyte Multilayers with Poly(allylamine hydrochloride) as the Top Layer. *J. Phys. Chem. B* **2017,** *121*, 1158-1167.
(5) Diamanti, E.; Andreozzi, P.; Anguiano, R.; Yate, L.; Gregurec, D.; Politakos, N.; Ziolo, R. F.; Donath, E.; Moya, S. E., The effect of top-layer chemistry on the formation of supported lipid bilayers on polyelectrolyte multilayers: primary versus quaternary amines. *Phys. Chem. Chem. Phys.* **2016,** *18*, 32396-32405.
(6) Wang, Y. F.; Guo, X. C.; Pan, R. H.; Han, D.; Chen, T.; Geng, Z. H.; Xiong, Y. F.; Chen, Y. J., Electrodeposition of chitosan/gelatin/nanosilver: A new method for constructing biopolymer/nanoparticle composite films with conductivity and antibacterial activity. *Mat. Sci. Eng. C-Mater.* **2015,** *53*, 222-228.
(7) Liu, S.; Liu, S.; Liu, X.; Zhao, J.; Cui, W.; Fan, C., Antibacterial antiadhesion membranes from silver-nanoparticle-doped electrospun poly(L-lactide) nanofibers. *J. Appl. Polym. Sci.* **2013,** *129*, 3459-3465.
(8) Liu, Y.; Chen, W.; Kim, H. I., Antibacterial activity of pH-sensitive genipin cross-linked chitosan/poly(ethylene glycol)/silver nanocomposites. *Polym. Advan. Technol.* **2012,** *23*, 8-14.

(9) Kim, C. Y.; Xu, L.; Lee, E. H.; Choa, Y. H., Magnetic Silicone Composites with Uniform Nanoparticle Dispersion as a Biomedical Stent Coating for Hyperthermia. *Adv. Polym. Tech.* **2013,** *32*, E714-E723.
(10) Li, W. T.; Wang, M. H.; Li, Y. J.; Sun, Y.; Li, J. C., Linker-free layer-by-layer self-assembly of gold nanoparticle multilayer films for direct electron transfer of horseradish peroxidase and H2O2 detection. *Electrochim. Acta* **2011,** *56*, 6919-6924.
(11) Tian, S. J.; Liu, J. Y.; Zhu, T.; Knoll, W., Polyaniline/gold nanoparticle multilayer films: Assembly, properties, and biological applications. *Chem. Mater.* **2004,** *16*, 4103-4108.
(12) Pallotta, A.; Parent, M.; Clarot, I.; Luo, M.; Borr, V.; Dan, P.; Decot, V.; Menu, P.; Safar, R.; Joubert, O.; Leroy, P.; Boudier, A., Blood Compatibility of Multilayered Polyelectrolyte Film Containing Immobilized Gold Nanoparticles. *Part. Part. Syst. Charact.* **2017,** *34*, 1600184.
(13) Luo, M.; Boudier, A.; Clarot, I.; Maincent, P.; Schneider, R.; Leroy, P., Gold Nanoparticles Grafted by Reduced Glutathione With Thiol Function Preservation. *Colloid Interface Sci. Commun.* **2016,** *14*, 8-12.
(14) Decher, G., Fuzzy Nanoassemblies: Toward Layered Polymeric Multicomposites. *Science* **1997,** *277*, 1232-1237.
(15) Tournebize, J.; Boudier, A.; Joubert, O.; Eidi, H.; Bartosz, G.; Maincent, P.; Leroy, P.; Sapin-Minet, A., Impact of gold nanoparticle coating on redox homeostasis. *Int. J. Pharm.* **2012,** *438*, 107-16.
(16) Tournebize, J.; Boudier, A.; Sapin-Minet, A.; Maincent, P.; Leroy, P.; Schneider, R., Role of gold nanoparticles capping density on stability and surface reactivity to design drug delivery platforms. *ACS Appl. Mater. Interfaces* **2012,** *4*, 5790-9.
(17) Tournebize, J.; Sapin-Minet, A.; Schneider, R.; Boudier, A.; Maincent, P.; Leroy, P., Simple spectrophotocolorimetric method for quantitative determination of gold in nanoparticles. *Talanta* **2011,** *83*, 1780-3.
(18) Pallotta, A.; Boudier, A.; Leroy, P.; Clarot, I., Characterization and stability of gold nanoparticles depending on their surface chemistry: Contribution of capillary zone electrophoresis to a quality control. *J. Chromatogr. A* **2016,** *1461*, 179-84.
(19) Sauerbrey, G., Verwendung von Schwingquarzen zur Wägung dünner Schichten und zur Mikrowägung. *Z. Phys.* **1959,** *155*, 206-222.
(20) Suh, J.; Paik, H. J.; Hwang, B. K., Ionization of Poly(ethylenimine) and Poly(allylamine) at Various pH's. *Bioorganic Chem.* **1994,** *22*, 318-327.
(21) Patra, C. N.; Priya, R.; Swain, S.; Kumar Jena, G.; Panigrahi, K. C.; Ghose, D., Pharmaceutical significance of Eudragit: A review. *Future J. Pharm. Sci.* **2017,** *3*, 33-45.
(22) Placido, T.; Fanizza, E.; Cosma, P.; Striccoli, M.; Curri, M. L.; Comparelli, R.; Agostiano, A., Electroactive layer-by-layer plasmonic architectures based on Au nanorods. *Langmuir* **2014,** *30*, 2608-18.
(23) Gu, Y.; Weinheimer, E. K.; Ji, X.; Wiener, C. G.; Zacharia, N. S., Response of Swelling Behavior of Weak Branched Poly(ethylene imine)/Poly(acrylic acid) Polyelectrolyte Multilayers to Thermal Treatment. *Langmuir* **2016,** *32*, 6020-6027.
(24) Richert, L.; Engler, A. J.; Discher, D. E.; Picart, C., Elasticity of Native and Cross-Linked Polyelectrolyte Multilayer Films. *Biomacromolecules* **2004,** *5*, 1908-1916.
(25) Mermut, O.; Lefebvre, J.; Gray, D. G.; Barrett, C. J., Structural and Mechanical Properties of Polyelectrolyte Multilayer Films Studied by AFM. *Macromolecules* **2003,** *36*, 8819-8824.

2.2. Conclusion

Si la nature du polymère cationique utilisé influe grandement sur la stabilité des films, l'utilisation d'un tampon de dissolution sans ions phosphate permet d'obtenir un chargement en AuNP plus important. Nous avons montré que ces anions divalents déstabilisaient le film. En prenant en compte toutes les optimisations (tampon tris + surcharge), nous pourrions réduire le nombre de couches nécessaires à environ 350 (contre 1500 au départ) soit une diminution de plus de 4 fois. Si le dépôt reste relativement important, la construction devient envisageable et compatible avec une automatisation ainsi qu'une fabrication en série.

DISCUSSION ET PERSPECTIVES

Durant ce travail de doctorat, nous avons développé des films multicouches formés de polyélectrolytes et capables d'immobiliser des AuNP. Ces films ont montré une inertie intéressante vis-à-vis des protéines et de diverses molécules physiologiques. Leur capacité à intégrer des AuNP est importante et a encore pu être améliorée par changement du milieu de dissolution des polymères (près de 10^{12} AuNP/cm²/cycle). L'objectif du projet est d'obtenir un réservoir capable de libérer un principe actif (NO) de manière contrôlée dans le temps. Les trois points principaux développés au cours du doctorat ont été : le développement de méthodologies dédiées au contrôle des AuNP pour pouvoir produire des lots de qualité pharmaceutique, l'optimisation de leur chargement dans des films LbL et l'évaluation de la biocompatibilité de ces derniers. La prochaine étape à développer reste la nitrosation et la libération de NO par les films. Enfin quelques perspectives seront développées

Les AuNP comme matières premières pharmaceutiques.

Les AuNP sont contrôlées par mesure de leurs différents paramètres physico-chimiques (diamètre hydrodynamique, potentiel zéta, profil électrophorétique …). La mise en place de ce contrôle qualité est nécessaire car les AuNP sont considérées dans notre montage comme des matières premières pharmaceutiques. La plus-value de l'électrophorèse capillaire repose sur la détermination de la pureté de la population nanoparticulaire et l'obtention d'un profil d'impuretés. De plus, une méthode de dosage spécifique de l'or a été développée et permet à la fois d'évaluer le rendement de synthèse (discrimination de l'or sous forme ionique et nanoparticulaire) et de quantifier la quantité d'AuNP contenue dans les films.

La prochaine étape du contrôle qualité des AuNP requiert le couplage de l'ECZ avec un spectromètre de masse, permettant l'identification des impuretés organiques (inhérentes à

la synthèse) mais aussi leur quantification pour le suivi de stabilité des lots produits. Cette étape est nécessaire pour l'utilisation d'AuNP comme matière première pharmaceutique.

Biocompatibilité des films.

Parmi les points à développer, la biocompatibilité des films est cruciale. Le principal point faible reproché à la construction, lors de différents dépôts du projet, est l'absence du contrôle de l'adhésion protéique sur le film. Même si les expérimentations ont montré une adsorption limitée à la surface du film, à long terme il n'est pas exclu d'observer une adsorption protéique massive (en particulier les protéines de la coagulation) en surface des films [107]. Un tel dépôt aurait deux conséquences principales : une baisse d'activité par la présence d'une gangue de fibrine [108], mais surtout l'induction de caillots sanguins et/ou la mise en place d'un phénomène de resténose [61, 109]. L'ajout d'une couche polymérique composée de PAA greffé avec du poly(éthylène glycol) (PEG) (sous forme de copolymère à blocs ou en forme de peigne) pourrait empêcher l'apparition de ces effets secondaires. Une surface recouverte de PEG entrainera une plus grande inertie du DM par une non-adsorption des protéines [110, 111]. Cela diminuera par la même occasion l'inflammation locale [112], aboutissant à une meilleure tolérance du DM.

Concernant les méthodes analytiques, l'amélioration des limites de détection et la validation de la méthode de quantification de l'or dans les milieux cellulaires/tissulaires restent nécessaires pour envisager une étude de biodistribution complète. Même si l'absence de dissémination des AuNP a été prouvée par les expérimentations en ECZ, QCM et contraintes de cisaillements, des études devront être menées, grâce entre autre à cette méthode. Il sera alors possible d'évaluer l'accumulation de ces AuNP au niveau d'organes

clés dans le métabolisme et l'élimination tels que le foie, la rate, les reins ou les poumons [113].

Films libérant du NO.

A l'heure actuelle, le principal point bloquant reste l'obtention de films libérant du NO de façon contrôlée dans le temps. La fonctionnalisation des AuNP par des RSNO est réalisable avec une charge importante en NO par AuNP, mais actuellement leur incorporation au sein de films multicouches n'a pas été réalisée. De plus, pour aboutir à la durée de libération souhaitée, l'augmentation du réservoir est la deuxième étape. Des changements dans la construction du film sont aussi possibles avec l'introduction de couches dites « barrières » qui limiteraient la diffusion du NO [114]. Ces couches permettraient de limiter l'apparition d'une phase de « burst » (court laps de temps après implantation dans lequel il y aurait une libération massive de principe actif) observée dans les modèles de libération de NO [3]. Des solutions sont actuellement en cours de développement au laboratoire et sont sous étude de brevetabilité.

Perspectives et aspect clinique.

Un autre problème peut être soulevé : les films déposés à la surface des stents sont-ils compatibles avec les contraintes mécaniques de ces derniers ? Le film peut altérer les propriétés mécaniques du stent (modification de l'élasticité) et ainsi gêner voire empêcher son expansion une fois placé dans le vaisseau. Les études réalisées en QCM ont montré que les films déposés avaient une élasticité et une viscosité égale à celle de l'acier (certainement due à la présence d'AuNP à l'intérieur du film, article 6). C'est cette résistance importante qui pourrait venir bloquer le déploiement correct du stent. A l'inverse, le déploiement du

stent peut endommager le film. En effet, lorsque le stent est déposé dans le vaisseau, les fils qui le composent (pour les stents tressés) subissent des déformations et des frottements [115], notamment dans les segments mobiles des artères (fosses iliaques) [116]. Ces phénomènes pourraient entrainer un décollement partiel ou total du film entrainant une perte de son action et une éventuelle toxicité par la libération de débris (polymères et/ou AuNP) dans le système circulatoire. De plus, même si les nouveaux alliages développés pour les stents ainsi que l'amélioration des techniques de fabrication (découpe laser, surface plus lisse …) les rendent de plus en plus biocompatibles, l'apport de NO à dose physiologique par un stent actif permettrait de limiter les phénomènes responsables de la resténose ainsi que le stress engendré par la pose d'un tel dispositif [59, 61, 62].

Un des points fort du système développé reste sa modularité. Les films peuvent être adaptés à d'autres dispositifs médicaux ainsi qu'à d'autres pathologies en modifiant le principe actif ou les NP utilisées. Il serait tout à fait envisageable d'y intégrer des nanoparticules d'argent pour une action antibactérienne du dispositif. En clinique, les DMI (toutes classes confondues) sont soumis à deux limitations majeures. Premièrement, les maladies nosocomiales [117] qui sont un risque majeur pour la survie du patient, notamment avec les DMI à visée cardiovasculaire. L'action antibactérienne du NO (ou d'un autre PA) aurait deux actions bénéfiques : limiter l'apparition des infections nosocomiales d'une part, mais aussi réduire l'apparition de bactéries multi-résistantes. Deuxièmement, dans de nombreux cas, les patients recevant un DMI sont fragiles, poly-pathologiques (60 à 80 % des patients atteints de diabète présentent une hypertension artérielle [118] …) ce qui entraine une baisse de l'immunité couplée à un retard de cicatrisation. Ces facteurs entretiennent le cycle de l'inflammation et favorisent l'apparition d'effets secondaires comme la resténose. Une action anti-inflammatoire, *via* l'apport d'un PA (ou plusieurs ayant une complémentarité

d'action), par le DMI permettrait d'agir localement sur les facteurs favorisant l'inflammation et de faciliter la cicatrisation.

Enfin, l'impression 3D, particulièrement adaptable aux polymères [119], est une voie envisagée. Les DMI créés par cette technique seraient personnalisés en fonction de chaque patient et/ou pathologie. Cependant, le coût de la technologie reste relativement élevé et relativement peu répandu dans les hôpitaux à l'heure actuelle. Enfin, les températures nécessaires à la formation d'une impression 3D seraient incompatibles avec l'utilisation de NO.

CONCLUSION

Le but principal de ce travail de doctorat a été de poser les bases d'un nouveau type de DM faisant appel aux nanotechnologies et à la science des polymères. Un des premiers problèmes soulevés a été l'absence de caractérisation suffisante des AuNP pour une utilisation pharmaceutique. Des solutions ont été proposées pour faciliter leur caractérisation et des pistes sont actuellement à l'étude pour obtenir des AuNP parfaitement définies. Dans un deuxième temps, le revêtement de surface développé s'est avéré stable et relativement inerte laissant présager de sa biocompatibilité. Malgré cela, des évolutions restent nécessaires pour aboutir à une version définitive capable de libérer des principes actifs sur de longues périodes. Parmi les moyens mis en œuvre, certains se sont avérés réalisables (optimisation des conditions de construction, surcharge en AuNP) et d'autres font actuellement l'objet d'une procédure de brevetabilité et n'ont pas été développés dans ce manuscrit. Toutes ces expérimentations ont permis d'obtenir des films de mieux en mieux caractérisés et de comprendre leur interaction avec des objets nanoparticulaires. Ils devront par la suite être testés sur des lignées cellulaires pour évaluer leur cytocompatibilité, puis *in vivo* pour s'assurer de leur action bénéfique.

Pour conclure ce travail de thèse, les films multicouches nanostructurés pour le développement de stents innovant représentent un pas en avant vers la création d'un nouveau type de décorations de surface appliquées au domaine biomédical.

.

BIBLIOGRAPHIE

[1] W.H. Organization, WHO Global Model Regulatory Framework for Medical Devices including in vitro diagnostic medical devices, (2017).

[2] http://ansm.sante.fr/Activites/Mise-sur-le-marche-des-dispositifs-medicaux-et-dispositifs-medicaux-de-diagnostic-in-vitro-DM-DMIA-DMDIV/DM-classes-IIa-IIb-III-et-DMIA-Communication-et-liste/%28offset%29/4 (consulté le 17/05/17).

[3] G. Acharya, C.H. Lee, Y. Lee, Optimization of cardiovascular stent against restenosis: factorial design-based statistical analysis of polymer coating conditions, PloS one, 7 (2012) e43100.

[4] M. Luo, A. Boudier, I. Clarot, P. Maincent, R. Schneider, P. Leroy, Gold Nanoparticles Grafted by Reduced Glutathione With Thiol Function Preservation, Colloid and Interface Science Communications, 14 (2016) 8-12.

[5] J. Tournebize, A. Boudier, O. Joubert, H. Eidi, G. Bartosz, P. Maincent, P. Leroy, A. Sapin-Minet, Impact of gold nanoparticle coating on redox homeostasis, Int J Pharm, 438 (2012) 107-116.

[6] OMS, Les 10 principales causes de mortalité dans le monde en 2015 (http://www.who.int/mediacentre/factsheets/fs310/fr/ consulté le 07/09/17), (2016).

[7] R.S. Vasan, E.J. Benjamin, The Future of Cardiovascular Epidemiology, Circulation, 133 (2016) 2626-2633.

[8] D. Mozaffarian, E.J. Benjamin, A.S. Go, D.K. Arnett, M.J. Blaha, M. Cushman, S.R. Das, S. de Ferranti, J.-P. Després, H.J. Fullerton, V.J. Howard, M.D. Huffman, C.R. Isasi, M.C. Jiménez, S.E. Judd, B.M. Kissela, J.H. Lichtman, L.D. Lisabeth, S. Liu, R.H. Mackey, D.J. Magid, D.K. McGuire, E.R. Mohler, C.S. Moy, P. Muntner, M.E. Mussolino, K. Nasir, R.W. Neumar, G. Nichol, L. Palaniappan, D.K. Pandey, M.J. Reeves, C.J. Rodriguez, W. Rosamond, P.D. Sorlie, J. Stein, A. Towfighi, T.N. Turan, S.S. Virani, D. Woo, R.W. Yeh, M.B. Turner, Heart Disease and Stroke Statistics—2016 Update, A Report From the American Heart Association, (2015).

[9] M. Writing Group, E.J. Benjamin, M.J. Blaha, S.E. Chiuve, M. Cushman, S.R. Das, R. Deo, S.D. de Ferranti, J. Floyd, M. Fornage, C. Gillespie, C.R. Isasi, M.C. Jiménez, L.C. Jordan, S.E. Judd, D. Lackland, J.H. Lichtman, L. Lisabeth, S. Liu, C.T. Longenecker, R.H. Mackey, K. Matsushita, D. Mozaffarian, M.E. Mussolino, K. Nasir, R.W. Neumar, L. Palaniappan, D.K. Pandey, R.R. Thiagarajan, M.J. Reeves, M. Ritchey, C.J. Rodriguez, G.A. Roth, W.D. Rosamond, C. Sasson, A. Towfighi, C.W. Tsao, M.B. Turner, S.S. Virani, J.H. Voeks, J.Z. Willey, J.T. Wilkins, J.H.Y. Wu, H.M. Alger, S.S. Wong, P. Muntner, Heart Disease and Stroke Statistics—2017 Update: A Report From the American Heart Association, Circulation, 135 (2017) e146-e603.

[10] A.J. Lusis, Atherosclerosis, Nature, 407 (2000) 233-241.

[11] A. Gistera, G.K. Hansson, The immunology of atherosclerosis, Nat Rev Nephrol, 13 (2017) 368-380.

[12] M. Kelm, J. Schrader, Control of coronary vascular tone by nitric oxide, Circulation research, 66 (1990) 1561.

[13] E.D. Motley, K. Eguchi, M.M. Patterson, P.D. Palmer, H. Suzuki, S. Eguchi, Mechanism of Endothelial Nitric Oxide Synthase Phosphorylation and Activation by Thrombin, Hypertension, 49 (2007) 577.

[14] C.N. Hess, R. Kou, R.P. Johnson, G.K. Li, T. Michel, ADP Signaling in Vascular Endothelial Cells: ADP-DEPENDENT ACTIVATION OF THE ENDOTHELIAL ISOFORM OF NITRIC-OXIDE SYNTHASE REQUIRES THE EXPRESSION BUT NOT THE KINASE ACTIVITY OF AMP-ACTIVATED PROTEIN KINASE, The Journal of biological chemistry, 284 (2009) 32209-32224.

[15] F. Kuhr, J. Lowry, Y. Zhang, V. Brovkovych, R.A. Skidgel, Differential regulation of inducible and endothelial nitric oxide synthase by kinin B1 and B2 receptors, Neuropeptides, 44 (2010) 145-154.

[16] G. Garcia-Cardena, R. Fan, V. Shah, R. Sorrentino, G. Cirino, A. Papapetropoulos, W.C. Sessa, Dynamic activation of endothelial nitric oxide synthase by Hsp90, Nature, 392 (1998) 821-824.

[17] V. Rizzo, D.P. McIntosh, P. Oh, J.E. Schnitzer, In Situ Flow Activates Endothelial Nitric Oxide Synthase in Luminal Caveolae of Endothelium with Rapid Caveolin Dissociation and Calmodulin Association, Journal of Biological Chemistry, 273 (1998) 34724-34729.

[18] M.E. Davis, I.M. Grumbach, T. Fukai, A. Cutchins, D.G. Harrison, Shear Stress Regulates Endothelial Nitric-oxide Synthase Promoter Activity through Nuclear Factor κB Binding, Journal of Biological Chemistry, 279 (2004) 163-168.

[19] M. Hecker, A. Mulsch, E. Bassenge, R. Busse, Vasoconstriction and increased flow: two principal mechanisms of shear stress-dependent endothelial autacoid release, American Journal of Physiology - Heart and Circulatory Physiology, 265 (1993) H828.

[20] V.B. Schini-Kerth, Vascular biosynthesis of nitric oxide: effect on hemostasis and fibrinolysis, Transfusion Clinique et Biologique, 6 (1999) 355-363.

[21] J. Loscalzo, G. Welch, Nitric oxide and its role in the cardiovascular system, Progress in cardiovascular diseases, 38 (1995) 87-104.

[22] M.E. Mendelsohn, S. O'Neill, D. George, J. Loscalzo, Inhibition of fibrinogen binding to human platelets by S-nitroso-N-acetylcysteine, The Journal of biological chemistry, 265 (1990) 19028-19034.

[23] P.M. Bath, D.G. Hassall, A.M. Gladwin, R.M. Palmer, J.F. Martin, Nitric oxide and prostacyclin. Divergence of inhibitory effects on monocyte chemotaxis and adhesion to endothelium in vitro, Arteriosclerosis and thrombosis : a journal of vascular biology, 11 (1991) 254-260.

[24] P. Kubes, M. Suzuki, D.N. Granger, Nitric oxide: an endogenous modulator of leukocyte adhesion, Proceedings of the National Academy of Sciences of the United States of America, 88 (1991) 4651-4655.

[25] D.S. Marks, J.A. Vita, J.D. Folts, J.F. Keaney, G.N. Welch, J. Loscalzo, Inhibition of neointimal proliferation in rabbits after vascular injury by a single treatment with a protein adduct of nitric oxide, Journal of Clinical Investigation, 96 (1995) 2630-2638.

[26] U.C. Garg, A. Hassid, Nitric oxide-generating vasodilators and 8-bromo-cyclic guanosine monophosphate inhibit mitogenesis and proliferation of cultured rat vascular smooth muscle cells, Journal of Clinical Investigation, 83 (1989) 1774-1777.

[27] K. Fukuo, T. Inoue, S. Morimoto, T. Nakahashi, O. Yasuda, S. Kitano, R. Sasada, T. Ogihara, Nitric oxide mediates cytotoxicity and basic fibroblast growth factor release in cultured vascular smooth muscle cells. A possible mechanism of neovascularization in atherosclerotic plaques, Journal of Clinical Investigation, 95 (1995) 669-676.

[28] F. Hinder, H.D. Stubbe, H. Van Aken, R. Waurick, M. Booke, J. Meyer, Role of nitric oxide in sepsis-associated pulmonary edema, American journal of respiratory and critical care medicine, 159 (1999) 252-257.

[29] G.R. May, P. Crook, P.K. Moore, C.P. Page, The role of nitric oxide as an endogenous regulator of platelet and neutrophil activation within the pulmonary circulation of the rabbit, British journal of pharmacology, 102 (1991) 759-763.

[30] M. Gilchrist, C. Hesslinger, A.D. Befus, Tetrahydrobiopterin, a Critical Factor in the Production and Role of Nitric Oxide in Mast Cells, Journal of Biological Chemistry, 278 (2003) 50607-50614.

[31] F. Obermeier, V. Gross, J. Schölmerich, W. Falk, Interleukin-1 production by mouse macrophages is regulated in a feedback fashion by nitric oxide, Journal of Leukocyte Biology, 66 (1999) 829-836.

[32] S.H. Snyder, Nitric oxide: first in a new class of neurotransmitters, Science, 257 (1992) 494-496.

[33] C.F. Zorumski, I. Yukitoshi, Nitric oxide and hippocampal synaptic plasticity, Biochemical Pharmacology, 46 (1993) 777-785.

[34] V.L. Dawson, NITRIC OXIDE: ROLE IN NEUROTOXICITY, Clinical and Experimental Pharmacology and Physiology, 22 (1995) 305-308.

[35] V.L. Dawson, T.M. Dawson, E.D. London, D.S. Bredt, S.H. Snyder, Nitric oxide mediates glutamate neurotoxicity in primary cortical cultures, Proceedings of the National Academy of Sciences of the United States of America, 88 (1991) 6368-6371.

[36] L.J. Ignarro, Biosynthesis and Metabolism of Endothelium-Derived Nitric Oxide, Annual Review of Pharmacology and Toxicology, 30 (1990) 535-560.

[37] S. Moncada, Nitric Oxide in the Vasculature: Physiology and Pathophysiology, Annals of the New York Academy of Sciences, 811 (1997) 60-69.

[38] C. Boulanger, T.F. Lüscher, Release of endothelin from the porcine aorta. Inhibition by endothelium-derived nitric oxide, Journal of Clinical Investigation, 85 (1990) 587-590.

[39] T. Nakaki, M. Nakayama, R. Kato, Inhibition by nitric oxide and nitric oxide-producing vasodilators of DNA synthesis in vascular smooth muscle cells, European journal of pharmacology, 189 (1990) 347-353.

[40] B.C. Kone, Nitric oxide synthesis in the kidney: isoforms, biosynthesis, and functions in health, Seminars in nephrology, 24 (2004) 299-315.

[41] S.J. Zieman, D.A. Kass, Advanced glycation endproduct crosslinking in the cardiovascular system: potential therapeutic target for cardiovascular disease, Drugs, 64 (2004) 459-470.

[42] W. Schmid, A. Lee, J. Son, E. Koller, I. Volf, Hypochlorite-oxidized low density lipoproteins reduce production and bioavailability of nitric oxide in RAW 264.7 macrophages by distinct mechanisms, Life sciences, 83 (2008) 50-58.

[43] D.W. Landry, J.A. Oliver, The pathogenesis of vasodilatory shock, The New England journal of medicine, 345 (2001) 588-595.

[44] S. Lopez-Sanz, N.R. Farinas, R.S. Vargas, R.D. Martin-Doimeadios, A. Rios, Methodology for monitoring gold nanoparticles and dissolved gold species in culture medium

and cells used for nanotoxicity tests by liquid chromatography hyphenated to inductively coupled plasma-mass spectrometry, Talanta, 164 (2017) 451-457.

[45] S. Morr, N. Lin, A.H. Siddiqui, Carotid artery stenting: current and emerging options, Medical Devices (Auckland, N.Z.), 7 (2014) 343-355.

[46] P.W. Serruys, H. Emanuelsson, W. van der Giessen, A.C. Lunn, F. Kiemeney, C. Macaya, W. Rutsch, G. Heyndrickx, H. Suryapranata, V. Legrand, J.J. Goy, P. Materne, H. Bonnier, M.-C. Morice, J. Fajadet, J. Belardi, A. Colombo, E. Garcia, P. Ruygrok, P. de Jaegere, M.-A. Morel, Heparin-Coated Palmaz-Schatz Stents in Human Coronary Arteries, Early Outcome of the Benestent-II Pilot Study, 93 (1996) 412-422.

[47] HAS, Utilisation des endoprothèses (stents) coronaires en France en 2014 (2016).

[48] G. Vergnol, E. Renard, F. Haroun, P. Guerin, A. Seron, C. Bureau, G. Loirand, V. Langlois, Electrografting of a biodegradable layer as a primer adhesion coating onto a metallic stent: in vitro and in vivo evaluations, Journal of Materials Science: Materials in Medicine, 24 (2013) 2729-2739.

[49] J.M. Ino, E. Sju, V. Ollivier, E.K.F. Yim, D. Letourneur, C. Le Visage, Evaluation of hemocompatibility and endothelialization of hybrid poly(vinyl alcohol) (PVA)/gelatin polymer films, Journal of Biomedical Materials Research Part B: Applied Biomaterials, 101 (2013) 1549-1559.

[50] S.L. Chin-Quee, S.H. Hsu, K.L. Nguyen-Ehrenreich, J.T. Tai, G.M. Abraham, S.D. Pacetti, Y.F. Chan, G. Nakazawa, F.D. Kolodgie, R. Virmani, N.N. Ding, L.A. Coleman, Endothelial cell recovery, acute thrombogenicity, and monocyte adhesion and activation on fluorinated copolymer and phosphorylcholine polymer stent coatings, Biomaterials, 31 (2010) 648-657.

[51] A.J. Coury, K.B. Stokes, P.T. Cahalan, P.C. Slaikeu, Biostability considerations for implantable polyurethanes, Life Support Syst, 5 (1987) 25-39.

[52] D. Bakker, C.A. van Blitterswijk, S.C. Hesseling, H.K. Koerten, W. Kuijpers, J.J. Grote, Biocompatibility of a polyether urethane, polypropylene oxide, and a polyether polyester copolymer. A qualitative and quantitative study of three alloplastic tympanic membrane materials in the rat middle ear, Journal of biomedical materials research, 24 (1990) 489-515.

[53] P.W. Serruys, Y. Onuma, D. Dudek, P.C. Smits, J. Koolen, B. Chevalier, B. de Bruyne, L. Thuesen, D. McClean, R.J. van Geuns, S. Windecker, R. Whitbourn, I. Meredith, C. Dorange, S. Veldhof, K.M. Hebert, K. Sudhir, H.M. Garcia-Garcia, J.A. Ormiston, Evaluation of the second generation of a bioresorbable everolimus-eluting vascular scaffold for the treatment of de novo coronary artery stenosis: 12-month clinical and imaging outcomes, Journal of the American College of Cardiology, 58 (2011) 1578-1588.

[54] R. Hill, A. Bagust, A. Bakhai, R. Dickson, Y. Dündar, A. Haycox, R. Mujica Mota, A. Reaney, D. Roberts, P. Williamson, W. T, Coronary artery stents: a rapid systematic review and economic evaluation. Available from: https://www.ncbi.nlm.nih.gov/books/NBK62314/, Health Technology Assessment Southampton (UK), (2004).

[55] J. Daemen, P. Wenaweser, K. Tsuchida, L. Abrecht, S. Vaina, C. Morger, N. Kukreja, P. Juni, G. Sianos, G. Hellige, R.T. van Domburg, O.M. Hess, E. Boersma, B. Meier, S. Windecker, P.W. Serruys, Early and late coronary stent thrombosis of sirolimus-eluting and paclitaxel-eluting stents in routine clinical practice: data from a large two-institutional cohort study, Lancet, 369 (2007) 667-678.

[56] I. Iakovou, T. Schmidt, E. Bonizzoni, et al., Incidence, predictors, and outcome of thrombosis after successful implantation of drug-eluting stents, Jama, 293 (2005) 2126-2130.

[57] L. Mauri, W.H. Hsieh, J.M. Massaro, K.K. Ho, R. D'Agostino, D.E. Cutlip, Stent thrombosis in randomized clinical trials of drug-eluting stents, The New England journal of medicine, 356 (2007) 1020-1029.

[58] S.J. Pocock, Safety of drug-eluting stents: demystifying network meta-analysis, The Lancet, 370 (2007) 2099-2100.

[59] M.R. Bennett, M. O'Sullivan, Mechanisms of angioplasty and stent restenosis: implications for design of rational therapy, Pharmacology & therapeutics, 91 (2001) 149-166.

[60] D.L. Fischman, M.B. Leon, D.S. Baim, R.A. Schatz, M.P. Savage, I. Penn, K. Detre, L. Veltri, D. Ricci, M. Nobuyoshi, et al., A randomized comparison of coronary-stent placement and balloon angioplasty in the treatment of coronary artery disease. Stent Restenosis Study Investigators, The New England journal of medicine, 331 (1994) 496-501.

[61] M.R. Bennett, In-stent stenosis: pathology and implications for the development of drug eluting stents, Heart, 89 (2003) 218-224.

[62] A.W. Carpenter, M.H. Schoenfisch, Nitric oxide release: part II. Therapeutic applications, Chem Soc Rev, 41 (2012) 3742-3752.

[63] M. Joner, A.V. Finn, A. Farb, E.K. Mont, F.D. Kolodgie, E. Ladich, R. Kutys, K. Skorija, H.K. Gold, R. Virmani, Pathology of drug-eluting stents in humans: delayed healing and late thrombotic risk, Journal of the American College of Cardiology, 48 (2006) 193-202.

[64] S.C. Woodward, P.S. Brewer, F. Moatamed, A. Schindler, C.G. Pitt, The intracellular degradation of poly(epsilon-caprolactone), Journal of biomedical materials research, 19 (1985) 437-444.

[65] A. de Mel, N. Naghavi, B.G. Cousins, I. Clatworthy, G. Hamilton, A. Darbyshire, A.M. Seifalian, Nitric oxide-eluting nanocomposite for cardiovascular implants, Journal of materials science. Materials in medicine, 25 (2014) 917-929.

[66] C. Sorragi, S.M. Shishido, M.E. Lemos, S. Marcondes, E. Antunes, M.H. Krieger, In vitro evaluation of the safe margin, antithrombotic and antiproliferative actions for the treatment of restenosis: Nitric oxide donor and polymers, Cell biochemistry and function, 29 (2011) 207-214.

[67] N. Naghavi, A. de Mel, O.S. Alavijeh, B.G. Cousins, A.M. Seifalian, Nitric oxide donors for cardiovascular implant applications, Small, 9 (2013) 22-35.

[68] C.d.c. Européennes, Directive 93/42/CEE relative aux dispositifs médicaux., (1993).

[69] C.d.l.U.E. Parlement Européen, Directive 2007/47/CE relative aux dispositifs médicaux., (2007).

[70] R.R. Costa, J.F. Mano, Polyelectrolyte multilayered assemblies in biomedical technologies, Chemical Society reviews, 43 (2014) 3453-3479.

[71] G. Decher, Fuzzy nanoassemblies: Toward layered polymeric multicomposites., Science, 277 (1997) 1232-1237.

[72] K. Sato, S. Takahashi, J. Anzai, Layer-by-layer thin films and microcapsules for biosensors and controlled release, Analytical sciences : the international journal of the Japan Society for Analytical Chemistry, 28 (2012) 929-938.

[73] M.C. Berg, L. Zhai, R.E. Cohen, M.F. Rubner, Controlled drug release from porous polyelectrolyte multilayers, Biomacromolecules, 7 (2006) 357-364.

[74] Z. Kadlecova, L. Baldi, D. Hacker, F.M. Wurm, H.A. Klok, Comparative study on the in vitro cytotoxicity of linear, dendritic, and hyperbranched polylysine analogues, Biomacromolecules, 13 (2012) 3127-3137.

[75] Y. Yi, H.J. Kim, P. Mi, M. Zheng, H. Takemoto, K. Toh, B.S. Kim, K. Hayashi, M. Naito, Y. Matsumoto, K. Miyata, K. Kataoka, Targeted systemic delivery of siRNA to cervical cancer model using cyclic RGD-installed unimer polyion complex-assembled gold nanoparticles, Journal of controlled release : official journal of the Controlled Release Society, 244 (2016) 247-256.

[76] R. Taniguchi, Y. Miura, H. Koyama, T. Chida, Y. Anraku, A. Kishimura, K. Shigematsu, K. Kataoka, T. Watanabe, Adequately-Sized Nanocarriers Allow Sustained Targeted Drug Delivery to Neointimal Lesions in Rat Arteries, Molecular pharmaceutics, 13 (2016) 2108-2116.

[77] I. Brigger, C. Dubernet, P. Couvreur, Nanoparticles in cancer therapy and diagnosis, Adv Drug Deliv Rev, 54 (2002) 631-651.

[78] E. Roger, J.C. Gimel, C. Bensley, A.S. Klymchenko, J.P. Benoit, Lipid nanocapsules maintain full integrity after crossing a human intestinal epithelium model, Journal of controlled release : official journal of the Controlled Release Society, 253 (2017) 11-18.

[79] J. Hardie, Y. Jiang, E.R. Tetrault, P.C. Ghazi, G.Y. Tonga, M.E. Farkas, V.M. Rotello, Simultaneous cytosolic delivery of a chemotherapeutic and siRNA using nanoparticle-stabilized nanocapsules, Nanotechnology, 27 (2016) 374001.

[80] M.E. Davis, Z.G. Chen, D.M. Shin, Nanoparticle therapeutics: an emerging treatment modality for cancer, Nature reviews. Drug discovery, 7 (2008) 771-782.

[81] Y.F. Wang, X.C. Guo, R.H. Pan, D. Han, T. Chen, Z.H. Geng, Y.F. Xiong, Y.J. Chen, Electrodeposition of chitosan/gelatin/nanosilver: A new method for constructing biopolymer/nanoparticle composite films with conductivity and antibacterial activity, Mat Sci Eng C-Mater, 53 (2015) 222-228.

[82] M. Jager, C. Zilkens, K. Zanger, R. Krauspe, Significance of nano- and microtopography for cell-surface interactions in orthopaedic implants, Journal of biomedicine & biotechnology, 2007 (2007) 69036.

[83] G. Balasundaram, M. Sato, T.J. Webster, Using hydroxyapatite nanoparticles and decreased crystallinity to promote osteoblast adhesion similar to functionalizing with RGD, Biomaterials, 27 (2006) 2798-2805.

[84] J. Tournebize, A. Boudier, A. Sapin-Minet, P. Maincent, P. Leroy, R. Schneider, Role of gold nanoparticles capping density on stability and surface reactivity to design drug delivery platforms, ACS applied materials & interfaces, 4 (2012) 5790-5799.

[85] M.T. Ortega, J.E. Riviere, K. Choi, N.A. Monteiro-Riviere, Biocorona formation on gold nanoparticles modulates human proximal tubule kidney cell uptake, cytotoxicity and gene expression, Toxicology in vitro : an international journal published in association with BIBRA, 42 (2017) 150-160.

[86] X. Li, M. Soler, C.I. Ozdemir, A. Belushkin, F. Yesilkoy, H. Altug, Plasmonic nanohole array biosensor for label-free and real-time analysis of live cell secretion, Lab on a chip, 17 (2017) 2208-2217.

[87] J.M. Dennison, J.M. Zupancic, W. Lin, J.H. Dwyer, C.J. Murphy, Protein Adsorption to Charged Gold Nanospheres as a Function of Protein Deformability, Langmuir, 33 (2017) 7751-7761.

[88] L. Karmani, D. Labar, V. Valembois, V. Bouchat, P.G. Nagaswaran, A. Bol, J. Gillart, P. Leveque, C. Bouzin, D. Bonifazi, C. Michiels, O. Feron, V. Gregoire, S. Lucas, T. Vander Borght, B. Gallez, Antibody-functionalized nanoparticles for imaging cancer: influence of conjugation to gold nanoparticles on the biodistribution of 89Zr-labeled cetuximab in mice, Contrast media & molecular imaging, 8 (2013) 402-408.

[89] M. Singh, D.C. Harris-Birtill, S.R. Markar, G.B. Hanna, D.S. Elson, Application of gold nanoparticles for gastrointestinal cancer theranostics: A systematic review, Nanomedicine : nanotechnology, biology, and medicine, 11 (2015) 2083-2098.

[90] D. Kim, Y.Y. Jeong, S. Jon, A drug-loaded aptamer-gold nanoparticle bioconjugate for combined CT imaging and therapy of prostate cancer, ACS nano, 4 (2010) 3689-3696.

[91] A.N. Kharlamov, A.E. Tyurnina, V.S. Veselova, O.P. Kovtun, V.Y. Shur, J.L. Gabinsky, Silica-gold nanoparticles for atheroprotective management of plaques: results of the NANOM-FIM trial, Nanoscale, 7 (2015) 8003-8015.

[92] A. Warnecke, P. Luessen, J. Sandmann, M. Ikic, S. Rossa, F.M. Gutzki, D.O. Stichtenoth, D. Tsikas, Application of a stable-isotope dilution technique to study the pharmacokinetics of human 15N-labelled S-nitrosoalbumin in the rat: possible mechanistic and biological implications, Journal of chromatography. B, Analytical technologies in the biomedical and life sciences, 877 (2009) 1375-1387.

[93] J. Tournebize, A. Sapin-Minet, R. Schneider, A. Boudier, P. Maincent, P. Leroy, Simple spectrophotocolorimetric method for quantitative determination of gold in nanoparticles, Talanta, 83 (2011) 1780-1783.

[94] B.D. Chithrani, A.A. Ghazani, W.C.W. Chan, Determining the Size and Shape Dependence of Gold Nanoparticle Uptake into Mammalian Cells, Nano Lett, 6 (2006) 662-668.

[95] J.D. Trono, K. Mizuno, N. Yusa, T. Matsukawa, K. Yokoyama, M. Uesaka, Size, concentration and incubation time dependence of gold nanoparticle uptake into pancreas cancer cells and its future application to X-Ray Drug Delivery System, Journal of radiation research, 52 (2011) 103-109.

[96] ICH-Q2(R1), Note for Guidance on Validation of Analytical Procedures : Text and Methodology. Ref. CPMP/ICH/381/95.

[97] F.a.D. Administration, Guidance for Industry, Bioanalytical Method Validation, Revision 1, Septembre 2013, (2013).

[98] F. d'Orlye, A. Varenne, P. Gareil, Size-based characterization of nanometric cationic maghemite particles using capillary zone electrophoresis, Electrophoresis, 29 (2008) 3768-3778.

[99] B. Franze, I. Strenge, C. Engelhard, Separation and detection of gold nanoparticles with capillary electrophoresis and ICP-MS in single particle mode (CE-SP-ICP-MS), Journal of Analytical Atomic Spectrometry, 32 (2017) 1481-1489.

[100] D. Mozhayeva, C. Engelhard, Separation of Silver Nanoparticles with Different Coatings by Capillary Electrophoresis Coupled to ICP-MS in Single Particle Mode, Analytical chemistry, 89 (2017) 9767-9774.

[101] V. Baldim, A. Ismail, P. Taladriz-Blanco, S. Griveau, M.G. de Oliveira, F. Bedioui, Amperometric Quantification of S-Nitrosoglutathione Using Gold Nanoparticles: A Step toward Determination of S-Nitrosothiols in Plasma, Analytical chemistry, 88 (2016) 3115-3120.

[102] L.L. Perissinotti, A.G. Turjanski, D.A. Estrin, F. Doctorovich, Transnitrosation of Nitrosothiols: Characterization of an Elusive Intermediate, J Am Chem Soc, 127 (2005) 486-487.

[103] T. Boudou, T. Crouzier, K. Ren, G. Blin, C. Picart, Multiple functionalities of polyelectrolyte multilayer films: new biomedical applications, Advanced materials, 22 (2010) 441-467.

[104] G. Decher, Fuzzy Nanoassemblies: Toward Layered Polymeric Multicomposites, Science, 277 (1997) 1232-1237.

[105] FDA, Indirect Food additives: Adhesives and components of coating, 21CFR175.320, (2017).

[106] FDA, Sevelamer - Full prescribing information, (2017).

[107] P. Thevenot, W. Hu, L. Tang, SURFACE CHEMISTRY INFLUENCE IMPLANT BIOCOMPATIBILITY, Current topics in medicinal chemistry, 8 (2008) 270-280.

[108] M. Vafa Homann, D. Johansson, H. Wallen, J. Sanchez, Improved ex vivo blood compatibility of central venous catheter with noble metal alloy coating, Journal of biomedical materials research. Part B, Applied biomaterials, 104 (2016) 1359-1365.

[109] I.H. Jaffer, J.C. Fredenburgh, J. Hirsh, J.I. Weitz, Medical device-induced thrombosis: what causes it and how can we prevent it?, Journal of Thrombosis and Haemostasis, 13 (2015) S72-S81.

[110] R. Michel, S. Pasche, M. Textor, D.G. Castner, Influence of PEG Architecture on Protein Adsorption and Conformation, Langmuir, 21 (2005) 12327-12332.

[111] H. Du, P. Chandaroy, S.W. Hui, Grafted poly-(ethylene glycol) on lipid surfaces inhibits protein adsorption and cell adhesion, Biochimica et Biophysica Acta (BBA) - Biomembranes, 1326 (1997) 236-248.

[112] G.L. Ackland, A. Gutierrez Del Arroyo, S.T. Yao, R.C. Stephens, A. Dyson, N.J. Klein, M. Singer, A.V. Gourine, Low-molecular-weight polyethylene glycol improves survival in experimental sepsis, Critical care medicine, 38 (2010) 629-636.

[113] W.H. De Jong, W.I. Hagens, P. Krystek, M.C. Burger, A.J. Sips, R.E. Geertsma, Particle size-dependent organ distribution of gold nanoparticles after intravenous administration, Biomaterials, 29 (2008) 1912-1919.

[114] S. Pavlukhina, S. Sukhishvili, Polymer assemblies for controlled delivery of bioactive molecules from surfaces, Adv Drug Deliv Rev, 63 (2011) 822-836.

[115] G.E. Ragkousis, N. Curzen, N.W. Bressloff, Simulation of longitudinal stent deformation in a patient-specific coronary artery, Medical engineering & physics, 36 (2014) 467-476.

[116] G. Choi, L.K. Shin, C.A. Taylor, C.P. Cheng, In Vivo Deformation of the Human Abdominal Aorta and Common Iliac Arteries With Hip and Knee Flexion: Implications for the Design of Stent-Grafts, Journal of Endovascular Therapy, 16 (2009) 531-538.

[117] J.P. Guggenbichler, O. Assadian, M. Boeswald, A. Kramer, Incidence and clinical implication of nosocomial infections associated with implantable biomaterials – catheters, ventilator-associated pneumonia, urinary tract infections, GMS Krankenhaushygiene interdisziplinär, 6 (2011) Doc18.

[118] N.R.C. Campbell, R.E. Gilbert, L.A. Leiter, P. Larochelle, S. Tobe, A. Chockalingam, R. Ward, D. Morris, R.T. Tsuyuki, S.B. Harris, L'hypertension chez les diabétiques de type 2: Mise à jour sur le traitement pharmacologique, Canadian Family Physician, 57 (2011) e347-e353.

[119] C.L. Ventola, Medical Applications for 3D Printing: Current and Projected Uses, Pharmacy and Therapeutics, 39 (2014) 704-711.

Films polymériques pour le développement de stents innovants

La prise en charge d'urgence des pathologies ischémiques repose dans un premier temps sur la thrombolyse et/ou l'angioplastie puis dans un second temps sur des mesures hygiéno-diététiques. L'angioplastie consiste en la destruction de l'obstruction située dans l'artère et est souvent suivie (dans 70 % des cas) par la pose d'une endoprothèse également appelée stent. Malgré des innovations thérapeutiques importantes (stents libérant des principes actifs), des problèmes de thrombose et de resténose au niveau du site lésé sont observés. Or, le monoxyde d'azote, NO, un gazotransmetteur de l'organisme, possède des propriétés intéressantes pour lutter contre ce phénomène, à concentration physiologique.

Dans ce travail, nous avons développé un film nanostructuré permettant de recouvrir un stent, avec pour objectif final une délivrance contrôlée de NO. Cette couverture incorpore des nanoparticules d'or (AuNP), choisies pour leur importante capacité de greffage avec des donneurs de NO. Celles-ci sont piégées au sein des couches d'un film constitué de polyélectrolytes : le polycation, les AuNP et le polyanion interagissant ensemble par des interactions électrostatiques.

Le chapitre 1 propose une revue de la littérature sur l'utilisation croissante des nanotechnologies dans le domaine des dispositifs médicaux. Dans ce contexte biomédical spécifique, les AuNP doivent être considérées comme des matières premières pharmaceutiques. Le chapitre 2 présente les méthodologies analytiques développées en ce sens. Ces méthodes, en complément des techniques physicochimiques plus classiquement utilisées, seront appliquées à l'ensemble des lots de nanoparticules produits. Des premiers essais de greffage de NO ont été menés à l'aide d'une macromolécule modèle. Le chapitre 3 se concentre sur la formation et l'optimisation des films nanostructurés. Les AuNP ont été incorporées dans des films multicouches qui démontrent une stabilité importante (> 1 an) et sont capables d'en immobiliser un grand nombre (jusqu'à 10^{12} AuNP/cm²/cycle). Pour augmenter leur taux de chargement au sein des films, une étude d'optimisation a été réalisée. Un enrichissement des films en AuNP est possible en modifiant les conditions de préparation. Enfin, ces films présentent une inertie face à des protéines, des cellules immunocompétentes et du sang total.

L'ensemble de ces résultats permet de poser des bases solides pour le développement de stents innovants à couverture active.

Mots clés : Nanoparticules d'or, contrôle qualité, films polymériques multicouches, stent, resténose.

Polymeric films for innovative stent development

Emergency management of ischemic pathologies is initially based on thrombolysis and/or angioplasty and secondly on hygiene-dietetic measures. Angioplasty consists of the destruction of the obstacle located in the artery and is often followed (in 70% of cases) by stent implantation. Despite therapeutic innovations (drug eluting stents), problems of thrombosis and restenosis in the injured site are observed. Yet, nitric oxide, NO, a gaseous transmitter is characterized by interesting properties against this phenomenon at the physiological concentration.

In this work, we developed a nanostructured film that would be able to deliver NO in order to cover a stent. This coating entraped gold nanoparticles (AuNP) characterized by a high capacity of NO donor grafting. They were incorporated into layers of a polyelectrolyte film: polycation, AuNP and polyanion interacting by electrostatic bounds.

The first chapter stands a literature review on the increased use of nanotechnologies in the medical device field. In this specific biomedical context, AuNP must be considered as pharmaceutical raw material. Chapter 2 presents analytical methods developed in this way. These methodologies, completed by more classical physicochemical technics, will be applied to all the synthetized batches. First NO grafting tests were performed using a model macromolecule. Chapter 3 concentrates on nanostructured film formation and optimization. AuNP were incorporated into films and they presented an important stability (> 1 year) and films were able to immobilize a large number of AuNP (up to 10^{12} AuNP/cm²/cycle). To increase their inclusion rate an optimization step was realized. The film enrichment with AuNP was possible by the modification of the preparation conditions. Lastly, the films were inert towards proteins, immunocompetent cells and whole blood.

These results allow lying solid bases for the future development of innovative stents with active coating.

Key-words: Gold nanoparticles, quality control, layer-by-layer polymeric films, stent, restenosis